

GEORGIA INSTITUTE OF TECHNOLOGY
OFFICE OF CONTRACT ADMINISTRATION
SPONSORED PROJECT INITIATION

Date: October 12, 1976

Project Title: Fluidized Carbon Coated Particles Reactor Concept

Project No: E-26-624

Project Director: Dr. R. A. Karam

Sponsor: U. S. Energy Research and Development Administration; Oak Ridge Operations

Agreement Period: From 10/1/76 Until 12/31/76

Type Agreement: Contract No. E(40-1)-5273

Amount: \$40,000 ERDA
3,911 GIT (E-26-320)
\$43,911

Reports Required: Final Report

Sponsor Contact Person (s):

Technical Matters

Contractual Matters

(thru OCA)

Mr. Walker Love
Research Contracts, Procedures and Reports Branch
Contract Division
U. S. Energy Research and Development Administration
Oak Ridge Operations
P. O. Box E
Oak Ridge, Tennessee 37830

Defense Priority Rating: None

Assigned to: Nuclear Engineering (School/Laboratory)

COPIES TO:

Project Director
Division Chief (EES)
School/Laboratory Director
Dean/Director-EES
Accounting Office
Procurement Office
Security Coordinator (OCA)
Reports Coordinator (OCA)

Library, Technical Reports Section
Office of Computing Service
Director, Physical Plant
EES Information Office
Project File (OCA)
Project Code (GTRI)
Other _____

GEORGIA INSTITUTE OF TECHNOLOGY
OFFICE OF CONTRACT ADMINISTRATION
SPONSORED PROJECT TERMINATION

no action
11

REVISED
(See Note)

Date: 2/17/78

Project Title: Fluidized Carbon Coated Particles Reactor Concept

Project No: E-26-624

Project Director: Dr. R.A. Karam

Sponsor: U.S. Department of Energy (Formerly U.S. Energy Research & Development Administration); Oak Ridge Operations

Effective Termination Date: 12/31/77

Clearance of Accounting Charges: 12/31/77

Grant/Contract Closeout Actions Remaining:

- Final Invoice and Closing Documents
- Final Fiscal Report
- Final Report of Inventions
- Govt. Property Inventory & Related Certificate 11 Aug 77
- Classified Material Certificate
- Other: _____

NOTE: THIS PROJECT WAS REACTIVATED FOR SUBMISSION OF REVISED FINAL REPORT.

Assigned to: Nuclear Engineering (School/Laboratory)

COPIES TO:

- | | |
|----------------------------|------------------------------------|
| Project Director | Library, Technical Reports Section |
| Division Chief (EES) | Office of Computing Services |
| School/Laboratory Director | Director, Physical Plant |
| Dean/Director-EES | EES Information Office |
| Accounting Office | Project File (OCA) |
| Procurement Office | Project Code (GTRI) |
| Security Coordinator (OCA) | Other _____ |
| Reports Coordinator (OCA) | |

BOUND BY THE NATIONAL LIBRARY BINDERY CO. OF GA.
and title page? Imperfect volumes delay return of binding. Thanks.

108

E-26-624

FINAL REPORT (REVISED)

SUSPENDED-BED REACTOR PRELIMINARY
DESIGN $U^{233} - Th^{232}$ CYCLE

By

R. A. Karam, A. Alapour, and C. C. Lee

Prepared for

The U. S. Energy Research and Development Administration
under Contract No. E(40-1)-5273

November

1977



SCHOOL OF NUCLEAR ENGINEERING
GEORGIA INSTITUTE OF TECHNOLOGY
ATLANTA, GEORGIA 30332

SUSPENDED-BED REACTOR PRELIMINARY DESIGN

U^{233} - Th^{232} CYCLE

by

R. A. Karam, A. Alapour, and C. C. Lee
School of Nuclear Engineering
Georgia Institute of Technology

Prepared for the U.S. Energy Research and Development Administration
under contract No. E(40-1)-5273

TABLE OF CONTENTS

	FOREWORD	1
	SUMMARY	2
I.	INTRODUCTION	17
II.	SUSPENDED-BED REACTOR CONCEPT	23
	II.1 Introduction	23
	II.2 Thermal Hydraulics for Fluidized-and-Fixed-Bed Regimes	27
	II.2.1 Heat Transport	27
	II.2.2 Fluidized and Fixed-Bed Regimes	34
	II.2.2.1 Fluidized Bed	34
	II.3 Thermodynamic Optimization Study for Gas Cooled Reactors	38
	II.3.1 Gas-Cycle Studies	39
	II.3.2 Gas/Steam Binary Cycle	44
	II.4 Fuel Design	51
	II.4.1 General Considerations of Coated Particles	51
	II.4.2 Coated Particle Fuel - A Review	51
	II.4.3 Suspended-Bed Reactor Fuel Design	61
	II.5 Physics Calculations	65
	II.5.1 Core Specifications	65
	II.5.2 Blanket	71
	II.5.3 Cross Section Generation	76
	II.5.4 Reactor Calculations	76
	II.5.5 The Suspended-Bed Reactor Cylindrical Calculations . .	83
	II.6 Selection of Pipe Material and Sizes	87

II.7	Decay Heat Removal	94
II.8	Consideration Leading to Choice of Suspended-Bed Reactor Parameters	98
II.9	Preliminary Final Design of Suspended-Bed Reactor	110
III.	RECOMMENDED RESEARCH AND DEVELOPMENT PROGRAM	127

APPENDICES

A.	GENERAL CONSIDERATION OF NATURAL URANIUM AND THORIUM RESERVES AND IMPLICATION ON NUCLEAR POWER GROWTH	131
A.1	Uranium Reserves	132
A.2	The Thorium Resource	140
A.3	Energy from Assured Reserves	142
A.4	Electrical Energy Needs and Nuclear Power Growth	144
B.	THORIUM-BASED REACTORS	150
B.1	General Background	151
B.2	Physics Parameters	153
B.2.1	Breeding	153
B.2.2	Doubling Time and Specific Power	167
B.2.3	Breeder Strategy	171
B.2.3.1	Metallic Pu-Th Interim Breeders	175
B.2.4	Coolant Void Coefficient	176
B.2.5	Doppler Coefficient	178
B.2.6	Protactinium Production	178
B.2.7	U-232 Production	179
B.2.8	Transuranium Elements Production	184
B.2.9	Delayed Neutron Fraction	185

APPENDICES

C.	HEAT CONDUCTION THROUGH THREE SHELLS	186
D.	THERMAL HYDRAULICS CODE	195
E.	GAS-STEAM BINARY CYCLE.	202
REFERENCES	213

LIST OF TABLES

Table S-I.	SBR Design Specifications (Dicarbide Fuel)	6
Table S-II.	SBR Design Specifications (Coated Metallic Fuel)	8
Table II-4-I.	Advanced BISO Fertile Particle Description	53
Table II-4-II.	Effective Conversion Factors for Advanced BISO Fuel Particles.	59
Table II-4-III.	Mechanical Properties of Fuel Materials.	63
Table II-5-I.	Comparison of Material Volume Fractions of SBR with Typical GCFR and LMFBR	72
Table II-5-II.	Fissile and Fertile Material Requirements and Con- version Ratios, as a Function of Coolant Volume Frac- tion in the Dicarbide Spherical Suspended-Bed Reactor.	79
Table II-5-III.	Fissile and Fertile Material Requirements and Conversion Ratios as a Function of Void Fraction in Metallic Spherical SBR Reactor	80
Table II-5-IV.	SBR Comparison with Other 1000 MW _e Reactors.	81
Table II-5-V.	Physics Parameters for Cylindrical Reactors	84
Table II-6-I.	Mechanical, Physical, and Nuclear Properties of V-Ti(20%), Zircalloy 2 and 4, and S.S. 316	89
Table II-6-II.	Effects of Pipe Material on Neutronic Performance.	90
Table II-6-III.	Design Properties of Pipes	93
Table II-7-I.	Mass of Graphite Block Required to Remove Decay Heat for 1, 12, and 24 hours After Shutdown.	95
Table II-7-II.	Temperature Distribution for Various Sizes of Pipes.	97
Table II-9-I.	Material Constants Used in Calculation	119
Table II-9-II.	SBR Design Specifications Dicarbide Fuel	121
Table II-9-III.	SBR Design Specifications (Coated Metallic Fuel)	123
Table A-1-I.	U.S. Uranium Resources as of January 1, 1975 (Tons of U ₃ O ₈)	132
Table A-1-II.	Potential Resources--January 1, 1976	132
Table A-1-III.	Reasonably Assured Uranium Reserves (as of January 1, 1975, 1000 tons)	139

Table A-2-I.	Estimates of U.S. Thorium Resources	140
Table A-2-II.	Estimates of the U.S. Uranium Fuel Resources	140
Table A-2-III.	Estimated U.S. Thorium Resources (thousand tons)	141
Table A-3-I.	U.S. Nuclear Electrical Capacity Forecasts as of February 1974 (thousands of megawatts)	143
Table B-2-I.	Atom Densities in Heavy Water Cooled (U ²³³ -Th ²³²)O ₂ Reactors and in Sodium-Cooled (Pu ²³⁹ -U ²³⁸)O ₂ Reactors	161
Table B-2-II.	Breeding Performance of (U ²³³ -Th ²³²)O ₂ in D ₂ O- Cooled Reactor	162
Table B-2-III.	Breeding Performance of (Pu ²³⁹ -Th ²³²)O ₂ in D ₂ O- Cooled Reactor	163
Table B-2-IV.	Breeding Performance of (Pu ²³⁹ -U ²³⁸)O ₂ in Sodium- Cooled Reactor	164
Table B-2-V.	Group Cross Sections for Slowly Saturating Fission Products (in barns).	165
Table B-2-VI.	Group Cross Sections for Rapidly Saturating and Nonsaturating Fission Products and Xe ¹³⁵ (in barns).	166
Table B-2-VII.	Thermal Conductivity k _f of Some Fuel Materials (Btu/he-ft-°F)	172
Table B-2-VIII.	Relative Hazards of Transuranium Elements in Th ²³² and U ²³² and U ²³⁸ Fuel Cycles.	185
Table B-2-IX.	Delayed Neutrons per Fission (Source Ref. 90).	185

LIST OF FIGURES

	Page
Fig. S-1. Suspended-Bed Reactor.	5
Fig. S-2. Binary Cycle Efficiency, lbs Gas Needed/lb Steam Generated, Gas Turbine Outlet Temperature, Reactor Inlet Temperature and Compression Inlet Temperature All vs Compression Ratio	11
Fig. S-3. Binary Cycle Efficiency, lbs Gas Needed per lb Steam Generated, Gas Turbine Outlet Temperature, Reactor Inlet Temperature and Compressor in Temperature All vs Compression Ratio	12
Fig. S-4. Suspended-Bed Reactor Binary Cycle	13
Fig. S-5. Program of Study Block Diagram	16
Fig. I-1. Arrangement of Tubes for Suspended-Bed Reactor	20
Fig. II-3-1. Gas Cycle Efficiency vs Compression Ratio for One Stage Compression.	40
Fig. II-3-2. Gas Cycle Efficiency vs Compression Ratio for Two Stage Compression.	42
Fig. II-3-3. Gas Cycle Efficiency vs Compression Ratio at Several Temperatures and Recuperator Effectiveness	43
Fig. II-3-4. Optimum Gas-Steam Binary Cycle	45
Fig. II-3-5. Optimum Gas-Steam Binary Cycle	46
Fig. II-3-6. Binary Cycle Efficiency, lbs Gas Needed/lb Steam Generated, Gas Turbine Outlet Temp., and Comp. Inlet Temp. All vs Compression Ratio	48
Fig. II-3-7. Binary Cycle Efficiency, lbs Gas Needed per lb Steam Generated, Gas Turbine Outlet Temp., Reactor Inlet Temp. and Compressor in Temp. All vs Compression	49
Fig. II-4-1. TRISO Fuel Particle Coating Failure Diagram.	54
Fig. II-4-2. BISO Fuel Particle Coating Failure Diagram	55
Fig. II-4-3. Assumed Pressure Vessel Failure Fraction vs (a) Fast Neutron Fluence or (b) Kernel Burnup for TRISO UC ₂ fuel. (From Ref. 21).	56
Fig. II-4-4. TRISO Fuel Particle Coating Failure Diagram.	57

Fig. II-4-5.	Effect of a Rapid Thermal Excursion From 1250 ^o to 1425 ^o , 1600 ^o , or 1800 ^o C and Back to 1250 ^o C on Pressure Vessel Failure in TRISO UC ₂ as a Function of (a) Fast Neutron Exposure or (b) Kernel Burnup for Fuel Experiencing 78% FIMA at a Fast Neutron Exposure of 8 x 10 ²¹ nvt. (From Ref. 21)..	58
Fig. II-5-1.	Geometrical Description of the Suspended Bed-Reactor	66
Fig. II-5-2.	Pictorial View of Pipe Arrangement	67
Fig. II-5-3.	A Section of Pipe Showing Core and Blanket Arrangements.	68
Fig. II-5-4.	A Sketch of the Suspended-Bed Reactor Pipe Showing Insulation	69
Fig. II-5-5.	Unit Cell in Suspended-Bed Reactor	70
Fig. II-5-6.	Bottom Axial Blanket	74
Fig. II-5-7.	Axial Blanket.	75
Fig. II-5-8.	Critical Mass vs Coolant Volume Fraction	77
Fig. II-5-9.	Conversion Ratio vs Coolant Volume Fraction.	78
Fig. II-5-10.	Fundamental Mode Neutron Spectrum of the SBR and the the LMFBR.	82
Fig. II-5-11.	Spatial Power Distribution in the SBR.	85
Fig. II-5-12.	Assembly in Transition; k _{eff} < 0.37	86
Fig. II-8-1.	Power Density vs Fuel Particle Particle Diameter in Fluidized Bed	99
Fig. II-8-2.	Gas Outlet Temperature vs Particle Diameter.	100
Fig. II-8-3.	Pressure Loss vs Bed Height (Fluidized Bed).	101
Fig. II-8-4.	Power Density vs Particle Diameter at Various Gas Pressures (Fluidized Bed).	102
Fig. II-8-5.	Power Density vs Particle Diameter at Various Gas Inlet Temperatures (Fluidized Bed)	103
Fig. II-8-6.	Power Density vs Gas Velocity in Suspended-Bed Reactor	104
Fig. II-8-7.	Gas Outlet Temperature vs Gas Velocity (Suspended-Bed Reactor)	106

Fig. II-8-8.	Pressure Drop vs Gas Velocity (Suspended-Bed Reactor) . .	107
Fig. II-8-9.	Power Density and Pressure Loss vs Gas Velocity Bed Void Fractions	108
Fig. II-8-10.	Power Density and Pressure Loss vs Gas Velocity at Various Bed Void Fractions	109
Fig. II-9-1.	Binary Cycle Efficiency vs Compression Ratio at Various Pressure Loss Ratio.	111
Fig. II-9-2.	Binary Cycle Efficiency and Core Inlet Temperature vs Gas Cycle Pressure Loss Ratio at Various Compression Ratios	112
Fig. II-9-3.	Power Density vs Compression Ratio at Various Void Fractions.	113
Fig. II-9-4.	Pressure Loss vs Compression Ratio (Dicarbide Fuel). . .	114
Fig. II-9-5.	Overall Binary Efficiency vs Compression Ratio for Various Void Fractions (Dicarbide Fuel).	115
Fig. II-9-6.	Power Density vs Compression Ratio for Various Void Fractions (Metallic Fuel).	116
Fig. II-9-7.	Pressure Loss Ratio vs Compression Ratio for Various Void Fractions (Metallic Fuel)	117
Fig. II-9-8.	Overall Binary Efficiency vs Compression Ratio for Various Voids (Metallic Fuel)	118
Fig. II-9-9.	Suspended-Bed Reactor Binary Cycle	125
Fig. II-9-10.	Suspended-Bed Reactor.	126
Fig. III-1.	Program of Study Block Diagram	130
Fig. A-2-1.	Relative Abundance of Nuclear Fuels in the Earth's Crust (Basis, Ref. 54)	141
Fig. A-4-1.	Electrical Energy Needs and Various Scenarios of Nuclear Power Growth	146
Fig. B-2-1.	Neutron Yield per Neutron Absorbed, η vs Energy of Neutron Absorbed (Source Ref. 52).	154
Fig. B-2-2.	Fission Cross-Section of ^{232}Th and ^{238}U	157

Fig. B-2-3.	Fission Cross Sections of U^{233} , U^{235} , and Pu^{239} as a Function of Energy (source Ref. 44)	177
Fig. B-2-4.	Nuclear Reactions Occurring in the Neutron Irradiation of Thorium	180
Fig. B-2-5.	Nuclear Reactions Occurring in the Neutron Irradiation of Uranium	181
Fig. B-2-6.	Time Factor (T.F.) $\equiv (e^{-0.0099t} - e^{-0.3647t})$ vs t (years)	183

FOREWARD

This report describes the preliminary design of the Suspended-Bed Reactor fueled with Th²³² - U²³³ coated particles and to be considered as an alternative to LMFBR's. It was prepared by R. A. Karam, A. Alapour, and C. C. Lee of the Georgia Institute of Technology under contract E(40-1)-5273. Mr. William Kitterman, who in addition to being a Project Manager for ERDA, was a motivating force for the project. Youssef Chacal's contribution in the art work is gratefully acknowledged.

SUMMARY

SUSPENDED-BED REACTOR PRELIMINARY DESIGN U^{233} - Th^{232} CYCLE

The Division of International Security Affairs (ISA), Energy Research and Development Administration (ERDA), awarded Georgia Institute of Technology a 6-man-months contract to perform a preliminary system design and analysis of a stationary nuclear electric power station which is based on the Suspended-Bed Reactor concept (SBR) and which might be, by design, non-proliferating.

The SBR Concept

When a fluid stream, either gas or liquid, is passed through a bed of granular material and the velocity of the stream is gradually increased, a point is reached such that the drag force resisting the flow of the fluid is equal to the weight of the particles in the bed. Any further increase in the fluid velocity would lead to expansion of the bed, i.e. the particles are separated resulting in a greater area for the passage of the fluid; this limits the pressure drop across the bed. This condition corresponds to the limit of stability of a packed (fixed) bed and marks the transition to the fluidized or suspended state. If the fluid velocity is held constant at this point, the force of the fluid balances the weight of the particles, and the contact among particles tends to cease. The surface of the bed adjusts itself just like a liquid, and the particles will remain suspended as long as the fluid flows at that velocity.

As the fluid velocity is increased still further, an intensive mixing of the bed begins and, finally on increasing the gas velocity still more, carry-over of particles from the container occurs. A fluidized condition exists for only a specific range of fluid velocities. Below this range, the bed is stationary or fixed, and above it the particles would be transported out of the bed. If a screen is placed at the top of the bed to prevent the flow of particles out of the bed, a fixed-bed condition would prevail again. The drag force under these conditions is much higher than the weight of the bed; consequently all the particles would be held up against the screen while the fluid is allowed through. This is the basis of the Suspended-Bed Reactor concept.

Coated particles about 2 mm in diameter are used as the fuel. The coatings consist of three layers: (1) low density pyrolytic graphite, 70 μ thick, (2) silicon carbide pressure vessel, 30 μ thick, and (3) ZrC layer, 50 μ thick, to protect the pressure vessel from moisture and oxygen. The fuel kernel can be either uranium-thorium dicarbide or metal.

The coated particles are suspended by helium gas (coolant) in a cluster of pressurized tubes. The upward flow of helium fluidizes the coated particles. As the flow rate increases, the bed of particles is lifted upward to the core section. The particles are restrained at the upper end of the core by a suitable screen. The overall particle density in the core is just enough for criticality condition. Should the helium flow cease, the bed in the core section will collapse, and the particles will flow downward into the section where the increased physical spacings among the tubes brings about a safe shutdown. By immersing this section of the tubes in a large graphite block to serve as a heat sink, dissipation of decay heat becomes manageable. This eliminates the need for emergency core cooling systems.

The inherent advantages of this concept are:

- No pressure vessel is required.
- No control rods are required. Costly drive mechanisms and uneven flux distortion are eliminated.
- Truly fail-safe operation with respect to decay heat removal.
- No clad for the fuel is required. This reduces the waste-disposal problem.
- No emergency core cooling is needed.
- On-line fueling operation. This eliminates costly shutdown.
- High temperature operation resulting in two distinct advantages:
(1) high thermodynamic efficiency and (2) process heat for making steel, methane from coal, etc.
- High burnup, 100,000 MWD/ton or more.
- Coated particles retain fission products effectively.
- Breeding ratio can be tailored to be close to 1.0 if desired.
- High breeding ratio and low doubling time are possible.
- Helium gas is a very safe coolant.

The SBR Design

Figure S-1 shows the overall Suspended-Bed Reactor design. Design parameters are listed in Table S-I for the dicarbide coated fuel. Table S-II lists design parameter for the metallic fuel coated particles.

A comprehensive analysis of ways to increase the efficiency of thermal energy conversion to electricity, based on current technologies, led to the adoption of an optimized steam cycle "topped" by a simple gas-turbine cycle, the combination of which yields a significant increase in the thermodynamic

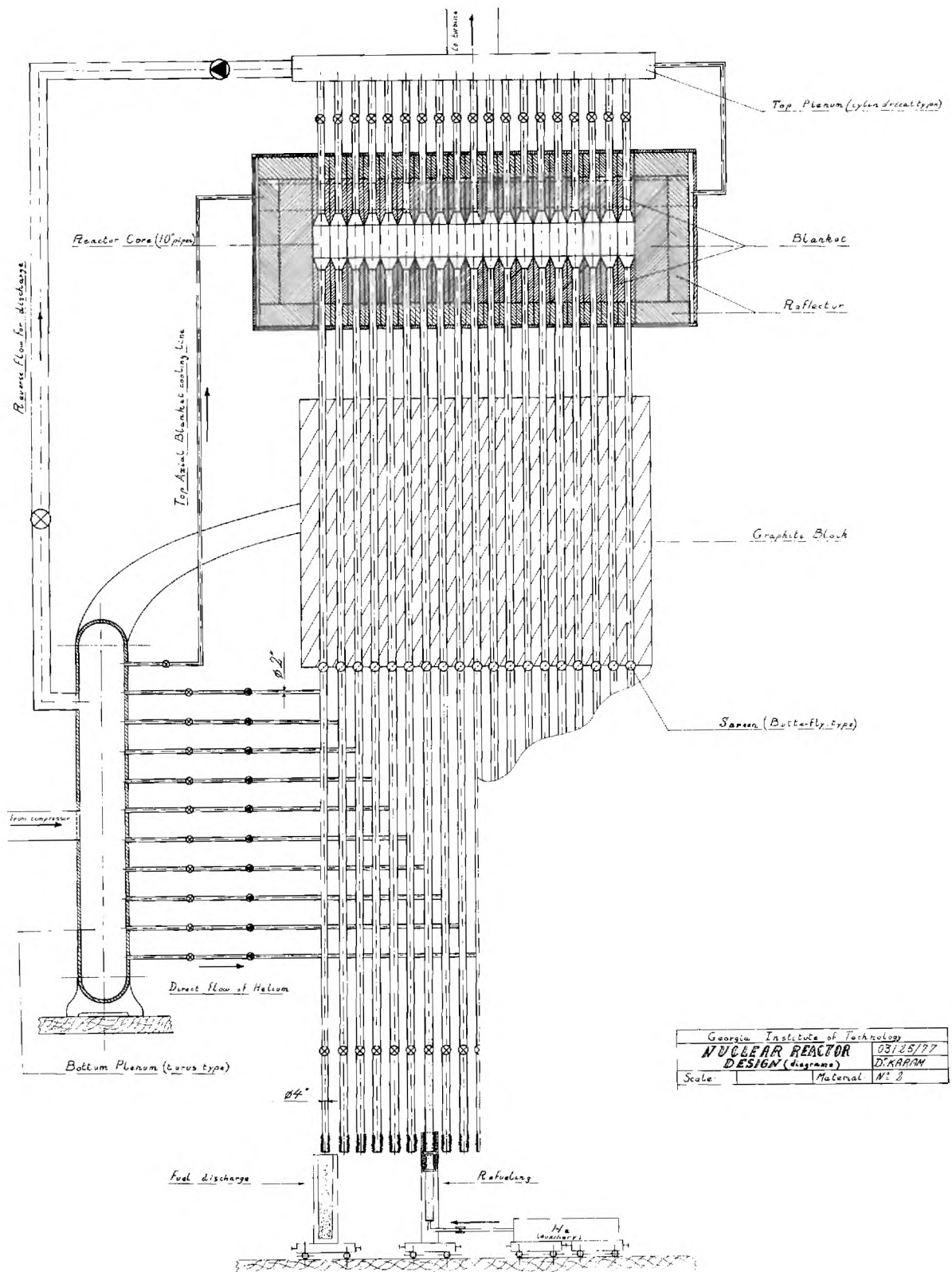


Figure S-1. Suspended-Bed Reactor.

Table S-I. SBR Design Specifications
Dicarbide Fuel

<u>GENERAL</u>	
Electric Power, MW _e	1160.0
Binary Cycle Overall Thermal Efficiency, %	40.0
Core Power Density, MW/m ³	290.0
Core Volume, m ³	10.0
Core Height, m	1.0
 <u>GAS CYCLE</u> 	
He Gas Static Pressure, psi	1000.0
Gas Compressor Compression Ratio	1.2
Core Gas Inlet Temperature, °F	590.0
Core Gas Outlet Temperature, °F	1500.0
Comp./Gas-Turb. Efficiency, %	90.0
Total Gas Cycle Pressure Loss Ratio, %	14.0
Gas Volume Fraction in Core (Void), %	60.0
Gas Mass Flow Rate, kg _{gas} /hr	3.963 x 10 ⁶
Gas Superficial Velocity, m/sec	19.1
Gas Pressure Drop in Core, psi	120.0
 <u>STEAM GENERATOR</u> 	
Steam Generator Gas Inlet Temperature, °F	1464.0
Steam Generator Gas Outlet Temperature, °F	509.0
Gas Temperature at Pinch Point, °F	700.0
Pound Gas per Pound Steam Generated	0.8415
Steam Generator Outlet Temperature, °F	1000.0
Steam Generator Feed Water Temperature, °F	486.0
 (continued) 	

Table S-I. SBR Design Specifications
Dicarbide Fuel (continued)

STEAM CYCLE

Superheated Steam Pressure/Temperature (Steam Turb. Inlet), psia/°F	2000/1000
N ^o of Resuperheaters	0.0
N ^o of Feed Water Heaters	6.0
Condenser Pressure/Temperature, in. Hga/°F	2/101
Quality of Steam at Low Pressure Turb. Exit, %	15.0
Steam Flow Rate, kg/hr	4.709 x 10 ⁶
Pumping Requirement, MWe	32.0
Thermal Efficiency of Steam Cycle Alone, %	43.0
Net Power Generated by Steam Cycle, MWe	1310.0
Steam Turbine/Pump Efficiency, %	85.0

FUEL

Fuel Particle Diameter, cm	0.17
Fuel Kernel Diameter (U ²³³ -Th ²³²)C ₂ , cm	0.14
Fuel Particle Total Coating Thickness, cm	0.015
Pyrolytic Graphite Layer Thickness (First Layer), cm	0.0070
Silicon Carbide Layer Thickness (Second Layer), cm	0.0030
Zirconium Carbide Layer Thickness (Third Layer), cm	0.0050
Maximum Fuel Temperature, °F	2400.0
Maximum Temperature Drop through the Fuel Kernel, °F	290.0
Terminal Velocity of Fuel Particles, m/sec	8.7
Fuel Kernel Max. Volumetric Heat Source Strength, MW/m ³	1.830 x 10 ⁵
Fertile Mass Core/Blanket, kg	10,963/57,590
Fissile Mass, kg	2600.0
Specific Power, MW/kg	1.1
Enrichment, Inner Core/Outer Core, %	16.0/22.88
Initial Breeding Ratio	1.06
Power Peaking Factor	1.21

Table S-II. SBR Design Specifications
(Coated Metallic Fuel)

<u>GENERAL</u>	
Electrical Power, MW _e	902.0
Binary Cycle Overall Thermal Efficiency, %	41.0
Core Power Density, MW/m ³	220.0
Core Volume, m ³	10.0
Core Height, m	1.0
<u>GAS CYCLE</u>	
He Gas Static Pressure, psi	1000.0
Gas Compressor Compression Ratio	1.2
Core Gas Inlet Temperature, °F	590.0
Core Gas Outlet Temperature, °F	1500.0
Comp./Gas-Turb. Efficiency, %	90.0
Total Gas Cycle Pressure Loss Ratio, %	12.0
Gas Volume Fraction in Core (Void), %	55.0
Gas Mass Flow Rate, kg _{gas} /hr	3.017 x 10 ⁶
Gas Superficial Velocity, m/sec	14.7
Gas Pressure Drop in Core, psi	98.0
<u>STEAM GENERATOR</u>	
Steam Generator Gas Inlet Temperature, °F	1452.0
Steam Generator Gas Outlet Temperature, °F	512.0
Gas Temperature at Pinch Point, °F	700.0
Pound Gas Required per Pound Steam Generated	0.8551
Steam Generator Outlet Temperature, °F	1000.0
Steam Generator Feed Water Temperature, °F	486.0

(continued)

Table S-II. SBR Design Specifications
(Coated Metallic Fuel-continued)

STEAM CYCLE

Superheated Steam Pressure/Temperature, psia/°F	2000/1000
N ^o of Resuperheater	0.0
N ^o of Feed Water Heaters	6.0
Cond. Pressure/Temperature, in. Hga/°F	2/101
Quality of Steam, %	15.0
Steam Flow Rate, kg/hr	3.528 x 10 ⁶
Pumping Requirement, MWe	24.0
Thermal Efficiency of Steam Cycle Alone, %	43.0
Net Power Generated by Steam Cycle, MWe	983.3
Steam Turbine/Pump Efficiency, %	85.0

FUEL

Fuel Particle Diameter, cm	0.17
Fuel Kernel Diameter (U ²³³ -Th ²³²), cm	0.14
Fuel Particle Total Coating Thickness, cm	0.0150
Pyrolytic Graphite Layer Thickness, cm	0.0070
Silicon Carbide Layer Thickness, cm	0.0030
Zirconium Carbide Layer Thickness, cm	0.0050
Maximum Fuel Temperature, °F	2000.0
Maximum Temperature Drop for Fuel Kernel, °F	94.0
Terminal Velocity of Fuel Particles, m/sec	9.3
Fuel Kernel Max. Volumetric Heat Source Strength, MW/m ³	1.217 x 10 ⁵
Fertile Mass Core/Blanket, kg	17,479/63,584
Fissile Mass, kg	3348.0
Specific Power	1.21
Enrichment, Inner Core/Outer Core, %	12.8/18.3
Conversion Ratio	1.17

efficiency. Features of this binary cycle are shown in Figures S-2 and 3 for reactor outlet temperatures of 1500°F and 1800°F, respectively. Figure S-4 shows a schematic of the reactor binary cycle. Inherent features of this cycle are:

- Exploitation of high temperature benefits become possible without necessitating higher temperature steam cycle technology. This is accomplished by simply passing the high temperature gas through the gas turbine first and then to the steam generator.
- Recuperators which are required for direct gas cycle are not needed in this design. The hot gas coming out of the turbine is cooled while producing superheated steam for the steam cycle. Gas leaving the steam generator is still hot, 500-600°F. It is compressed and sent back to the reactor. This gas cycle is very similar to what is now in HTGR's, except for a key component, an addition of a gas turbine. This addition and optimization of the whole cycle yields a significant improvement in overall efficiency.
- Because the gas cycle used in this design has a low efficiency, it matches in a natural way the gas turbine technology, i.e. small size and small MW rating, 100-250 MWe.
- The gas pressure drop of this gas/steam binary cycle is expected to decrease to about half of that characteristic of direct gas cycles, primarily because of eliminating the recuperator.
- Inlet temperature to the reactor would be lower than that associated with gas cycle.
- The complete elimination of the reheater.

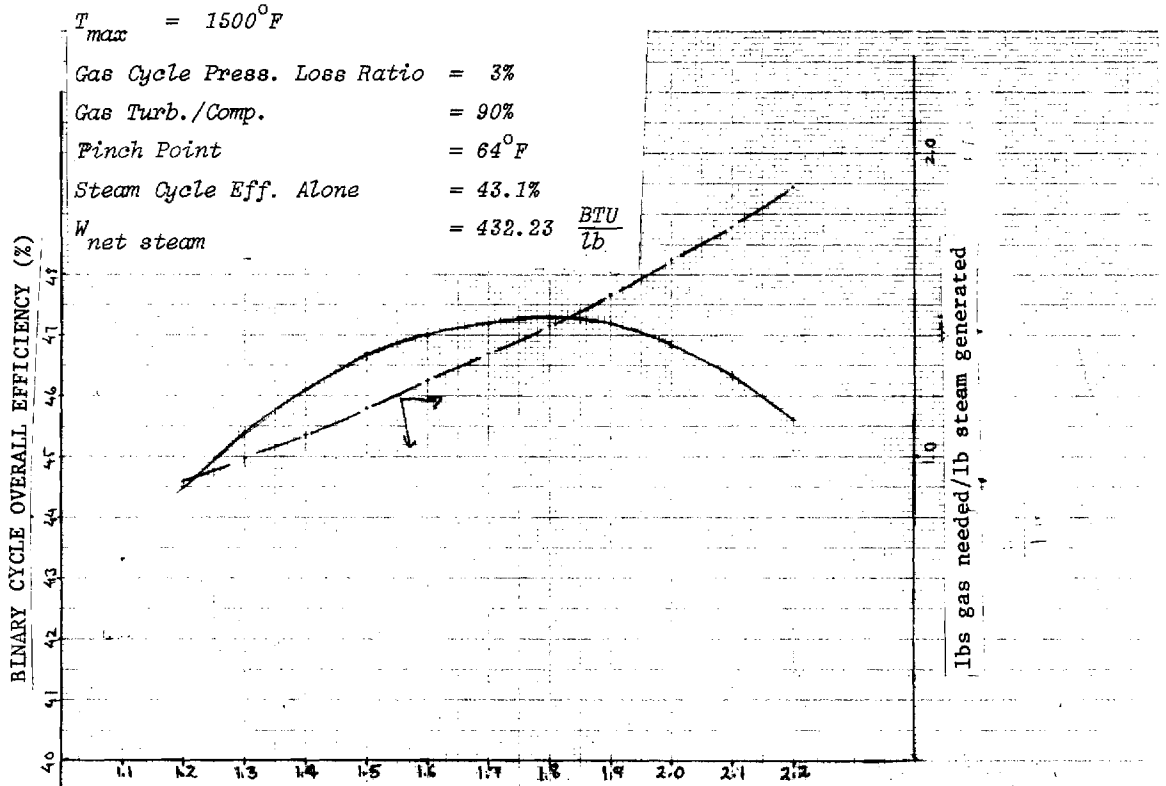
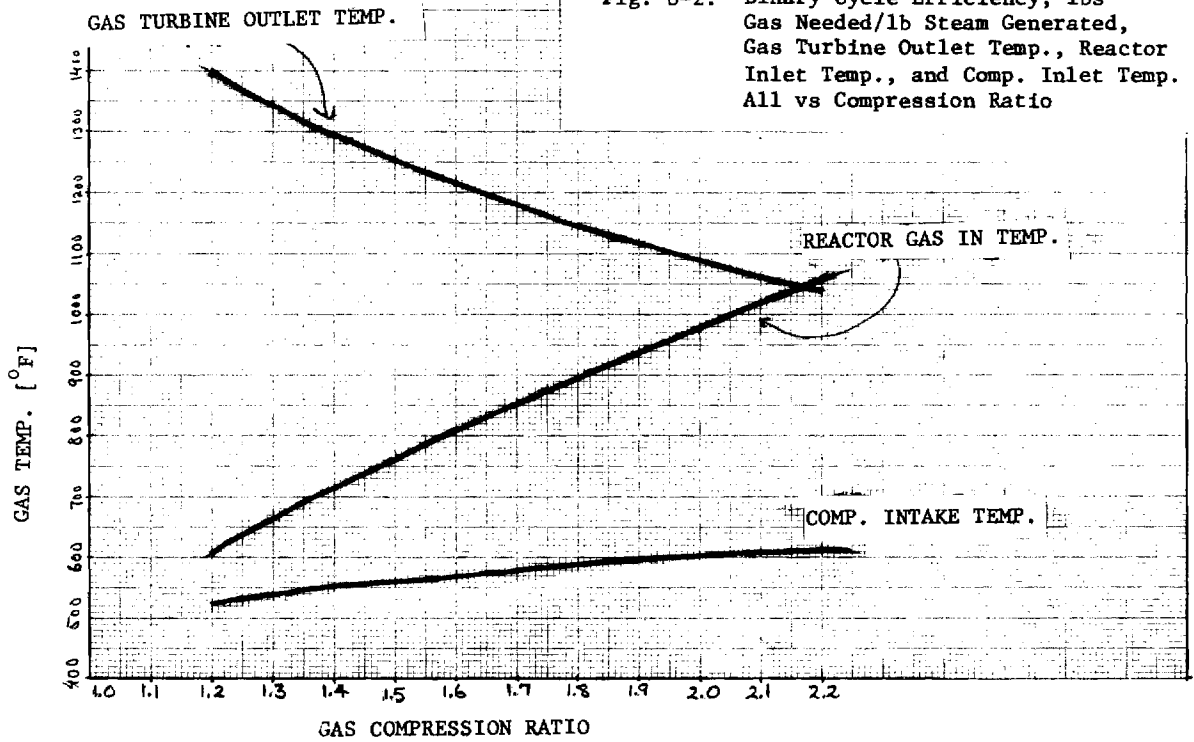


Fig. S-2. Binary Cycle Efficiency, lbs Gas Needed/lb Steam Generated, Gas Turbine Outlet Temp., Reactor Inlet Temp., and Comp. Inlet Temp. All vs Compression Ratio



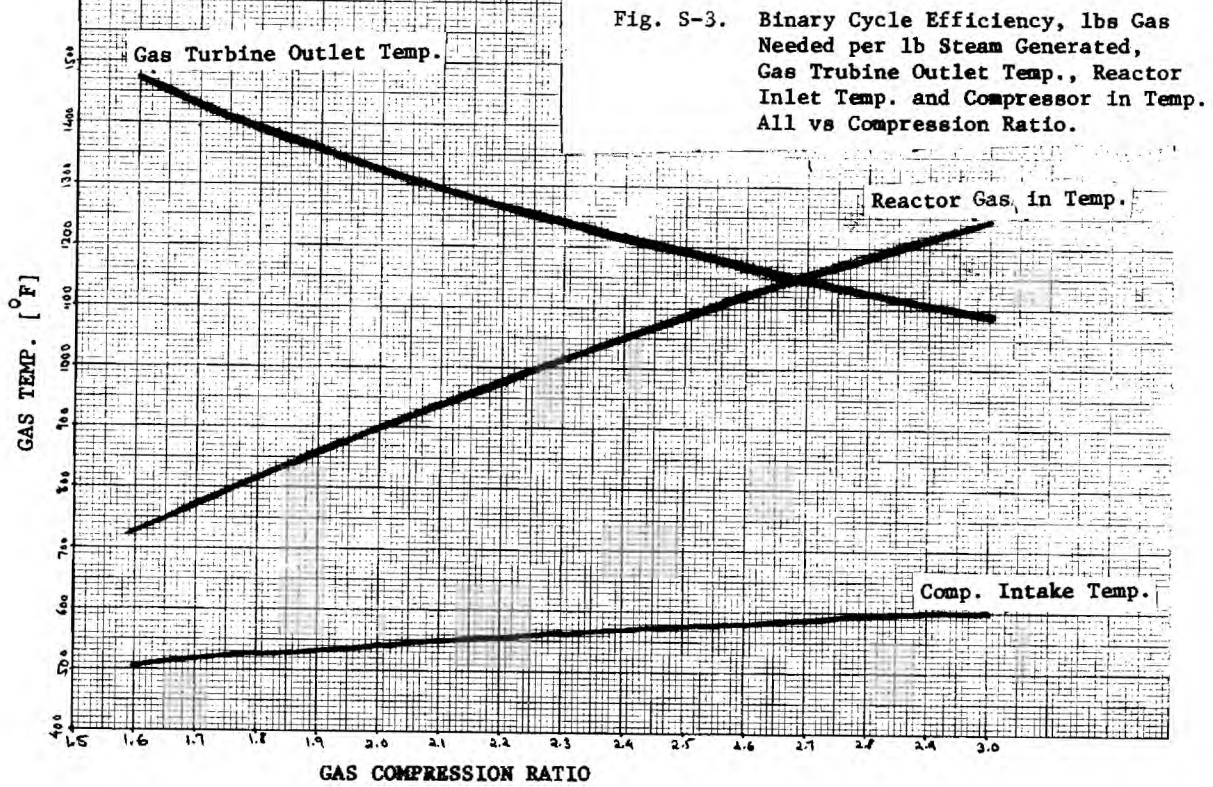
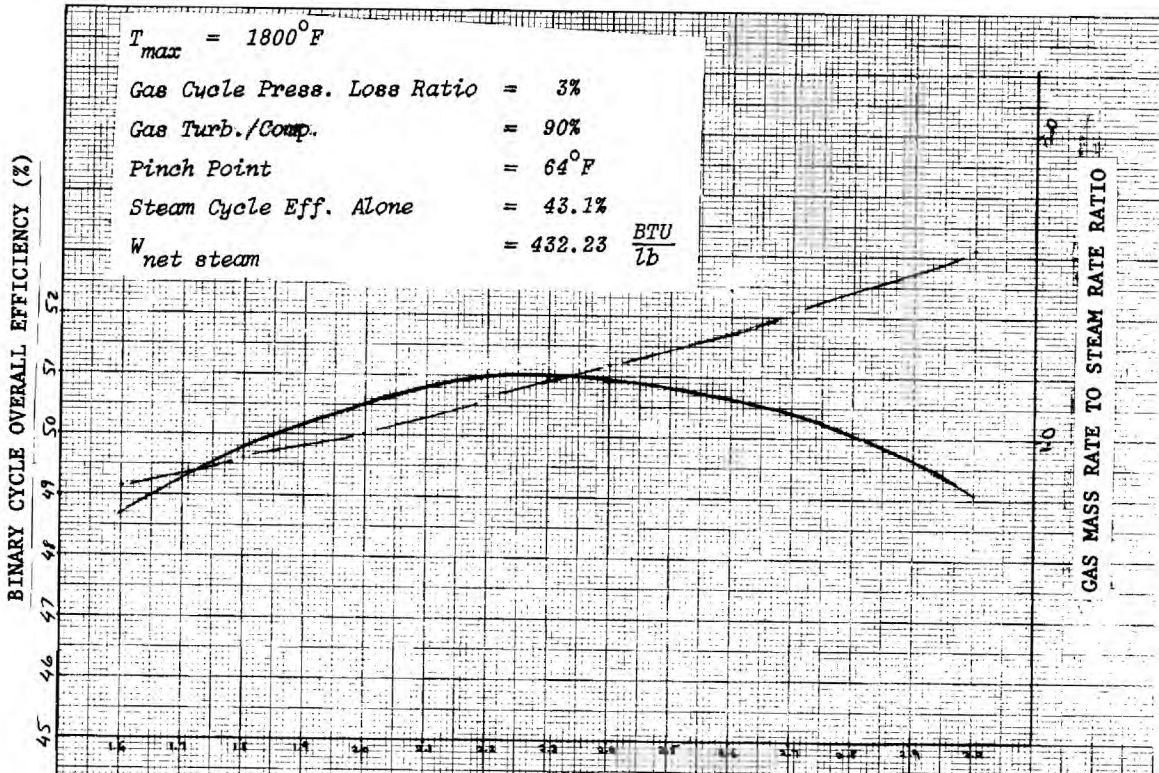


Fig. S-3. Binary Cycle Efficiency, lbs Gas Needed per lb Steam Generated, Gas Turbine Outlet Temp., Reactor Inlet Temp. and Compressor In Temp. All vs Compression Ratio.

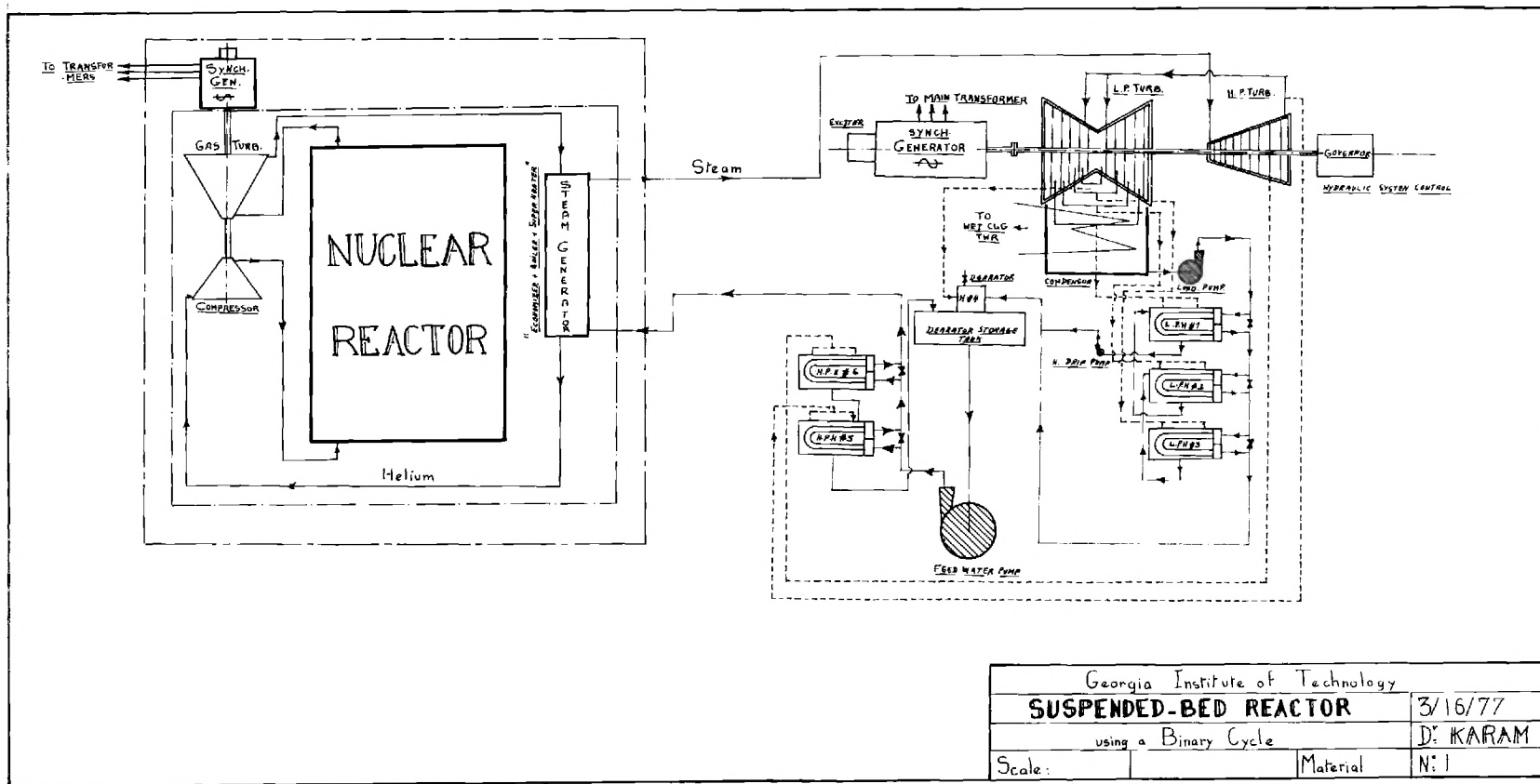


Figure S-4. Suspended-Bed Reactor Binary Cycle.

Research and Development Program

The first point that should be emphasized is that the Suspended-Bed Reactor concept is not really limited to any one type of fuel or coolant. For example, if the coated particle fuel should prove unsuitable in a suspended-bed operation due to breakage or erosion, it is quite possible to use coated particles fixed in a matrix of a material with high thermal conductivity shaped into disks with holes drilled through the disk for the passage of the coolant. The disks can be suspended in "guides" just like the coated particles. Thus, the fail-safe or nearly fail-safe features of the Suspended-Bed Reactor are not really tied to particles.

Nevertheless, if coated particles are to be used in a Suspended-Bed Reactor, it is necessary to experimentally determine the erosion rate of the outer layer under normal operating conditions, i.e. helium velocity and temperature and, later, irradiating condition. In addition to erosion, it is important to determine the breakage rate due to normal handling, i.e. fluidization and suspension of the particles in the core region. Another important factor is whether or not, at operating temperatures, the particles tend to stick to each other after long-term operation.

The pressure drop through the reactor is a very important design parameter which has important implications on performance and economics. This one parameter affects the breeding ratio, doubling time, overall thermodynamic efficiency and eventually the cost of electricity. It is, therefore, important to conduct an experimental program aimed at minimizing the pressure drop before any final fuel design is chosen. The state of the art of calculating pressure drops in fixed or fluidized beds is not accurate. Thus an experimental program for measuring the pressure drop as a function of particle

size and density at various coolant velocities is necessary.

Suspending fuel, whether coated particles or disks, in a core region is certainly possible, and there is no doubt whatsoever about its feasibility. But it needs to be demonstrated with the goal of assessing the ease with which reactors can be controlled.

A block diagram of the program envisioned for the SBR final design is shown in Figure S-5. The work heretofore concentrated on the thermodynamic and thermal hydraulic optimization under realistic engineering constraints. We have not exhausted, due to time limitations, the possibilities for optimum fuel design. Many possibilities exist whereby the fuel volume fraction and the power density would increase and, at the same time, the pressure drop would decrease. The benefits of such optimization translate directly into cheaper energy cost. The block diagram in Figure S-5 represents a scheme to optimize the condition for a self-sustaining energy source at the cheapest cost. Our analysis, which is based on considerations of physics and thermal hydraulics, indicates that a doubling time for the SBR as short as ten years or even shorter is very possible.

Engineering and Safety Constraints

Engineering and Safety Constraints

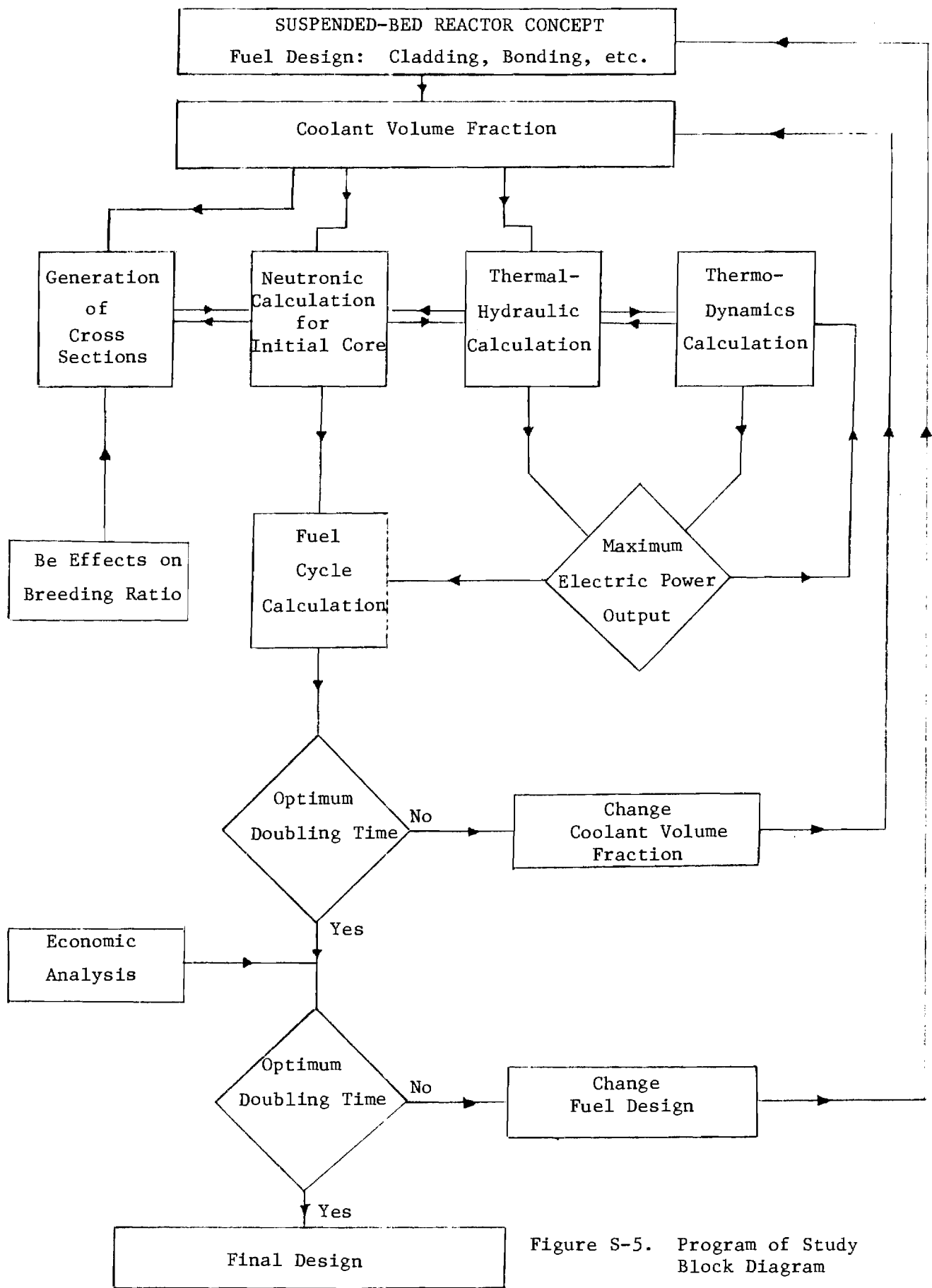


Figure S-5. Program of Study Block Diagram

I. INTRODUCTION

The Division of International Security Affairs, Energy Research and Development Administration (ERDA), held a meeting on August 18, 1976 at ERDA Headquarters to discuss the possibility of limiting proliferation by design specifications. Tentative design features circulated at the meeting by ISA for a reactor system that is nearly proliferation-proof were:

- A. No fuel element withdrawal during the life of the reactor.
- B. Subsequent to startup, no requirement for the addition of enriched fissile fuel for the life of the reactor.
- C. After an initial short "burn-in" period, fuel shall contain isotopic species which can only be removed by high technology such as isotope separation devices which can not be handled without a massive protective shielding.
- D. Reactor shall be refueled with fertile material only, either periodically or continuously.
- E. Any reprocessing shall be accomplished inside the biological shield only. No fuel shall be removed outside the biological shield during normal operations. Only fission products shall be permitted outside biological shield in suitable shielded containers.
- F. Core shall contain low critical mass of special nuclear material (SNM). If any fuel is diverted, reactor will be shutdown.

G. Reactor shall not be designed for "breeder" operation which accumulates excess SNM. Performance shall be based upon "sustainer" operation, i.e., breeding ratio being approximately one. If any of the bred fuel is diverted the reactor will be shutdown.

H. High thermodynamic efficiency in the production of electricity.

Two main reactor concepts were discussed: the gaseous fuel reactor and the fluidized-bed reactor. Interest in both concepts dates back to the early fifties. A review of the early considerations of these concepts is found in Ref. 1. Currently the National Aeronautics and Space Administration is actively supporting the development of the gaseous core concept. Features of this concept were discussed at the meeting by Dr. Karlheinz Thom of NASA.

The fluidized-bed reactor concept which was totally different from previously considered concepts⁽²⁻⁶⁾ was discussed by R. A. Karam of the Georgia Institute of Technology. The initial concept as presented on August 18, 1976 comprised the following: pyrolytic carbon coated ²³³(U - Th)C₂ particles are fluidized and cooled by helium in a cluster of pressurized tubes. The tubes are arranged as shown in Fig. I-1. The upward flow of helium fluidizes the coated particles. As the flow rate increases the bed of particles are lifted upward to the core section. The particles are restrained at the upper end of the core by a suitable screen. The overall particle density in the core is just enough for criticality condition. Should the helium flow cease, the bed in the core section will collapse, and the particles will flow

downward into the flaired section where the increased physical spacings among the tubes brings about a safe shutdown. By immersing the flaired section of the tubes in a pool of water, removal of decay heat becomes possible and this eliminates the need for emergency core cooling system. The inherent advantages of this concept are:

- No pressure vessel is required.
- No control rods are required. Costly drive mechanisms and uneven flux distortion are eliminated.
- Truly fail-safe operation with respect to decay heat removal.
- No clad for the fuel is required. This reduces the waste-disposal problem.
- No emergency core cooling is needed.
- On-line fueling operation. This eliminates costly shutdown.
- High temperature operation resulting in two distinct advantages:
(1) high thermodynamic efficiency and (2) process heat for making steel, methane from coal, etc.
- High burnup, 100,000 MWD/ton or more.
- Coated particles retain fission products effectively.
- Breeding ratio can be tailored to be close to 1.0 if desired.
- Helium gas is safe, inert coolant.

Based upon the above considerations ERDA's ISA awarded Georgia Tech a 6 man-months contract to perform a preliminary system design and analysis of a stationary nuclear electric power station which could meet the tentative specifications, cited above, for non-proliferating power reactors.

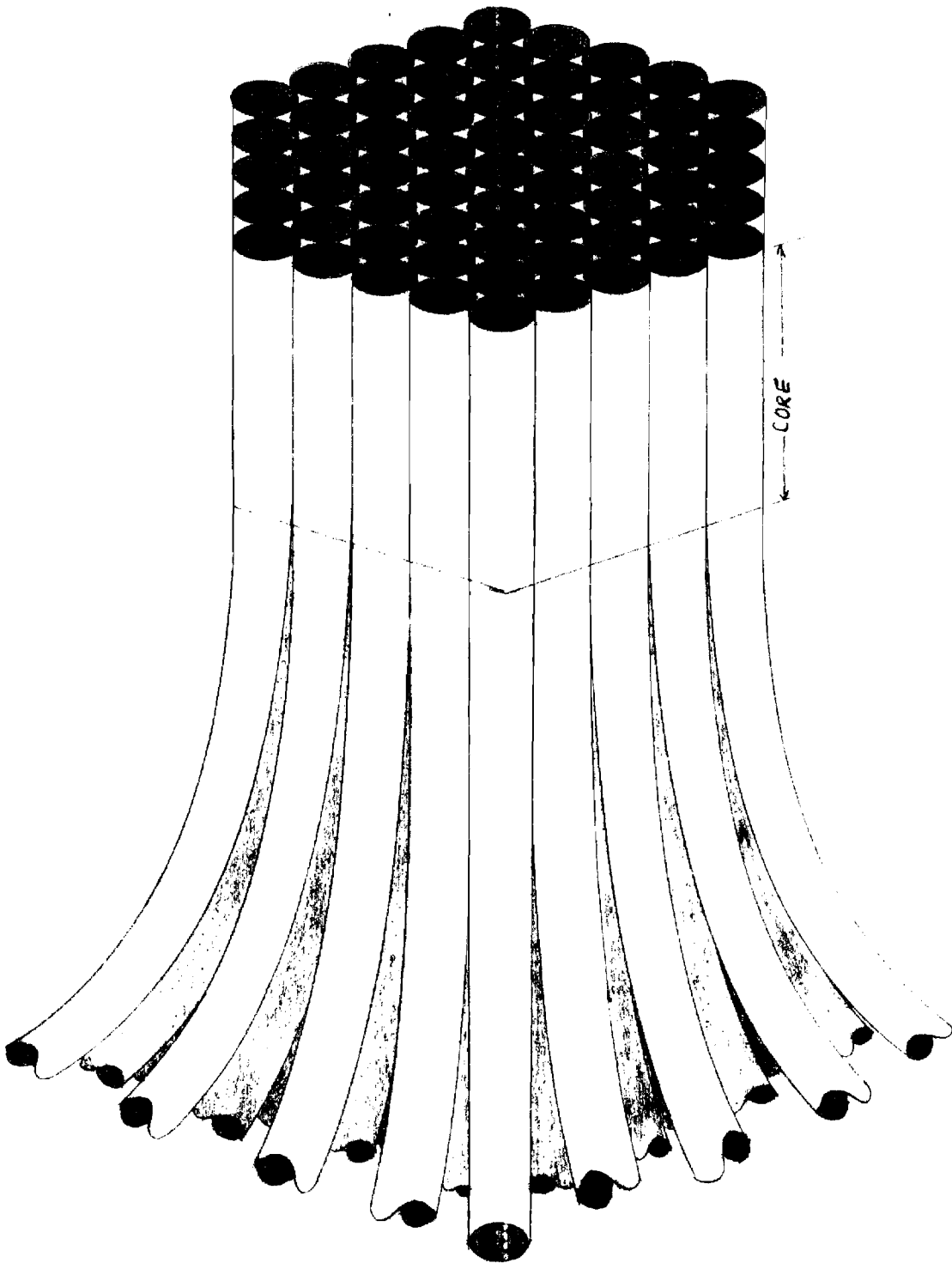


Fig. I-1. Arrangement of Tubes for Suspended-Bed Reactor

This report contains the preliminary design and consists of the following chapters:

- I. Introduction
- II. Suspended-Bed Reactor System Design
 1. Introduction
 2. Thermal hydraulics for fluidized and fixed bed regimes
 3. Thermodynamic optimization study of gas cooled reactors
 4. Suspended-bed reactor fuel design
 5. Physics calculation
 6. Selection of pipe material and sizes
 7. Decay heat removal
 8. Considerations leading to SBR parameters
 9. The preliminary design of the suspended bed reactor
- III. Recommend Research and Development Program
- Appendix A. General Considerations of Natural Uranium on Thorium Reserves and Implication on Nuclear Power Growth
 1. Uranium reserves
 2. The thorium resource
 3. Energy from assured reserves
 4. Electrical energy needs and nuclear power growth
- Appendix B. Thorium Based Reactors
 1. General background
 2. Physics parameters
 - 2.1. Breeding
 - 2.2. Doubling time and specific power
 - 2.3. Breeding strategy
 - 2.3.1 Metallic Pu-Th Interim Breeders

- 2.4. Coolant void coefficient
 - 2.5. Doppler coefficient
 - 2.6. Protactinium Production
 - 2.7. Uranium -232 production
 - 2.8. Transuranium elements production
 - 2.9. Delayed neutron fraction
- Appendix C. Heat Conduction Through Successive Spherical Shell
- Appendix D. Computer Program
- Appendix E. Gas-Steam Binary Cycle

II. SUSPENDED-BED REACTOR CONCEPT

1. Introduction

When a fluid stream, either gas or liquid, is passed through a bed of granular material and the velocity of the stream is gradually increased, a point is reached such that the drag force resisting the flow of the fluid is equal to the weight of the particles in the bed. Any further increase in the fluid velocity would lead to expansion of the bed, i.e. the particles are separated resulting in a greater area for the passage of the fluid; this limits the pressure drop across the bed. This condition corresponds to the limit of stability of a packed (fixed) bed and marks the transition to the fluidized or suspended state. If the fluid velocity is held constant at this point, the force of the fluid balances the weight of the particles, and the contact among particles tends to cease. The surface of the bed adjusts itself just like a liquid, and the particles will remain suspended as long as the fluid flows at that velocity.

As the fluid velocity is increased still further, an intensive mixing of the bed begins and, finally on increasing the gas velocity still more, carry-over of particles from the container occurs. A fluidized condition exists for only a specific range of fluid velocities. Below this range, the bed is stationary or fixed, and above it the particles would be transported out of the bed. If a screen is placed at the top of the bed to prevent the flow of particles out of the bed, a fixed-bed condition would prevail again. The drag force under these conditions is much higher than the weight of the bed; consequently all the particles would be held up against the screen while

the fluid is allowed through. This is the basis of the suspended-bed reactor concept.

In the fluidized regime, the bed is expanded to a volume greater than that of the fixed bed, and the particles are in continuous oscillation, colliding with one another and moving from point to point within the bed. The macroscopic properties of the bed, however, are characteristic of a liquid. Buoyancy, hydrostatic pressure, and absence of resistance to shear stresses are a few examples. The overall flow pattern depends on the fluid medium and the size, shape and density of the particles being fluidized. Generally there are two distinct types of flow patterns: particulate and aggregative. Particulate fluidization refers to the bed expansion under uniform distribution. Particulate fluidization occurs with liquid-solid systems, and gas-solid systems when the particles are very fine. Aggregative fluidization is regarded as an excess of fluid passing through the bed in the form of bubbles, giving rise to essentially a two-phase system. Aggregative fluidization occurs with gas-solid systems and sometimes with liquid-solid systems when the solids are of high density.

Important parameters frequently encountered in studying fixed/fluidized beds are the pressure drop through the bed (ΔP), the bed height (H), the superficial velocity, terminal velocity, and porosity of the bed. The superficial velocity is defined as the velocity that the fluid would have if there were no particles, i.e. the velocity of fluid before entering the bed. The terminal velocity is the velocity of free falling particles in the medium. The porosity or void fraction is regarded as the ratio of the volume of fluid to the total volume of the bed (fluid and particles).

"A fluid surface" characterizes the fluidized-bed in the fluidized region.

At porosities higher than 0,8, however, the high degree of turbulence may cause large fluctuations at the top of the bed that a particular level can no longer be defined. As a result of increasing the superficial velocity even further to the value of terminal velocity, the transition from fluidized-bed to vertical slurry occurs. At this stage the particles are carried over from the bed by the fluid medium, unless the particles are stopped by a restricting screen. In this case, the particles are stacked up to the top of the bed and form a suspended-bed.

Coated particles about 2 mm in diameter are used as the fuel. The coatings consist of three layers: (1) low density prolytic graphite, 70 μ thick, (2) silicon carbide pressure vessel, 30 μ thick, and (3) ZrC layer, 50 μ thick, to protect the pressure vessel from moisture and oxygen. The fuel kernel can be either uranium-thorium dicarbide or metal.

The coated particles are suspended by helium gas (coolant) in a cluster of pressurized tubes. The upward flow of helium fluidizes the coated particles. As the flow rate increases the bed of particles is lifted upward to the core section. The particles are restrained at the upper end of the core by a suitable screen. The overall particle density in the core is just enough for criticality condition. Should the helium flow cease, the bed in the core section will collapse, and the particles will flow downward into the section where the increased physical spacings among the tubes brings about a safe shutdown. By immersing this section of the tubes in a pool of water or a suitable heat sink, removal of decay heat becomes possible. This eliminates the need for emergency core cooling systems.

This chapter contains the following sections:

1. Introduction
2. Thermal Hydraulics for Fluidized- and Fixed-Bed Regimes
3. Thermodynamic Optimization Study for Gas Cooled Reactors
4. Suspended-Bed Reactor Fuel Design
5. Physics Calculation Including Core and Blanket Specifications
6. Selection of Pipe Material and Sizes
7. Decay Heat Removal
8. Considerations Leading to SBR Parameters
9. The Preliminary Final Design of the Suspended-Bed Reactor

2. Thermal Hydraulics for Fluidized- and Fixed-Bed Regimes

2.1 Heat Transport

The amount of heat, $Q(Z)$, removed by the helium gas as it passes through the bed to a point Z along the axial height is

$$Q(Z) = \dot{m} C_p (T_g(Z) - T_{gin}) \quad (1)$$

where \dot{m} = mass transfer rate = $G A_b$,

G = mass flow rate per unit area,

A_b = area of the bed,

C_p = heat capacity at constant pressure,

$T_g(Z)$ = temperature of the gas as a function of the axial distance, Z , and

T_{gin} = inlet temperature of the gas.

The quantity $Q(Z)$ is also the heat generated by the fuel in the bed at Z , i.e.

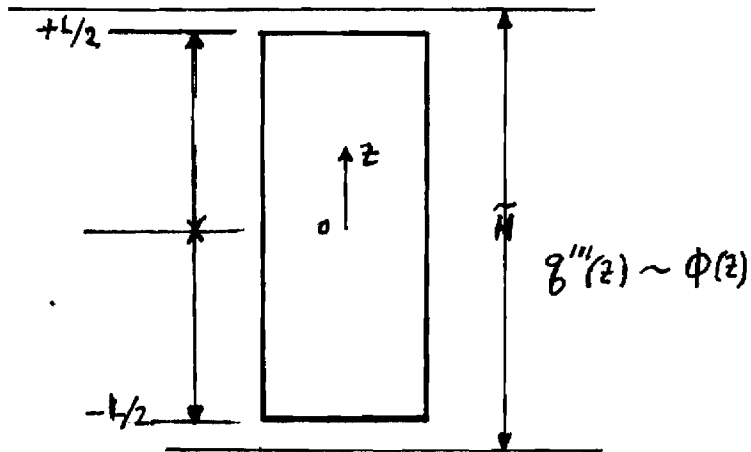
$$Q(Z) = \int_{-L/2}^Z q'''(Z) dV_f \quad (2)$$

where $q'''(Z) = q_c''' \cos\left(\frac{\pi Z}{\tilde{H}}\right)$ = volumetric heat source as a function of Z .

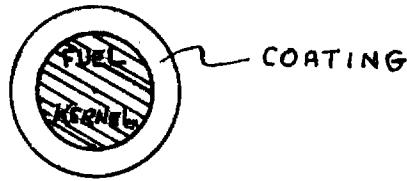
q_c''' = volumetric thermal heat source assumed constant radially,

\tilde{H} = extrapolated height of core bed, at which neutron flux goes to zero,

V_f = volume of fuel kernels per unit length of bed (see sketches a and b)



- a. Sketch illustrating relationships of $Q(z)$, $q'''(z)$ and bed height



- b. Fuel kernel and fuel particle

Fig. II-2-1. Sketches illustrating (a) bed height; $Q(z)$, $q'''(z)$ and (b) fuel kernel.

Define ϵ as the void fraction in the bed; it may also be expressed as

$$\epsilon = \frac{\text{volume of gas}}{\text{volume of bed}} = \frac{V_g}{V_b} = \frac{V_g}{V_p + V_g} \quad (3)$$

where V_p and V_g are the volume of the particles and the gas respectively.

The volume of the particles may also be expressed as:

$$V_p = (1-\epsilon)V_b \quad (4)$$

since

$$v_f/v_p = \left(\frac{D_f}{D_p}\right)^3 \quad (5)$$

where D_f and D_p are the diameters of the fuel kernel and particle respectively, then

$$v_f = (1-\epsilon) \left(\frac{D_f}{D_p}\right)^3 v_b \quad (6)$$

or

$$dv_f = (1-\epsilon) \left(\frac{D_f}{D_p}\right)^3 A_b dz \quad (7)$$

Consequently,

$$\begin{aligned} Q(Z) &= \int_{-L/2}^Z q_c''' \cos\left(\frac{\pi Z}{\tilde{H}}\right) (1-\epsilon) \left(\frac{D_f}{D_p}\right)^3 A_b dz \\ &= (1-\epsilon) \left(\frac{D_f}{D_p}\right)^3 A_b q_c''' \frac{\tilde{H}}{\pi} \left\{ \sin \frac{\pi Z}{\tilde{H}} + \sin \frac{\pi L}{2\tilde{H}} \right\} \end{aligned} \quad (8)$$

Equating (1) and (8), yields

$$T_g(Z) = T_{gin} + \frac{1-\epsilon}{G C_p} \left(\frac{D_f}{D_p}\right)^3 q_c''' \frac{\tilde{H}}{\pi} \left[\sin\left(\frac{\pi Z}{\tilde{H}}\right) + \sin \frac{\pi L}{2\tilde{H}} \right] \quad (9)$$

At $Z = L/2$

$$T_g(\text{out}) = T_{gin} + \frac{1-\epsilon}{G C_p} \left(\frac{D_f}{D_p}\right)^3 q_c''' \frac{\tilde{H}}{\pi} \left(2 \sin \frac{\pi L}{2\tilde{H}} \right) \quad (10)$$

Also

$$\Delta T_{p \rightarrow g}(Z) = (T_p - T_g)_c \cos\left(\frac{\pi Z}{\tilde{H}}\right) \quad (11)$$

where $\Delta T_{p \rightarrow g}(Z)$ is the difference in temperature between the particle surface and the gas at point Z and $(T_p - T_g)_c$ is the difference at the bed center.

The heat transfer equation relating T_p , T_g and q_c''' is

$$q_c''' dV_f = h(T_p - T_g)_c dA_p \quad (12)$$

where h = heat transfer coefficient for the film between the gas and particle surface

$$V_p = N \frac{\pi}{6} D_p^3, \quad N \text{ is number of particles}$$

$$A_p = N \pi D_p^2,$$

$$\text{from which } V_p = A_p \frac{D_p}{6}. \quad (13)$$

substituting (13) into (4) one gets

$$A_p = \frac{6(1-\epsilon) V_b}{D_p} \quad (14)$$

$$\text{and thus } dA_p = \frac{6(1-\epsilon)}{D_p} A_b dz. \quad (15)$$

Combining (15) and (7) into (12) yields

$$\left(T_p - T_g\right)_c = q_c''' \left(\frac{D_f}{D_p}\right)^3 \frac{D_p}{6h} \quad (16)$$

Substituting (16) into (11) yields

$$\Delta T_{p \rightarrow g}(Z) = q_c''' \left(\frac{D_f}{D_p}\right)^3 \frac{D_p}{6h} \cos\left(\frac{\pi Z}{\tilde{H}}\right) \quad (17)$$

or equivalently,

$$T_p(Z) = T_g(Z) + q_c''' \left(\frac{D_f}{D_p}\right)^3 \frac{D_p}{6h} \cos\left(\frac{\pi Z}{\tilde{H}}\right) \quad (18)$$

Replacing $T_g(Z)$ by its equivalent from (9) into (18) gives

$$\begin{aligned} T_p(Z) = T_{gin} + \frac{1-\varepsilon}{G C_p} \left(\frac{D_f}{D_p}\right)^3 q_c''' \frac{\tilde{H}}{\pi} \left[\sin \frac{\pi Z}{\tilde{H}} + \sin\left(\frac{\pi L}{2\tilde{H}}\right) \right] \\ + \frac{D_p}{6h} \left(\frac{D_f}{D_p}\right)^3 q_c''' \cos\left(\frac{\pi Z}{\tilde{H}}\right) \end{aligned} \quad (19)$$

The maximum surface temperature of the particles is obtained by differentiating (19) with respect to Z and equating the result to zero. The expression is

$$Z_{(T_p)_{\max}} = \frac{\tilde{H}}{\pi} \tan^{-1} \left[\frac{\tilde{H}}{\frac{\pi G C_p D_p}{(1-\varepsilon) 6h}} \right] \quad (20)$$

The amount of heat, q , conducted through a shell around the spherical fuel kernel can be shown (see Appendix C) as

$$q = A_f \left[\frac{k_c}{\frac{D_f}{2} \left(1 - \frac{D_f}{D_p} \right)} \right] (T_s - T_p) \quad (21)$$

where A_f = surface of the fuel kernel
 k_c = thermal conductivity of shell
 T_s = temperature at the surface of fuel kernel
 T_p = temperature at outer surface of shell.

For three layer shell Equation (21) becomes (see Appendix C)

$$q = A_f \left[\frac{k_{c1}}{\frac{D_f}{2} \left(1 - \frac{D_f}{D_{c1}} \right)} \right] (T_s - T_{c1})$$

$$q = A_{c1} \left[\frac{k_{c2}}{\frac{D_{c1}}{2} \left(1 - \frac{D_{c1}}{D_{c2}} \right)} \right] (T_{c1} - T_{c2})$$

$$q = A_p \left[\frac{k_{c3}}{\frac{D_p}{2} \left(1 - \frac{D_p}{D_{c2}} \right)} \right] (T_{c2} - T_{c1})$$

where k_{c1} , k_{c2} and k_{c2} are the thermal conductivity of the inner, middle and outer shells respectively. The amount of heat conducted at a point Z is the volumetric heat source at that point times the volume of the fuel particle, or

$$q(Z) = q'''(Z) V_f = \frac{\pi}{6} D_f^3 q'''(Z) \quad (22)$$

Also, the quantity $(T_s - T_p)$ at z is related to $(T_s - T_p)_c$, the difference at the center line, times $\cos \frac{\pi Z}{\tilde{H}}$.

At $z = 0$

$$q(0) = \frac{\pi}{6} D_f^3 q_c''' = \pi D_f^2 \left[\frac{k_c}{\frac{D_f}{2} \left(1 - \frac{D_f}{D_p}\right)} \right] (T_s - T_p) \quad (23)$$

From which

$$(T_s - T_p)_c = \frac{D_f q_c'''}{6} \left[\frac{D_f \left(1 - \frac{D_f}{D_p}\right)}{2 k_c} \right] \quad (24)$$

With this relation, $T_s(z)$ becomes

$$T_s(z) = T_p(z) + \frac{D_f}{6} q_c''' \left[\frac{D_f \left(1 - \frac{D_f}{D_p}\right)}{2 k_c} \right] \cos \left(\frac{\pi Z}{\tilde{H}} \right) \quad (25)$$

where $T_p(z)$ is given in Eq. (19). With these equations the maximum fuel kernel surface temperature is found at

$$Z_{(T_s)_{\max}} = \frac{\tilde{H}}{\pi} \tan^{-1} \left[\frac{\tilde{H}}{\frac{\pi G C_p}{1-\epsilon} \left\{ \frac{D_p}{6h} + \frac{D_f}{6} \frac{1}{\left(\frac{D_f}{D_p}\right)^3} \left[\frac{D_f \left(1 - \frac{D_f}{D_p}\right)}{2k_c} \right] \right\}} \right] \quad (26)$$

Similarly the maximum fuel center line temperature, T_m occurs at

$$Z_{(T_m)_{\max}} = \frac{\tilde{H}}{\pi} \tan^{-1} \left[\frac{\tilde{H}}{\frac{\pi G C_p}{(1-\epsilon)} \left\{ \frac{D_p}{6h} + \frac{D_f}{6} \frac{1}{\left(\frac{D_f}{D_p}\right)^3} \left[\frac{D_f \left(1 - \frac{D_f}{D_p} + \frac{D_f}{4k_f}\right)}{2k_c} \right] \right\}} \right] \quad (27)$$

2.2 Fluidized and Fixed-Bed Regimes

2.2.1 Fluidized Bed

In a fluidized bed the optimum Reynolds number at which the heat transfer coefficient is maximum is Ref. (7).

$$Re_{opt} = \frac{Ar}{18 + 5.22\sqrt{Ar}} \quad (28)$$

where $Ar = g \cdot \frac{D_p^3}{\nu^2} \cdot \frac{\rho_p - \rho_g}{\rho_g}$ Archimedes Number

$$g = 981 \left[\frac{\text{cm}}{\text{sec}^2} \right] \quad \text{gravity acceleration}$$

$$\nu = \frac{\mu_g}{\rho_g} \left[\frac{\text{cm}^2}{\text{sec}} \right] \quad \text{dynamic viscosity of the gas}$$

$$\mu_g \equiv \left[\frac{\text{g}_r}{\text{cm sec}} \right] \quad \text{viscosity of the gas}$$

$$\rho_g \equiv \left[\frac{\text{g}_r}{\text{cm}^3} \right] \quad \text{density of the gas}$$

$$\rho_p \equiv \left[\frac{\text{g}_r}{\text{cm}^3} \right] \quad \text{density of the particles}$$

$$D_p \equiv \left[\text{cm} \right] \quad \text{diameter of the particle}$$

The quantities, ρ_g and μ_g , are valuated at the mean temperature of the gas in the reactor. The inlet gas temperature is normally set; the outlet temperature is calculated so that the maximum tolerable fuel temperature is not exceeded. The maximum tolerable fuel temperature for

the coated dicarbide particles was set at 2400^oF, the same value as used in the HTGR technology. In practice the calculation of the T_{g out} was accomplished by an iterative procedure. An initial guess on the value of T_g was made, then it was calculated. The procedure was repeated under the constraint that nowhere along the bed height the maximum temperature for the fuel is exceeded.

The mass flow velocity is related to R_{e opt}, from Eq. (28), by the relation

$$G_{opt} = \frac{R_{e (opt)} \mu_g}{D_p} \frac{g_r}{\text{cm}^2 \cdot \text{sec}} \quad (29)$$

and

$$U_{opt} = \frac{G_{opt}}{\rho_g \times 100} \left(\frac{\text{m}}{\text{sec}} \right) \quad (30)$$

where G = mass flow rate per unit area

and U = gas superficial velocity, i.e. velocity fluid would have if there were no particles in bed.

The dependence of the void fraction on (Re)_{opt} is given by the relation⁽⁸⁾

$$\epsilon = \left[\frac{18 R_{e (opt)} + .36 R_{e opt}^2}{A_r} \right]^{0.21} \quad (31)$$

The appropriate heat transfer coefficient for the gas film is given by the Chu equation⁽⁹⁾

$$h = 5.7 \left(\frac{1}{P_r} \right)^{2/3} \times \left(\frac{R_{e opt}}{1-\epsilon} \right)^{-0.78} \times C_p \times G_{opt} \left[\frac{\text{watt}}{\text{cm}^2 \cdot \text{o}_F} \right] \text{ if } \frac{R_{e opt}}{1-\epsilon} < 30 \quad (32)$$

and

$$h = 1.77 \left(\frac{1}{P_r} \right)^{2/3} \times \left(\frac{Re_{opt}}{1-\epsilon} \right)^{-0.44} \times C_p \times G_{opt} \left[\frac{\text{watt}}{\text{cm}^2 \cdot \text{°F}} \right] \text{ if } \frac{Re_{opt}}{1-\epsilon} > 30 \quad (33)$$

where $P_r = \frac{C_p \mu_g}{k_g}$ Prandtl No ≈ 0.67

Pressure drop for the fluid is calculated by (10)

$$\Delta P = (\rho_p - \rho_g) (1-\epsilon) \times H \times g \times (14.22/9810) \text{ psi} \quad (34)$$

2.2.2 Fixed Beds

In fixed beds the void fraction, ϵ , and the gas velocity can be specified. The gas density and viscosity are averaged over the gas temperature in the reactor bed. The heat transfer coefficient is obtained by (33) and (34) with a fixed void fraction. The pressure drop for the fixed bed is: (11,12)

$$\Delta P = C \frac{H \times 100}{D_p} \left[U^2 \times \frac{\rho_g}{2g} \right] \left[\frac{1-\epsilon}{\epsilon^3} \right] \left(\frac{1.41}{100} \right) \text{ psi}$$

$C \equiv \text{constant} \sim (\text{Ref. 7}).$

A computer program has been written incorporating all these equations. For a given gas inlet temperature, and for fixed bed and void fraction, the code calculates the power density, the gas outlet temperature under the constraint that the maximum fuel temperature does not exceed a preset value, the gas velocity and the pressure drop. The size of the particle,

the coating thickness up to three layers, and bed-height are input parameters. Appendix D list the code which was written for the CDC CYBER-74 and a sample output is included.

3. Thermodynamic Optimization Study for Gas Cooled Reactors

The helium cooled Suspended-Bed Reactor has the potential of reaching high gas outlet temperatures, perhaps 1800^oF or higher. Currently the HTGR's of General Atomics operate at about 1500^oF. The AVR reactor in Germany reached helium exit temperature of 1740^oF.⁽¹³⁾ Apparently, the HTGR's could also achieve helium exit temperature of 1800^oF with a slight decrease in the power density.⁽¹⁴⁾ The main advantages of high temperature operation are: (1) significant improvement in the thermodynamic efficiency and (2) availability of high temperature process heat heretofore available only from fossil fuel. In this section we will review: (1) optimized direct gas-cycle and (2) binary cycle using both gas and steam.

The direct gas cycle has recently been reviewed by Fortescue and Quade⁽⁸¹⁾ for possible application in HTGR's. The primary interest in developing the gas cycle is to more fully exploit the high temperature potential. Additional benefits, cited by Fortescue and Quade are:

- (1) Gas turbines would eliminate the need for a high-temperature-input heat exchanger (steam generator).
- (2) Gas turbines would save on capital cost for equipment that would otherwise be needed for water treatment, feed water heating, and primary loop gas circulation.
- (3) Gas turbines would greatly facilitate dry cooling due to the high mean temperature of the gas turbine reject heat. This same feature can be applied in a supplementary waste heat vapor expansion cycle, using isobutane, to increase overall efficiency to greater than 50%.
- (4) Gas turbine would effect total plant simplification and consequent

capital and operational cost reduction.

Currently HTGR's gas outlet temperature is about 1400-1500^oF while the steam temperature is limited to 950-1000^oF because of design and economic considerations set by the technology of steam plants. The temperature differential between reactor gas outlet and steam is high, but more importantly, exploitation of higher temperatures which are quite easily attainable in HTGR's, can not be effectively used with current steam generator technology.

3.1 Gas-Cycle Studies

The helium gas-cycle efficiency was calculated as a function of compression ratio, the compressor's outlet to inlet pressure, and recuperator effectiveness. Details of the equations used in the calculations are given in Appendix E. The results are shown in Fig. II-3-1. Specific mass flow rates, relative exhaust volume as a function of compression ratio, and the T-S diagram are also shown. These results were obtained with a single stage compression, no intercooling, with top and bottom temperatures fixed at 1500^oF and 105^oF respectively.

The results in Fig. II-3-1 clearly show that the recuperator effectiveness plays an important role in improving the overall efficiency of the gas turbine. Using the practical value for recuperator effectiveness of 0.8 and a compression ratio of 2.5, with other conditions as specified in Fig. II-3-1, we find the optimum gas-cycle efficiency to be 37%. HTGR's steam cycle efficiency is about 40%; consequently, based on efficiency alone, direct cycle is not better.

A two stage compression with intercooling was also used. The results and appropriate conditions are shown in Fig. II-3-2. It is seen that the efficiency is hardly changed. These results are also in close agreement with those reported in Ref. (14).

Figure II-3-3 shows gas cycle efficiency as a function of compression ratio for several gas temperatures and recuperator effectiveness. An increase in recuperator effectiveness of 5% would increase cycle efficiency by about 2% at a given temperature. Also, at a given recuperator effectiveness, an increase in gas outlet temperature of 200^oF would increase cycle efficiency by about 2%.

It should be noted that a direct gas cycle for HTGR's, optimized as indicated in Fig. II-3-1, would increase the inlet gas temperature to the reactor by about 200-350^oF over current designs, i.e., from 650^oF to 950^oF. This would decrease the thermal power density which is already low. Improving the efficiency to about 50% by supplementary waste heat vapor expansion cycle, using isobutane, is certainly possible, but there is no experience with this technology and the advantages of simplicity, dry cooling, and compactness of the overall plant would be compromised. Additionally, isobutane is highly flammable material. An alternative to the binary cycle proposed by Fortescue and Quade⁽¹⁴⁾ which uses optimum gas cycle efficiency and low efficiency vapor expansion cycle, is a binary cycle which uses low efficiency gas cycle and optimum efficiency steam cycle. This not only would solve the high temperatures limitations of present HTGR's steam cycles but also would solve the problem of size limitations of gas turbine technology.

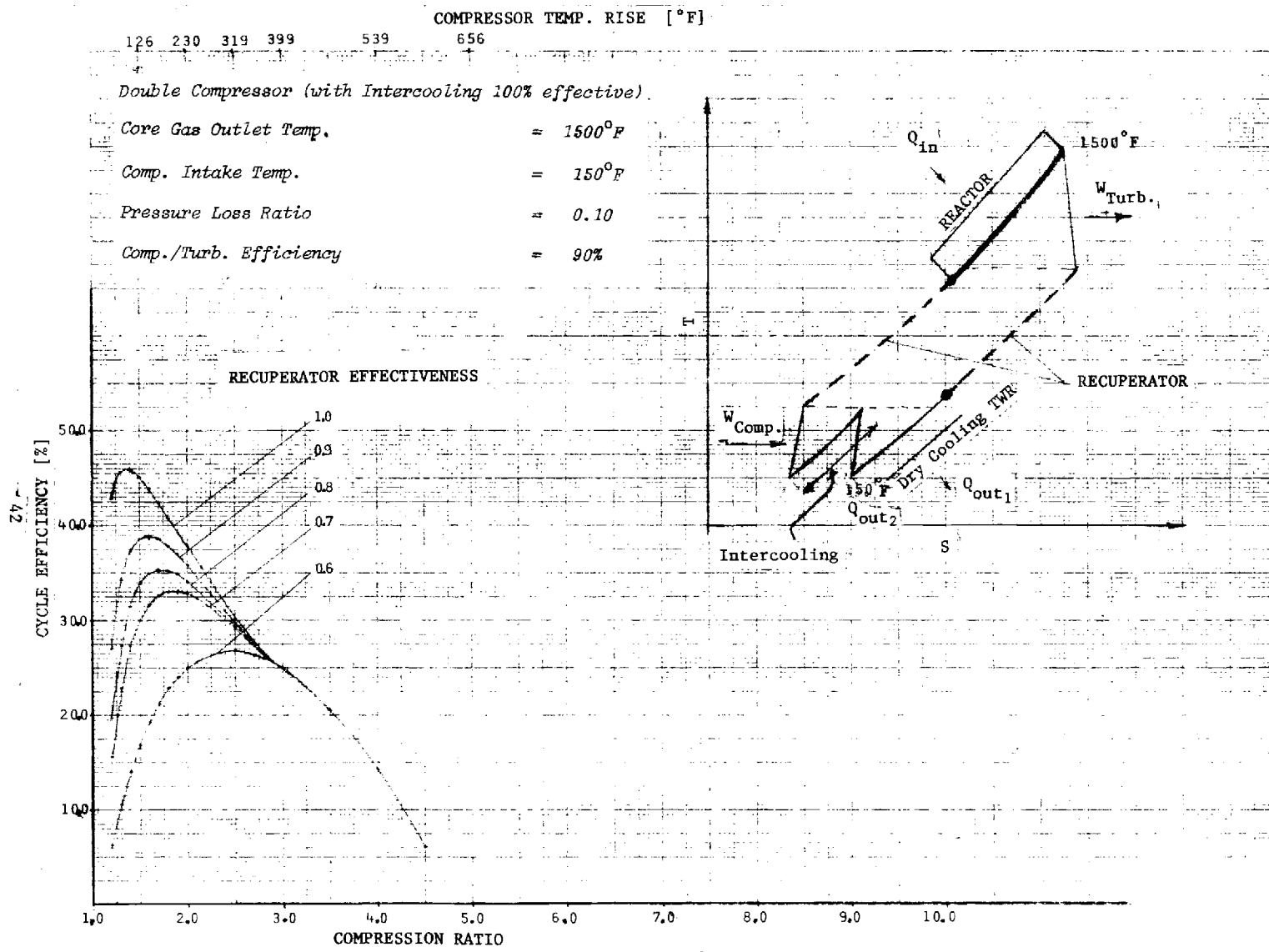


Fig. II-3-2. Gas Cycle Efficiency vs Compression Ratio for Two Stage Compression

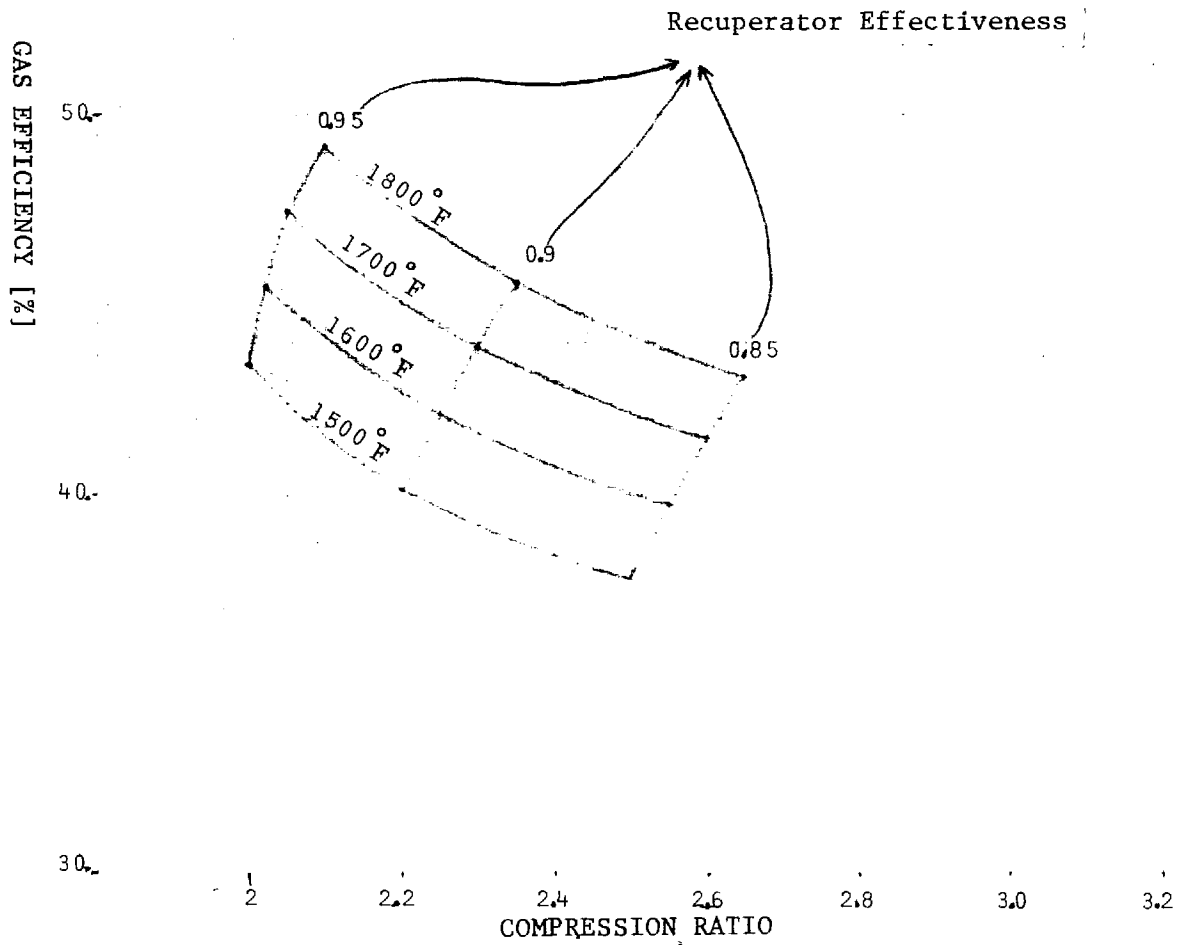


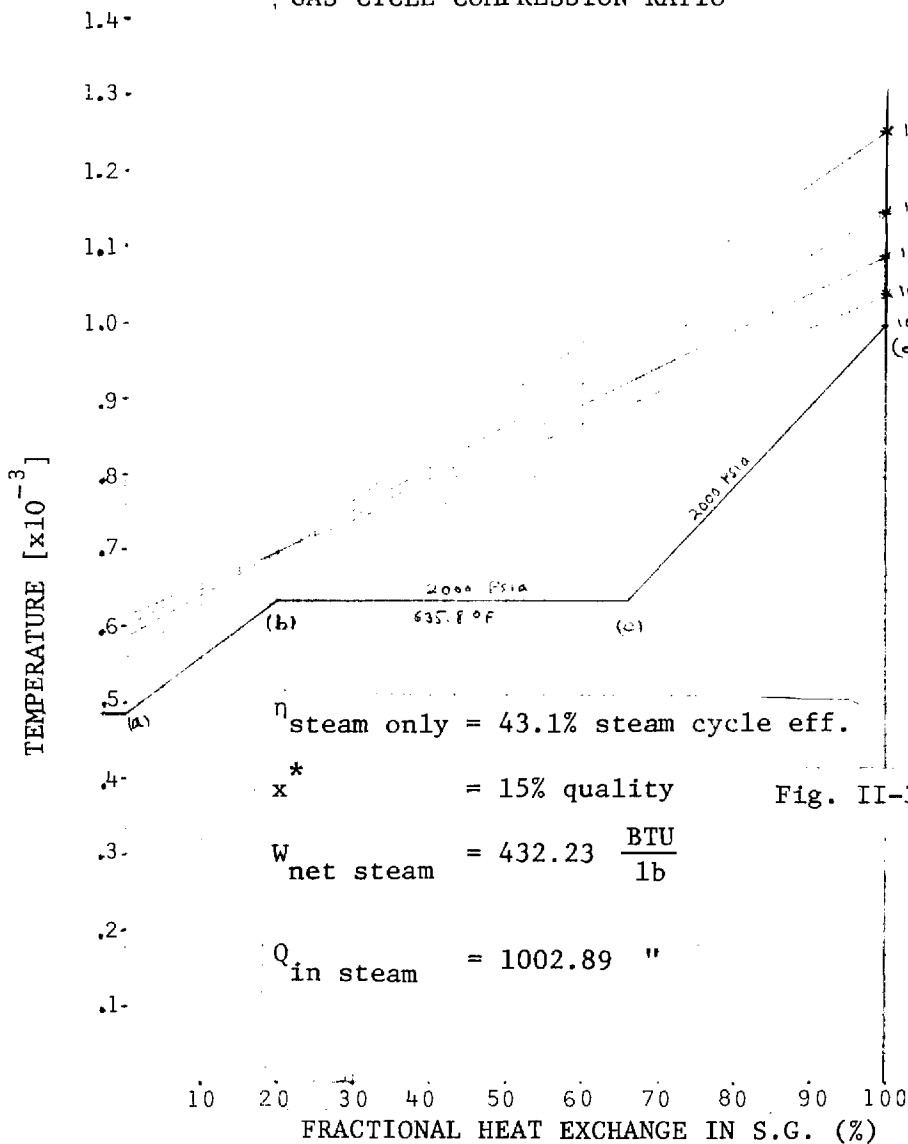
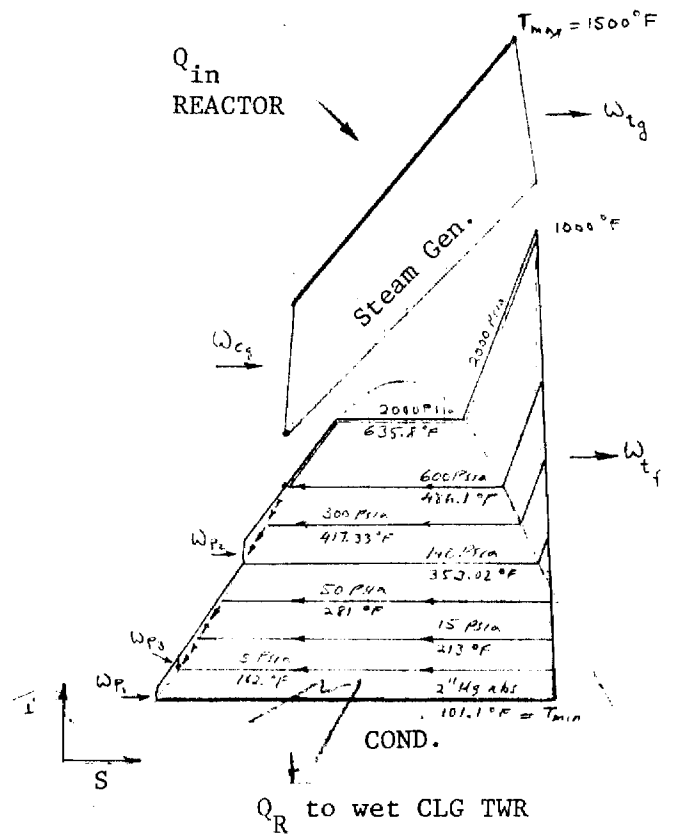
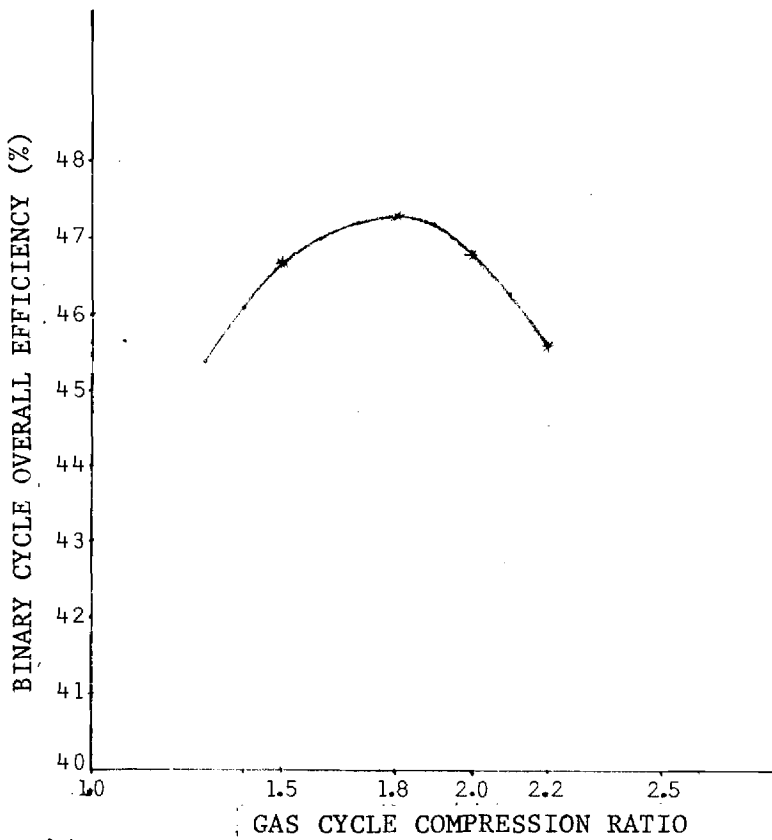
Fig. II-3-3. Gas Cycle Efficiency vs Compression Ratio at Several Temperatures and Recuperator Effectiveness

3.2 Gas/Steam Binary Cycle

Optimum gas/steam binary cycles for reactor gas outlet temperatures of 1500^oF and 1800^oF are summarized in Figs. II-3-4 and II-3-5 respectively. For 1500^oF gas outlet temperature, the steam cycle efficiency was 43.1% and the combined binary efficiency was greater than 47% (see Fig. II-3-4). The corresponding values for 1800^oF gas outlet temperature were 43.1% for the steam cycle and 51% for the binary cycle. Other data pertinent to these calculations are given in Figs. II-3-4 and 5. Details of the calculations are given in Appendix E.

Advantages of this design are as follows:

- (1) Exploitation of high temperature benefits are now possible without necessitating higher temperature steam cycle technology. This is accomplished by simply passing the high temperature gas through the gas turbine first and then to the steam generator.
- (2) Recuperators which are required for direct gas cycle are not needed in this design. The hot gas coming out of the turbine is cooled while producing superheated steam for the steam cycle. Gas leaving the steam generator is still hot ~500^oF. It is compressed and sent back to the reactor. This gas cycle is very similar to what is used now in HTGR's, except for a key component, an addition of a gas turbine. This addition and optimization of the whole cycle yields a significant improvement in overall efficiency.
- (3) Because the gas cycle used in this design has a low efficiency, it matches in a natural way the gas turbine technology, i.e., small size and small MW rating ~100-250 MWe.



1255 $^{\circ}F$ GAS INLET TEMP TO S.G.
 " " " " "
 1149 $^{\circ}F$ " " " " "
 1090 $^{\circ}F$ " " " " "
 1040 $^{\circ}F$ " " " " "
 1000 $^{\circ}F$ STEAM OUT
 (d)
 $T_{max} = 1500^{\circ}F$
 Pressure Loss Ratio in Gas Cycle = 3%
 Gas Turbine/Compr. Eff. = 90%
 Pinch Point in S.G. = 64'

$\eta_{steam\ only} = 43.1\%$ steam cycle eff.
 $x^* = 15\%$ quality
 $W_{net\ steam} = 432.23 \frac{BTU}{lb}$
 $Q_{in\ steam} = 1002.89$ "

Fig. II-3-4. Optimum Gas-Steam Binary Cycle.

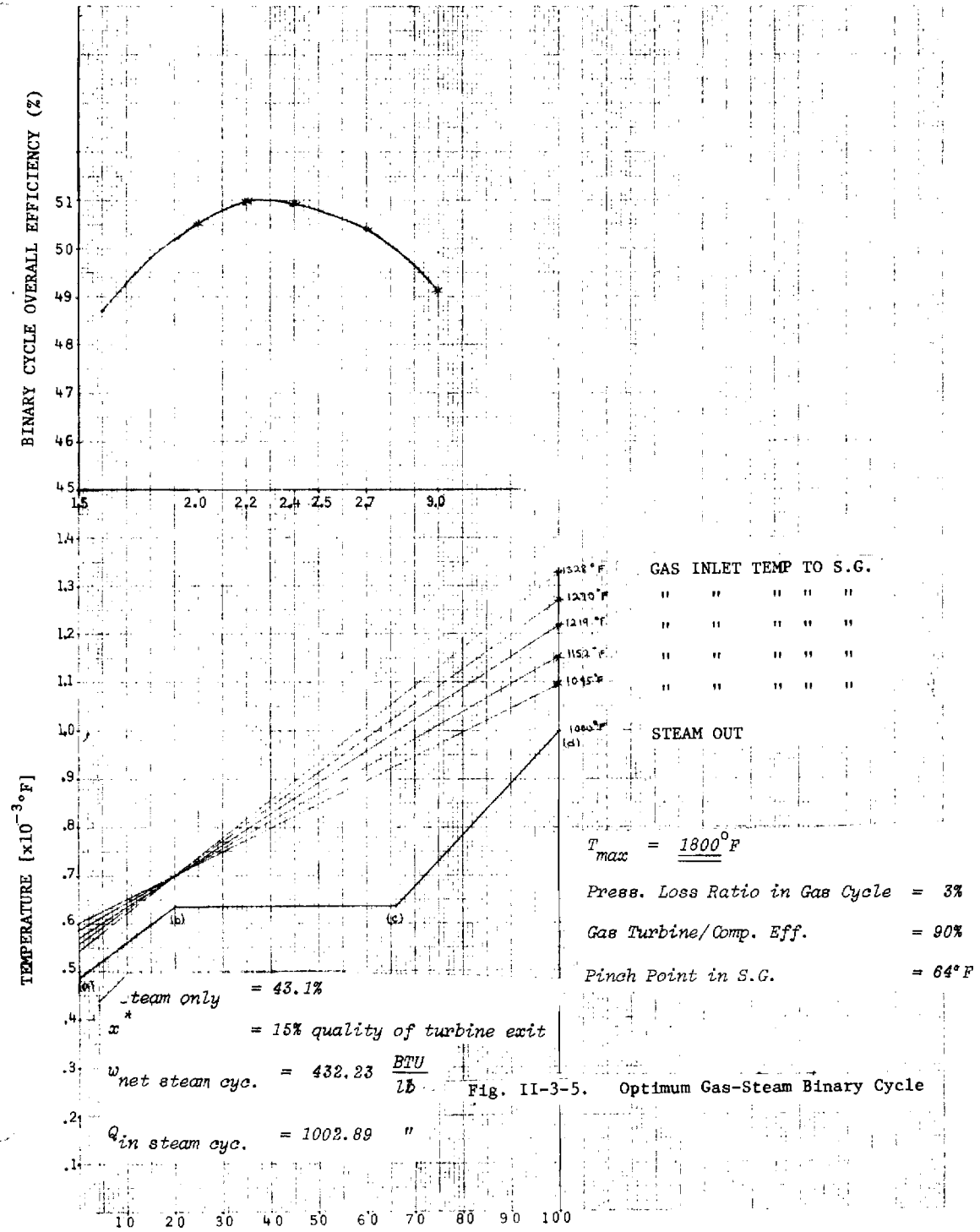


Fig. II-3-5. Optimum Gas-Steam Binary Cycle

- (4) The gas pressure drop of this gas/steam binary cycle is expected to decrease to about half of that characteristic of gas cycles, primarily because of eliminating the recuperator.
- (5) Inlet temperature to the reactor would be lower than that associated with gas cycle only.

The combination of a relatively efficient, technologically well developed steam cycle with a rather inefficient but well developed gas cycle, yields a significant advantage over existing thermal power converters.

The steam cycle shown in Fig. II-3-4 consists of six feed water heaters, five of which are closed loop heaters, one is open loop for deaeration purposes. The last heater is usually located at high elevation with respect to the boiler feed pumps to effect a continuous positive pressure at the input to the pumps and this eliminates cavitation and vibration. Steam at 2000 psi and 1000^oF from the steam generator goes to the high- and low-pressure turbines. Steam from the low-pressure turbine is extracted at various stages to heat the feed water. The rest of the steam goes to the condenser where the pressure is 2" Hg absolute. Here heat is rejected by the circulating water to the wet cooling towers.

Figure II-3-6 and 7 show the gas turbine outlet temperature, reactor gas-in temperature, compressor inlet temperature, and the pounds of gas needed per pound of steam generated, all versus gas compression ratio for outlet of 1500^oF and 1800^oF respectively. Also shown is the overall binary cycle efficiency as a function of compression ratio. It is interesting to note that at a compression ratio of 1.8 and T_{\max} for reactor gas outlet of 1500^oF, the optimized binary efficiency is 47.3%, but the turbine

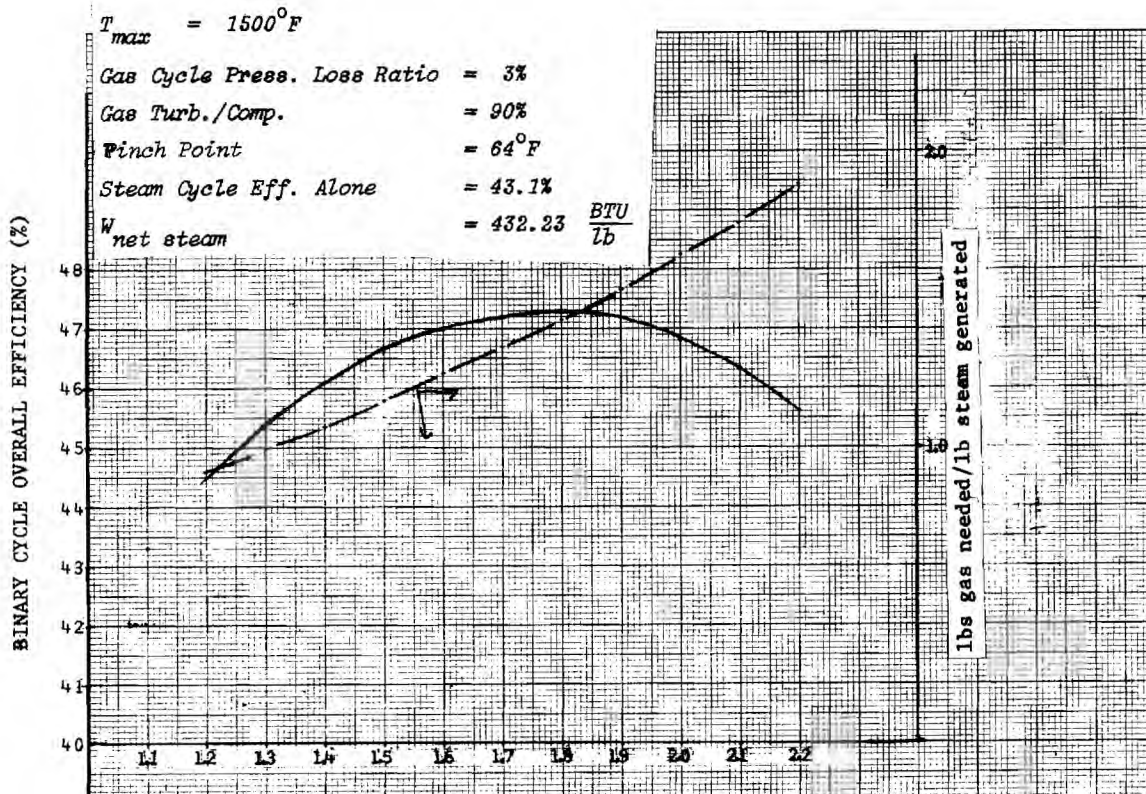
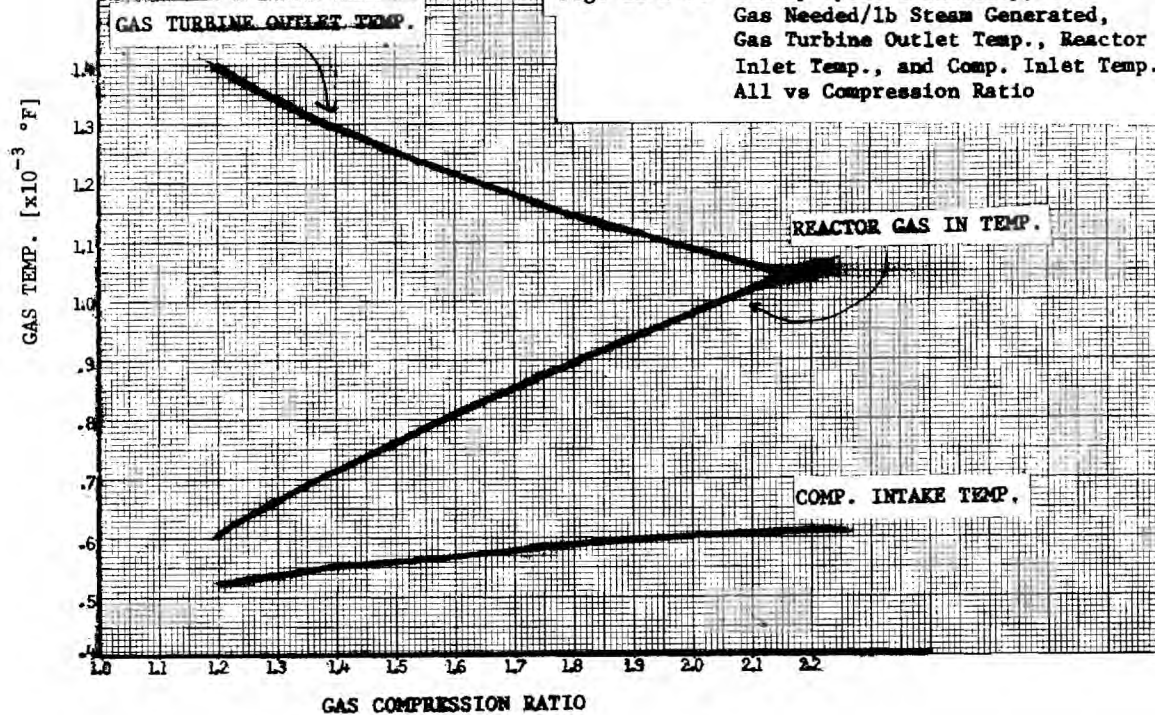


Fig. II-3-6. Binary Cycle Efficiency, lbs Gas Needed/lb Steam Generated, Gas Turbine Outlet Temp., Reactor Inlet Temp., and Comp. Inlet Temp. All vs Compression Ratio



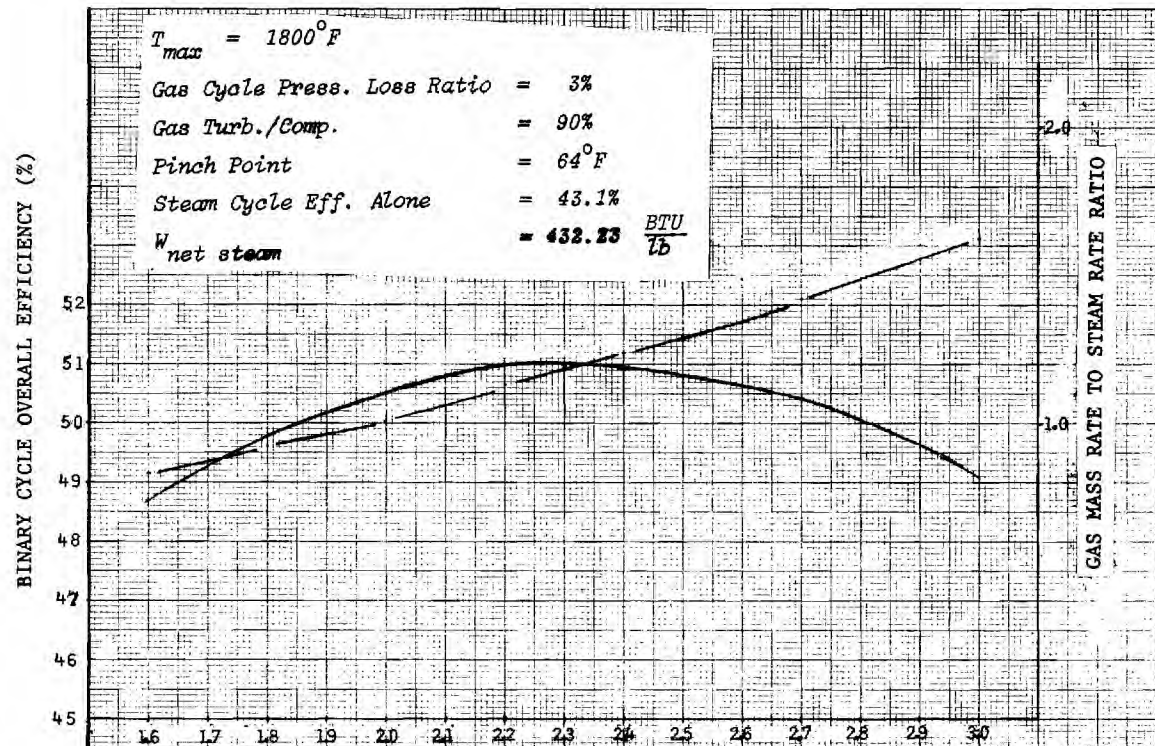
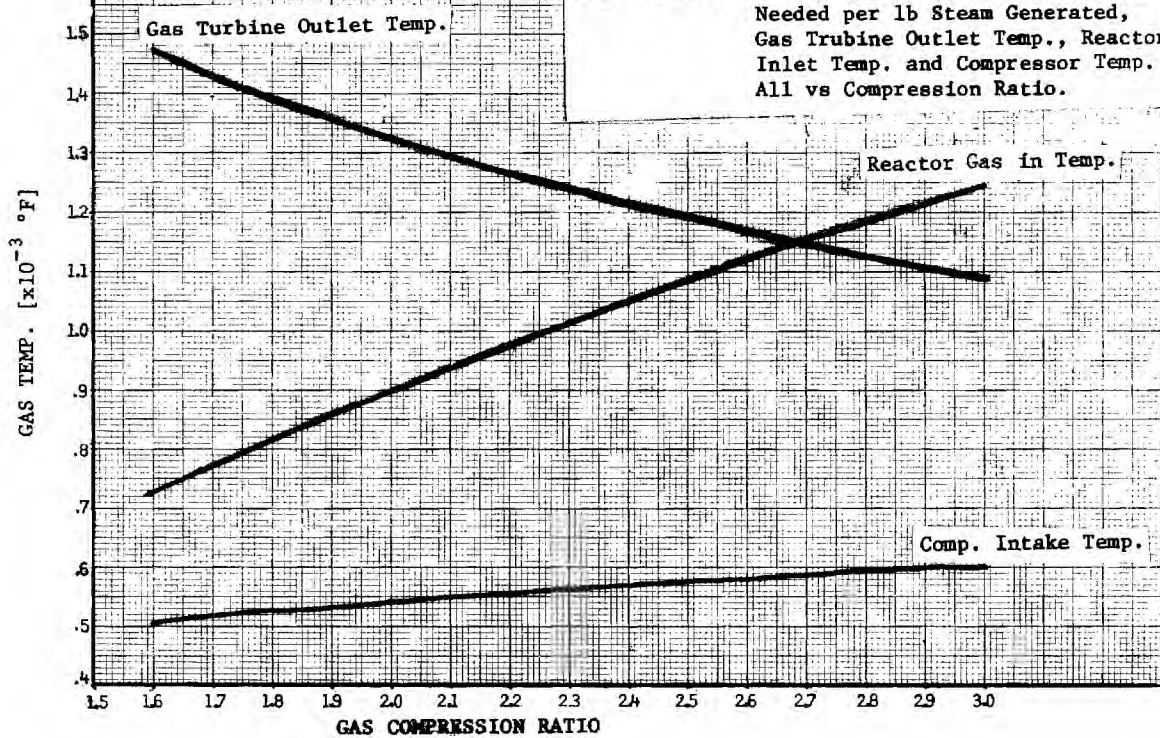


Fig. II-3-7. Binary Cycle Efficiency, lbs Gas Needed per lb Steam Generated, Gas Turbine Outlet Temp., Reactor Inlet Temp. and Compressor Temp. All vs Compression Ratio.



gas outlet temperature is only 1150^oF. This gas temperature and the steam cycle (shown in Fig. II-3-4) yields a steam cycle efficiency of 43.1%. This optimum binary cycle efficiency, however, corresponds to a reactor inlet temperature of 890^oF which is not really desirable because high gas flow rates would be required, and this could be costly. A better choice for operating compression ratios could be 1.4 to 1.5 where the efficiency is 46-46.7%, the inlet reactor temperature range is 710-760^oF, and the gas turbine outlet temperature is 1300-1250^oF. Optimum operating conditions from an economic point of view would require further analysis.

It is important to point out that the difference in the steam cycle efficiencies between this work and that of the HTGR's is primarily due to the fact that the compressors in this work are driven by the gas cycle, whereas the circulators in present HTGR technology are driven by steam. In addition to this work, the gas cycle produces additional electricity. For example, for a 1000 MWe plant operating at a compression ratio of 1.5, the binary cycle efficiency is 46.7% or the reactor produces 2140 MWth. The steam cycle alone produces 866 MWe and the net gas cycle is 134 MWe. The current HTGR technology with a 2140 MWth plant produces 856 assuming a steam cycle efficiency of 40%. In other words, the binary cycle described herein is over 16% better than HTGR technology under approximately the same operating condition.

4 Fuel Design

4.1 General Considerations of Coated Particles

The fuel particle design is a key factor which affects overall reactor performance. Physics and thermal hydraulics considerations show that the fuel particle design should have the following desirable characteristics:

1. large fuel volume fraction, or equivalently small coating material volume fraction
2. for better breeding performance, the higher the fuel density the better
3. high thermal conductivity for both coating layers and fuel kernel
4. high creep strength for long term irradiation in high temperature and pressure environments
5. good drop impact resistance and high crushing strength
6. optimum size to give the highest power density at the lowest pressure drop, and
7. high burnup performance.

4.2 Coated Particle Fuel - A Review

The development of coated particles fuel for thermal reactors (HTGR's and AVR's) and the developing coated particle technology for fast reactors^(15,16,17) provide an extensive experience to draw upon for the Suspended-Bed Reactor. A brief review of these fuels is useful.

Work on pyrolytic carbon coated particles has been going on for some time in many centers and laboratories around the world.^(18,19,20,21) As excellent review of the general properties of BISO and TRISO coated

particles was recently reported.⁽²¹⁾ The reference BISO and TRISO particles as well as some advanced BISO particles are described in Table II-4-I.⁽²²⁾ Generally, coating failure depends on the fuel temperature and irradiation time. Specifically there are two factors involved in irradiation time: (1) the fluence of neutrons above 100-200 KeV and (2) burnup. Figures II-4-1 and II-4-2, taken from (Ref. 21), illustrate respectively the coating failure zones for these particles as a function of irradiation time and fuel temperature. Figure II-4-3(a) shows TRISO particle failure as a function of fast neutron fluence in unit of 10^{21} nvt, at energies above 180 KeV. Figure II-4-3(b) shows TRISO particle failure as a function of fissile atom burnup, in units of % FIMA (fissions per initial heavy metal atom). TRISO particle failure as a function of temperature after exposure for different periods of irradiation is shown in Figure II-4-4. Finally rapid thermal excursion effects from 1250° to 1425° , to 1600° , or to 1800° C and back to 1250° C on pressure vessel failure in TRISO particles is shown in Figure II-4-5 as a function of fast neutron fluence (a) and kernel burnup (b). That the properties of these particles are excellent is obvious. In particular, the large burnup possible, shown in Figure II-4-3(b), is very attractive.

The General Atomic Corporation has also investigated⁽²²⁾ the breeding potential of HTGR's. To that end, some advanced designs of coated particles have been considered, namely BISO I, BISO II, and BISO III, all listed in Table II-4-I. The conversion ratio possible with these fuels are given in Table II-4-II.

Table II-4-I

Advanced BISO Fertile Particle Description

Particle System	Particle Parameters				
	Kernel Dia., μm	Buffer Thickness μm	Outer Coating Thickness μm	Total Coating Thickness μm	Kernel Volume Fraction
Reference TRISO-BISO	305 (TRISO)	50	100*	150	0.128
	500 (BISO)	85	75	160	0.227
Advanced BISO-I	500	60	65 (Si-PyC)	125	0.274
Advanced BISO-II	500	50	50 (Si-PyC)	100	0.364
Advanced BISO-III	500	40	35 (Si-PyC)	75	0.477

* Outer coating comprise 30 μm high density PyC, 35 μm SiC, and 35 μm high density PyC

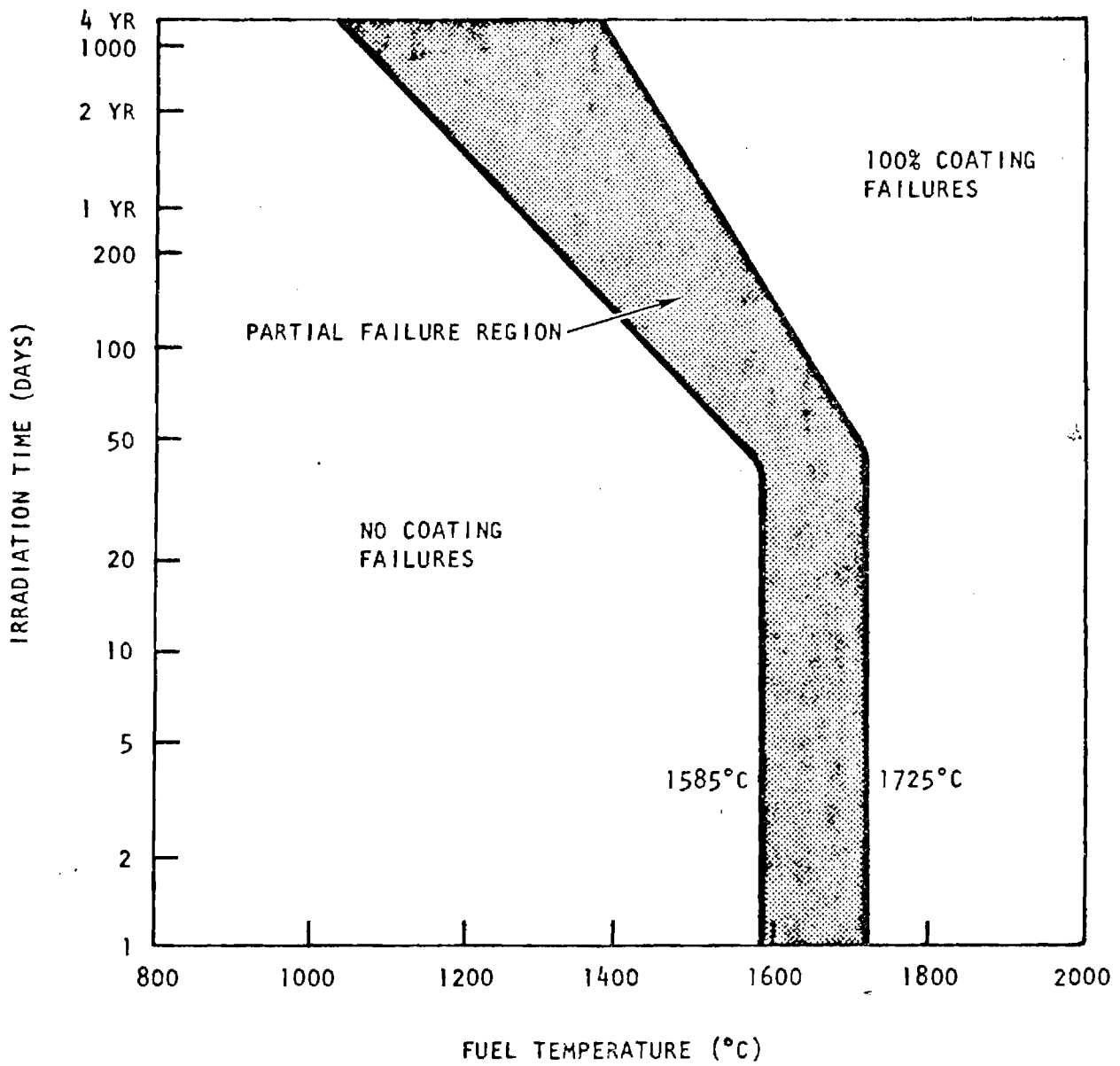


Fig. II-4-1. TRISO Fuel Particle Coating Failure Diagram

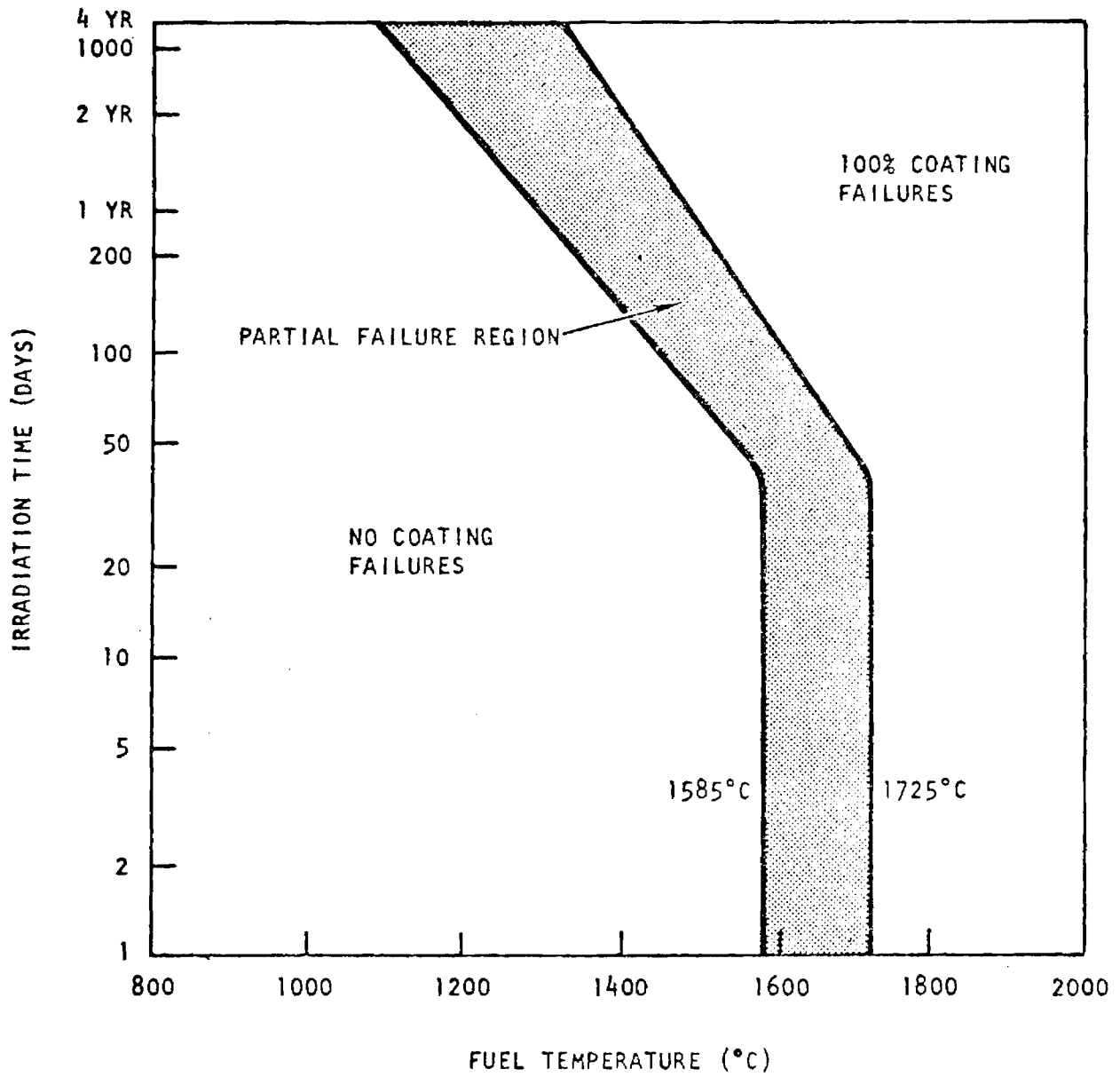


Fig. II-4-2. BISO Fuel Particle Coating Failure Diagram

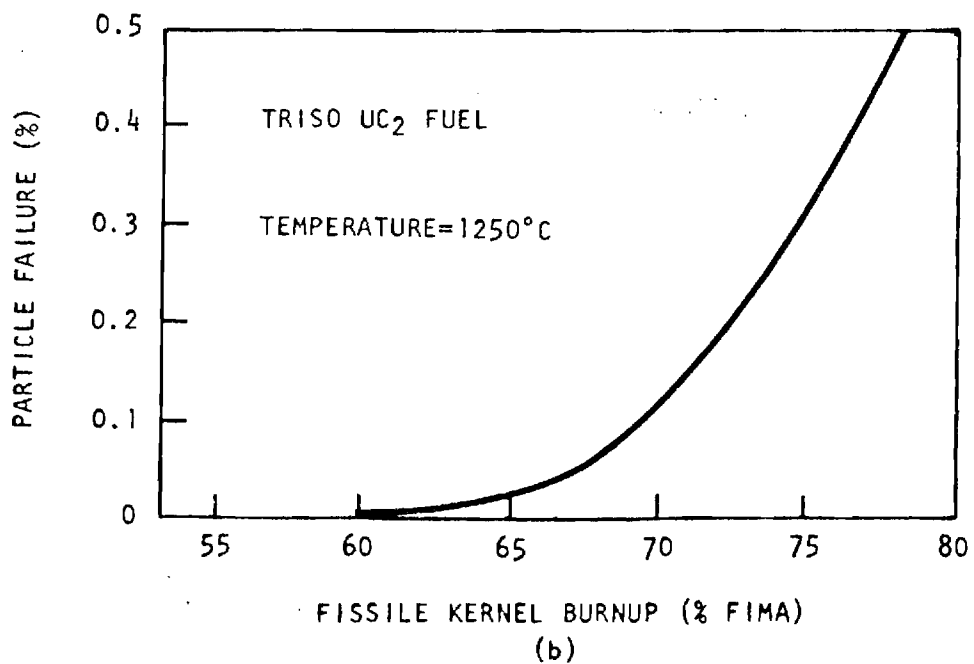
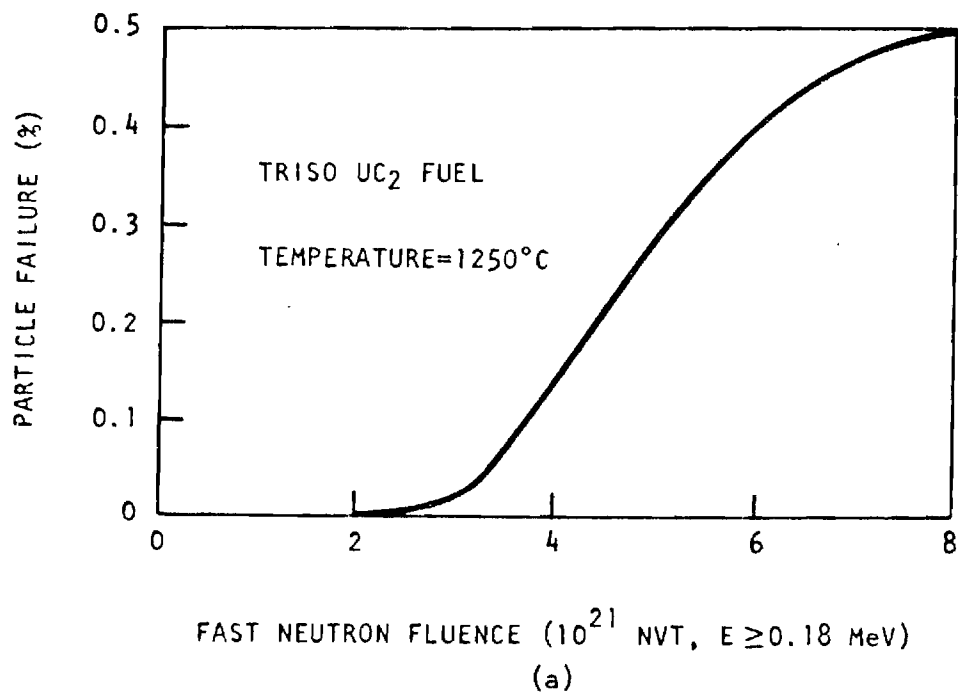


Fig. II-4-3. Assumed pressure vessel failure fraction vs (a) fast neutron fluence or (b) kernel burnup for TRISO UC₂ fuel. (From Ref. 21).

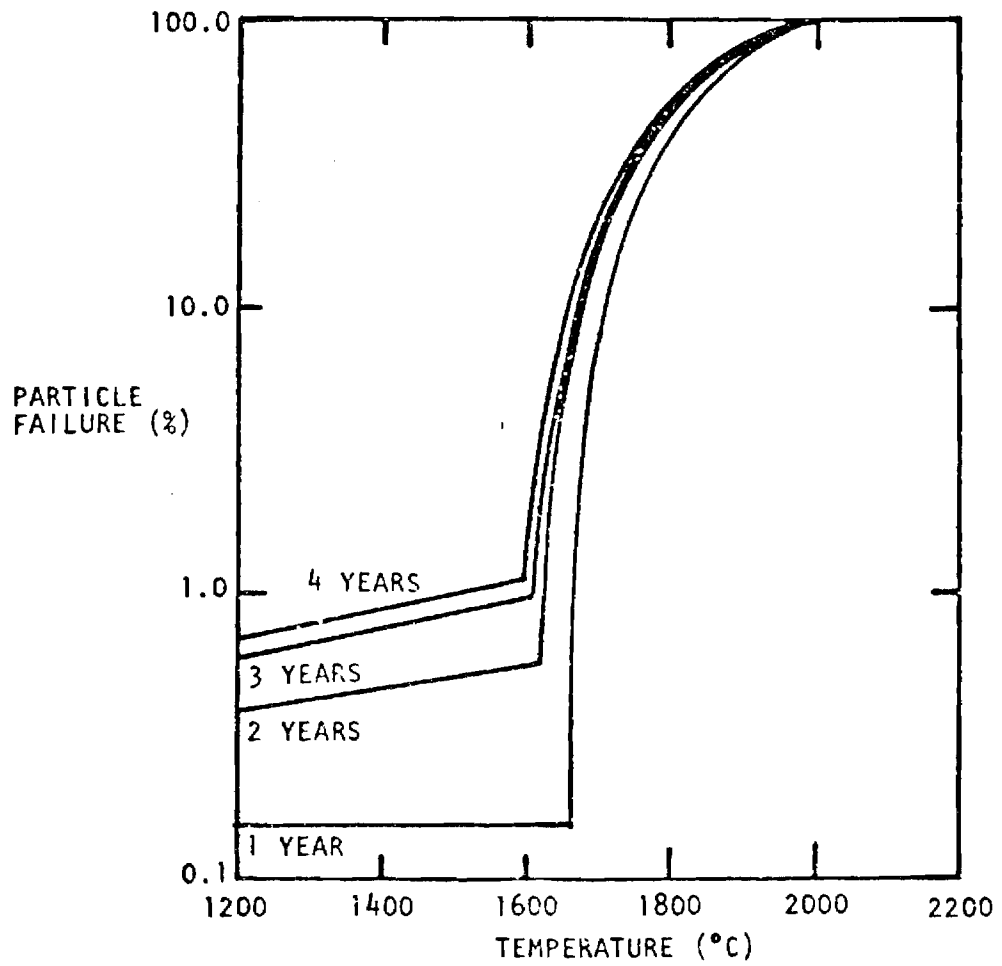


Fig. II-4-4. TRISO Fuel Particle Coating Failure Diagram

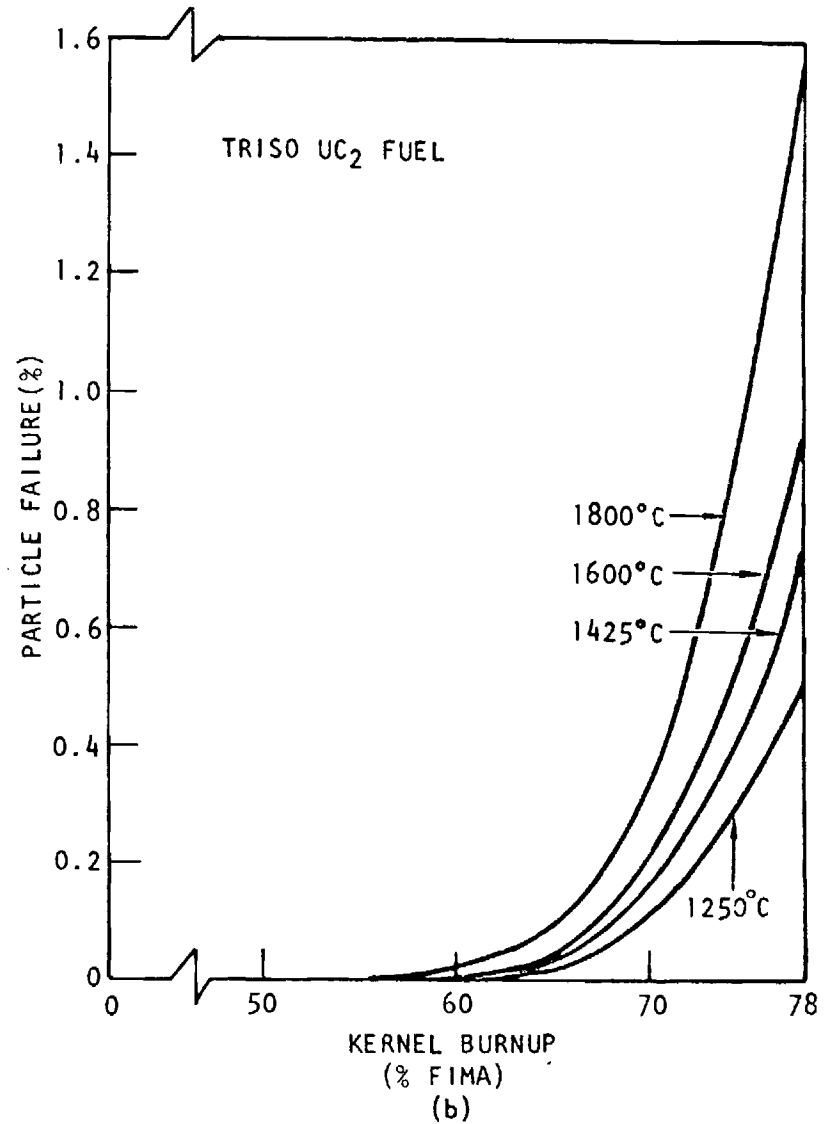
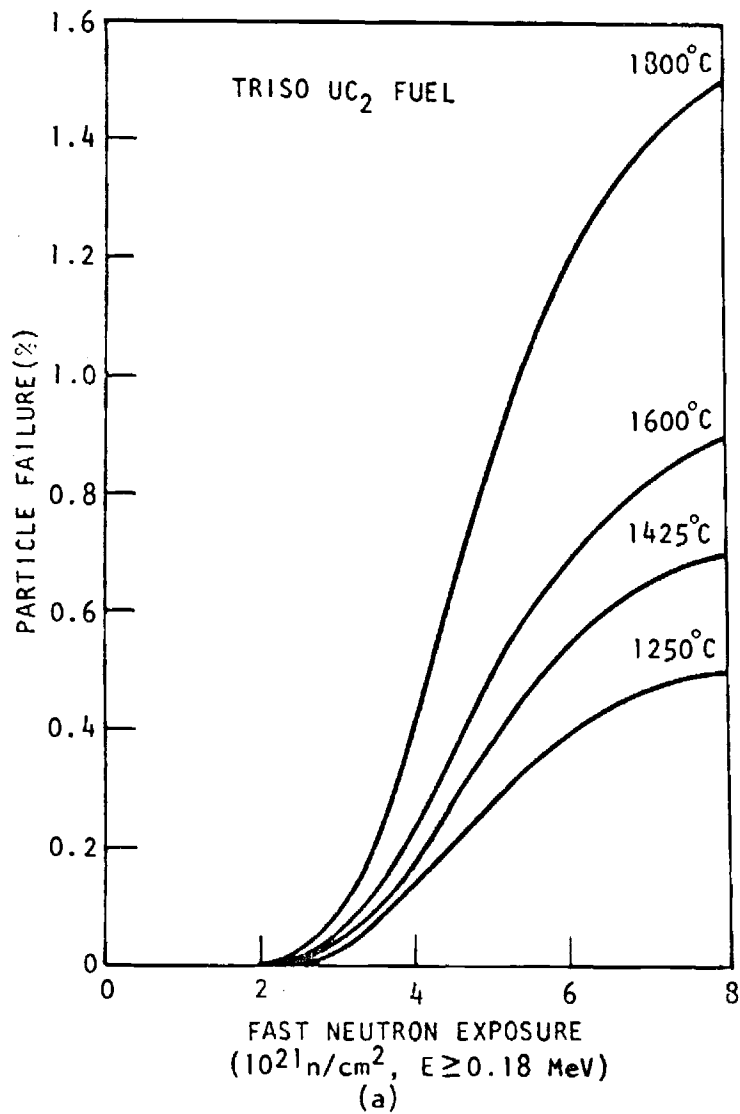


Fig. II-4-5. Effect of a rapid thermal excursion from 1250° to 1425°, 1600°, or 1800° and back to 1250° on pressure vessel failure in TRISO UC₂ as a function of (a) fast neutron exposure or (b) kernel burnup for fuel experiencing 78% FIMA at a fast neutron exposure of 8×10^{21} nvt. (From Ref. 21).

Table II-4-II. Effective Conversion Factors for Advanced BISO Fuel Particles

Reactor Type	Particle System ^a	Effective Conversion Ratio		Carbon to Thorium Atom Ratio	
HTGR Reference Fuel Rod and Fuel Block Design	BISO - I	0.84 ^a	0.75 ^b	115 ^a	130 ^b
	BISO - II	0.89 ^a	0.82 ^b	90 ^a	100 ^b
	BISO - III	0.93 ^a	0.87 ^b	70 ^a	80 ^b
HTGR Modified Fuel rod and block Design ^(c)	BISO - I	0.90		73 ^a	
	BISO - II	0.94		56 ^a	
	BISO - III	0.96		45 ^a	

(a) Power Density = 6.0 MWth/m³

(b) Power Density = 8.4 MWth/m³

(c) Coolant and fuel hole diameter = 1.857 cm in modified 8-row block. Fuel rod diameter increased while coolant channel decreased with respect to reference design.

It is seen that the conversion ratio increases as the carbon-to-thorium atom ratio decreases. Additionally, the coating thickness in the advanced BISO is significantly thinner than the reference BISO and TRISO particles. The advanced BISO's contain "Si-alloys coatings."⁽²²⁾ What these Si-alloys are was not stated. It was indicated, however, that Si-alloys, presumably SiC, exhibit higher strength than pyrolytic carbon and thus make it possible to have thinner coating.

The AVR fuel is also pyrolytic carbon coated particles placed in a graphite matrix and coated on the outside with a graphite shell about 5 mm. The AVR pebbles are spheres of about 6 cm diameter. In February 1974, the AVR reached helium exit temperature of about 1740^oF.⁽¹³⁾

Other coated particles designs have been considered for gas cooled fast reactors.^(15,16) These include:

1. carbide or oxide coated particles,
2. carbide or oxide fuel with stainless steel clad, and
3. carbide or oxide fuel with Vanadium-Ti alloy clad.

In many of the coated particle designs, SiC was selected as the pressure vessel material primarily because of its small interatomic spacing, absence of reaction with UC or UC₂ at high temperatures, low neutron capture cross section, good thermal conductivity, superior resistance to fuel migration, and superior strength.^(22,17) M. Dalle Donne, et al.⁽¹⁵⁾ have designed a mixed uranium plutonium carbide particles 1.4 mm diameter, with a triplex 120 μm thick coating (two layers of graphite and one silicon carbide) for use in a fast spectrum.

One of the main reasons for SiC coating being chosen for fast reactors is its superior performance under high fast neutrons fluence

$\sim 1 \times 10^{23}$ nvt. Because of its strength and irradiation tolerance SiC coatings are normally thin and this has a positive effect on the breeding ratio.

It is to be stressed, however, that the experience with coated particles in fast neutron spectra is quite limited. The Suspended-Bed Reactor has a relatively fast neutron spectrum, and, consequently, the coated particles selected for this reactor require proof testing.

4.3 Suspended-Bed Reactor Fuel Design

Two types of coated particles were chosen for the preliminary design of the Suspended-Bed Reactor: (1) (Th-U) C_2 kernel coated with triple layers of low density graphite buffer region, SiC pressure vessel and ZrC outer layer, and (2) (Th-U) metal kernel oxidized on the surface and coated with the same layers as the (Th-U) C_2 kernel. The kernel diameter in both cases was 1.4 mm. The thicknesses of the three layers were as follows: 70 μm low density graphite, 30 μm SiC, and 50 μm ZrC. These designs are similar to the German design described in (Ref. 16). The buffer layer, consisting of low density graphite ($< 1.0 \text{ g/cm}^3$), fulfill two important functions:

1. protects all other layers against fission product recoil effects,
2. provides free volume which would accommodate kernel swelling and fission products storage.

The thickness of the buffer region was determined as a function of kernel diameter (Ref. 16) which for our case would be 70 μm . The SiC layer provides two functions also:

1. serves as a pressure vessel
2. serves as barrier for fission products.

As the kernel expands due to thermal and irradiation swelling, the SiC is in tension. However, SiC has high thermal creep strength and very good mechanical properties with small dimensional variation - (0.3%). The ZrC layer primary function is to protect the SiC layer from attack by oxygen which may exist in low concentration in the helium coolant. Other material which could replace ZrC as a protective layer is Nb, NbC or perhaps Ni. ZrC, however, appears to be most adherent and is very resistant to thermal shock; thermal expansion coefficient is $6.6 \times 10^{-6}/^{\circ}\text{C}$ compared to $5.35 \times 10^{-6}/^{\circ}\text{C}$ for SiC.

The choice of a dicarbide kernel rather than oxide was primarily due to the excellent thermal conductivity of $(\text{U-Th})\text{C}_2$ which is 13.8 BTU/ $\text{m}^{\circ}\text{F ft.}$ versus 0.2 BTU/ $\text{m}^{\circ}\text{F ft.}$ for the oxide. This factor is important to power density and decay heat removal. Additionally, carbon has lower capture cross section than oxygen.

Metallic fuel kernel -- it is generally known that metallic thorium-uranium alloys exhibit superior irradiation stability over uranium alloys.⁽²³⁻²⁶⁾ The inherent advantages of this fuel are:

- (a) large fuel volume fraction
- (b) excellent thermal conductivity
- (c) high breeding ratio.

Among the disadvantages, the lack of experience requires a detailed development program.

The mechanical properties of the Suspended-Bed Reactor fuel design are listed in Table II-4-III.

Table II-4-III

Mechanical Properties of Fuel Materials

Properties	Unit	(U-Th)C ₂	Th	Buffer PyC	S _i C	ZrC
Young's modulus	psi		4.62x10 ⁶	2.4x10 ⁶	52.5x10 ⁶	2.0 x 10 ⁷
Ultimate tensile strength	psi		80x10 ³		46x10 ³	
Yield strength	psi		35x10 ³		46x10 ³	
Thermal expansion	°C ⁻¹		12.5x10 ⁻⁶	5.4x10 ⁻⁶	5.35x10 ⁻⁶	
Poison's ratio			0.27	0.24	0.25~0.3	
Thermal conductivity	$\frac{\text{watts}}{\text{m}^{\circ}\text{C}}$	23.9	45 (600°C)	75 (800°C)	36 (800°C)	20.5 (800°C)
Density	$\frac{\text{gm}}{\text{cm}^3}$	9.3	11.72	1.05	3.2	6.7
Melting point	°C		3092°F	6710°F	3997°F	6400°F

At high temperature thorium will react with the carbon coating. To prevent this, it is proposed that a layer on the surface of metal be oxidized before applying the buffer low density graphite. Another alternative to low density graphite, SiC and ZrC coatings is to use Cr, V, or V-Ti alloy. M Dalle Donne, et al⁽¹⁵⁾ indicated that metallic coatings can be applied on practically any size kernel. However, the particle should be designed so as to accommodate diameter variation and fission gas pressure buildup. Vanadium-titanium (20%) alloy has been found to be very compatible with thorium metal⁽²⁷⁾ under long term irradiation and high temperature. It has, however, lower thermal conductivity than either SiC or graphite. On the other hand, it may have better impact resistance, better wear resistance, and higher crushing strength. A fuel coated with V-Ti (20%) may be a potential fuel for the Suspended-Bed Reactor.

5. Physics Calculations

5.1 Core Specification

The Suspended-Bed Reactor consists of a core comprising two radial regions: inner core with a radius of 125 cm and an outer core extending from 125 cm to 178 cm. The core weight is one meter. The axial and radial blankets are 50 cm thick and are surrounded by 30 cm graphite reflectors. A sketch of the reactor is shown in Fig. II-5-1.

The core region consists of 151 (10" S.S. 316) pipes arranged into an 8-ring hexagon (see Fig. II-5-2). Above and below the core region, the 10" pipes are reduced to 4" to provide space for the axial blanket. This is shown in Fig. II-5-3. At the top of the core inside each 10" pipe, a screen is placed to prevent the coated particles from being carried away with the helium coolant. In the core region within each 10" S.S. pipe, a stainless steel distributor is placed for the purpose of increasing the void fraction. The pipes are insulated on the inside with 50 mils ZrO_2 layer to allow high temperature operation (Fig. II-5-4).

A 10 m^3 volume for the core was selected. This is based on thermal hydraulic analysis which indicated that for the Suspended-Bed Reactor and the fuel particle size chosen, the range of power density possible was between 150-400 MW/m^3 . A choice of $250MW/m^3$ yields, for the 10 m^3 core, a total power of 2500 MWth.

The unit cell in the Suspended-Bed Reactor can be represented by a triangle with equal sides (see Fig. II-5-5). The small pipe at the center of the unit cell is a control element placed in the empty space among the large pipes. The total volume fraction of the empty space is 9% of the core volume and represents about 2% reactivity.

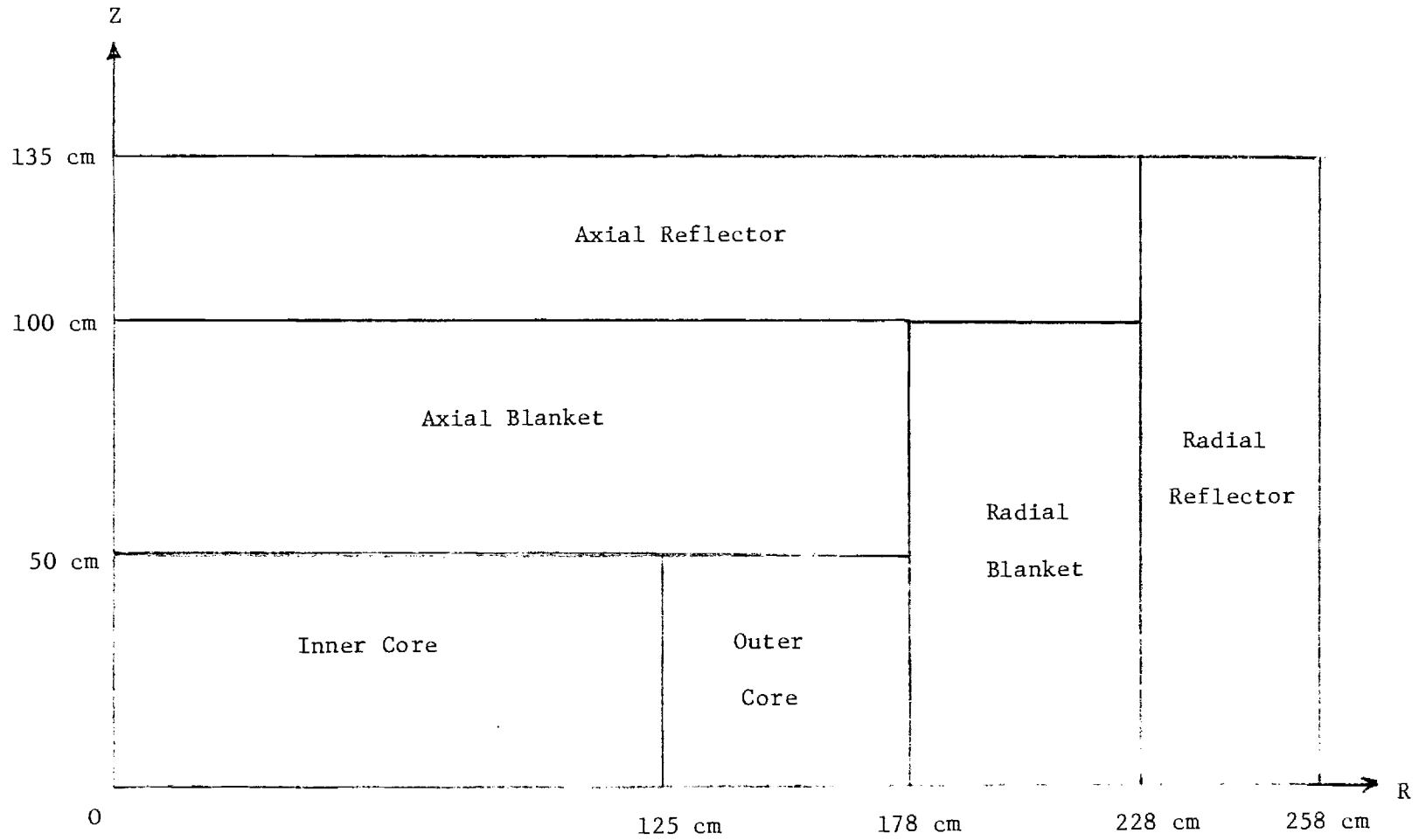


Fig. II-5-1. Geometrical Description of the Suspended Bed-Reactor

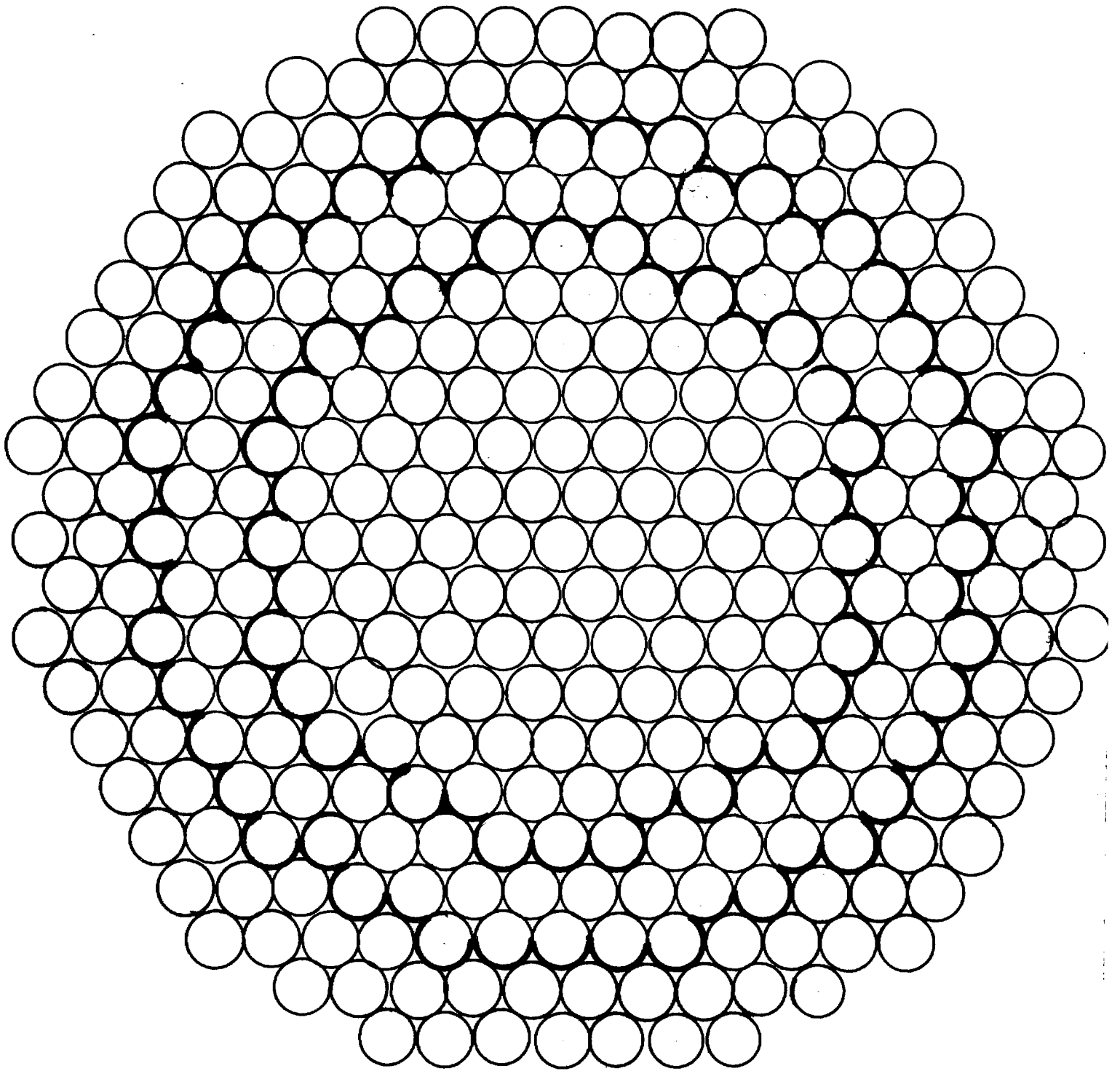


Fig. II-5-2. Pictorial View of Pipe Arrangement

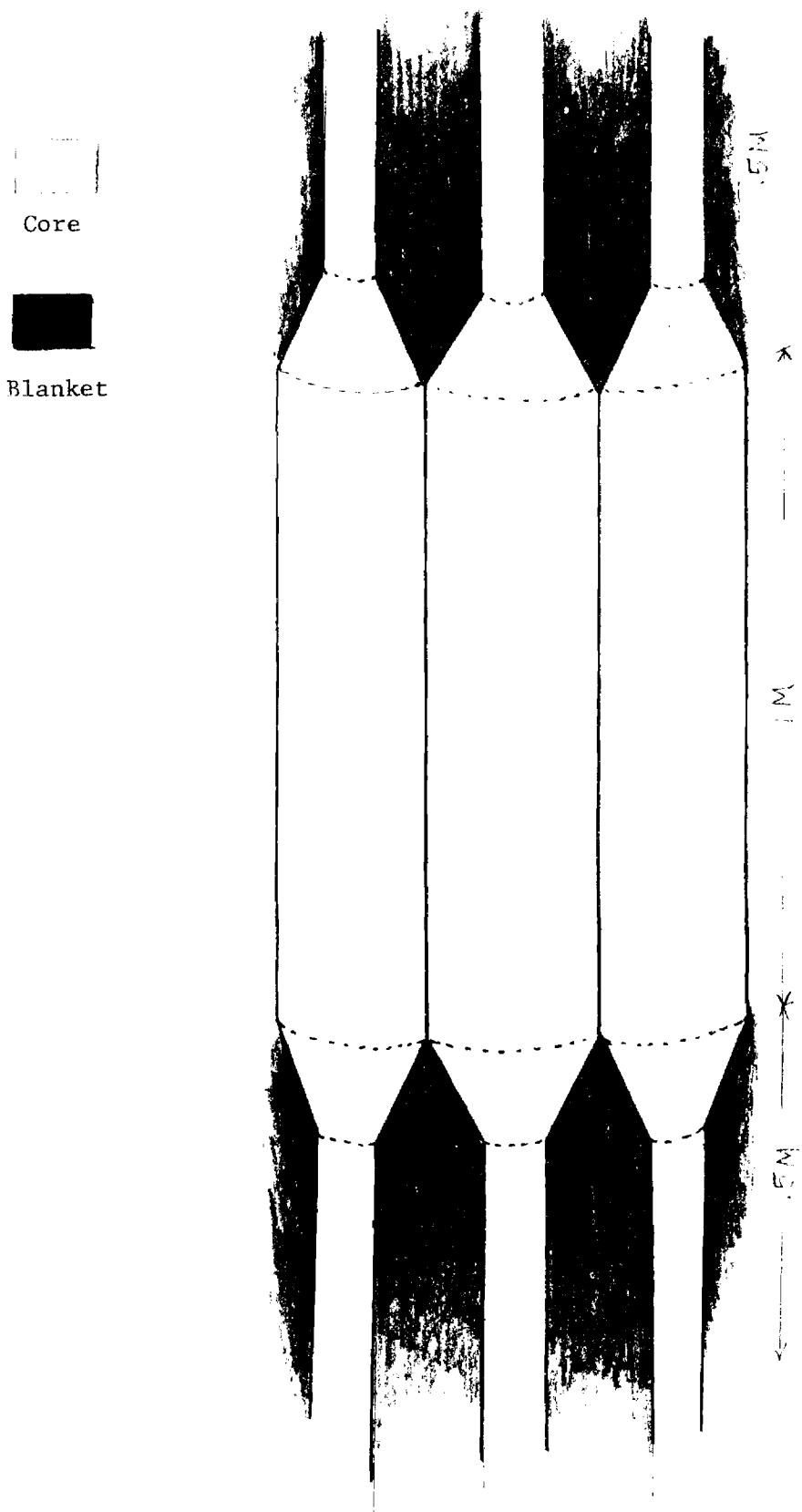


Fig. II-5-3. A Section of Pipe Showing Core and Blanket Arrangements

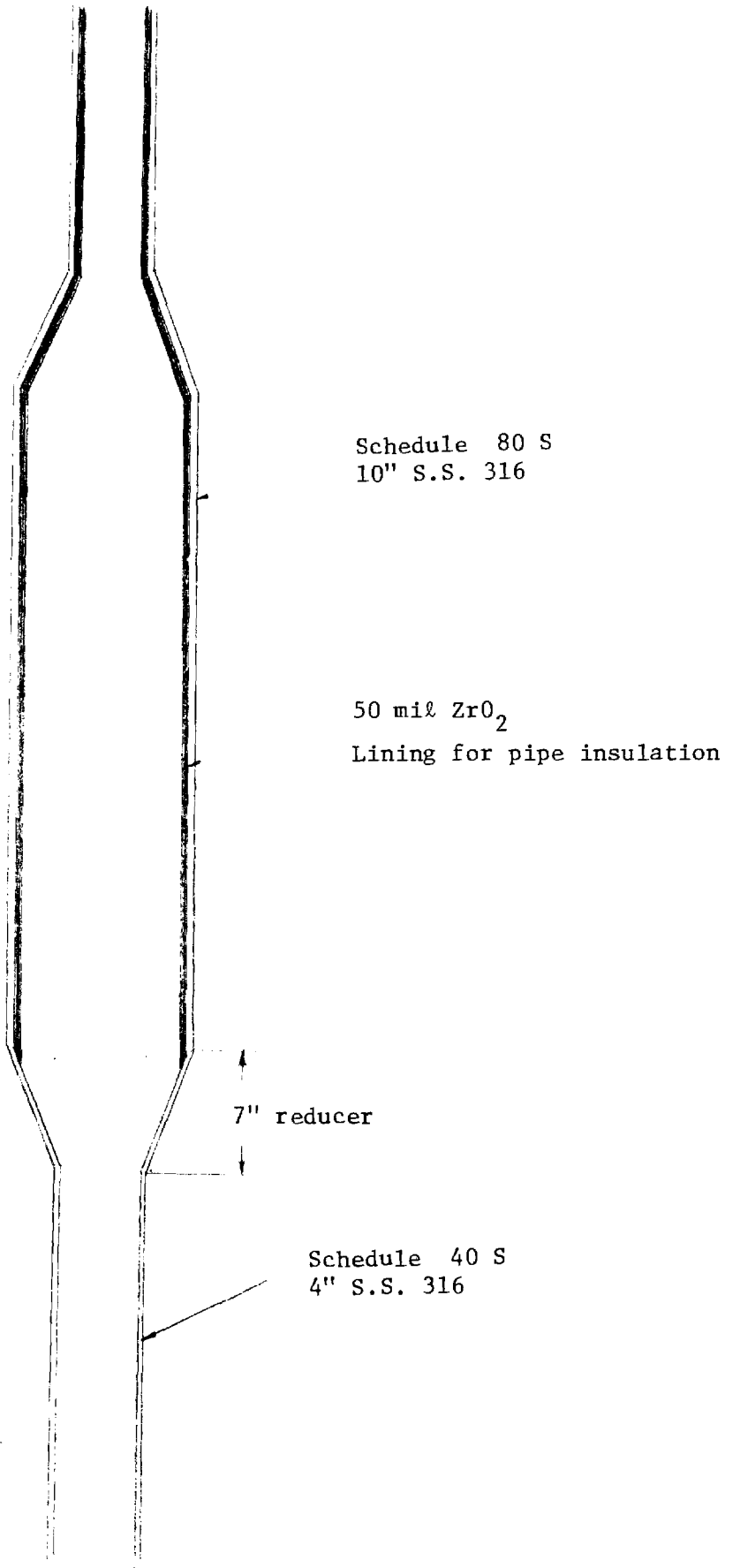


Fig. II-5-4. A Sketch of the Suspended-Bed Reactor Pipe Showing Insulation

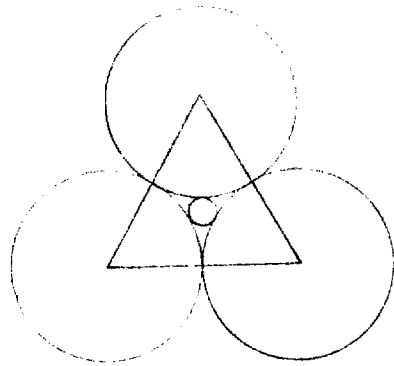


Fig. II-5-5. Unit Cell in Suspended-Bed Reactor

The stainless steel volume fraction is relatively insensitive to the pipe diameter. For example, the difference in volume fractions between 5" and 10" pipes is only 0.2%.

The material volume fractions for the Suspended-Bed Reactor are given in Table II-5-1. Component volume fractions in GCFR's and LMFBR are included for comparison.

5.2 Blanket Specifications

The specifications for the radial blanket are:

Radial Blanket

no. of blanket elements	102
kernel material	$(U^{233} \text{ Th}^{232})C_2$
coating material	ZrC-SiC-PyC
no. of particles per element	11,801,922
blanket height	1 M
pipe specification	10" schedule 80 S S.S. 316

Top Axial Blanket

blanket type	hexagonal element (fertile rods inserted in graphite matrix or Beo matrix) with a 4.5" diameter hole at center
no. of elements	253
no. of rods per element	18
no. of coolant channels	2
blanket pellet diameter	4.52 cm

Table II-5-I. Comparison of Material Volume Fractions of SBR with Typical GCFR and LMFBR

Reactor				SBR Dicarbide Kernel			SBR Metallic Kernel			GCFR (Ref. 28)	LMFBR (Ref. 29)
<u>Core</u>											
Coolant	Volume	Fraction		0.2886	0.361	0.433	0.325	0.361	0.397	0.640	0.406
Fuel	"	"		0.242	0.202	0.161	0.222	0.202	0.181	0.221	0.329
Stainless Steel	"	"		0.17	0.17	0.17	0.17	0.17	0.17	0.139	0.223
Kernel Coating	"	"		0.191	0.159	0.124	0.175	0.159	0.144		
Pipe Lining	"	"		0.0153	0.0153	0.0153	0.0153	0.0153	0.0153		
<u>Radial Blanket</u>											
Coolant	Volume	Fraction		0.23	0.23	0.23	0.23	0.23	0.23	0.34	0.274
Fertile	"	"		0.30	0.30	0.30	0.30	0.30	0.30	0.50	0.451
Stainless Steel	"	"		0.16	0.16	0.16	0.16	0.16	0.16	0.16	0.245
Graphite	"	"		0.22	0.22	0.22	0.22	0.22	0.22		
<u>Axial Blanket</u>											
Top Coolant	Volume	Fraction		0.27	0.27	0.27	0.27	0.27	0.27	0.640	0.406
Fertile	"	"		0.45	0.45	0.45	0.45	0.45	0.45	0.221	0.329
Stainless Steel	"	"		0.08	0.08	0.08	0.08	0.08	0.08	0.39	0.223
Graphite	"	"		0.20	0.20	0.20	0.20	0.20	0.20		
Bottom Coolant	"	"		0.12	0.12	0.12	0.12	0.12	0.12		
Graphite	"	"		0.20	0.20	0.20	0.12	0.12	0.12		
Stainless Steel	"	"		0.08	0.08	0.08	0.08	0.08	0.08		
Fertile	"	"		0.60	0.60	0.60	0.60	0.60	0.60		

Top Axial Blanket (contd.)

coolant channel size	1.78 cm x 45.72 cm x 27.3 cm
light of element	50 cm
length of each side of element	31.53 cm

Bottom Axial Blanket

blanket type	Hexgonal element (fertile rods inserted in graphite matrix or Beo matrix) with a 4.5" diameter hole at center
no. of elements	253
no. of rods per element	24
blanket pellet	452 cm
cladding thickness	1.27 mm
height of element	50 cm
length of each side of element	31.53 cm

Figures II-5-6 and II-5-7 show the details for bottom and top axial blankets.

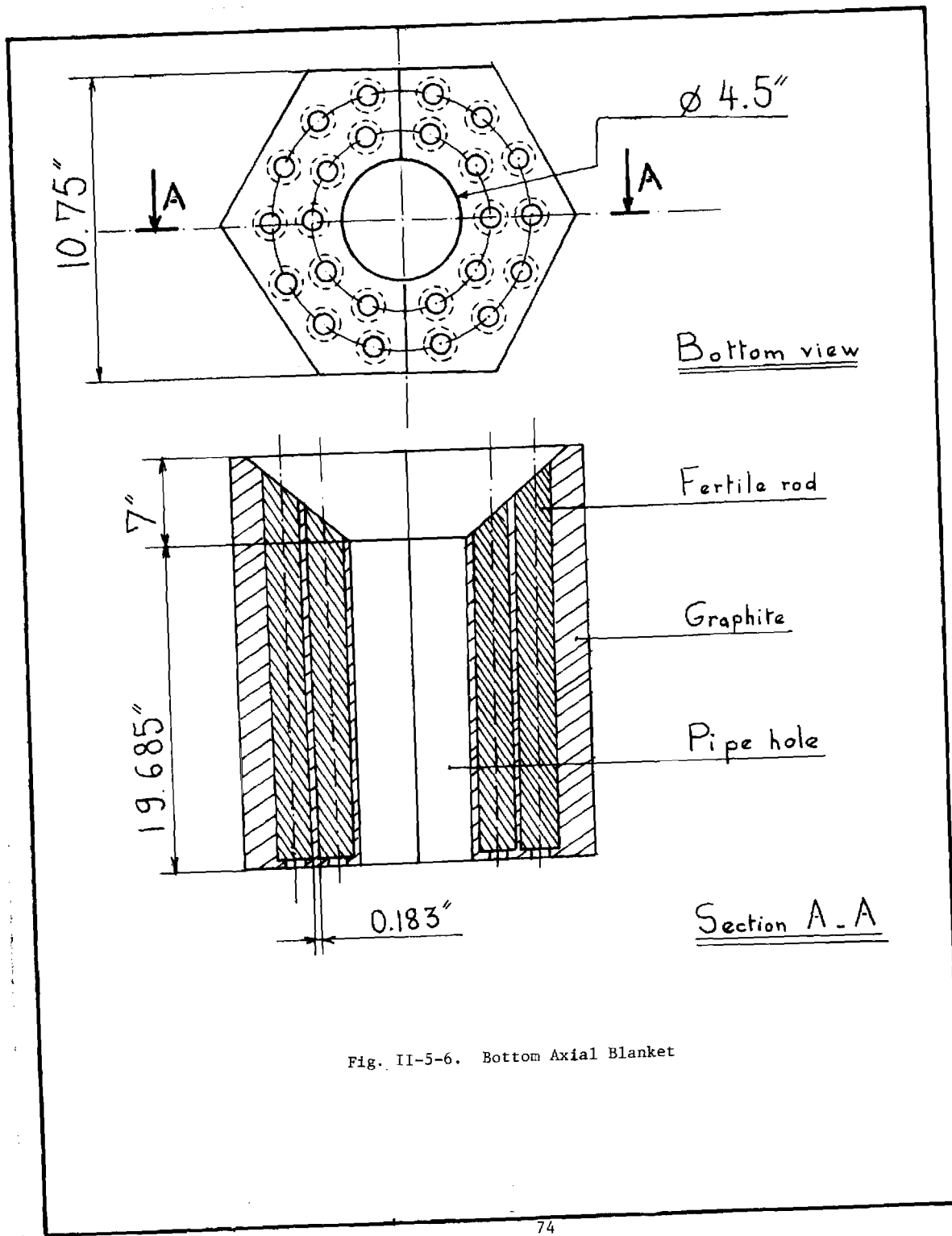


Fig. II-5-6. Bottom Axial Blanket

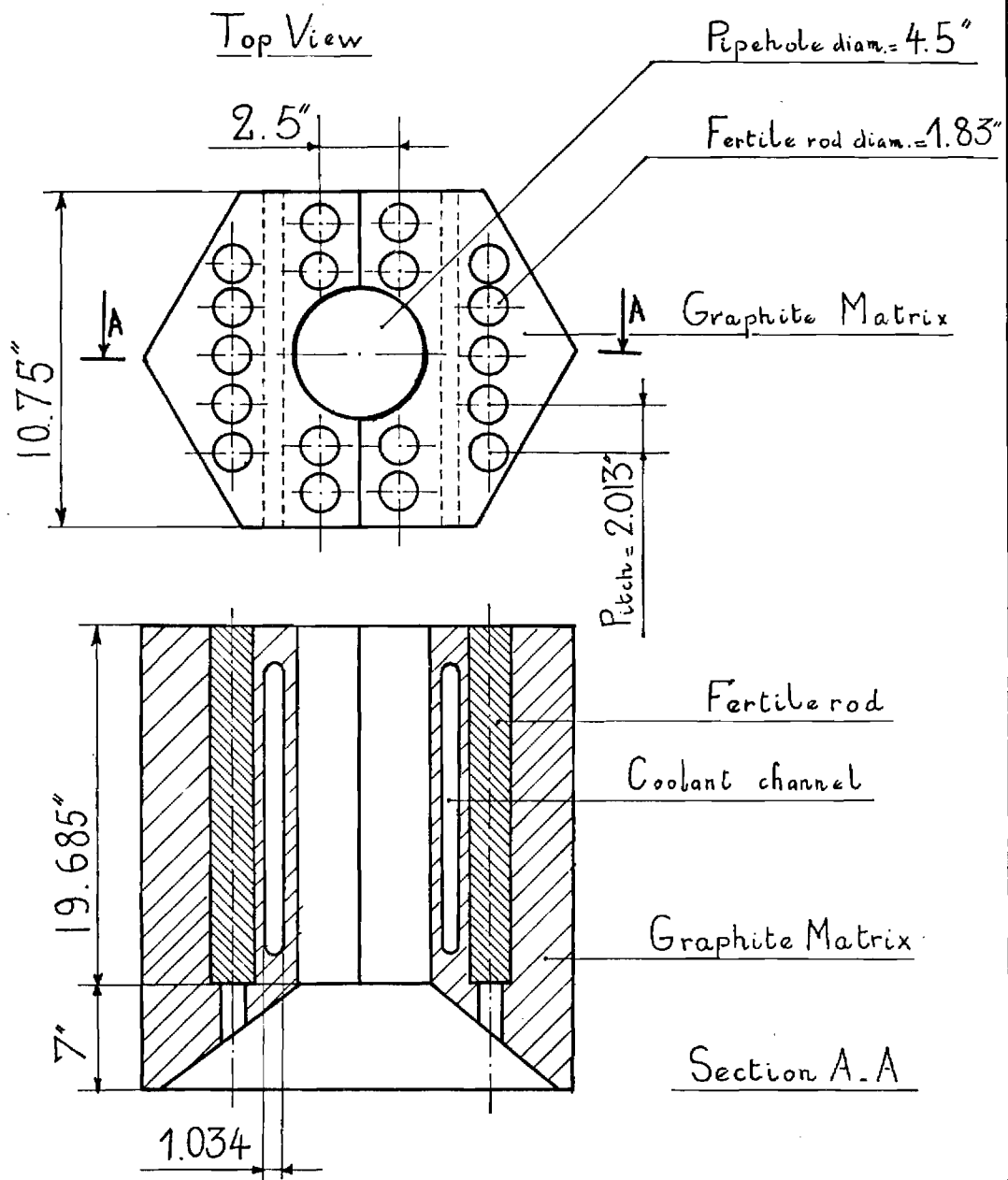


Fig. II-5-7. Top Axial Blanket

5.3 Cross Section Generation

The MC² code,⁽³⁰⁾ which utilizes the narrow resonance treatment, equivalence theory and an exact Legendre treatment for slowing down, was used. A total of about 2000 energy groups covered the energy range of 15 MeV to 0.75 eV. A thermal group was added. ENDF/B Version III data were used.

The unit cell specification accounted for self-shielding. The kernels were assumed homogeneous and energy self-shielding was taken into consideration by the narrow resonance treatment in MC². The cross section sets generated for the Suspended-Bed Reactor consisted of 25 broad energy groups averaged over the fundamental mode spectrum of each composition.

5.4 Reactor Calculations

A set of spherical calculations were performed with the two basic fuel kernels chosen for the Suspended-Bed Reactor: dicarbide and metallic kernels. These calculations were used to delineate the dependence of critical mass and conversion ratio on coolant volume fraction (Fig. II-5-9 and II-5-10). The calculations comprised a one-region core, 35-cm blanket and 32-cm graphite reflector. Tables II-5-II and II-5-III show the results for the dicarbide and metallic fuels respectively.

Table II-5-IV compares the parameters of Suspended-Bed Reactor in spherical geometry with comparable GCFR and an LMFBR parameters. The Suspended-Bed Reactor fundamental mode spectrum is compared with that of a typical LMFBR in Fig. II-5-11. It is noted that the Suspended-Bed Reactor spectrum is significantly softer than that of an LMFBR but much

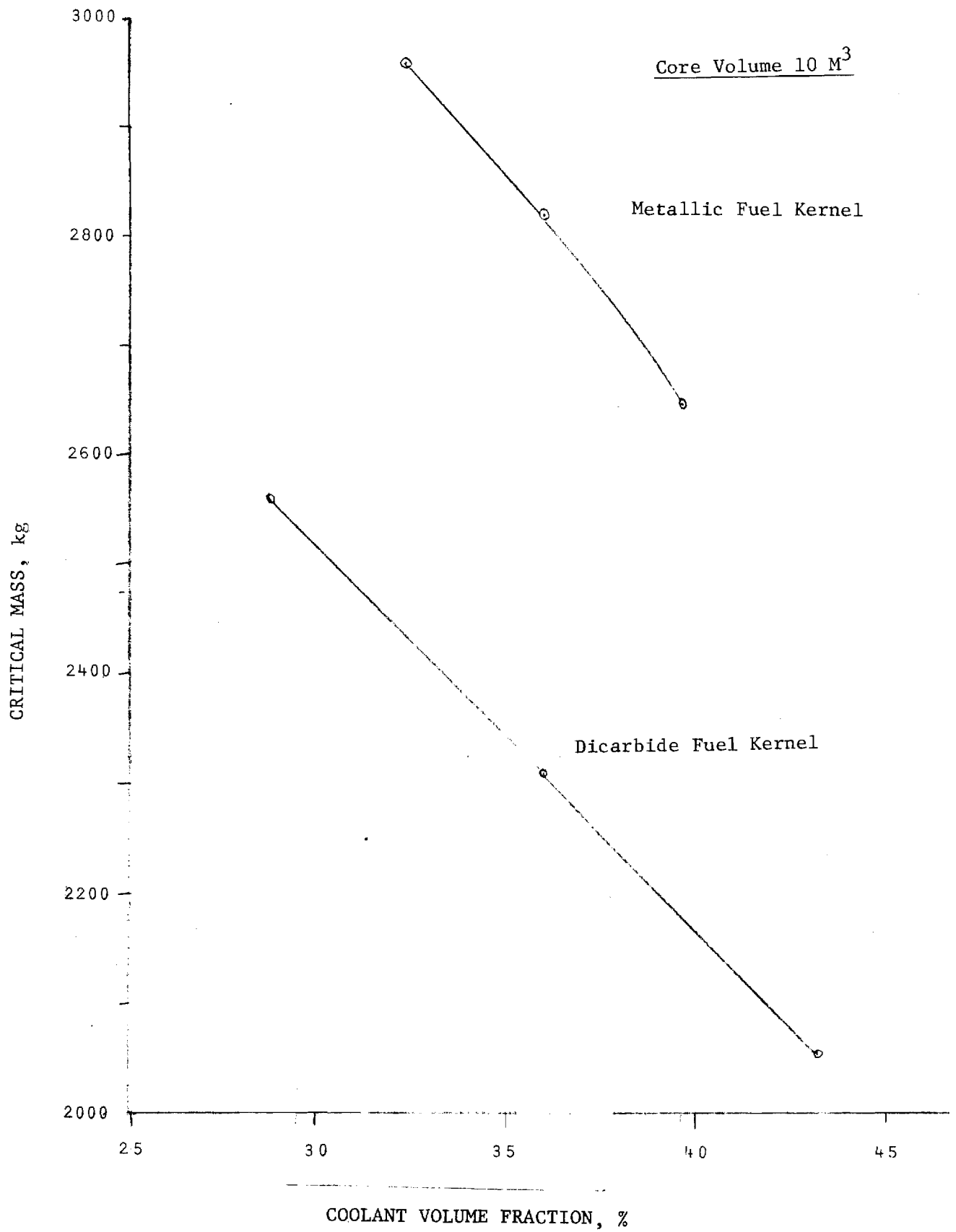


Fig. II-5-8. Critical Mass vs Coolant Volume Fraction

Core Volume $10 M^3$

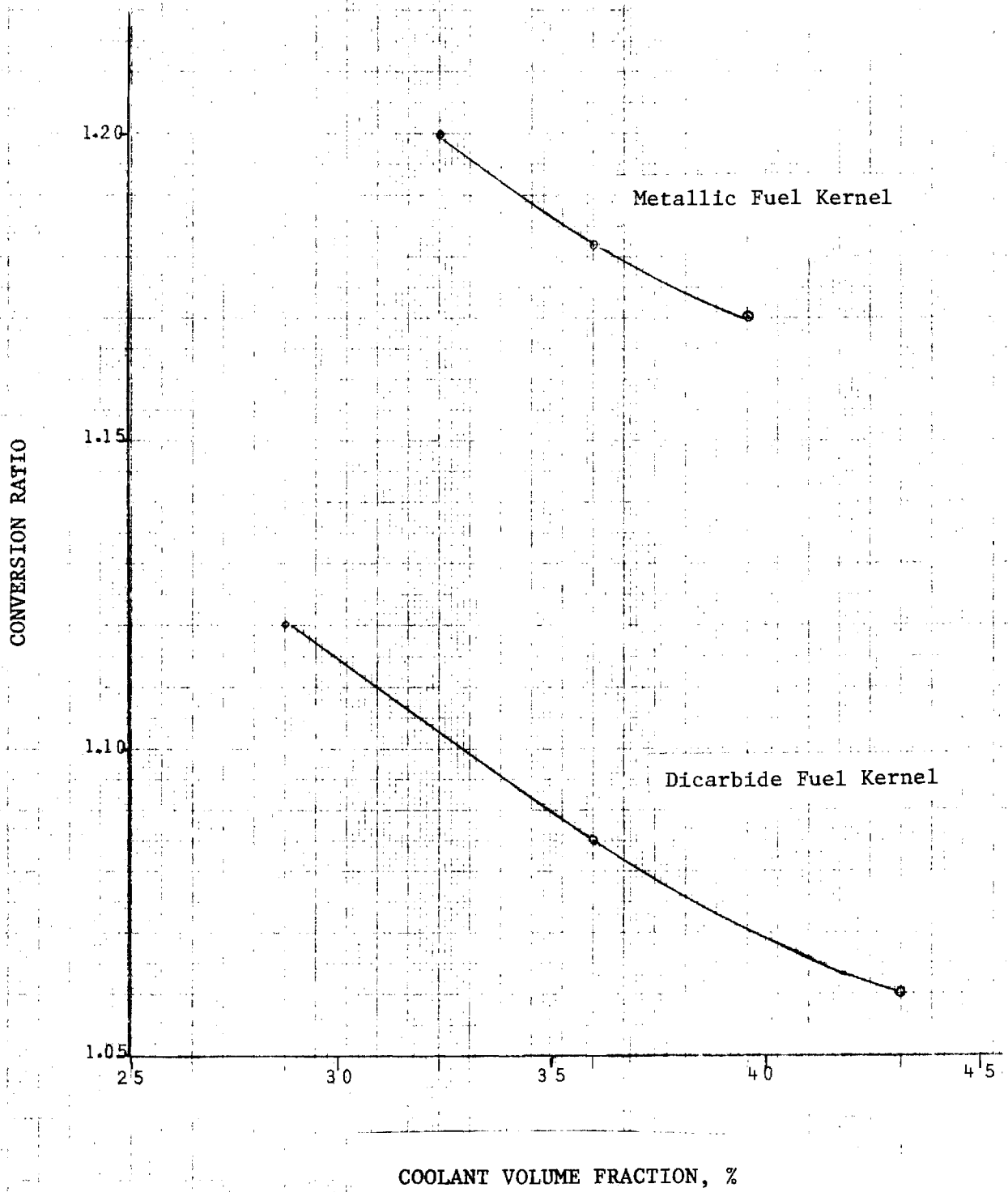


Fig. II-5-9. Conversion Ratio vs Coolant Volume Fraction

Table II-5-II

Fissile and Fertile Material Requirements and Conversion Ratios as a Function of Coolant Volume Fraction in Dicarbide Spherical Suspended-Bed Reactor

Core Geometry	Spherical, Dicarbide					
	10	6.4	10	11.67	10	10.4
Core Volume, m ³	28.86	28.86	36.1	36.1	43.3	43.3
Coolant Volume Fraction (%)	1.12	1.13	1.085	1.09	1.06	1.07
Conversion Ratio	12	13	13.5	13	15	15
Critical Enrichment (%)	2564	1709	2311	2597	2054	2136
Fissile Inventory (kg)	18875	11491	14816	17254	11633	12099
Fertile Inventory Core (kg)	62365	48368	62365	66086	25839	64236
Blanket (kg)	21439	13206	17127	19851	13687	14235
Total Heavy Metal Inventory In-core (kg)						

Table II-5-III

Fissile and Fertile Material Requirements and Conversion Ratios as a Function of Coolant Volume Fraction in the Metallic Spherical Suspended-Bed Reactor

Core Geometry	Spherical, Metallic					
	5.9	10	10	12.8	10	13.1
Core Volume, m ³	5.9	10	10	12.8	10	13.1
Coolant Volume Fraction (%)	32.5	32.5	36.1	36.1	39.7	39.7
Breeding Ratio	1.2	1.191	1.182	1.18	1.174	1.17
Critical Enrichment (%)	124	11	11.5	11	12	11.5
Fissile Inventory (kg)	1911	2965	2818	3450	2646	3322
Fertile Inventory Core (kg)	14017	23988	20230	27913	19491	25570
Blanket (kg)	46200	62365	62365	72654	62365	73275
Total Heavy Metal Inventory In-core (kg)	15928	26952	23048	27913	22137	28892

Table II-5-IV. SBR Comparison with Other 1000 MWe Reactors

Reactor Type	Suspended-Bed Reactor		GCFR (Ref. 31)	LMFBR (Ref. 32)
	Dicarbide Kernel	Metallic Kernel	Oxide	Oxide
Fuel	Dicarbide Kernel	Metallic Kernel	Oxide	Oxide
Particle Coating	ZrC - SiC - PyC	ZrC - SiC - PyC		
Clad Material			S.S.	S.S.
Blanket Material	Th metal in Graphite Matrix	Th metal in Graphite Matrix	ThO ₂	UO ₂
Coolant	He	He	He	Na
Core Power Density MW/m ³	250	250	240	380
Core Volume, (m ³)	10	10	10.306	6.3
Specific Power, Mw/kg	1.08	0.887	0.827	1.0
Critical Mass, kg	2311	2818	2910	2400
Conversion Ratio	1.08	1.18	1.21	1.20

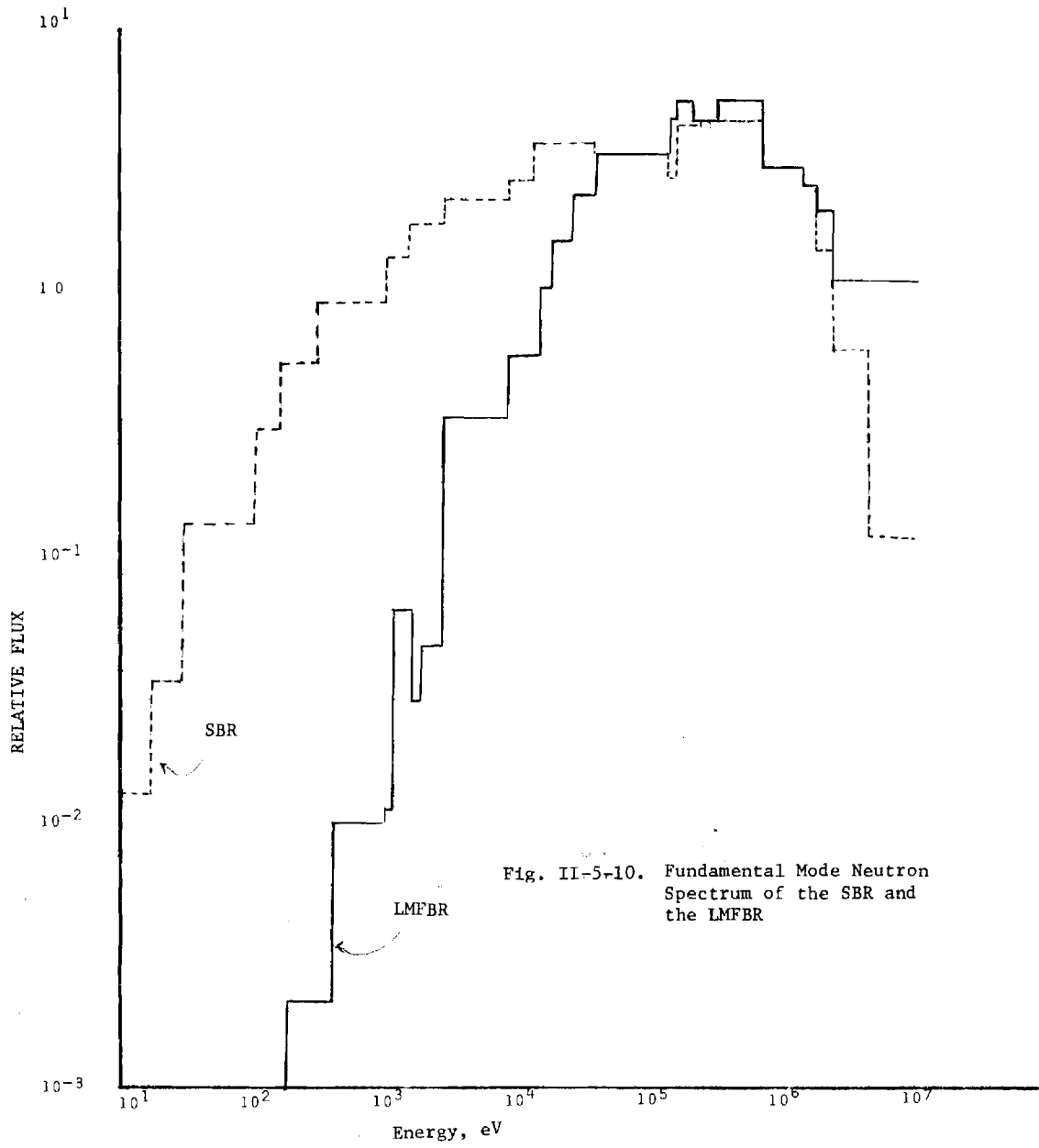


Fig. II-5-10. Fundamental Mode Neutron Spectrum of the SBR and the LMFBR

harder than the LWR's.

The void coefficient of the coolant in the Suspended-Bed Reactor is small ($- 0.003\% \Delta k/k$), but negative.

5.5 The Suspended-Bed Reactor Cylindrical Calculations

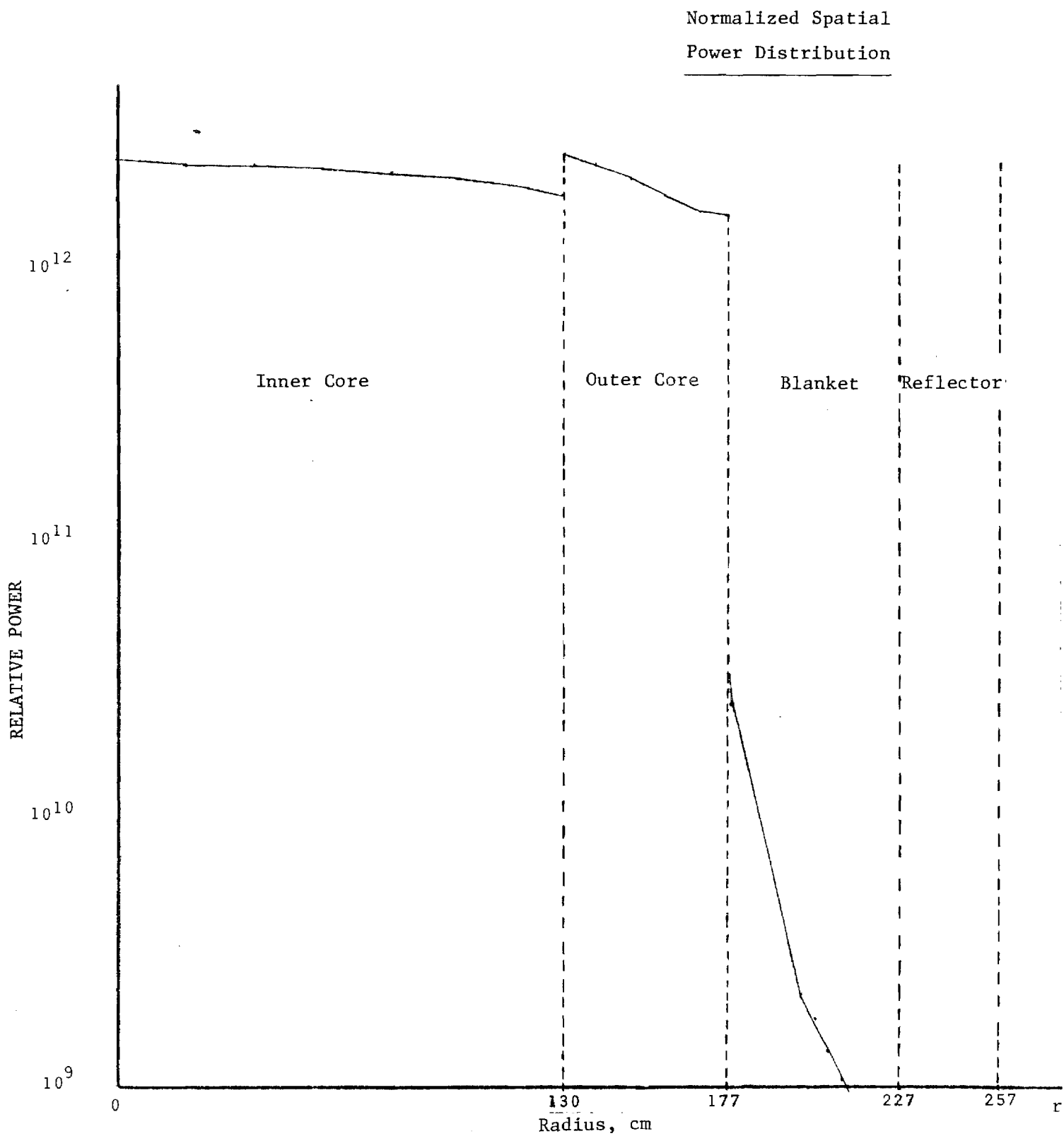
The physics parameters of the Suspended-Bed Reactor, as sketched in Fig. II-5-1 were calculated in cylindrical geometry. Table II-5-V summarizes the results. Figure II-5-11 shows the spatial power distribution.

When the reactor is shutdown the suspended bed collapses and the reactivity of the assembly in transition (see Fig. II-5-12) is less than 0.87.

Table II-5-V. Physics Parameters for Cylindrical Reactors

Parameter	Dicarbide Fuel	Metallic Fuel
Core volume, m ³	10.0	10.0
Inner core, m ³	5.64	5.64
Outer core, m ³	4.54	4.54
Enrichment		
inner core	16.0 %	12.8%
outer core	22.88%	18.3%
Total fissile inventory		
inner core, kg	1170.0	1507.0
outer core, kg	1430.0	1841.0
Total fertile		
inner core, kg	6143.0	10,266.0
outer core, kg	4820.0	7213.0
axial blanket, kg	41,166.0	41,166.0
radial blanket, kg	16,424.0	22,418.0
Conversion ratio	1.06	1.17
Power peaking factor	1.21	1.21
Heavy metal loading per particle, gm	0.0134	0.0175
Total number of particles	1.0128×10^9	1.19×10^9
Number of fuel particles per pipe	6.66×10^9	7.829×10^6

Fig. II-5-11. Spatial Power Distribution in the SBR



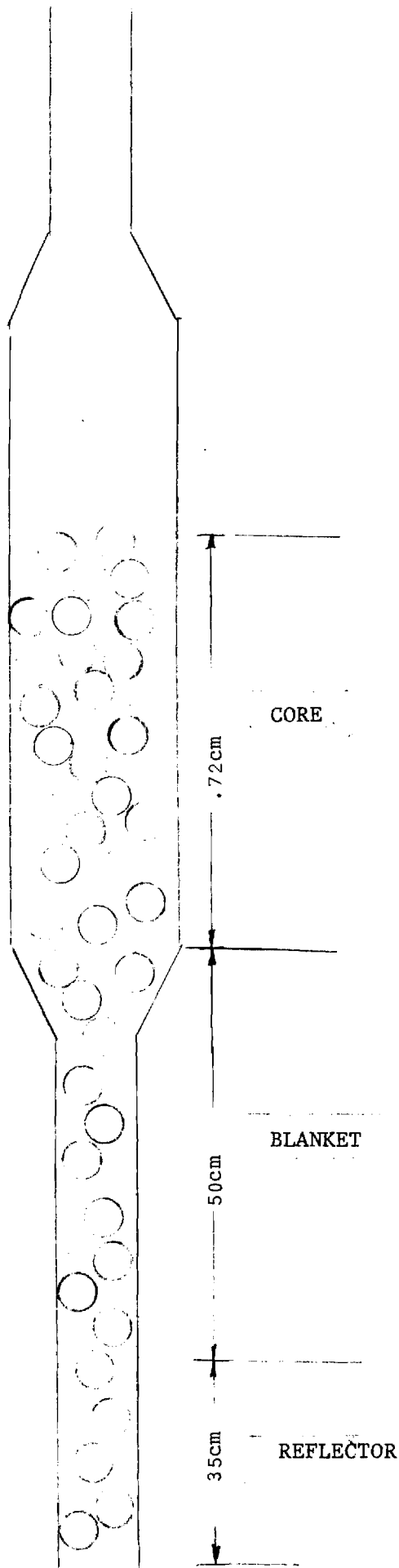


Fig. II-5-12. Assembly in Transition; $k_{eff} < 0.87$

6. Selection of Pipe Material and Sizes

The essential requirements for pipes' material in the Suspended-Bed Reactor are:

- (a) high melting point
- (b) high mechanical and creep strength for high temperature and high pressure operation
- (c) retention of satisfactory physical and mechanical properties at high temperature (1000°F) and pressure (1000) psi for long-term irradiations
- (d) compatibility with carbide
- (e) low cost.

Metals and alloys of particular interests are stainless steel 316, zircalloy and vanadium Ti ~ 20%.

Studies involving V-Ti alloys have indicated⁽²⁷⁾ that the 20% Ti-Vanadium alloy shows, (1) very little irradiation-induced swelling due to the absence of helium void formation, (2) hardly any irradiation-induced high temperature embrittlement, (3) relatively high creep strength which is maintained for long term irradiations, and (4) higher mechanical strength than S.S. 316 or zircalloy at high temperatures, to 800°C (1472°F). Thus, the V-20 Ti alloy appears to be a very promising pipe material. However, it is quite expensive; only a small amount of vanadium is produced commercially. The cost is approximately \$30/lb. With massive production, it is possible that the cost can be drastically decreased.

Zircalloy is widely used as a cladding material in thermal reactors due to its low thermal absorption cross sections. But in a fast reactor, the neutron spectrum is hard; the advantages of small thermal cross section are not significant. As a result, structural materials, such as stainless

steel with fairly high thermal absorption, can be used in fast reactor. Stainless steel is well developed and widely used in industry. It is the cheapest metal with reasonably good mechanical and irradiation behavior in high temperature and pressure environments. These are the main reasons why we chose stainless steel as a piping material for the Suspended-Bed Reactor.

The comparisons of mechanical, physical and nuclear properties for these three kinds of materials are listed in Table II-6-I. (33-35)

One-dimensional diffusion calculations were performed using V-Ti(20%) Zr and S.S. as piping material to study their effects on critical mass and breeding ratio. The results are shown in Table II-6-II. It is seen that with V-Ti one has almost the same breeding ratio as with stainless steel.

Pipe Size

The selection of pipe size mainly depends on the following factors:

- (a) cost
- (b) V.F. (volume fraction) of pipe material
- (c) removal of decay heat
- (d) operating pressure and operating temperature.

The general formula, recommended by the Power Boiler Section of the ASME boiler code and the ANSI code for pressure piping, is:

$$P/S = \frac{2(tm-C)}{D-2y(tm-C)}$$

Table II-6-I. Mechanical, Physical, and Nuclear Properties of
V-Ti(20%), Zircalloy 2 and 4, and S.S. 316

	<u>Unit</u>	<u>V-Ti 20%</u>	<u>Zircalloy 2,4</u>	<u>S.S. 316</u>
Melting point	$^{\circ}\text{F}$	3200 $^{\circ}\text{F}$	3310 $^{\circ}\text{F}$	2550-2650 $^{\circ}\text{F}$
Density	$\frac{\text{gm}}{\text{cm}^3}$	5.75	6.5	7.92
Linear thermal expansion	10^{-6} per $^{\circ}\text{C}$	9.4	5.9	19.7
Thermal conductivity	cal/cm/sec $^{\circ}\text{C}$	0.047	0.035 (25 $^{\circ}\text{C}$) 0.0315 (300 $^{\circ}\text{C}$)	0.035 (100 $^{\circ}\text{C}$) 0.050 (500 $^{\circ}\text{C}$)
Yield strength (0.2 % offset)	10^3 psi	30(25 $^{\circ}\text{C}$) 21 (1000 $^{\circ}\text{F}$) 19.5 (1300 $^{\circ}\text{F}$)	42 (25 $^{\circ}\text{C}$)	
Tensile strength	10^3 psi	75 (25 $^{\circ}\text{C}$) 69.2 (1000 $^{\circ}\text{F}$) 46.0 (1300 $^{\circ}\text{F}$)	70 (25 $^{\circ}\text{C}$)	100 (25 $^{\circ}\text{C}$) 95 (500 $^{\circ}\text{C}$) 85 (700 $^{\circ}\text{C}$) 52 (900 $^{\circ}\text{C}$)
Creep strength		good	bad	fair
Compatibility with carbide		good	unknown	good
Irradiation behavior		good	fair	fair
Thermal absorption cross section	barn	4.88	0.18	3.0

Table II-6-II

Effects of Pipe Material on Neutronic Performance

Pipe material	S. S.	Zr	V-Ti(20%)
Enrichment	12%	12%	12%
Relative Breeding Ratio	1.0	0.99	1.0
Relative critical mass	1	0.97	0.86

where

- P = maximum internal operating pressure in lb/in²
- S = allowable stress in material due to internal pressure
- t_m = minimum pipe wall thickness in inches
- C = allowance for threading, mechanical strength, and/or corrosion, in inches
- D = outside diameter of pipe, inches
- y = a coefficient having values as follows:
- 0.4 up to, and including, 1050^oF
 - 0.5 for 1100^oF
 - 0.7 for 1150^oF, and above.

Calculations show that the volume fraction of S.S. 316 corresponding to the required thickness to have internal operating pressure 1000 psi at temperature 1000^oF almost stay constant as pipe sizes are increased from 1 1/2" to the 10". For the Suspended-Bed Reactor it is economical to keep the number of pipes in the core reasonably low. However, removal of decay heat requires that pipes, 4" or smaller, be used.

The pipe size chosen for the core region was 10", schedule No. 80S. The pipe size above and below the core region is reduced to 4", schedule No. 40S. Additional benefits which result from this arrangement are:

1. adequate space among 4" pipes is provided to accommodate axial blanket and reflector so as to increase breeding ratio and decrease critical mass.
2. adequate space is provided to stack graphite blocks below the reactor for decay heat, heat sink.

3. adequate space is provided for the valves needed to control flow.

The schedule number given in A.S.T.M. specification A409 (corrosion resistant pipes) for 10" and 4" S.S. 316 pipes for service at 1000^oF and pressure 1000 psi is "80S" and "40S" and are listed in Table II-6-III.

Since the Suspended-Bed Reactor will have gas exit temperatures exceeding 1500^oF, it is necessary to insulate the pipes such that the temperature drop across the insulation is equal or greater than 500^oF. The material chosen for this purpose is ZrO₂. It has a high melting point (2600^oC) and a very low thermal conductivity (~.004 cal/cm-sec^oC). It is compatible with stainless steel.

Our calculations show that a 10-20 mils thick lining on the inside of each pipe would be more than enough to insulate the pipes. We chose 50 mils ZrO₂ coating.

Table II-6-III

Design Properties of Pipes

nominal pipe size and outside diameter	schedule number	wall thickness inches	inside diameter inches	Cross-Sectional		weight of pipe lb/ft
				metal area sq. in.	flow area sq. in.	
4 D = 4.500	40S	.237	4.026	3.17	12.73	10.79
10 D = 10.750	80S	.500	9.750	16.1	74.7	54.7

7. Decay Heat Removal

After a reactor has been shut down, large amounts of heat continue to be generated in the fuel due to the presence of fission products. Measures must be taken to ensure removal of this heat, especially if shutdown is a consequence of interruption of coolant flow.

In the Suspended-Bed Reactor, if the coolant flow is decreased rapidly, the fuel particles will fall to the bottom by gravity force where physical spacing among pipes and poison in the pipes will bring about safe shutdown. The graphite blocks among the pipes serve as decay sink and helps keep temperatures low without causing any material damage for a period of at least 24 hours.

The purpose of this section is to calculate the amount of graphite required to withstand decay heat for at least a period of one day with no coolant flow at all.

The following assumptions are made:

- a. total power = 2500 Mwt
- b. peak power density = 300 MW/m³
- c. maximum bed center line temperature = 3200^oF
- d. maximum pipe wall temperature = 1200^oF
- e. average temperature rise of graphite block = 1000^oF

The total amount of graphite is determined by:

$$M = \frac{1}{C_p \cdot \Delta T} \int_0^t p(t) dt$$

where M is the mass of graphite

C_p is the specific heat of graphite

Δt is the temperature rise in graphite block

$\int_0^t p(t)dt$ is the integral of decay power over cooling time, i.e.

the total decay heat during t .

The result of calculations are given in Table II-7-I.

Table II-7-I
Mass of Graphite Block Required to Remove
Decay Heat for 1, 12, and 24 hours After Shutdown.

Time After Shutdown		
1 hour	12 hours	24 hours
Decay heat in MWD		
3.9	13.4	21.5
Total amount of graphite (density = 1.8 g)		
20 m ³	68.7 m ³	110 m ³

It is seen that the amount of graphite required to accommodate decay heat for one day following shut down is only 110 m³ which is equivalent to a solid cylinder of 3.27 m radius and 3.27 m height.

The calculation of the temperature across the 4" pipe profile was done with the following equations:

a. Temperature across the pipe wall

$$T_i - T_o = \frac{q''' r_i^2}{2 Ks} \ln \frac{r_o}{r_i}$$

T_i = pipe inside wall temperature

T_o = pipe outside wall temperature

r_i = pipe inside radius

r_o = pipe outside radius

Ks = thermal conductivity of pipe material

q''' = power density

b. Temperature across the bed:

$$T_{\phi} - t_1 = \frac{q''' r_i^2}{4 k_e}$$

T_φ: bed center line temperature

K_e: bed effective thermal conductivity

The bed effective thermal conductivity is about one-tenth of the particle overall thermal conductivity according to reference. (36)

Table II-7-II summarizes the results for various pipe sizes. It can be seen that only the 4" schedule 40S pipe meet the guidelines outlined earlier. The maximum fuel bed center-line temperature was 2894^oF considerably lower than design limits.

Table II-7-II

Temperature Distribution for Various Sizes of Pipes

Size	Maximum bed center line temperature	Maximum wall temperature	Graphite temperature
4"	2894 ^o F	739 ^o F	500 ^o F
6"	5820 ^o F	930 ^o F	500 ^o F
10"	14366 ^o F	1727 ^o F	500 ^o F

8. Considerations Leading to Choice of Suspended-Bed Reactor Parameters

Initially it was thought that fluidized bed reactors would yield superior power densities. However, it soon was realized that such was not the case. Figure II-8-1 shows the power density as a function of particle size for a coating thickness to diameter of kernel ratio of 1/10. Three bed heights were considered: 1, 2, and 3 meters. Gas pressure, inlet temperature and maximum fuel temperature were set at 1000 psi, 500°F and 2400°F respectively. The gas outlet temperature as a function of particle size is shown in Fig. II-8-2, The pressure loss as a function of bed height is shown in Fig. II-8-3. From these results, it was found that the maximum power density in fluidized beds is rather small ~ 12-30 MW/m³.

The gas static pressure affects the power density slightly. Figure II-8-4 shows the power density as a function of particle diameter at three pressures: 1000, 1500, and 2000 psi. Finally, the dependence of power density on gas inlet temperature is shown in Fig. II-8-5.

As a consequence of this study, it was realized that fluidized bed reactors have relative low power densities. The breeding ratio and good doubling times require high fuel volume fraction and high power density. To overcome these limitations, it was decided to increase the gas velocities and trap the coated particles in the core by means of a screen so that the reactor would be a suspended-bed-reactor, i.e. fixed bed in a suspended state.

A parametric study of the suspended-bed-reactor concept was performed. Figure II-8-6 shows power density vs gas velocity for various particle sizes. It is seen that for particles 2 mm diameter or smaller and gas velocities of 10-20 meters/sec the power densities possible are 200-300 Mw/m³. The

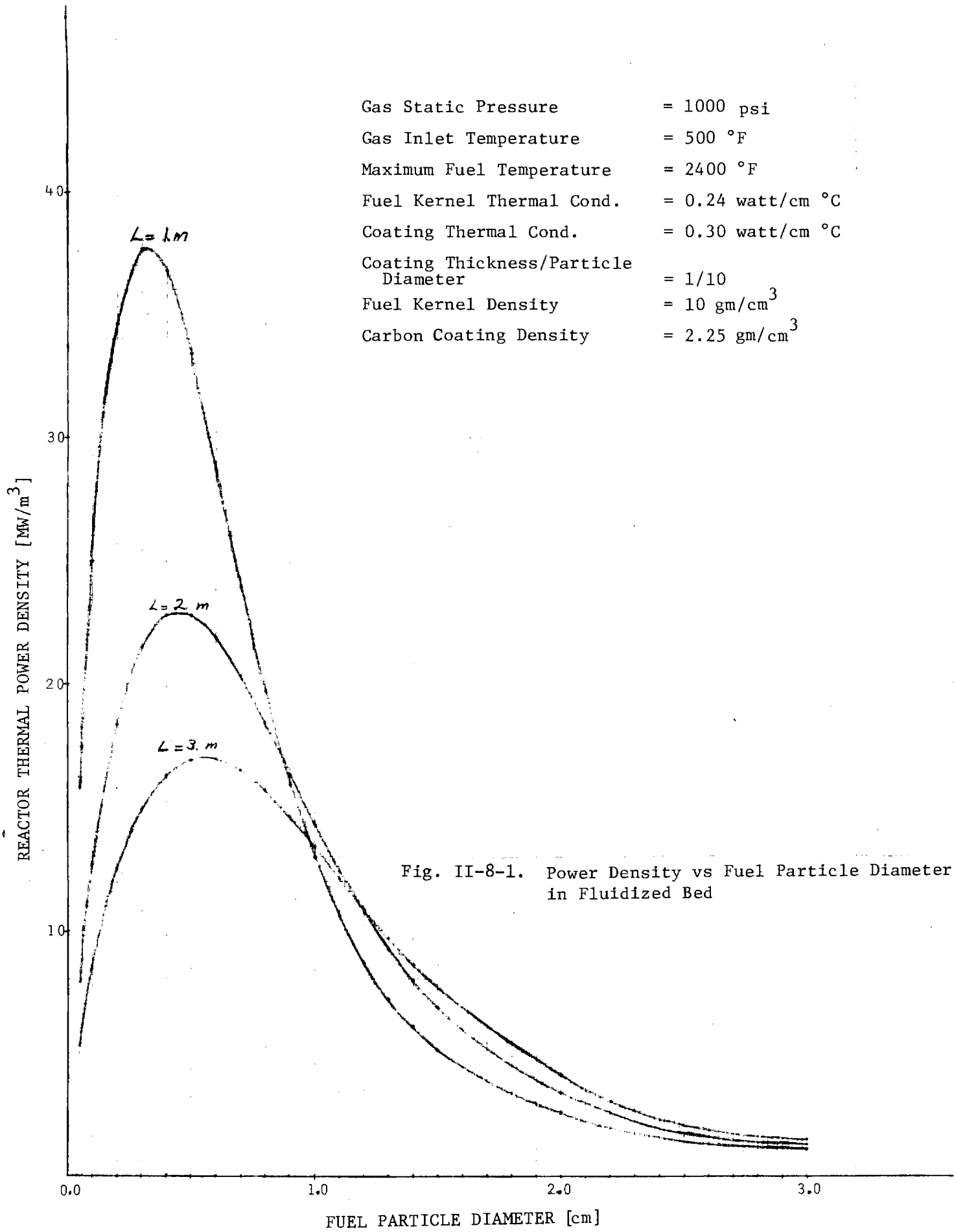
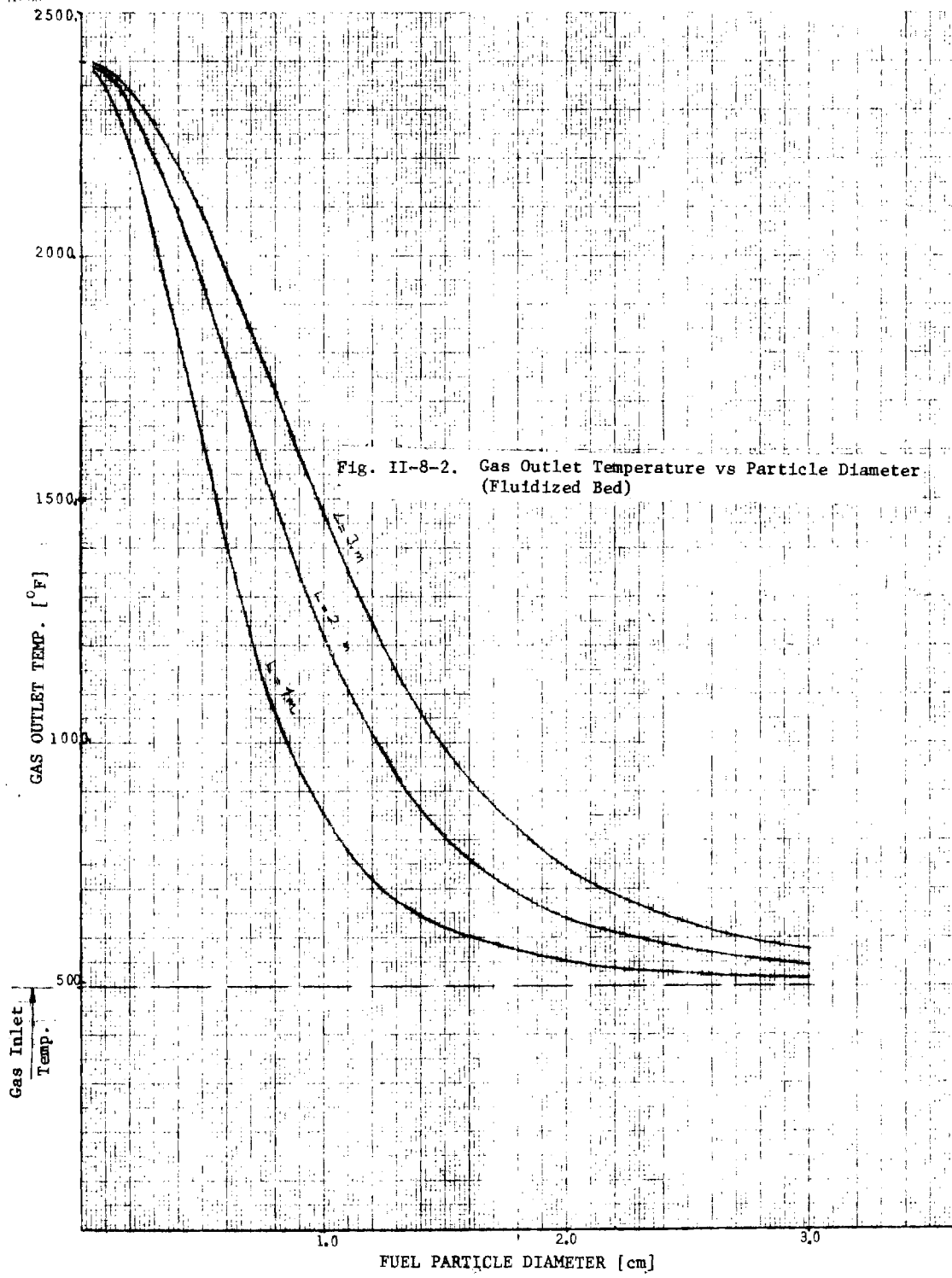


Fig. II-8-1. Power Density vs Fuel Particle Diameter in Fluidized Bed



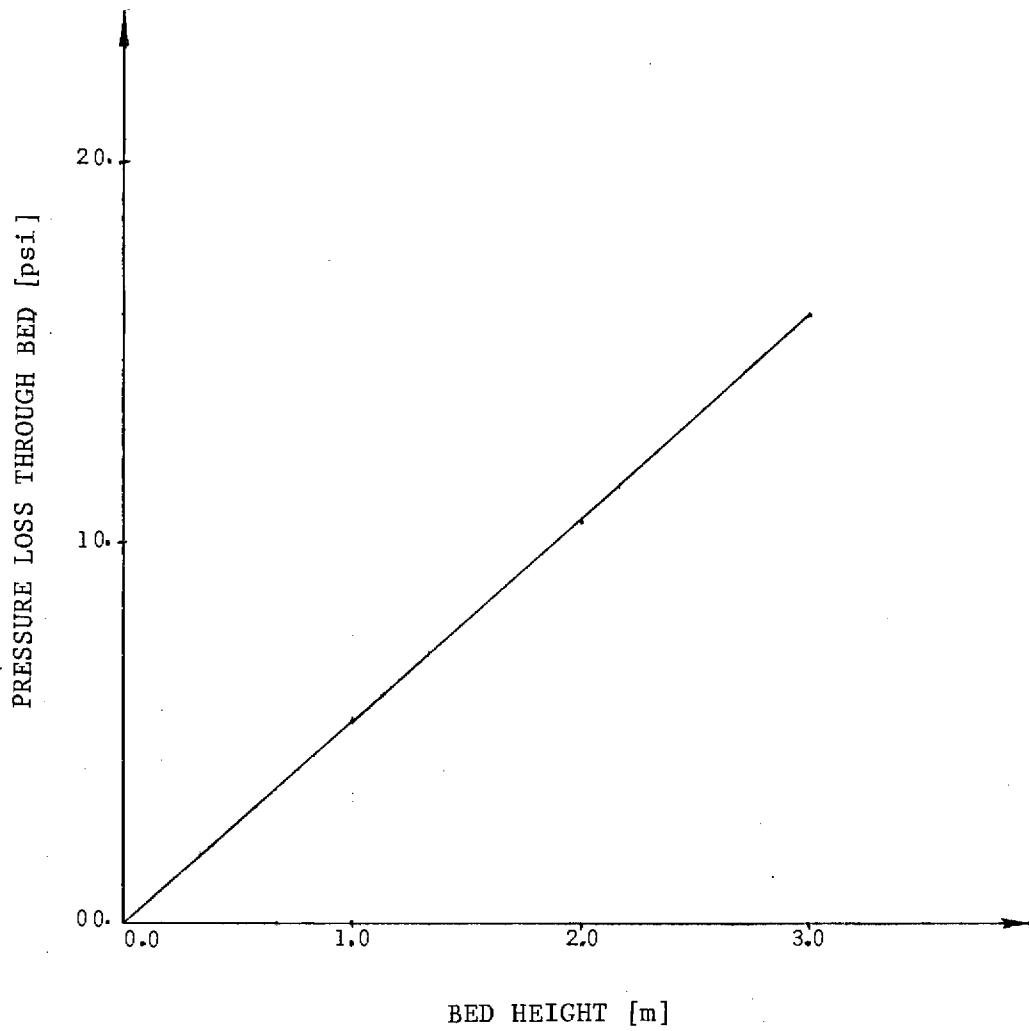
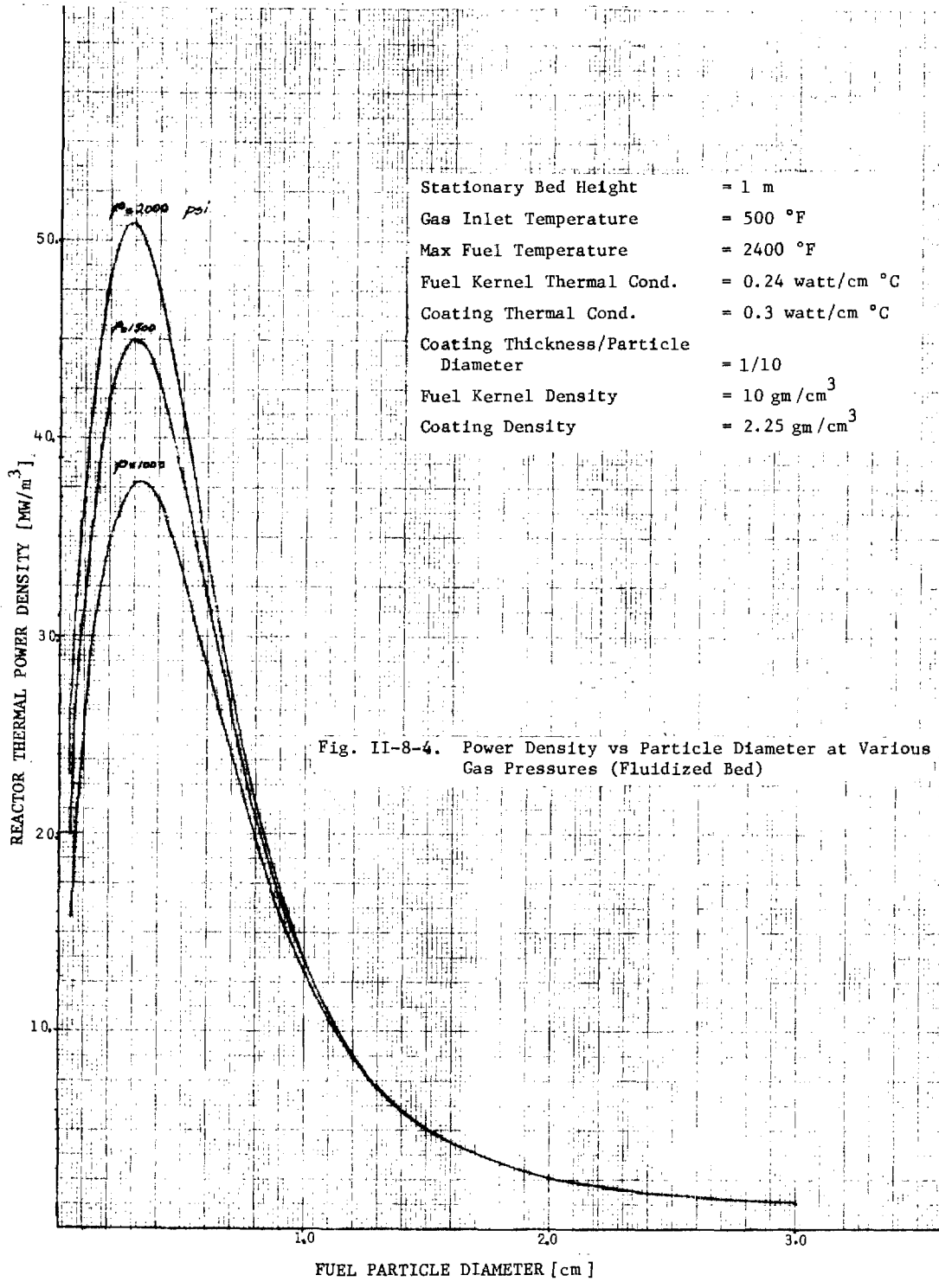
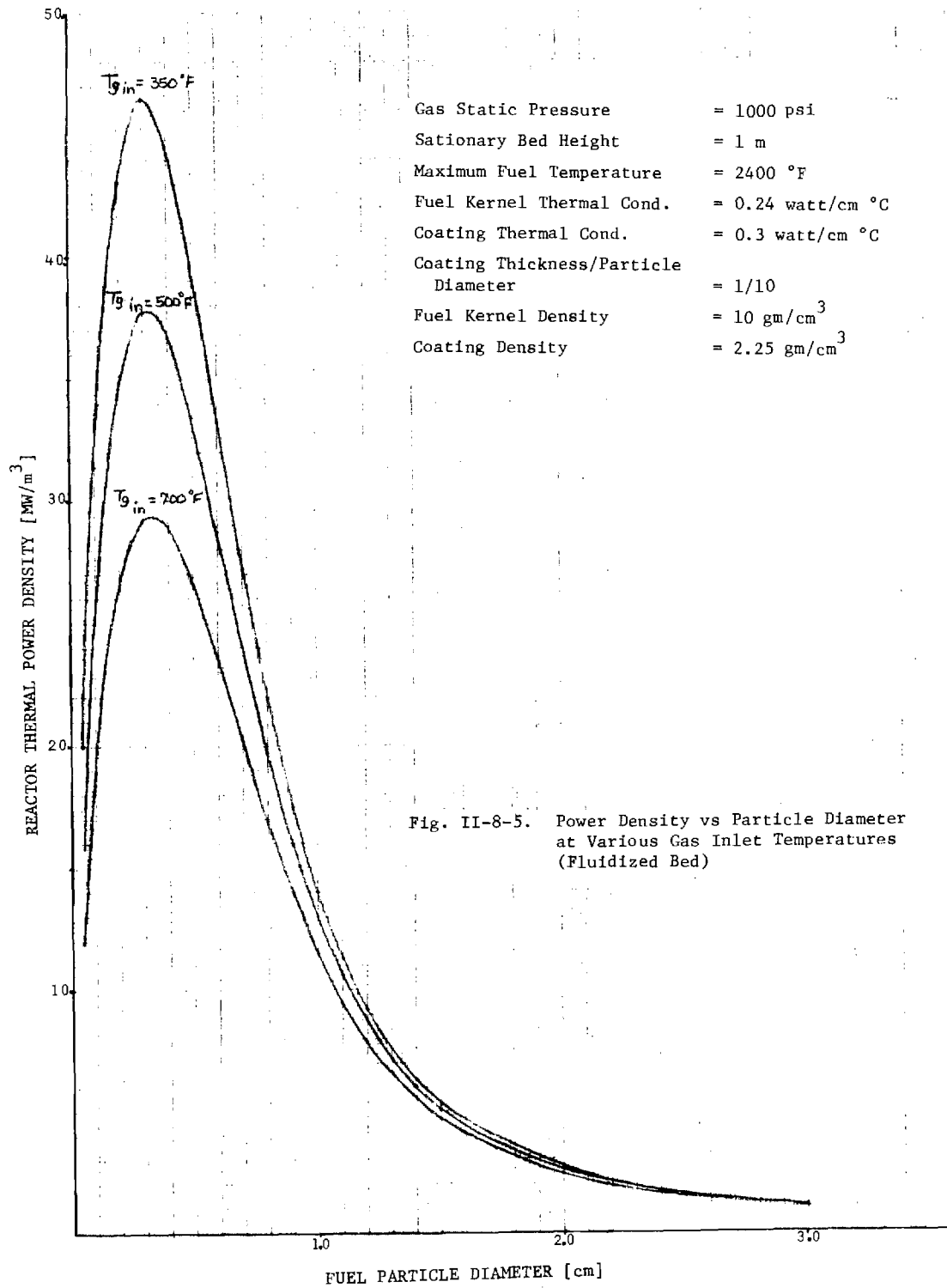


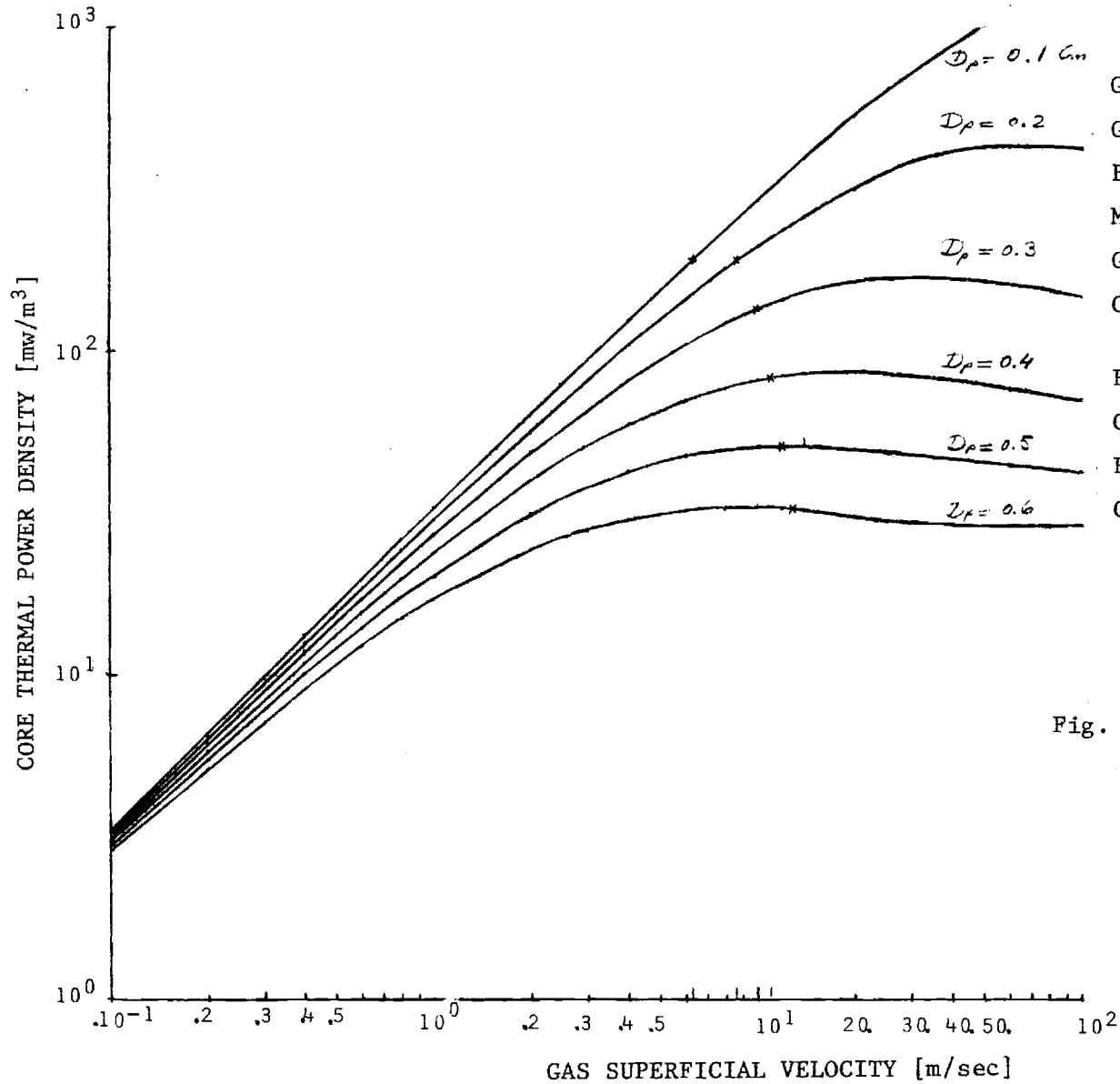
Fig. II-8-3. Pressure Loss vs Bed Height (Fluidized Bed)





Gas Static Pressure = 1000 psi
 Stationary Bed Height = 1 m
 Maximum Fuel Temperature = 2400 °F
 Fuel Kernel Thermal Cond. = 0.24 watt/cm °C
 Coating Thermal Cond. = 0.3 watt/cm °C
 Coating Thickness/Particle Diameter = 1/10
 Fuel Kernel Density = 10 gm/cm³
 Coating Density = 2.25 gm/cm³

Fig. II-8-5. Power Density vs Particle Diameter at Various Gas Inlet Temperatures (Fluidized Bed)



Gas Static Pressure = 1000 psi
 Gas Inlet Temperature = 500 °F
 Bed Height = 1 m
 Maximum Fuel Temperature = 2400 °F
 Gas Volume Fraction = 50%
 Coating Thickness/Particle Diameter = 1/10
 Fuel Kernel Thermal Cond. = 0.24 watt/cm °C
 Coating Thermal Cond. = 0.3 watt/cm °C
 Fuel Kernel Density = 10.0 gm/cm³
 Coating Density = 2.25 gm/cm³

Fig. II-8-6. Power Density vs Gas Velocity in Suspended-Bed Reactor

gas outlet temperature for each particle size as a function of gas velocity is shown in Fig. II-8-7. The corresponding pressure drop is shown in Fig. II-8-8. Figure II-8-9 shows the power density dependence on the void fraction and the corresponding pressure drop for 1 mm particles and Figure II-8-10 shows the same parameters for 2 mm particles.

The results indicate that power densities between 200-500 MW/m³ at acceptable pressure losses are indeed possible.

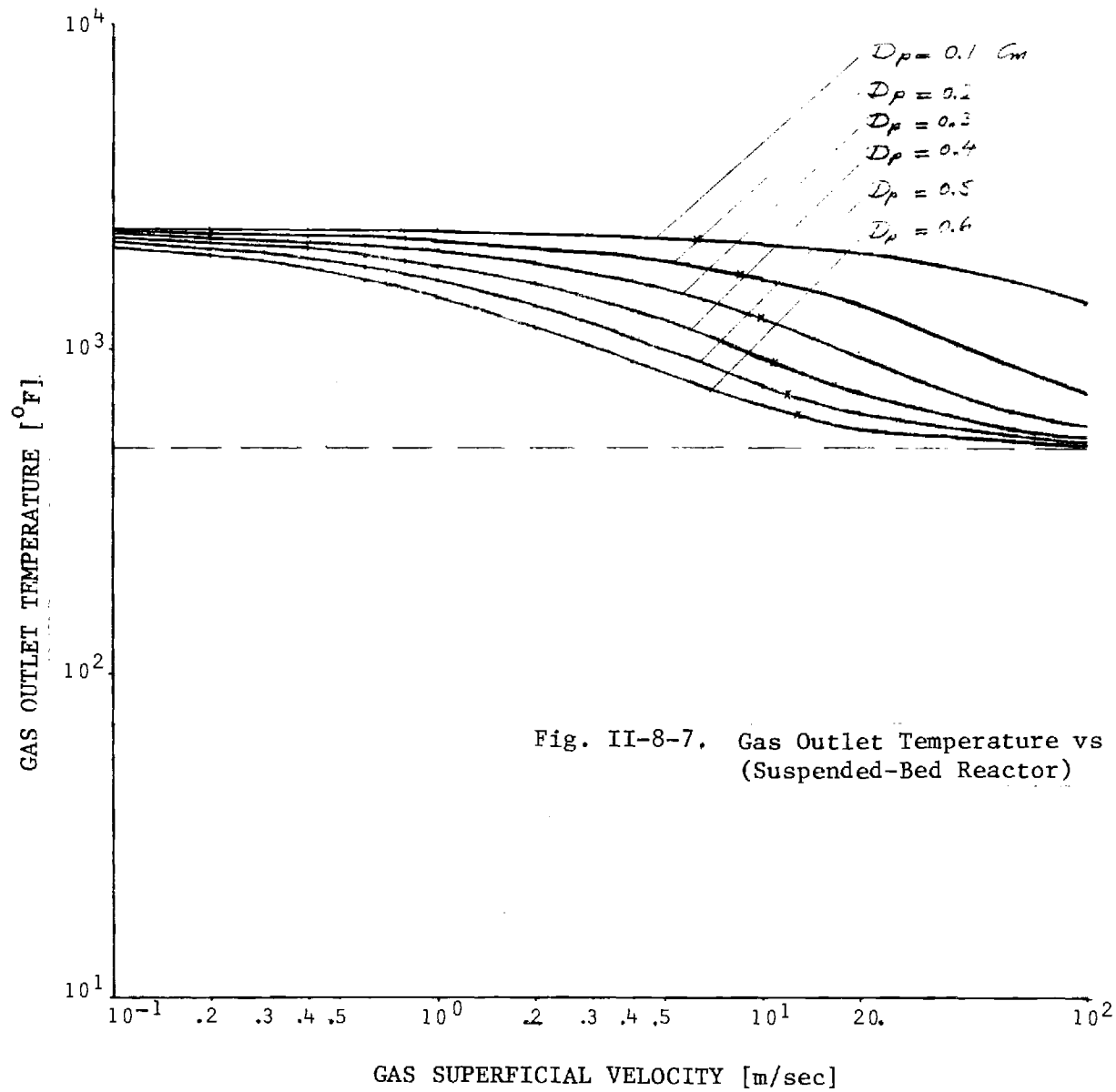


Fig. II-8-7. Gas Outlet Temperature vs Gas Velocity (Suspended-Bed Reactor)

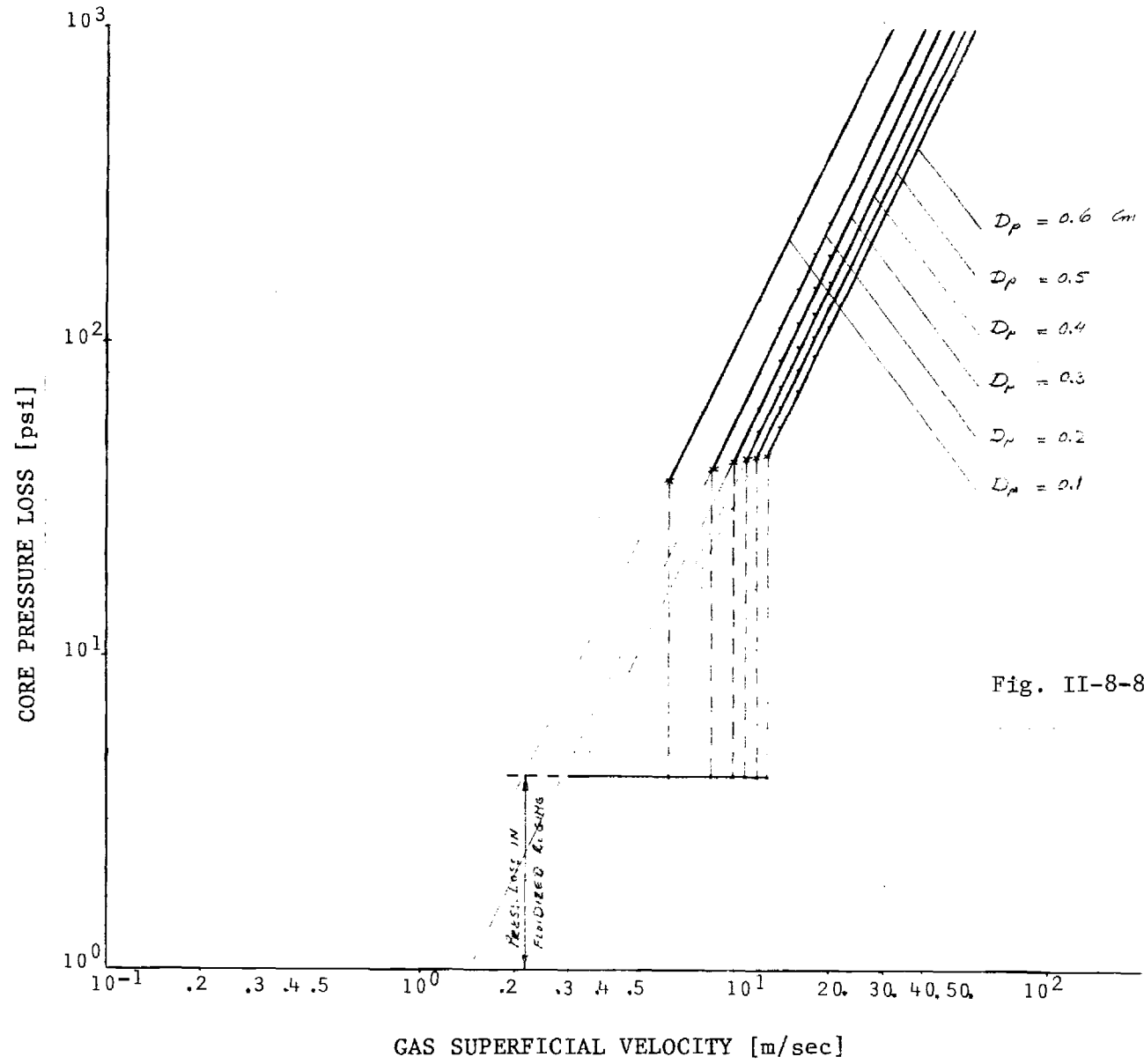


Fig. II-8-8. Pressure Drop vs Gas Velocity (Suspended-Bed Reactor)

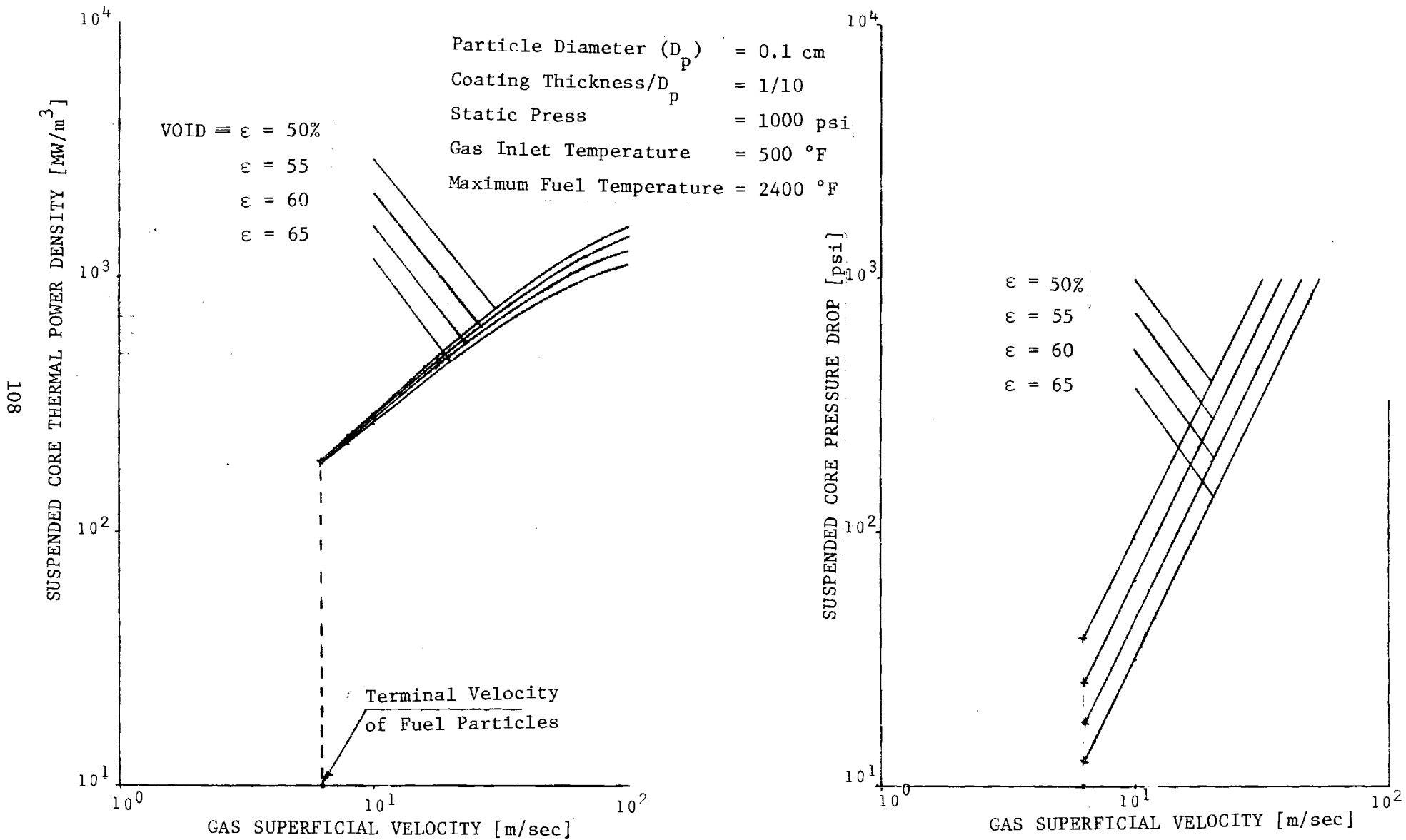


Fig. II-8-9. Power Density and Pressure Loss vs Gas Velocity at Various Bed Void Fractions

601

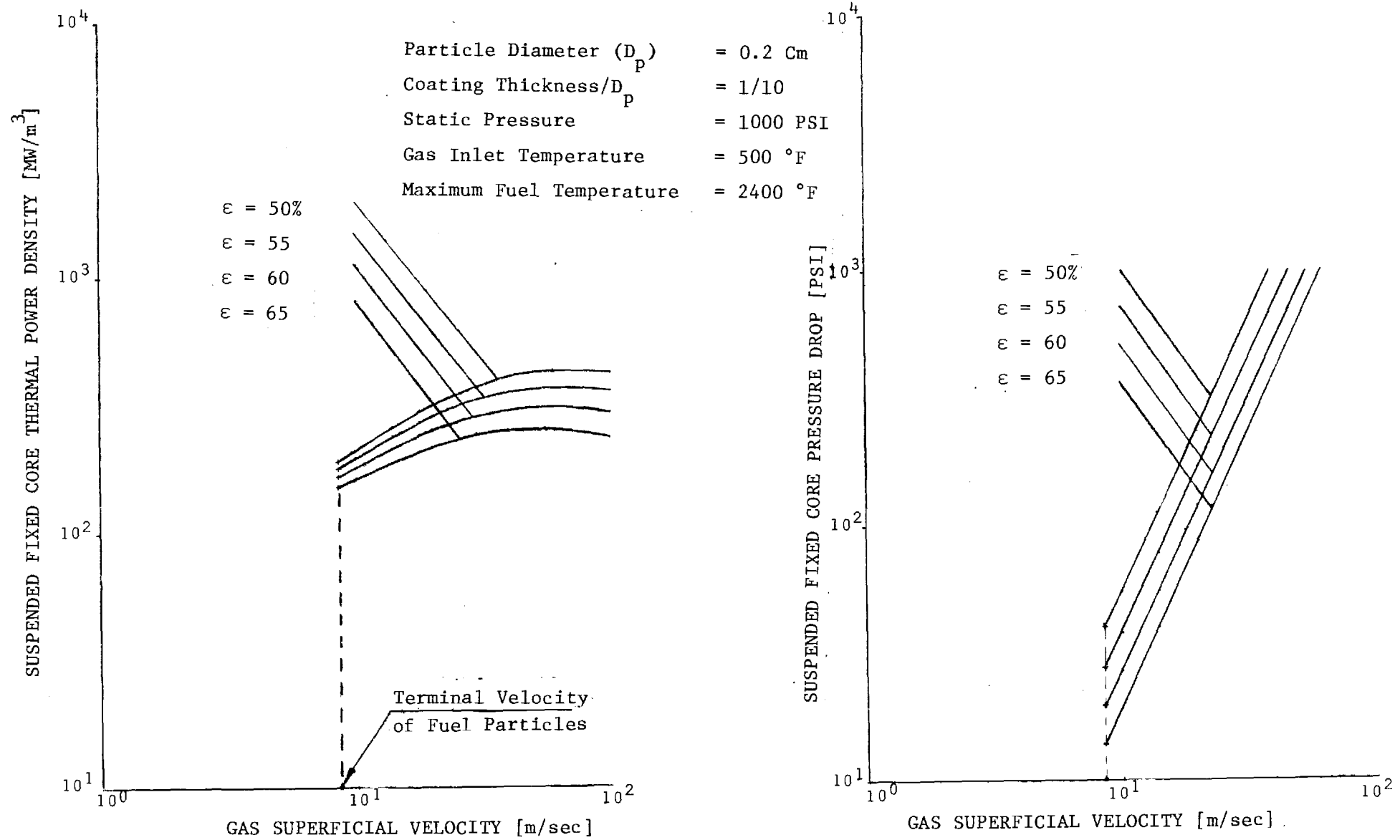


Fig. II-8-10. Power Density and Pressure Loss vs Gas Velocity at Various Bed Void Fractions

9. Preliminary Design of Suspended-Bed Reactor

Parametric optimization of a binary cycle, employing a combination of relatively low, direct gas cycle, efficiency and an indirect high efficiency steam cycle, was discussed in section 3 of this chapter. The dependence of the overall binary cycle efficiency on β , the pressure loss ratio, i.e. pressure drop in circuit, is shown in Fig. II-9-1 for β values between 0.01 and 0.09. Figure II-9-2 shows compressor outlet or core inlet temperature and overall binary cycle efficiency at various compression ratios, as a function of gas pressure loss ratio.

The power density as a function of compression ratio for various void fractions in the dicarbide fueled Suspended-Bed Reactor is shown in Fig. II-9-3. These results characterize the dicarbide fuel under the appropriate constraints specified in the figure. The pressure loss vs compression ratio is given in Figure II-9-4. The binary efficiency for various void fractions as a function compression ratio is shown in Fig. II-9-5.

The results for metallic fuel coated particles are given in Figures II-9-6, II-9-7, and II-9-8.

The maximum fuel temperature for the dicarbide and metallic fuels was set at 2400^oF and 2000^oF respectively. The gas outlet temperature was set at 1500^oF in all cases. The suspended-bed height was 1 meter and this represents a reasonable compromise between neutronic and pressure loss considerations.

The three layer coatings were 70 μ low density prolytic carbon, 30 μ SiC and 50 μ ZrC. Section 4 of this chapter discusses further the fuel design. Table II-9-I lists other material constants used in the calculation.

Steam Thermal Eff. Only	=	43.1 %
Quality of Steam Exit	=	15.0 %
Pumping Work Required	=	10.6 BTU/lb
Net Work by Steam	=	432.3 BTU/lb
Heat in Steam Generator	=	1002.8 BTU/lb
Pump and Steam Turbine Eff.	=	85.0 %
Comp. and Gas Turbine Eff.	=	90.0 %
Maximum Gas Temperature	=	1500 °F
Specific Heat Ratio for He, C_p/C_v	=	1.66
Specific Heat at Const. Pressure, C_p	=	1.248 BTU/lb °F

BINARY CYCLE OVERALL THERMAL EFFICIENCY (%)

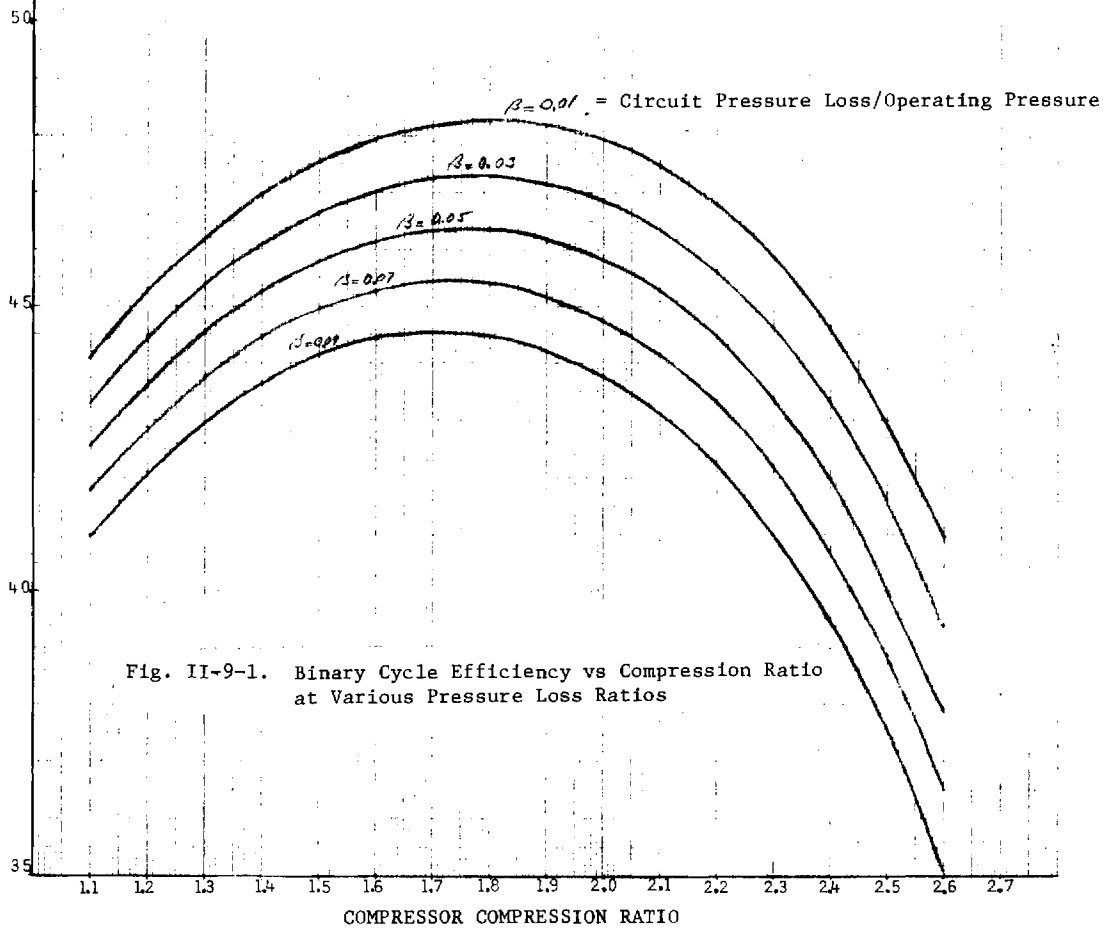
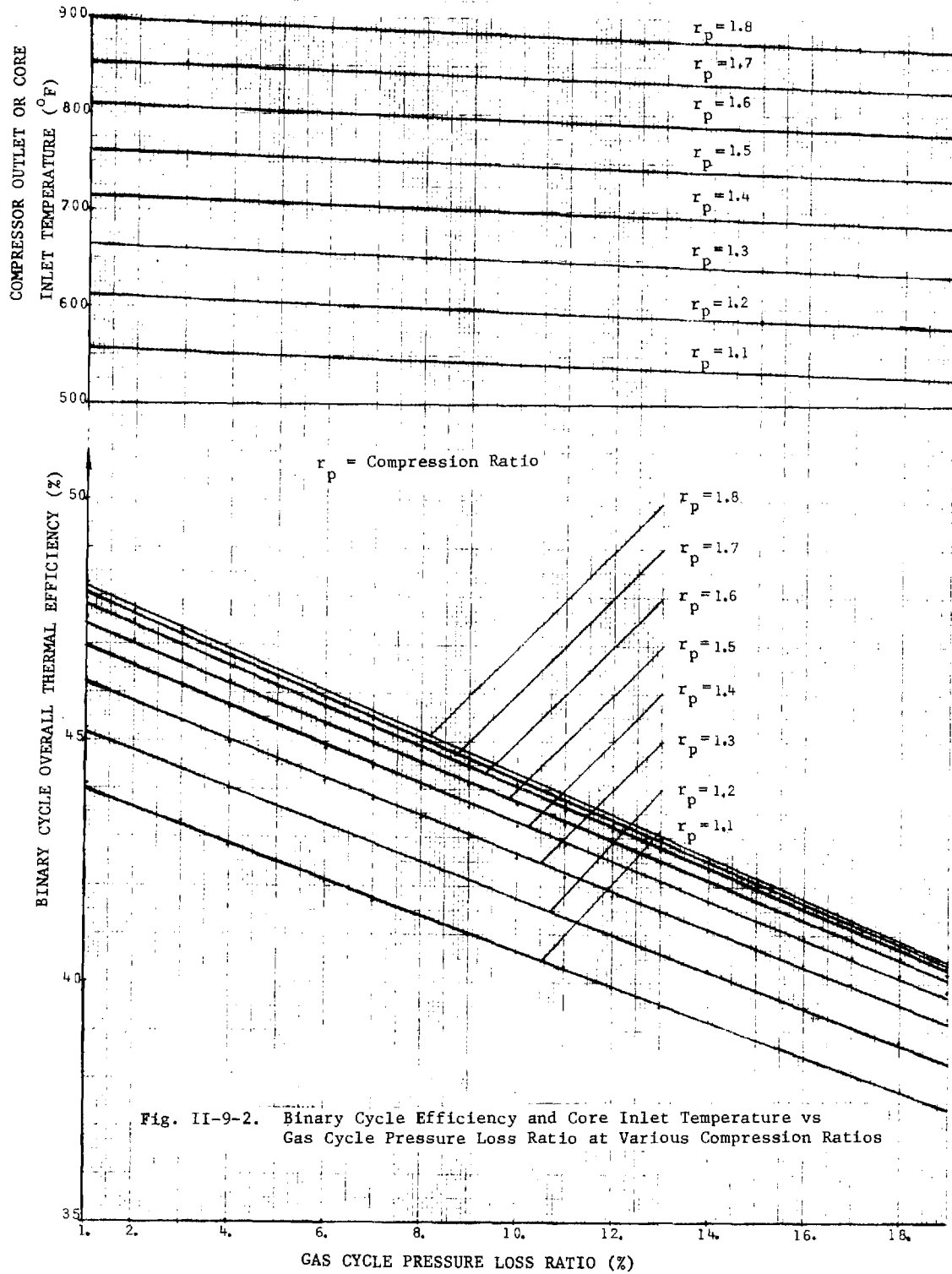
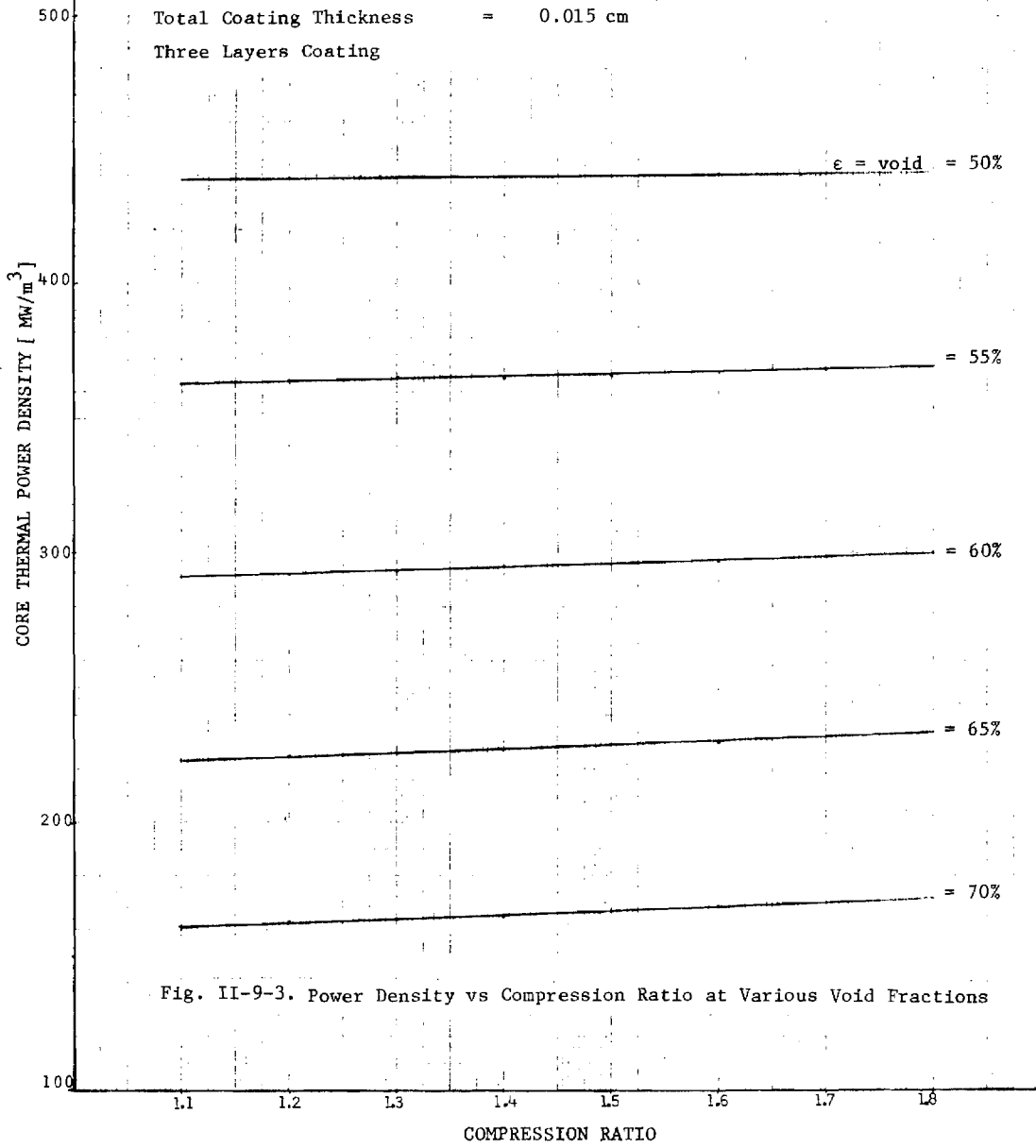


Fig. II-9-1. Binary Cycle Efficiency vs Compression Ratio at Various Pressure Loss Ratios



CARBIDE FUEL

Gas Static Pressure = 1000.00 psi
Core Height = 1.00 m
Core Outlet Temperature = 1500.00 °F
Maximum Fuel Temperature = 2400.00 °F
Particle Diameter = 0.17 cm
Total Coating Thickness = 0.015 cm
Three Layers Coating



Carbide Fuel

Fig. II-9-4. Pressure Loss vs Compression Ratio (Dicarbide Fuel)

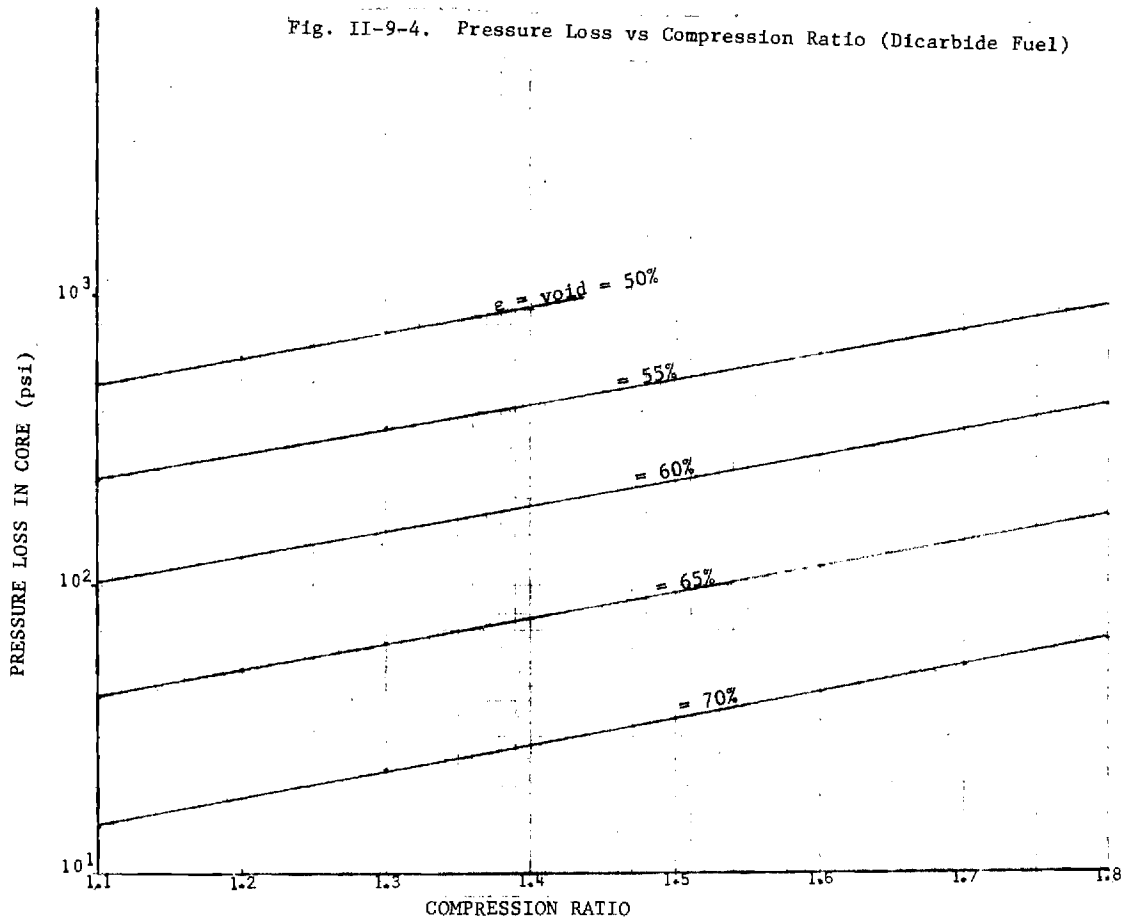
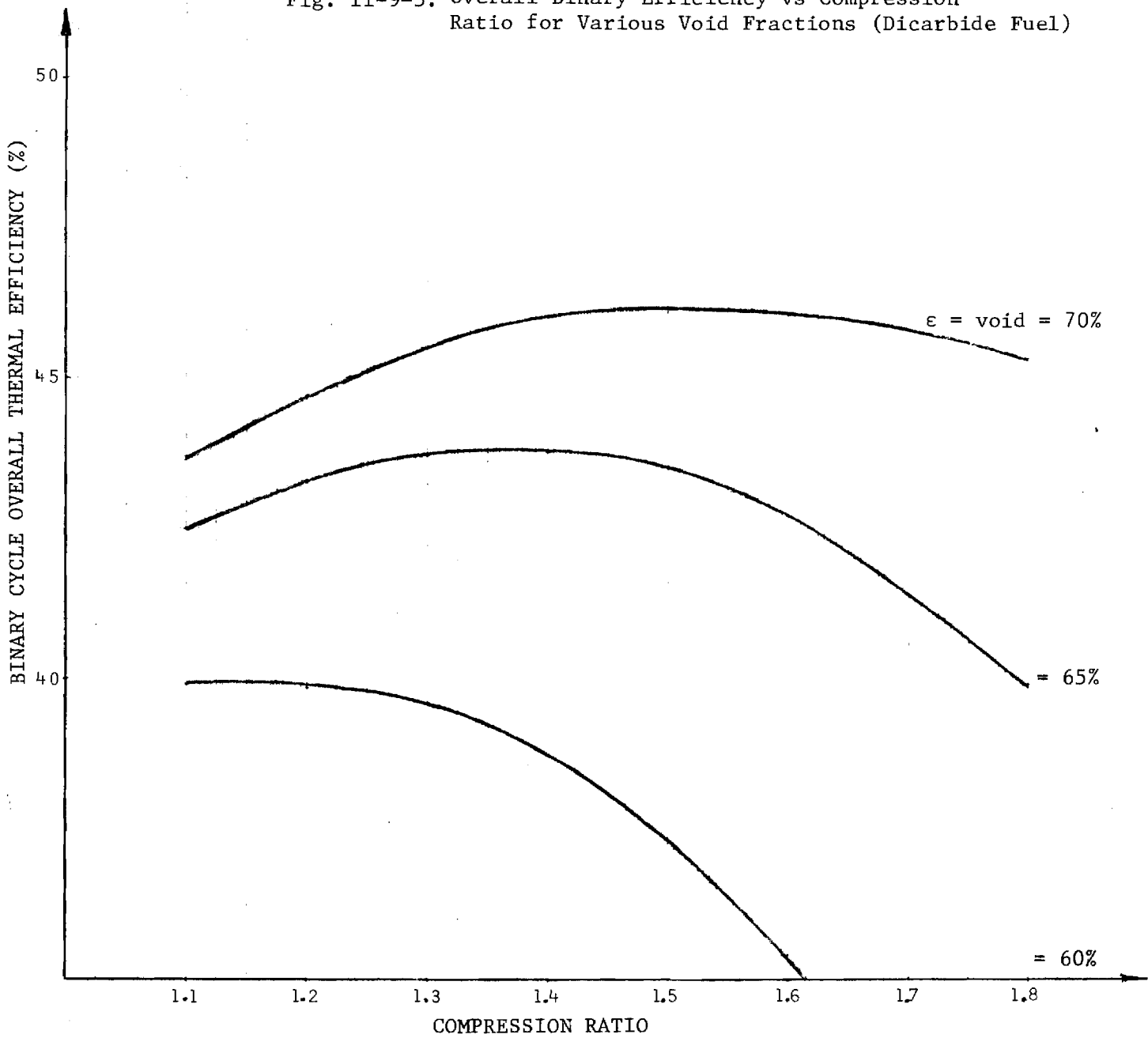


Fig. II-9-5. Overall Binary Efficiency vs Compression Ratio for Various Void Fractions (Dicarbide Fuel)



Metallic Fuel

Gas Static Pressure = 1000.0 psi
Core Height = 1.0 m
Core Gas Outlet Temperature = 1500.0 °F
Maximum Fuel Temperature = 2000.0 °F
Particle Diameter = 0.17 cm
Total Coating Thickness = 0.015 cm
Three Layers Coating

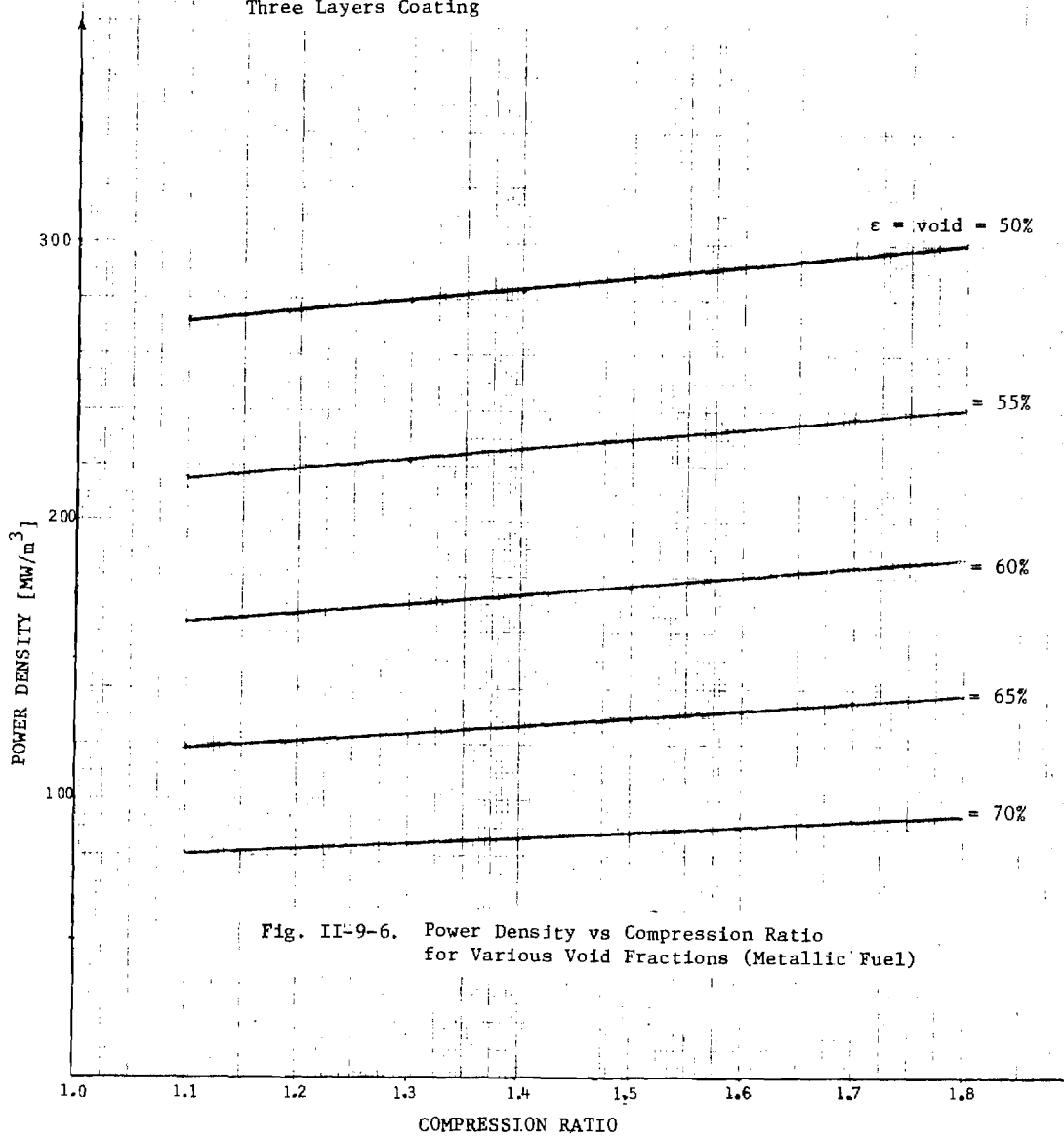
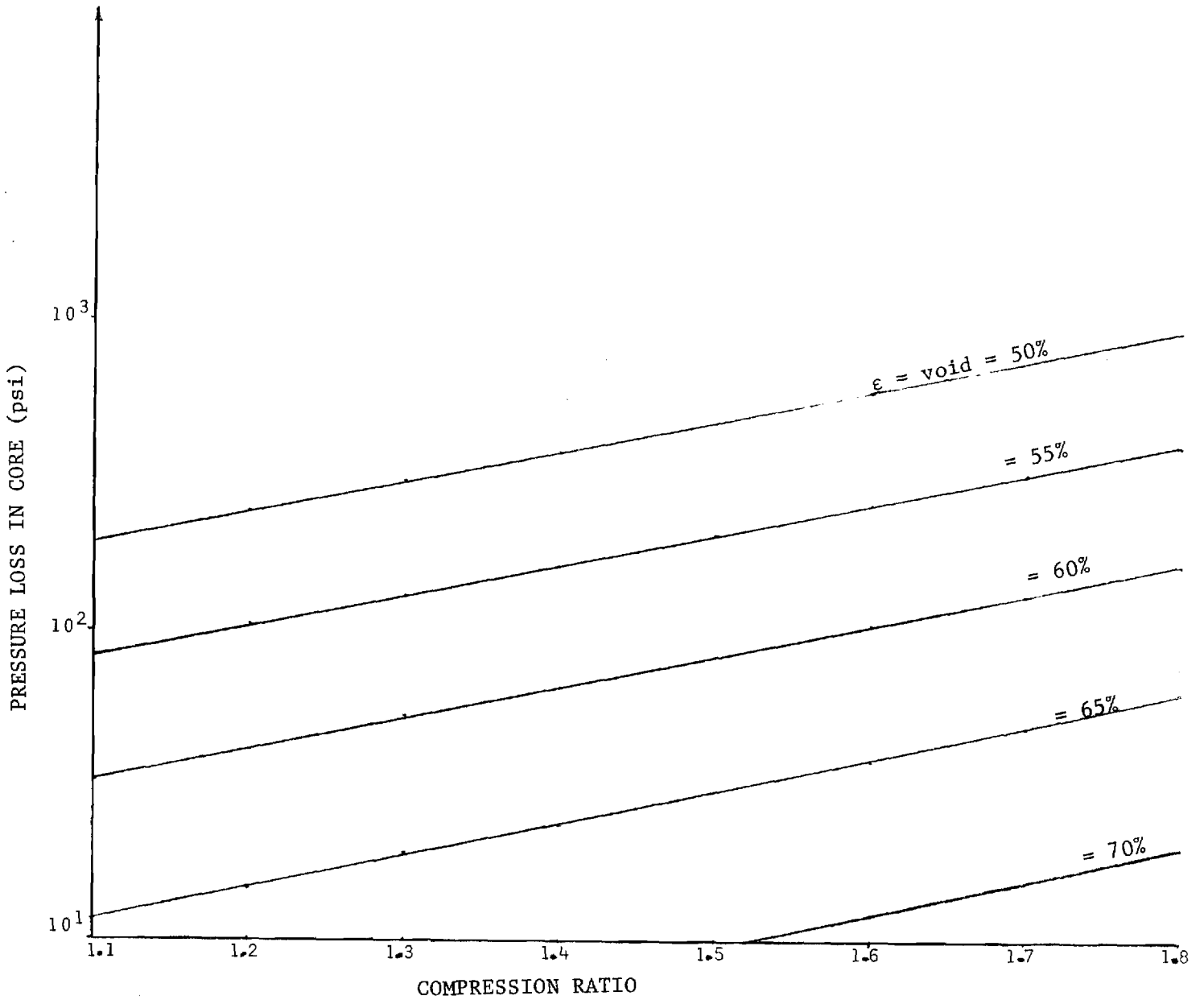


Fig. II-9-6. Power Density vs Compression Ratio for Various Void Fractions (Metallic Fuel)

Fig. II-9-7. Pressure Loss Ratio vs Compression Ratio for Various Void Fractions (Metallic Fuel)



Metallic Fuel

Fig. II-9-8. Overall Binary Efficiency vs Compression Ratio for Various Voids (Metallic Fuel)

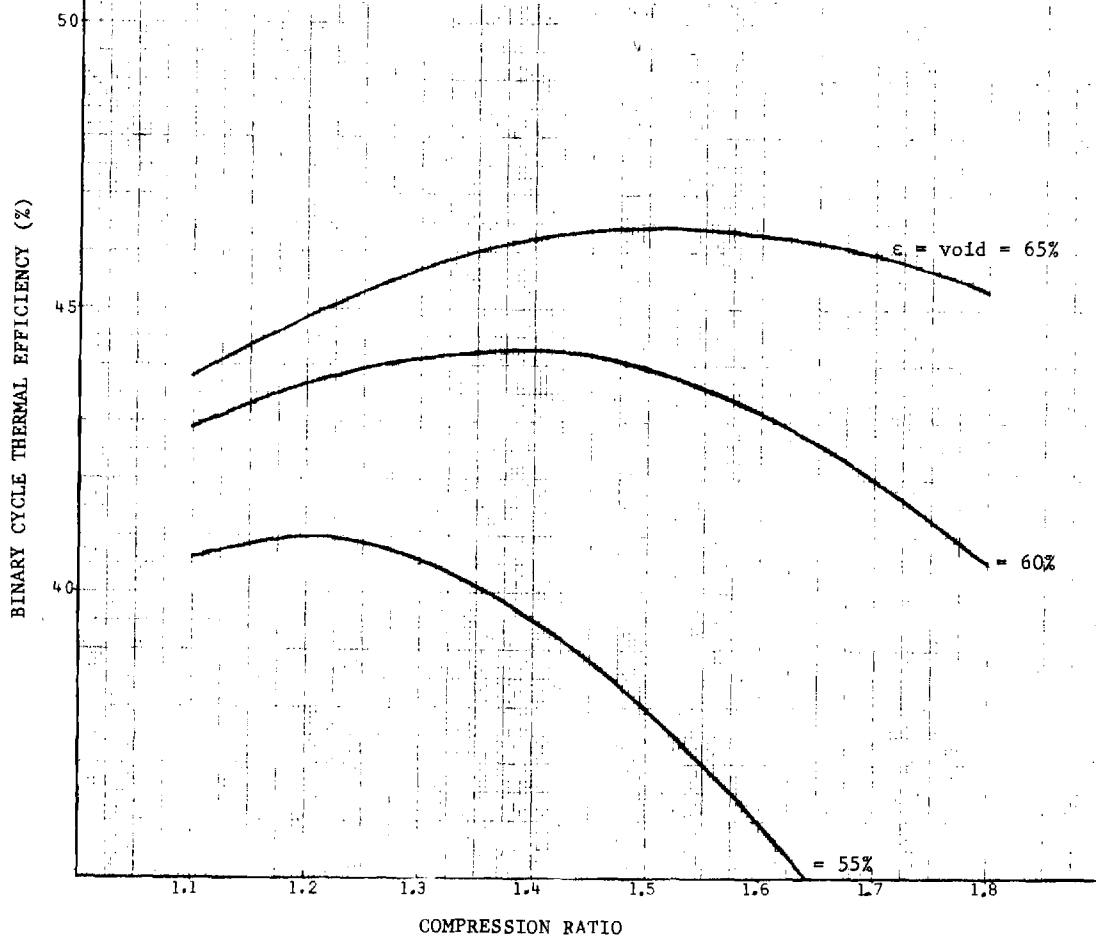


Fig. II-9-I. Material Constants Used in Calculation

FUEL KERNEL:

a. Dicarbide Fuel, $(U^{233}, Th^{232})C_2$	
Density of dicarbide fuel kernel, gm/cm^3	10.0
Thermal conductivity of dicarbide fuel $watt/cm^{\circ}C$	0.24
b. Metallic fuel, (U^{233}, Th^{232})	
Density of metal fuel, gm/cm^3	11.7
Thermal condition of metal fuel, $watt/cm^{\circ}C$	0.45

COATING

1st layer; density of low density pyro. graphite, gm/cm^3	1.0
Thermal conductivity of low density pyro. graphite, $watt/cm^{\circ}$	0.75
2nd layer; density of silicon carbide, gm/cm^3	3.2
Thermal conductivity of silicon carbide, $watt/cm^{\circ}C$	0.36
3rd layer; density of zirconium carbide, gm/cm^3	6.7
Thermal conductivity of zirconium carbide, $watt/cm^{\circ}C$	0.205

For the carbide fuel the maximum binary cycle efficiency for a void fraction of 60% occurs at a compression ratio of about 1.2 (Fig. II-9-5). The pressure loss in the core at this compression ratio is 120 psi (Fig. II-9-4). Assuming an additional pressure loss in the rest of the circuit of 20% or a total loss of 140 psi. The corresponding overall binary efficiency is 40%. The power density is 290 MW/m^3 . Table II-9-II summarizes the dicarbide Suspended-Bed Reactor design parameters.

For the metallic fuel, the same procedure for optimization, yields acceptable pressure losses at 55% void fraction for which the maximum binary cycle efficiency occurs at a compression ratio of 1.2. The pressure loss in the core is 100 psi, and the overall efficiency is 41%. The power density is 220 MW/m^3 . Table II-9-III summarizes the coated metallic fuel Suspended-Bed Reactor design parameters.

The overall Suspended-Bed Reactor binary cycle is shown schematically in Fig. II-9-9.

The overall Suspended-Bed Reactor is shown in Fig. II-9-10.

Table II-9-II. SBR Design Specifications
(Dicarbide Fuel)

<u>GENERAL</u>	
Electric Power, MW _e	1160.0
Binary Cycle Overall Thermal Efficiency, %	40.0
Core Power Density, MW/m ³	290.0
Core Volume, m ³	10.0
Core Height, m	1.0
<u>GAS CYCLE</u>	
He Gas Static Pressure, psi	1000.0
Gas Compressor Compression Ratio	1.2
Core Gas Inlet Temperature, °F	590.0
Core Gas Outlet Temperature, °F,	1500.0
Comp./Gas-Turb. Efficiency, %	90.0
Total Gas Cycle Pressure Loss Ratio, %	14.0
Gas Volume Fraction in Core (Void), %	60.0
Gas Mass Flow Rate, kg _{gas} /hr	3.963 x 10 ⁶
Gas Superficial Velocity, m/sec	19.1
Gas Pressure Drop in Core, psi	120.0
<u>STEAM GENERATOR</u>	
Steam Generator Gas Inlet Temperature, °F	1464.0
Steam Generator Gas Outlet Temperature, °F	509.0
Gas Temperature at Pinch Point, °F	700.0
Pound Gas per Pound Steam Generated	0.8415
Steam Generator Outlet Temperature, °F	1000.0
Steam Generator Feed Water Temperature, °F	486.0

(continued)

Table II-9-II. SBR Design Specifications
(Dicarbide Fuel-continued)

STEAM CYCLE

Superheated Steam Pressure/Temperature (Steam Turb. Inlet), psia/°F	2000/1000
N ^o of Resuperheaters	0.0
N ^o of Feed Water Heaters	6.0
Condenser Pressure/Temperature, in. Hga/°F	2/101
Quality of Steam at Low Pressure Turb. Exit, %	15.0
Steam Flow Rate, kg/hr	4.709 x 10 ⁶
Pumping Requirement, MWe	32.0
Thermal Efficiency of Steam Cycle Alone, %	43.0
Net Power Generated by Steam Cycle, MWe	1310.0
Steam Turbine/Pump Efficiency, %	85.0

FUEL

Fuel Particle Diameter, cm	0.17
Fuel Kernel Diameter (U ²³³ -Th ²³²)C ₂ , cm	0.14
Fuel Particle Total Coating Thickness, cm	0.015
Pyrolytic Graphite Layer Thickness (First Layer), cm	0.0070
Silicon Carbide Layer Thickness (Second Layer), cm	0.0030
Zirconium Carbide Layer Thickness (Third Layer), cm	0.0050
Maximum Fuel Temperature, °F	2400.0
Maximum Temperature Drop through the Fuel Kernel, °F	290.0
Terminal Velocity of Fuel Particles, m/sec	8.7
Fuel Kernel Max. Volumetric Heat Source Strength, MW/m ³	1.830 x 10 ⁵
Fertile Mass Core/Blanket, kg	10,963/57,590
Fissile Mass, kg	2600.0
Specific Power, MW/kg	1.1
Enrichment, Inner Core/Outer Core, %	16.0/22.88
Initial Breeding Ratio	1.06
Power Peaking Factor	1.21

Table II-9-III. SBR Design Specifications
(Coated Metallic Fuel)

<u>GENERAL</u>	
Electrical Power, MW _e	902.0
Binary Cycle Overall Thermal Efficiency, %	41.0
Core Power Density, MW/m ³	220.0
Core Volume, m ³	10.0
Core Height, m	1.0
 <u>GAS CYCLE</u> 	
He Gas Static Pressure, psi	1000.0
Gas Compressor Compression Ratio	1.2
Core Gas Inlet Temperature, °F	590.0
Core Gas Outlet Temperature, °F	1500.0
Comp./Gas-Turb. Efficiency, %	90.0
Total Gas Cycle Pressure Loss Ratio, %	12.0
Gas Volume Fraction in Core (Void), %	55.0
Gas Mass Flow Rate, kg _{gas} /hr	3.017 x 10 ⁶
Gas Superficial Velocity, m/sec	14.7
Gas Pressure Drop in Core, psi	98.0
 <u>STEAM GENERATOR</u> 	
Steam Generator Gas Inlet Temperature, °F	1452.0
Steam Generator Gas Outlet Temperature, °F	512.0
Gas Temperature at Pinch Point, °F	700.0
Pound Gas Required per Pound Steam Generated	0.8551
Steam Generator Outlet Temperature, °F	1000.0
Steam Generator Feed Water Temperature, °F	486.0
 (continued) 	

Table II-9-III. SBR Design Specifications
(Coated Metallic Fuel-continued)

STEAM CYCLE

Superheated Steam Pressure/Temperature, psia/°F	2000/1000
N ^o of Resuperheater	0.0
N ^o of Feed Water Heaters	6.0
Cond. Pressure/Temperature, in. Hga/°F	2/101
Quality of Steam, %	15.0
Steam Flow Rate, kg/hr	3.528 x 10 ⁶
Pumping Requirement, MWe	24.0
Thermal Efficiency of Steam Cycle Alone, %	43.0
Net Power Generated by Steam Cycle, MWe	983.3
Steam Turbine/Pump Efficiency, %	85.0

FUEL

Fuel Particle Diameter, cm	0.17
Fuel Kernel Diameter (U ²³³ -Th ²³²), cm	0.14
Fuel Particle Total Coating Thickness, cm	0.0150
Pyrolytic Graphite Layer Thickness, cm	0.0070
Silicon Carbide Layer Thickness, cm	0.0030
Zirconium Carbide Layer Thickness, cm	0.0050
Maximum Fuel Temperature, °F	2000.0
Maximum Temperature Drop for Fuel Kernel, °F	94.0
Terminal Velocity of Fuel Particles, m/sec	9.3
Fuel Kernel Max. Volumetric Heat Source Strength, MW/m ³	1.217 x 10 ⁵
Fertile Mass Core/Blanket, kg	17,479/63,584
Fissile Mass, kg	3348.0
Specific Power	1.21
Enrichment, Inner Core/Outer Core, %	12.8/18.3
Conversion Ratio	1.17

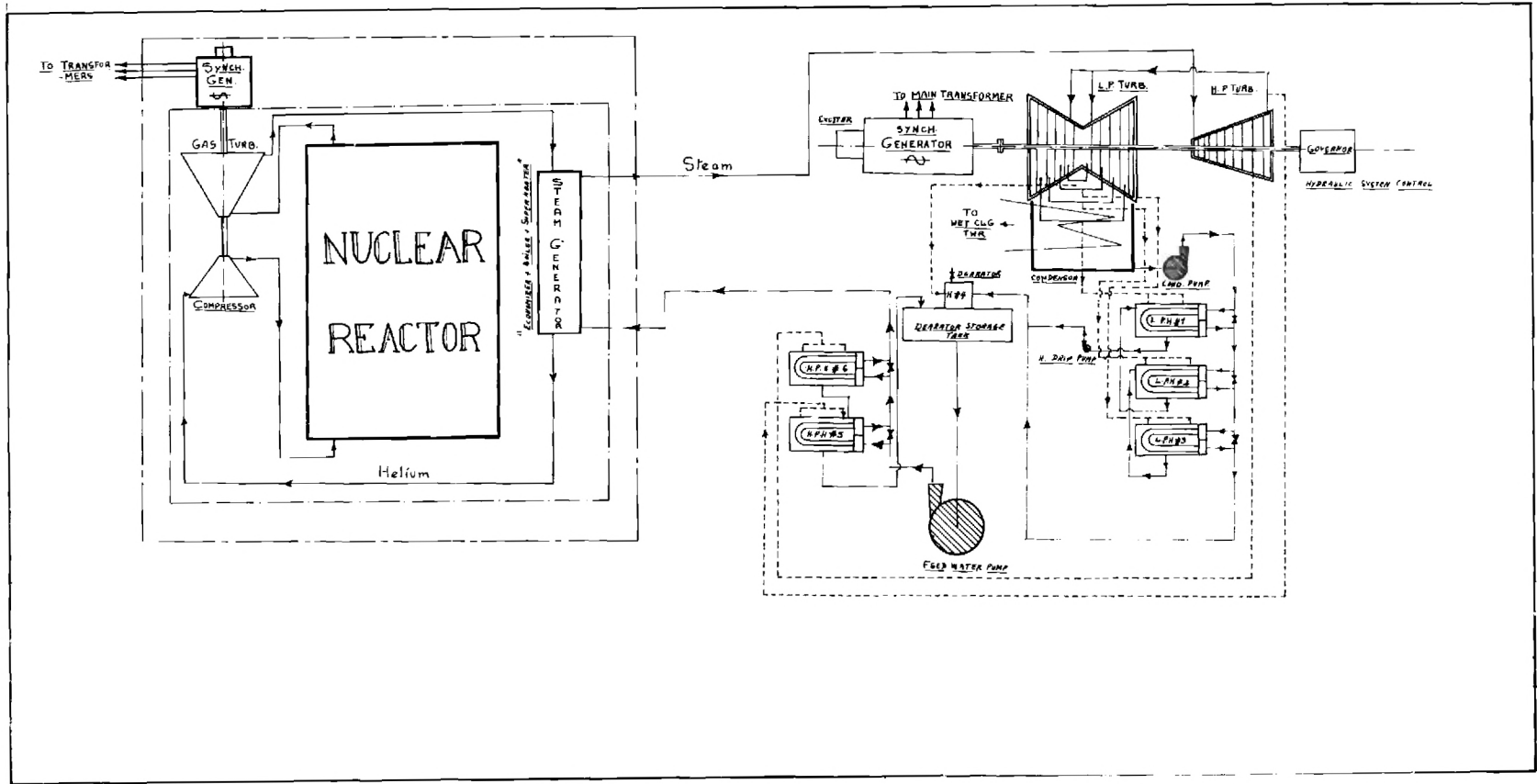


Figure II-9-9. Suspended-Bed Reactor Binary Cycle.

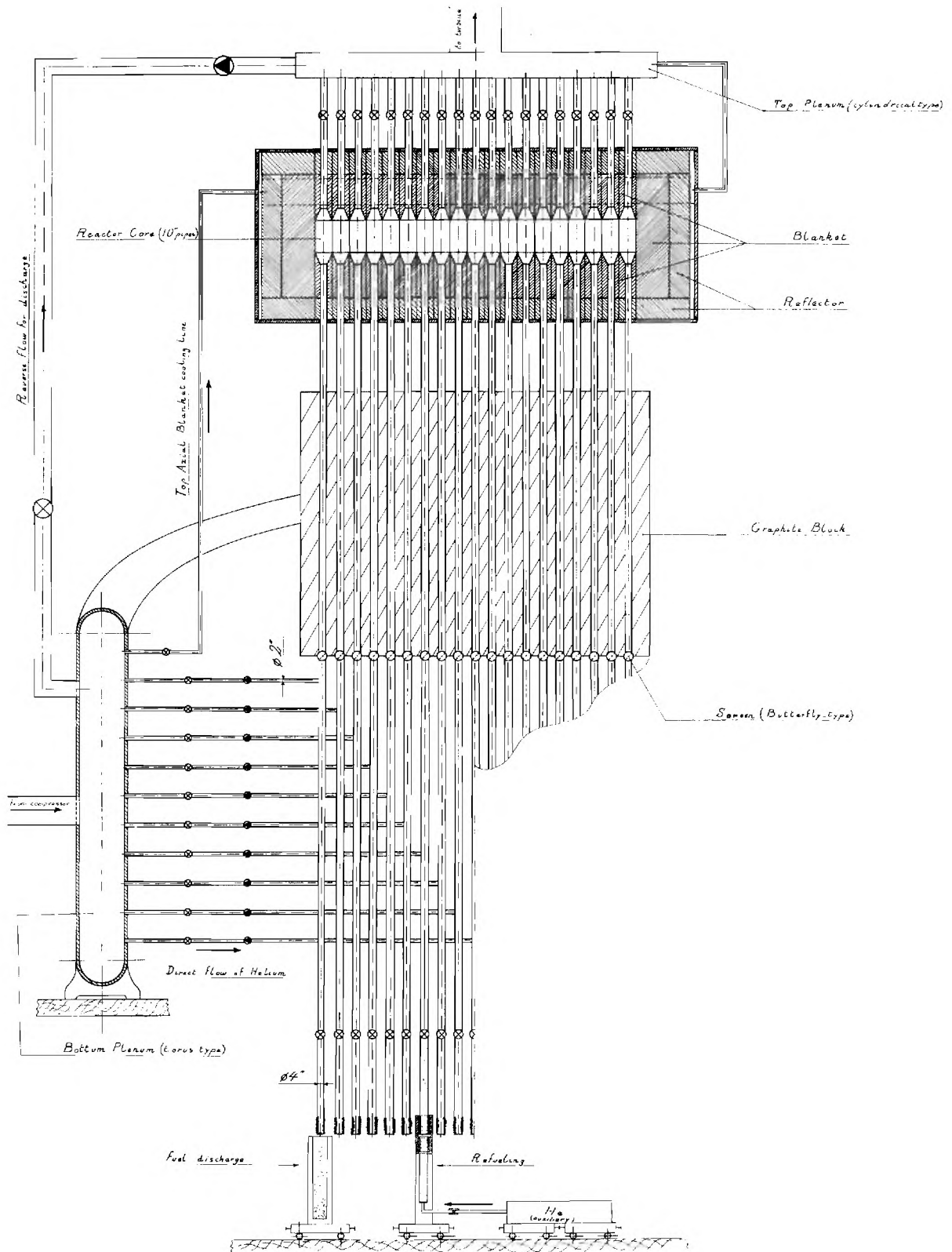


Figure II-9-10. Suspended-Bed Reactor.

III. RECOMMENDED RESEARCH AND DEVELOPMENT PROGRAM

The first point that should be emphasized is that the Suspended-Bed Reactor concept is not really limited to any one type of fuel or coolant. For example if the coated particle fuel should prove unsuitable in a suspended bed operation due to breakage or erosion, it is quite possible to use coated particles fixed in a matrix of a material with high thermal conductivity shaped into disks with holes drilled through the disk for the passage of the coolant. The disks can be suspended in "guides" just like the coated particles. Thus, the fail-safe or nearly fail-safe features of the Suspended-Bed Reactor are not really tied to particles.

Nevertheless, if coated particles are to be used in a Suspended-Bed Reactor, it is necessary to experimentally determine the erosion rate of the outer layer under normal operating conditions, i.e. helium velocity and temperature and later irradiating condition. In addition to erosion, it is important to determine the breakage rate due to normal handling, i.e., fluidization and suspending the particles in the core region. Another important factor is whether or not at operating temperatures the particles tend to stick to each other after long term operation.

The pressure drop through the reactor is a very important design parameter which has important implications on performance and economics. This one parameter affects the breeding ratio, doubling time, overall thermodynamic efficiency and eventually the cost of electricity. It is, therefore, important to conduct an experimental program aimed at minimizing the pressure drop before any final fuel design is chosen. The state

of the art of calculating pressure drops in fixed or fluidized beds is not accurate, perhaps within 50%. Thus an experimental program for measuring the pressure drop as a function of particle size and density at various coolant velocities is necessary.

Suspending fuel, whether coated particles or disks, in a core region is certainly possible, and there is no doubt whatsoever about its feasibility. But it needs to be demonstrated with the goal of assessing the ease with which reactors can be controlled.

A block diagram of the program we envision for the the SBR final design is shown in Fig. III-1-1. Our work heretofore concentrated on the thermodynamic and thermal hydraulic optimization under realistic engineering constraints. We have not exhausted, due to time limitations, the possibilities for optimum fuel design. Many possibilities exist whereby the fuel volume fraction and the power density would increase and at the same time the pressure drop would decrease. The benefits of such optimization translate directly into cheaper energy cost. The block diagram in Fig. III-1-1 represents a scheme to optimize the condition for a self-sustaining energy source at the cheapest cost. Our analysis which is based on considerations of physics and thermal hydraulics indicates that a doubling time for the SBR as short as 10 years or even shorter is very possible.

The fuel cycle calculation represents a significant effort which is essential. In particular, reactivity swings for each fuel cycle needs to be evaluated. Burnup effects on breeding ratio must be assessed. Protactinium effects on control should also be assessed. We currently are testing the appropriate codes which we are planning to use for the fuel cycle analysis.

Economic analysis also requires a significant effort, but it is necessary. Our activity in this area was limited to costing out components. It would be desirable to cooperate with Oak Ridge National Laboratory and perform this analysis for the Suspended-Bed Reactor. We welcome the opportunity.

Engineering and Safety Constraints

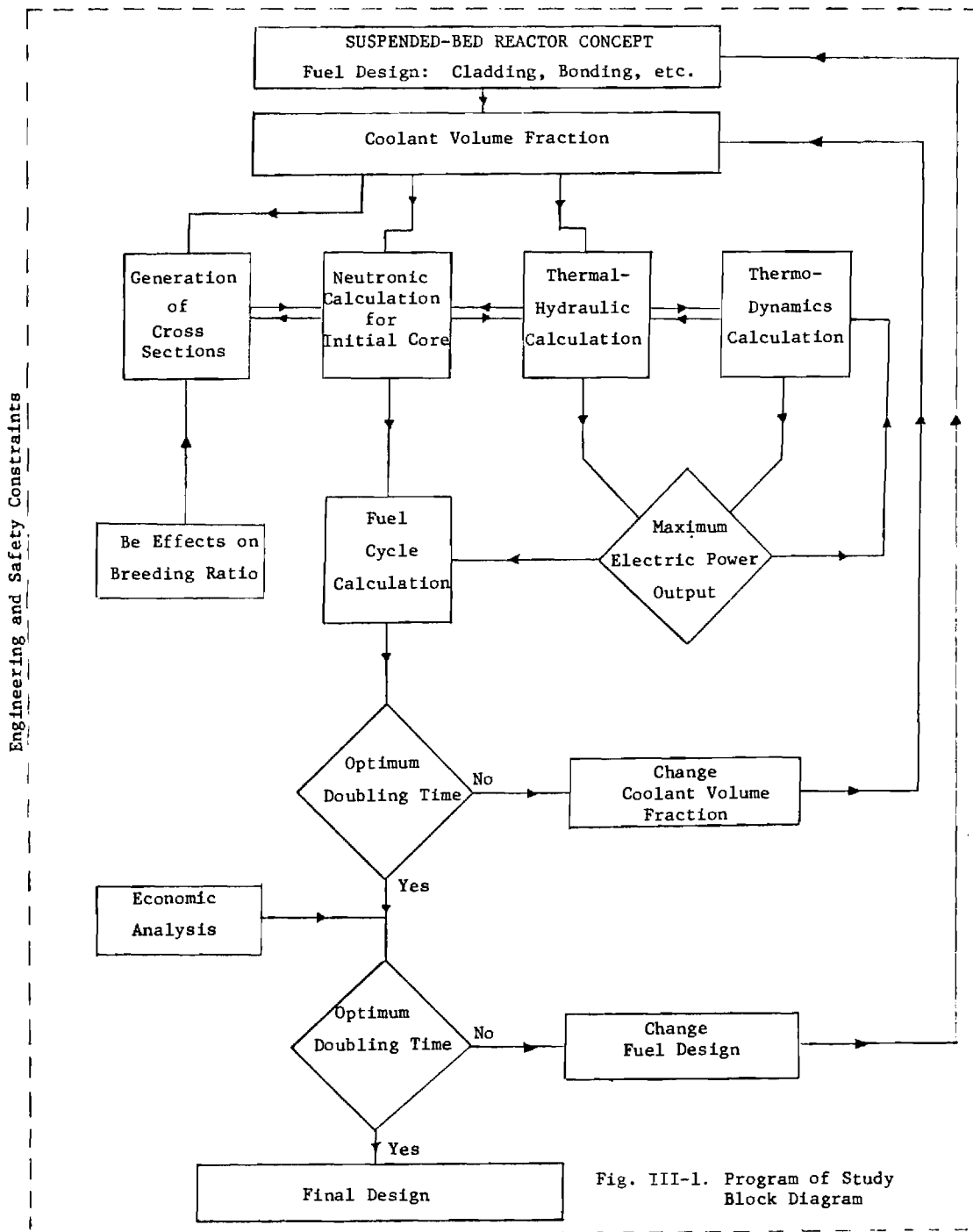


Fig. III-1. Program of Study Block Diagram

APPENDIX A

GENERAL CONSIDERATIONS OF NATURAL URANIUM AND THORIUM-
RESERVES AND IMPLICATION ON NUCLEAR POWER GROWTH

A.1 Uranium Reserves

INFO, December 1975, tabulated the U.S. uranium resources as given in Table A-1-I.

Table A-1-I U.S. Uranium Resources as of January 1, 1975
(Tons of U₃O₈)

Production Cost	Potential Reserves				Total
	Reasonably Assured Reserves	Probable	Possible	Speculative	
\$8	200,000	300,000	200,000	30,000	730,000
\$8-10 Increment	115,000	160,000	190,000	80,000	545,000
\$10	315,000	460,000	390,000	110,000	1,275,000
\$10-15 Increment	105,000	220,000	250,000	100,000	675,000
\$15	420,000	680,000	640,000	210,000	1,950,000
\$15-30 Increment	180,000	460,000	700,000	200,000	1,540,000
\$30	600,000	1,140,000	1,340,000	410,000	3,490,000
By-products(a) 1975-2000	90,000	--	--	--	90,000
TOTAL	690,000	1,140,000	1,340,000	410,000	3,580,000

Source: Energy Research and Development Administration.

Note: Numbers may not add to totals because of rounding.

(a) By-product of phosphate and copper production.

The potential U.S. resources reported by ERDA as of January 1, 1976 are given in Table A-1-II (information from ERDA--Weekly Announcements, March 19, 1976).

Table A-1-II Potential Resources--January 1, 1976

Class	Tons U ₃ O ₈		
	\$10	\$15*	\$30*
Probable	440,000	655,000	1,060,000
Possible	420,000	675,000	1,270,000
Speculative	145,000	290,000	590,000

* Includes lower cost resources

The data in Table A-1-II show a net decrease in the "probable resources" category of 80,000 tons of U_3O_8 . Exploration efforts in 1975 included 26 million feet of drilling in some 56,000 holes for an average depth of 465 feet per hole.

The Committee on Mineral Resources and the Environment (COMRATE) in a recent study of reserves and resources of uranium in the United States⁽³⁷⁾ concluded: "Current data on uranium reserves (in known deposits) are reliable, but estimates of potential undiscovered resources are of uncertain validity." Potential reserves are those reserves which are yet to be discovered although there is no guarantee that they will ever be discovered. ERDA's estimates of potential reserves are based on comparison of characteristics of known deposits and their geologic surroundings to similar geologic areas. Recent exploration efforts,⁽³⁸⁾ presumably guided by knowledge of geologic strata, have failed to expand the reserves.

The quantities of uranium that could be recovered at costs higher than \$30/lb U_3O_8 from known deposits appear to be very small.⁽³⁹⁾ Moreover, since variations in the grade of ore in a given deposit occur frequently, the recovery of the lower grade ore (or higher-cost uranium reserves) must be carried out at the same time as that of the high grade ore. This increases the average cost of recovery to the \$30/lb U_3O_8 level. If the low-grade ore is not recovered concurrently with the high grade ore, the resource would be lost because at that time the cost of recovery would be greatly increased.⁽³⁹⁾

The validity of the AEC estimates of potential resources in sandstone deposits was recently examined in a two-day conference at Albuquerque, New Mexico, December 12 and 13, 1974. Although participants in the

conference have had extensive experience with sandstone deposits, there was no agreement. Views varied from pessimistic to optimistic. The following observations⁽³⁷⁾ were offered as reasons that AEC estimates of resources will not be met:

1. The most favorable areas in some of the basins, e.g. in the Wind River Basin of Wyoming, may already have been explored.
2. The amount of U_3O_8 found per foot of exploratory drilling has decreased from 14.7 pounds to U_3O_8 per foot in 1955 to 4.7 pounds per foot in 1971 (mostly because of increased drill hole depths).
3. Drilling during 1971-73 increased AEC \$10 "reserves" by only 7,000 tons of U_3O_8 .
4. Drilling in certain areas that under the AEC system would have been estimated to contain potential resources has not been successful (underlined for emphasis).
5. Evidence of the existence of large low-grade (0.05 to 0.10%, U_3O_8) deposits of uranium in sandstones is lacking.
6. Exploration experience has contradicted projections involved in estimates of potential ore.
7. While known mineralization is widespread, a relatively few deposits contain the bulk of the reserves. About 95% of reserves are in 150 of the 4500 properties listed by the AEC.

Observations in support of AEC estimates were as follows:

1. There is a close correlation between past drilling effort (annual total footage) and amounts of uranium discovered.
2. Since knowledge of uranium deposits is incomplete, future exploration will very likely discover deposits of kinds unrecognized at present.

3. Higher prices in future will justify a search for lower grade ores than those mined at present.
4. There are mineralized areas already known that have not been fully explored, either because first results of drilling indicated submarginal grades, or because reserves in hand were adequate to sustain company production schedules.
5. Exploration effort to date is not an adequate index of the resources that could be discovered if the exploration effort were greatly increased. The uncertain market for uranium and the low profitability of the industry have not been conducive to vigorous exploration.

COMRATE⁽³⁷⁾ saw no quantitative basis for evaluating these contradictory observations. However, the extensive drilling, during 1975, reported recently by ERDA seems to confirm the pessimists' view on this point. COMRATE also rejects the optimistic estimates of uranium resources made by the Electric Power Research Institute (EPRI).⁽⁴⁰⁾

Some believe that exploration has been so extensive that all major reserves have been found.⁽⁴¹⁾

The black shales of the United States have been frequently mentioned as a potential source of uranium, particularly the Chattanooga shale in the east central United States. The Chattanooga shale at an average grade of .007% and an average recovery of 50%, requires nearly 30,000 tons of rock for every ton of U_3O_8 produced. Cost analysis (studied by COMRATE)⁽³⁷⁾ suggest that the cost per pound of U_3O_8 (1974 dollars) would be upwards of \$80. Even if such a price should prove acceptable, formidable problems of mining and milling, water supply, environmental protection, and capital

costs would have to be resolved. One recent analysis concludes⁽⁴²⁾ the energy cost of mining, milling, processing, and power generation from uranium from Chattanooga shale would be less than the yield of energy. Another analysis⁽⁴³⁾ concludes that some reactors produce rather little excess in energy beyond that required to fuel them with uranium from Chattanooga shale.

An independent check on the AEC estimates of the resource in the San Juan Basin in New Mexico was provided by 36 experts from industry, university and government.^(44,45) AEC's own estimate was 740,000 tons of U_3O_8 at costs of up to \$30/lb. Twelve experts estimated that the Basin contained less than 100,000 tons and four estimated more than 1 million tons. The median estimate was 150,000 tons and the average estimate was 450,000 tons. This illustrates further the urgent need for an accurate assessment of uranium reserves and points to the presence of error flags associated with the known reserves.

On a more practical level the confusion with respect to the availability of uranium as reflected by price stability is permeating the literature of the nuclear industry. Westinghouse announced⁽⁴⁶⁾ that the Company is seeking to free herself from contractual obligation to supply uranium to utility companies at pre-oil embargo prices. According to Westinghouse, dramatic uranium price increases could cause her to lose 2 billion dollars. Westinghouse estimates of the price of U_3O_8 in October, 1975 were \$24/lb.⁽⁴⁶⁾ In the March, 1976 issue of Nuclear News, chairman of the board of Westinghouse, Robert Kelley, talks about \$40/lb of U_3O_8 . Back in the October issue of Nuclear News (1975), William Minsch, a retired AEC senior attorney says, "Everybody has a fear of facing up to this drastic uranium shortage

that is closing in on us. We ought not to act like someone who thinks he has cancer, but is afraid to go to the doctor. It is better to know the truth and see what you can do about it. We have got to face up to this shortage of uranium. I think it would take a massive coordinated effort between government and domestic uranium industry . . ."

The concern about the magnitude of the uranium resources for the LWR industry is genuine. John Hagerton of the S. M. Stoller Corporation in an address to the Atomic Industrial Forum Conference on Energy Alternatives, February 19, 1975, Washington, D. C., correctly summarized the situation with this statement, "If nuclear power [LWR] is beholden to the nuclear physicist and reactor technologist for its progress to date, its future may well be in the hands of the hard-rock geologist and mining engineer." In an article on energy in the Wall Street Journal, March 29, 1976, the following statement appeared; "In 1966 this newspaper reported forecasts that there would be almost limitless supplies of power from nuclear power plants expected eventually to be the cheapest source of energy almost anywhere on the globe. It already has become clear, however, that nuclear power is no panacea. In fact, some observers consider it a sick industry. Its cost are escalating. Environmentalists are attacking it and some people think the world will run out of uranium before it runs out of oil."

Nuclear News (Mid-February 1976) reported that at least a dozen utilities were in various mining ventures trying to assure themselves adequate supplies of uranium. John Hogerton⁽⁴⁷⁾ says, "Today it is difficult to find a utility with nuclear commitments that is not concerned with some aspects of uranium supply. Some are concerned about lack of coverage for near-term or even close-in requirements. Others are concerned about

resources for the long-haul."

World assured reserves, according to the Nuclear Energy Agency of the Organization for Economic Cooperation and Development and the International Atomic Energy Agency as of January 1, 1975, are listed in Table II-2-III.⁽⁴⁸⁾ It is interesting to note that NEA/IAEA assessment of the U.S. reserves are lower than ERDA's figures.

Table A-1-III Reasonably Assured Uranium Reserves
(as of January 1, 1975, 1000 tons)

Cost Range	Reserves	
	< \$15/lb U ₃ O ₈	\$15-30/lb U ₃ O ₈
Algeria	28.0	-
Argentina	9.3	11.3
Australia	243.0	- ^a
Brazil	9.7	0.7
Canada ^b	144.0	22.0 ^c
Central African Republic	8.0	-
Denmark (Greenland)	-	6.0
Finland	-	1.9
France	37.0	18.0
Gabon	20.0	-
Germany	0.5	0.5
India	3.4	25.8
Italy	-	1.2
Japan	1.1	6.6
Korea	-	2.4
Mexico	5.0	1.0
Niger	40.0	10.0
Portugal	6.9	- ^a
South Africa	186.0	90.0
Spain	10.0	93.5
Sweden	-	300.0
Turkey	2.6	0.5
United Kingdom	-	1.8
United States ^d	320.0	134.0
Yugoslavia	4.2	2.3
Zaire	1.8	-
TOTAL (rounded)	1080.0	730.0

- a. Estimates of resources in this range have not been made and are, therefore, unknown. Exploration to date has concentrated on proving high-grade resources.
- b. Categories are by reference to price.
- c. Estimates in this price range are preliminary, restricted only to principal deposits, and thus are very conservative.
- d. Does not include 54,000 tons U as a by-product from phosphates or 15,000 tons U as a by-product from copper production which might be recovered in the period to the year 2000.

A.2 The Thorium Resource

Estimates of the thorium resource in the U.S., reported in WASH-1097 (1969), are given in Table A-2-I.

Table A-2-I Estimates of U.S. Thorium Resources

Up to Price of \$/lb ThO ₂	Total, Reasonable Assured plus Estimated Additional, Millions of Short Tons	
	USAEC ⁽⁴⁹⁾	USGS ⁽⁵⁰⁾
10	0.6	1.0
30	0.8	2.1
50	11	---
100	36	77
500	3000	---

Table A-2-I may be compared to estimates of the uranium resource, shown in Table A-2-II under the same range of recovery costs as reported in WASH-1097.

Table A-2-II Estimates of the U.S. Uranium Fuel Resources

Up to Price of \$/lb U ₃ O ₈	Reasonably Assured		Total, Reasonably Assured plus Estimated Additional	
	Millions of Short Tons			
	USAEC	USGS	USAEC	USGS
7	--	--	0.10	--
8	0.15	--	0.43	--
10	0.21	0.19	0.56	1.1
15	0.46	--	1.0	--
30	0.66	0.36	1.6	1.9
50	6	--	10	--
100	11	15	25	40
500	500	--	2000	4700

More recent estimates (as of May 1973⁽⁵¹⁾) of the thorium resource are given in Table A-2-III,

Table A-2-III Estimated U.S. Thorium Resources
(thousand tons)

Cutoff Cost (\$/lb ThO ₂)	Reasonably Assured	Estimated Additional	Total
10	65	335	400
30 ^a	200	400	600
50 ^a	3,200	7,400	10,600

^aIncludes lower cost resources

Relative abundance of thorium and uranium in the earth is sketched in Fig. A-2-1. (after Ref. 52) and shows that the thorium resource is about 3 times that of the uranium. Others⁽⁵³⁾ report that the estimate for the thorium resource is 10 times as big as that of the uranium.

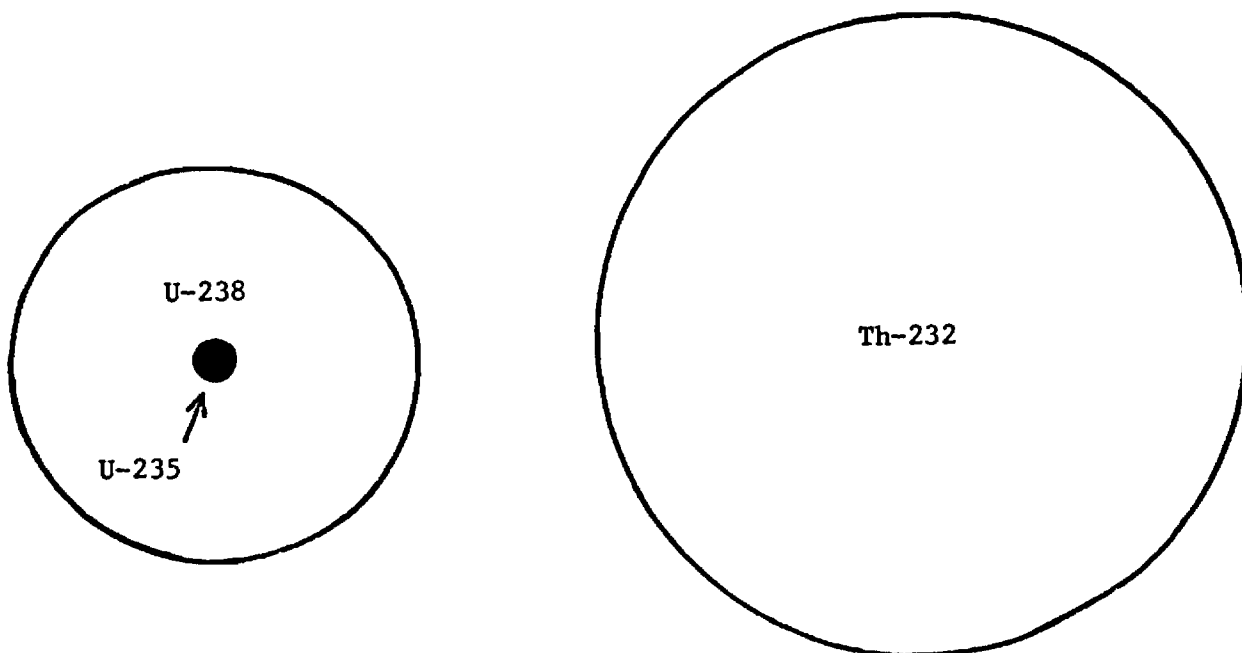


Fig. A-2-1. Relative Abundance of Nuclear Fuels in the Earth's Crust (Basis, Ref. 54).

It is realistic to expect that the estimates of the thorium resource have not been subjected to the same type of scrutiny as those of uranium. Nevertheless, a consensus emerges that: (1) the thorium resource, worldwide, is larger than the uranium resource, and (2) the U.S. reasonably assured resource at recovery cost of \$30/lb ThO₂ or less (i.e. 200,000 short tons, Table A-2-III) will be adequate to supply about 1000 power plants, of 1000 MWe each, practically indefinitely. It, therefore, appears that the thorium resource will be adequate to allow for growth in a thorium-based breeder concept.

A.3 Energy From Assured Reserves

That the LWR industry is facing difficulties due to uncertainties in uranium reserves is perhaps an understatement. If it is assumed that we can only be sure of about 700,000 short tons of U₃O₈, then the time span to exhaust this reserve, assuming 1000 nuclear plants each rated at 1000 MWe and operated at a load factor of 75% and a net thermal efficiency of 32%, would be short 5.4 years. More importantly, the entire 700,000 tons would be committed completely for only 125 (1000 MWe) plants, assuming the lifetime of a plant is 40 years.⁽⁵⁵⁾

Recently, financial problems have forced several utilities to delay and in some cases cancel construction of nuclear power plants. According to INFO (September, 1974) the total generating capacity, on order, under construction and operating was 237,194 MWe. As of March 8, 1976, the total generating capacity included in the three categories was 226,189 MWe, representing a net decrease of about 11,000 MWe. Orders for new power plants in 1975 totaled 5 compared to 27 in 1974 (INFO, December 1975). As of December 7, 1976, the total stands at 224,882 MWe (INFO, December 1976).

Regardless of the precise amount of uranium reserve which may ultimately be found, this source of energy for the LWR industry is quite limited. ERDA's forecasts for nuclear power growth⁽⁵⁶⁾ (WASH-1139 (1974)) are shown below in Table A-3-I.

Table A-3-I U.S. Nuclear Electrical Capacity Forecasts as of February 1974 (thousands of megawatts)

Year Case	1980	1985	1990	2000
A	85	231	410	850
B	102	260	500	1200
C	112	275	575	1400
D	102	250	475	1090

A key difference among cases A, B, and C is that the project time, from inception to licensing and operation, is 10, 8, and 6 years, respectively. Case D assumes a general reduction in the growth rate of electricity use. The total electric generating capacity in 1980 is forecast to be 680,000 MW compared to 700,000 MW for Case B, otherwise case D is similar to case B. Apparently it was assumed in this extensive work [WASH-1139 (74)] that the uranium resources will be adequate to justify the growth shown in Table A-3-I. A reasonable reaction to the shortage of uranium would be that utilities would only build nuclear power plants (LWR's) for which there are assured uranium reserves. This translates to 125,000 MW capacity under the assumptions of 700,000 short tons of U_3O_8 , 75% load factor, and 40 years plant life time. The annual production of fissile plutonium in 125 (1000 MWe) reactors is 125×170 kg or 21,000 kg (see Ref. 57 for plutonium production).

This amount of plutonium is only enough to fuel 6 to 7 LMFBR's of 1000 MWe capacity and is hardly enough to make much of an impact on future energy requirements.

Starting with 41,000 MWe nuclear capacity already installed in 1975 (INFO, February, 1976) and assuming an additional rate of 10,000 MWe per year, we will reach the limit of 125,000 MWe, described earlier, by 1984. The cumulative amount of fissile plutonium produced by that time would be 145,100 kg. Unless the installed capacity is increased beyond the 125,000 MWe level, the annual production of fissile plutonium from LWR's would level off at 21,000 kg. This inventory would, however, decrease significantly if the recycle of plutonium in LWR's, as proposed in WASH-1327, begins in 1977 or 1978. Burning the very limited inventory of plutonium in light water reactors will increase the likelihood that no breeder concept would have enough base-support with respect to fuel availability to make much of an impact on electrical energy needs.

A.4 Electrical Energy Needs and Nuclear Power Growth

Electric utilities usually plan their generating capacities according to projections based on estimates of growth in the population, economy and the standard of living. These projections necessarily anticipate demands 7-10 years ahead of time because it takes that long to bring power plants on line. The method of statistical analysis of past history and trend projection to predict energy requirements often fails to incorporate technical, social and political developments which affect such predictions. Nevertheless, trend projection is the only tool available for future energy needs assessment.

The Energy Research and Development Administration study, WASH-1139 (74), employed such statistical tools to forecast electrical energy needs and anticipated nuclear power growth between 1974 and 2000. The forecast is based on the Census Bureau's Series E population projection which indicates a total U.S. population of 228 million in 1980 and 271 million in the year 2000. It also assumes net immigration of 0.4 million a year and a fertility rate to replacement level. All of these assumptions are in agreement with recent trends. Estimates of the work force were based on age-groups within the total population, taking into account recent trends toward greater female participation in the labor force. These assumptions are then correlated with the Gross National Product (GNP) to predict future energy demands.

The total electrical energy demand between now and the year 2000 is represented by the upper left line shown in Fig. A-4-1. This forecast represents the slowest rate of growth studied in WASH-1139,⁽⁵⁶⁾ It assumed a decreased emphasis on the production of goods due to higher energy prices. It also assumed that maximum efforts would be made to conserve energy by increasing utilization efficiency and by changing temperature settings in heating and cooling homes and commercial buildings. Under these same conditions ERDA's study predicts a nuclear power growth of 85,000 MWe in 1980 to 850,000 MWe in the year 2000. This prediction is represented by the solid line in Fig. A-4-1. Extrapolation to the year 2030 is based on the data reported by J. Dietrich.⁽⁵⁸⁾ As mentioned earlier, ERDA's prediction does not consider the limitations of uranium reserves; consequently, the growth rate depicted in Fig. A-4-1 cannot be realized.

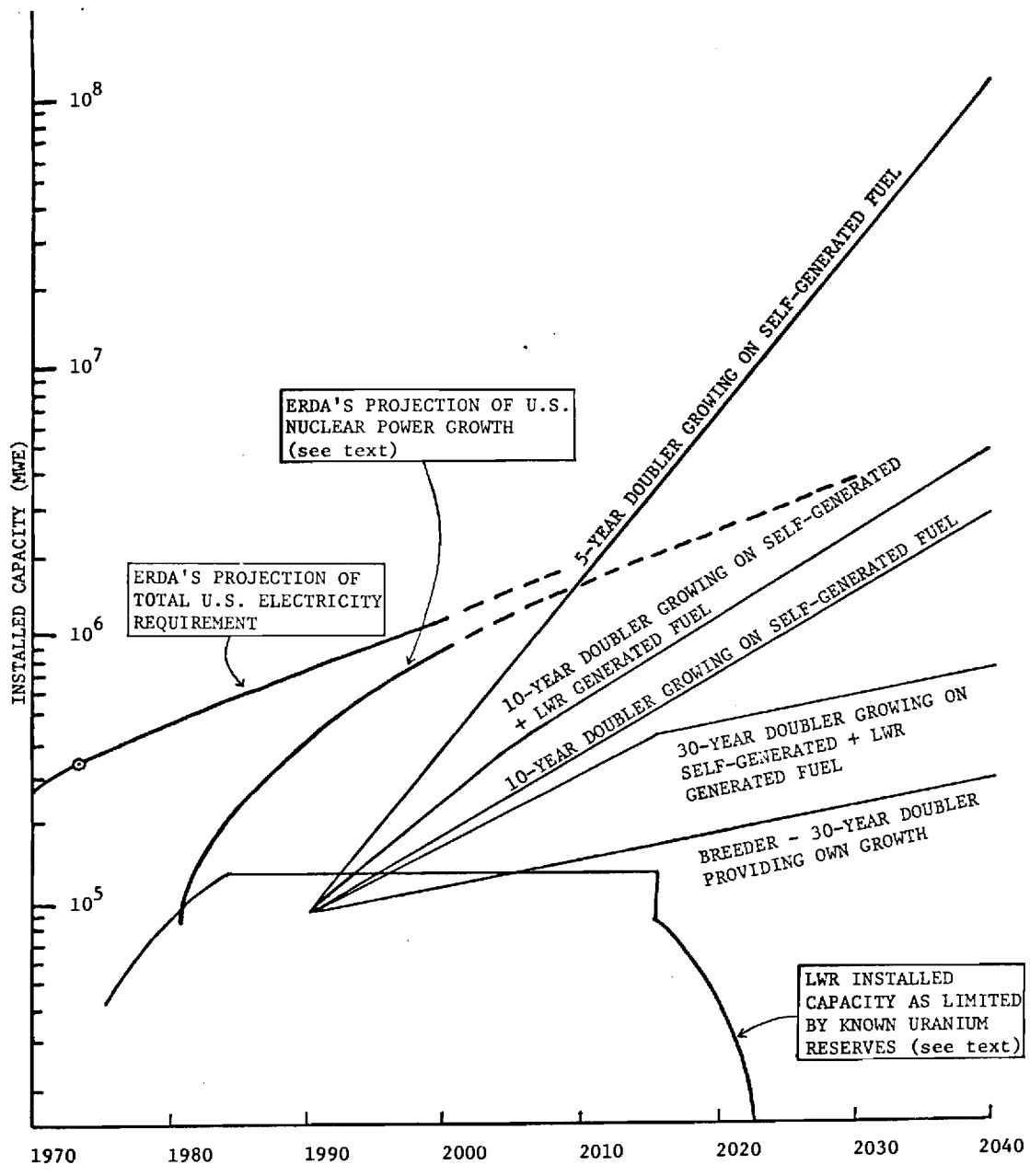


Fig. A-4-1. Electrical Energy Needs and Various Scenarios of Nuclear Power Growth

If one postulates that the growth of the LWR industry will continue until it reaches a level supportable by the U.S. proven reserves, and no more, then the total nuclear capacity possible would be 125,000 MWe assuming no plutonium recycle and 40-year plant lifetime. Should the uranium reserves, due to the greatly expanded exploration efforts, dramatically increase, ERDA's forecast of installed capacities can be reactivated. However, until major additional tracts of uranium deposits are found, it is prudent to follow a strategy based on what is, rather than on what might be. In this connection, one is reminded that on December 20, 1973, the Department of Interior leased 87 tracts in the Gulf of Mexico, off the shores of Mississippi, Alabama and Florida (MAFLA), for a fat \$1.49 billion. According to the Wall Street Journal (4/4/76), "The shallow Continental Shelf along the coastline of those states was virgin territory that brought a gleam to the oilman's eye." There was a great expectation that major finds in the Gulf of Mexico would be found and that these will force the Oil Producing Nations to roll back their prices. In 1976, however, drillers stunned geologists by coming up with 15 expensive holes so dry they were dusty. After a glum reassessment of their tracts, several oil companies had second thoughts and are relinquishing their rights to the leases.

The installed nuclear capacity in the U.S. in 1975 was 41,000 MWe (INFO, February 1976). If 10,000 MWe is added annually to the generating capacity, the 125,000 MWe level of LWR would be reached by 1984 and this level would stay constant for approximately 40 years unless changed by new discoveries of uranium deposits or by recycling plutonium. (Note that 700,000 short tons of U_3O_8 recoverable at cost up to \$30/lb is the basis for the 125,000 MWe capacity.) The quantities of uranium that could be

recovered at costs higher than \$30/lb from known deposits are very small according to ERDA.⁽⁵⁹⁾ The LWR projected generating capacity, as limited by the uranium reserve, is represented by the bottom curve in Fig. A-4-1. Flatness of this curve between 1984 and the year 2015 is due to the fact that all known reserves would have been committed to the installed capacity. Plutonium recycle is not considered because it is used more advantageously in breeders than in LWR's.

The fissile plutonium generated in LWR's is about 170 kg/1000 MWe or 272,000 kg by 1990, the year a breeder technology is assumed (optimistically) to come on line. Assuming a low fuel inventory of 3000 kg of fissile plutonium per breeder of 1000 MWe (comparable to LMFBR designs) and assuming that the fuel inventory is independent of the breeder's doubling time,^{*} we would have a breeder generating capacity of 90,000 MWe by 1990. The doubling time was varied: 30, 10, and 5 years were assumed and each breeder system was allowed to expand (1) at its own self-expanding rate (i.e. exponentially with characteristic doubling time) and (2) with additions from LWR generated plutonium. These curves are shown in Fig. A-4-1. (Note that the current estimates of the doubling time of the Clinch River Breeder Reactor, an LMFBR demonstration plant, is 34 years,⁽⁶⁰⁾ based on a breeding ratio of 1.20. Current estimates of breeding ratio tend to be high and consequently the doubling time may be as high as 60 years.

It is evident from Fig. A-4-1 that a breeder system with a doubling time of 30 years or longer does not have the potential to provide enough

* Note that this assumption is not valid; generally the doubling time is a function dependent on the fuel inventory, power density and the breeding ratio. For the purpose of trend projections, this dependence is not important.

electrical energy to cover projected requirements. In fact, even the 10-year doubler could not begin to cover requirements until the second half of the 21st century. The 5-year doubler would be ideal but unrealistic and perhaps unattainable when one considers fuel cycle delays and technology problems.

If projected electrical energy requirements are to be met and if no major new deposits of uranium are found, other sources than fission energy would have to be used extensively regardless of the LMFBR program.

There are those who question the continued growth of energy consumption. Indeed, the growth cannot be sustained indefinitely. It may even be desirable from the environmental point of view to deliberately plan no growth. These questions cannot be settled here and will have to be settled by society as a whole. Energy availability, however, will be a major factor which affects the direction society finally follows.

APPENDIX B

THORIUM-BASED REACTORS

THORIUM-BASED REACTORS

B.1 General Background

In response to a request in 1966 by the Congressional Joint Committee on Atomic Energy, the AEC organized a Thorium Systems Task Force for the purpose of an overall assessment of the Civilian Nuclear Power Program and the potential use of the thorium cycle in specific reactor designs. The task force was organized to essentially review and compile information, and to indicate the present status and the factors involved in the use of thorium in power reactors. Apparently the task force ". . . was not supposed to provide a comprehensive inquiry which would include national policy considerations, detailed assessment of the overall thorium cycle and power generation, and the effect of the introduction of a fast breeder on the use of thorium reactors."⁽⁶¹⁾ It was felt that LWR's will be the main vehicle with which the nuclear industry will make its start and eventually will be propagated through the successful entry of an economic fast breeder, presumably the LMFBR. The severe limitations on the LWR industry due to limited uranium reserves have already been discussed. The prospect for a successful debut of an LMFBR industry, acceptable to the public, remains cloudy and could go either way. Consider the recent statement by Dr. Robert C. Seamans, Jr., Administrator of ERDA,⁽⁶²⁾ "In conclusion, it must be emphasized that at this stage of LMFBR technology development we do not have all the answers necessary to determine the environmental acceptability, technical feasibility and economic competitiveness of LMFBR technology for widespread commercial deployment." Opponents of the LMFBR program consider it uneconomical, unnecessary, and unsafe. Public unease

has certainly been expressed about the widespread use of plutonium as indicated, for example, by the resolution of the National Council of Churches. More importantly, unless the doubling time of current LMFBR designs is improved drastically, this technology won't have the potential of meeting electrical energy needs.

Decreasing the doubling time with improvement in design is certainly possible. The French concept of heterogeneous cores,⁽⁶³⁾ as discussed in Ref. 64, essentially increases the overall volume fraction of fuel which increases the breeding ratio. Russian designs⁽⁶⁵⁾ contain lower sodium volume fractions and high fuel volume fractions and, therefore, have higher breeding ratios. Increasing the breeding ratio will decrease the doubling time (for further discussion of this see B-2-2). Improvements in doubling time are possible, but it is doubtful that such improvements would ultimately yield adequate doubling times unless the basic design of oxide fuel is changed to either carbide or metallic fuel whereby short doubling times are possible (more on this later).

A central factor which is the basis for most of the concern over LMFBR safety is the positive sodium-void coefficient. According to ERDA,⁽⁶⁶⁾ "Except for LMFBR designs in which a large positive reactivity worth zone could be suddenly and coherently voided as a result of a loss of flow accident accompanied by a total loss of control function, there is no possible initiator of an energetic core disruption prior to large scale loss of core integrity." Actually all current LMFBR designs have large positive central sodium-void coefficients and the loss of flow is not the only mechanism; sodium boiling could initiate uncontrollable transients with bad consequences.

In view of the facts that the LMFBR program as presently conceived:
(1) may not have the potential for meeting electrical energy needs any

time before the last part of the twenty first century (see Fig.A-4-1), (2) may prove to be uneconomical, (3) may continue to have problems with sodium-void coefficients, and (4) may be rejected by the public solely because of resistance to wide scale use of plutonium, it is most useful to consider alternative breeders with better breeding potential and safety characteristics. In the rest of this chapter we will review the general information on thorium-based reactors.

B.2 Physics Parameters

B.2.1 Breeding

A key parameter which characterizes the breeding potential of any reactor system is the production of neutrons per neutron absorbed in the fissile material. This parameter is known as η and its dependence on energy is shown in Fig. B-2-1. The striking feature of η ²³³ is that it is relatively independent of the incident neutron energy up to about 1 MeV. By contrast the η for Pu ²³⁹ is highly dependent on the neutron energy; it is lower than η ²³³ in the entire energy range below about 60 keV. The relationship of η for a particular isotope to the breeding potential of that isotope is given by the simple conversion ratio (CR) formula:

$$\overline{CR} = \overline{\epsilon\eta} - 1 - \overline{L}$$

where barred quantities represent averages over energy and spatial distributions.

$$\epsilon = 1 + \frac{\text{neutrons produced due to fissions in fertile material}}{\text{neutrons produced in fissile material}} \quad (1)$$

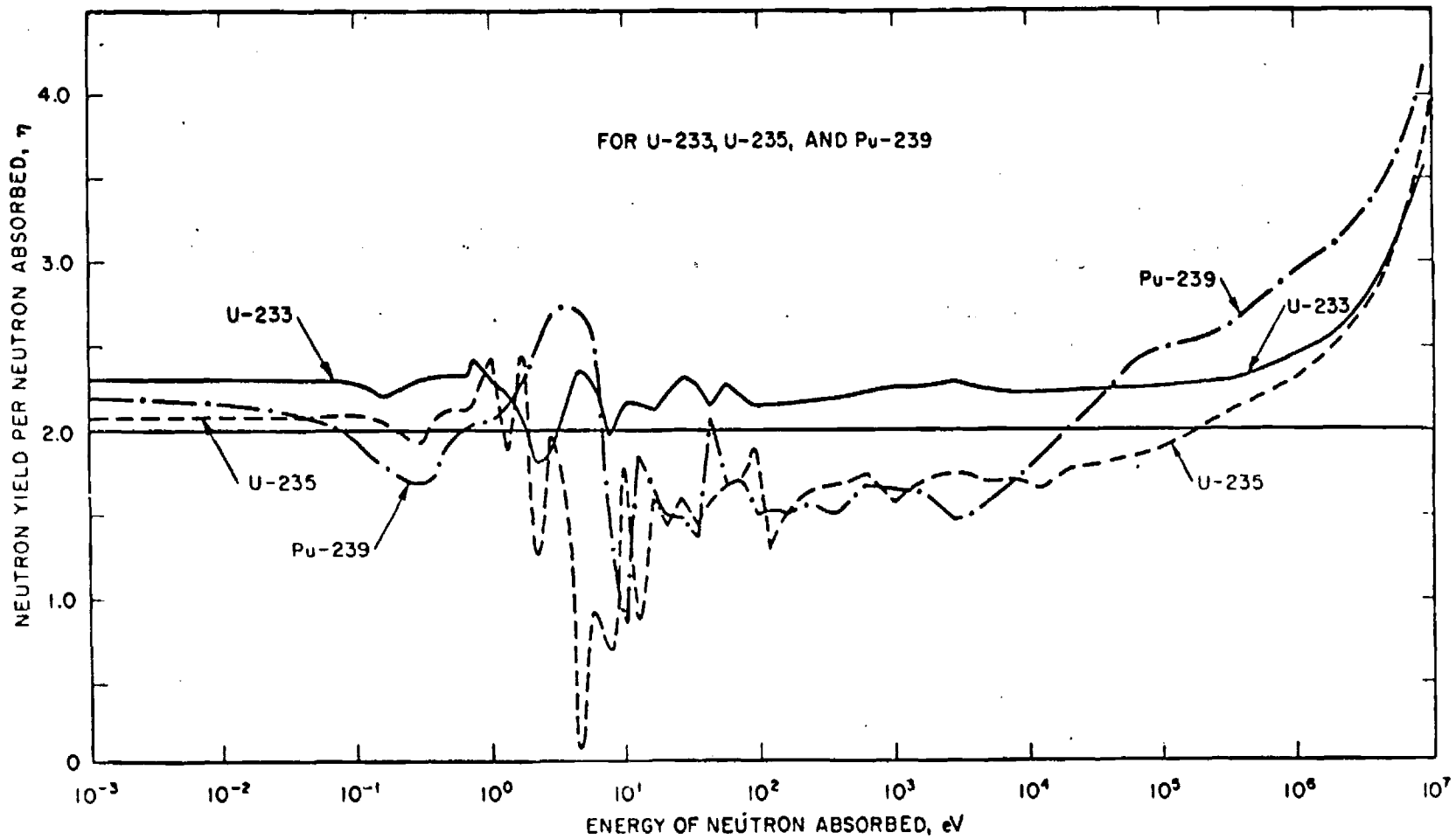


Fig. B-2-1 Neutron Yield per Neutron Absorbed, η vs Energy of Neutron Absorbed (Source Ref. 52).

and

L = neutrons lost parasitically and through leakage per neutron absorbed in the fissile fuel.

The conversion ratio measures the number of fertile atoms converted to fissile atoms for each fissile atom destroyed. If the value of \overline{CR} , averaged over the in-core fuel cycle time at equilibrium condition, is 1.0 or greater the conversion ratio becomes the breeding ratio, indicating that the reactor system can generate its own fissile material. It is highly desirable to have a breeding ratio much greater than 1.0 so that bred fuel in excess of what is needed by the operating plant may be used for expansion and growth.

The factor, ϵ , plays an important role in determining the final value of \overline{CR} . Because of lower fission threshold in U^{238} relative to thorium-232, the neutron yield in U^{238} is about four times that in Th^{232} . This property, which contributes significantly to \overline{CR} when the neutron spectrum is very hard, is apparently the main reason for the policy to develop the LMFBR with a U^{238} -based fuel rather than with a thorium cycle. In justifying this policy the AEC study, WASH-1097,⁽⁶¹⁾ cited some calculations performed by Okrent⁽⁶⁷⁾ prior to 1964 showing that for metallic fuel the conversion ratio in a small 1500 liter spherical core is 0.15 to 0.25 higher with U^{238} -Pu than with Th^{232} - U^{233} fuels. The fact that Okrent calculations apply to small metallic cores implies that the neutron spectrum was very hard. Consequently, the breeding potential of Pu^{239} would be expected to be better than U^{233} . The additional fission advantage of U^{238} over Th^{232} is gravy. Oxide, not metallic, fuel, however, is used in the LMFBR program and core sizes in excess of 8000 liters are typical. Both of these facts contribute

significantly to softening of the neutron spectrum and this renders the comparison irrelevant. Nevertheless, it is true that under comparable conditions ϵ for ^{238}U is higher than that for ^{232}Th and the fissions in ^{238}U relative to ^{232}Th , in typical LMFBR spectra, are approximately 4 to 1, (see Fig. B-2-2).

Increasing the value of the factor ϵ by including Be with thorium is possible on two counts: (1) the neutron production due to the Be (n,2n) reaction is about 25% of the production in ^{238}U in typical LMFBR spectra assuming equal atom density, and (2) the Be (γ ,n) reaction could increase the conversion ratio somewhat.

A high conversion ratio is desirable but, by itself, it does not guarantee a breeder concept which could grow fast enough to meet energy requirements. Along with a high conversion ratio it is desirable to have a low critical mass and a high power density. The doubling time which depends on all three variables is a better measure of the breeding performance of a reactor. In this regard the critical mass is dependent on the difference between the neutron yield and neutron absorption in the fissile isotope, i.e. $(\nu\sigma_f - \sigma_a)$. The larger the value of this quantity the lower the critical mass would be. Thus, if the critical mass is assumed to be inversely proportional to $\overline{\nu\sigma_f - \sigma_a}$ and if the breeding gain is assumed to be proportional to $\frac{1}{\epsilon\eta - 2}$, then the quantity, $\frac{1}{(\overline{\nu\sigma_f - \sigma_a})(\epsilon\eta - 2)}$, would be proportional to the doubling time. The doubling time is the time required for a breeder to double its fuel inventory and, for a given power density, is proportional to the critical mass divided by the breeding gain. The breeding gain is the breeding ratio minus one and it represents the excess fuel bred.

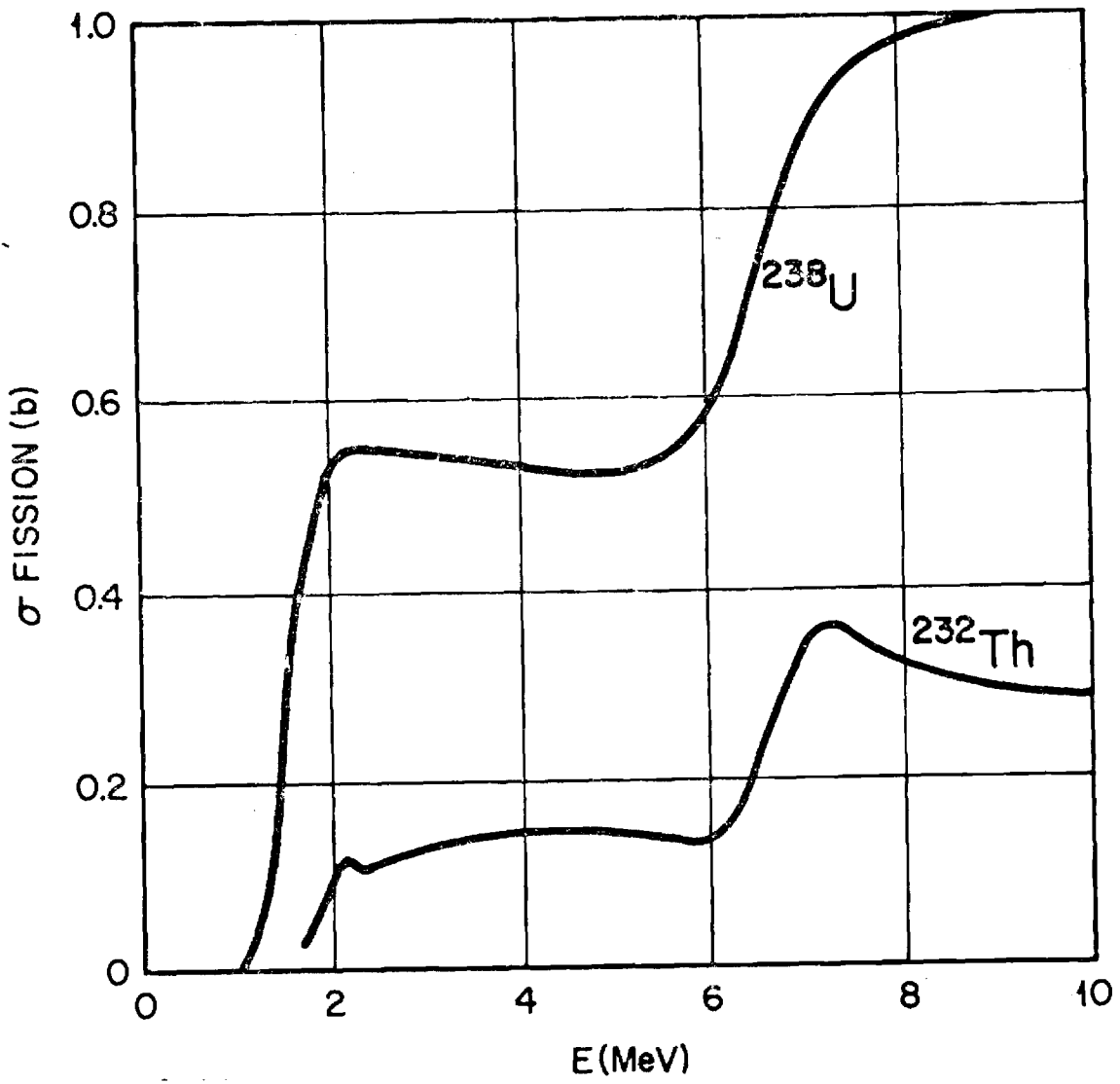


Fig. B-2-2. Fission Cross-Section of ^{232}Th and ^{238}U .

A comparison of the quantity, $\frac{1}{(\nu\sigma_f - \sigma_a)(\epsilon\eta - 2)}$, for U^{233} and Pu^{239} using multigroup formalism would be more meaningful with respect to breeding performance than conversion ratios. The values for the effective cross sections used in the comparison were recently generated⁽⁶⁸⁾ for the fundamental mode spectrum in the following reactors:

- $(U^{233} - Th^{232})O_2$ cooled by D_2O
- $(Pu^{239} - Th^{232})O_2$ cooled by D_2O
- $(Pu^{239} - U^{238})O_2$ cooled by sodium

The MC² code⁽³⁰⁾ which utilizes the narrow resonance treatment, equivalence theory for heterogeneity effects, and an exact legendre treatment for slowing down, was used. A total of about 2000 groups covered the energy range from 15 MeV to 0.43 eV. ENDF/B Version III data were used.

The unit-cell configuration of the D_2O reactors was fuel pins, 0.53 cm radius, surrounded by 0.1 cm thick zirconium clad (substituted for zircaloy) and 0.13 cm thick D_2O cooling jacket. The triangular unit-cell had a pitch to diameter ratio of 1.150.

The unit-cell configuration of the LMFBR reactor was a fuel pin, 0.28 cm radius, clad, 12 mil thick stainless steel, and an outer radius of 0.45 cm.

The homogenized atom densities of all three reactor compositions are given in Table B-2-I.

The values for the quantity, $\frac{1}{(\nu\sigma_f - \sigma_a)(\epsilon\eta - 2)}$, for each broad energy group are given in Tables B-2-II, B-2-III, and for all three reactors.

Examination of these tables reveals the following:

- (1) At energies above 100 KeV the breeding performance of $\text{Pu}^{239} - \text{Th}^{238}$ in an LMFBR is better than the breeding performance of $\text{U}^{233} - \text{Th}^{233}$ in a D_2O reactor. The improvement is primarily due to higher values of ϵ because of the higher fission rate in U^{238} .
- (2) Below about 50 keV the breeding performance of the $\text{U}^{233} - \text{Th}^{233}$ system is superior to the current LMFBR designs. This region extends all the way down to thermal energies.
- (3) The breeding performance of the $\text{U}^{233} - \text{Th}^{232}$ system could be improved further by including Be in the fuel composition. ^(69,70) MC² calculations ⁽³⁰⁾ indicate the neutron yield from the Be (n,2n) reaction is about 25% of the U^{238} fission yield. Additionally, the Be (γ ,n) reaction will add to the improvement.
- (4) Breeding below 20 keV and above thermal energies is not possible with plutonium systems. This is indicated in Table B-2-IV negative values for the quantity, $\frac{1}{(\nu\sigma_f - \sigma_a)(\epsilon\eta - 2)}$. The reason is that $\epsilon\eta$ is less than 2 (see Fig. III-2-1).
- (5) The best breeding potential for the $\text{U}^{233} - \text{Th}^{232}$ system is perhaps between 10 eV and 50 keV. In this energy range the $\nu\sigma_f - \sigma_a$ is large, the η^{233} is rather flat, and the effects of fission products are significantly less than in thermal reactors and hopefully manageable.

Fission product capture cross sections have been analyzed ⁽⁷¹⁾ by a combination of experimental results and statistical estimates for group cross sections for primary and secondary fission products covering the complete range of energies of interest to reactor calculations. Tables B-2-V, and B-2-VI, taken from Ref. 71, list the group cross sections for the slowly

and rapidly saturating fission products, respectively. It is seen from these data that the large capture resonances are below 10 eV. More work, however, is needed to assess the fission product effects on the breeding ratio of systems with average reaction rates in the energy region 10 eV - 50 keV.

Table B-2-I. Atom Densities in Heavy Water-Cooled ($U^{233}-Th^{232}$) O_2 and ($Pu^{239}-Th^{232}$) O_2 Reactors and in Sodium-Cooled ($Pu^{239}-U^{238}$) O_2 Reactors

Homogenized Atom Densities $\times 10^{-24}$																			
$(U^{233}-Th^{232})O_2$ in D_2O Coolant	<table border="1"> <thead> <tr> <th>U^{237}</th> <th>Th</th> <th>O</th> <th>D</th> <th>Zr</th> </tr> </thead> <tbody> <tr> <td>.00085483</td> <td>.0092365</td> <td>.030192</td> <td>.0200178</td> <td>.0085285</td> </tr> </tbody> </table>	U^{237}	Th	O	D	Zr	.00085483	.0092365	.030192	.0200178	.0085285								
	U^{237}	Th	O	D	Zr														
.00085483	.0092365	.030192	.0200178	.0085285															
$(Pu^{239}-Th^{232})O_2$ in D_2O Coolant	<table border="1"> <thead> <tr> <th>Pu^{239}</th> <th>Th</th> <th>O</th> <th>D</th> <th>Zr</th> </tr> </thead> <tbody> <tr> <td>.001190</td> <td>.008956</td> <td>.03030</td> <td>.0200198</td> <td>.0085285</td> </tr> </tbody> </table>	Pu^{239}	Th	O	D	Zr	.001190	.008956	.03030	.0200198	.0085285								
	Pu^{239}	Th	O	D	Zr														
.001190	.008956	.03030	.0200198	.0085285															
$(Pu^{231}-U^{238})O_2$ in Na Coolant	<table border="1"> <thead> <tr> <th>Pu^{239}</th> <th>Pu^{240}</th> <th>Pu^{241}</th> <th>Pu^{242}</th> <th>U^{238}</th> <th>O^{16}</th> <th>Na^{23}</th> <th>Fe</th> <th>Cr</th> </tr> </thead> <tbody> <tr> <td>.00307</td> <td>.00148</td> <td>.00033</td> <td>.00177</td> <td>.0136</td> <td>.023822</td> <td>.01227</td> <td>.008173</td> <td>.001776</td> </tr> </tbody> </table>	Pu^{239}	Pu^{240}	Pu^{241}	Pu^{242}	U^{238}	O^{16}	Na^{23}	Fe	Cr	.00307	.00148	.00033	.00177	.0136	.023822	.01227	.008173	.001776
	Pu^{239}	Pu^{240}	Pu^{241}	Pu^{242}	U^{238}	O^{16}	Na^{23}	Fe	Cr										
.00307	.00148	.00033	.00177	.0136	.023822	.01227	.008173	.001776											
	<table border="1"> <thead> <tr> <th>Ni</th> <th>Mo</th> </tr> </thead> <tbody> <tr> <td>.001217</td> <td>.0001494</td> </tr> </tbody> </table>	Ni	Mo	.001217	.0001494														
Ni	Mo																		
.001217	.0001494																		

Table B-2-II. Breeding Performance of $(U^{233}-Th^{232})O_2$
in D_2O -Cooled Reactor

Energy Group	E_{lower}, eV	$(\eta)_{U-233}$	$(\nu\sigma_f - \sigma_a)_{U-233}$	ϵ^*	$\frac{1}{(\nu\sigma_f - \sigma_a)(\epsilon\eta - 2)}$
1	0.60653×10^7	3.430	5.220	2.30470	3.2440×10^{-2}
2	0.36788×10^7	3.084	3.484	1.96920	8.3046×10^{-2}
3	0.22313×10^7	2.849	3.532	1.56136	1.1560×10^{-1}
4	0.13534×10^7	2.689	3.281	1.39831	1.7310×10^{-1}
5	0.82085×10^6	2.553	2.972	1.01046	5.8040×10^{-1}
6	0.38774×10^6	2.413	2.948	1.01000	8.2130×10^{-1}
7	0.18316×10^6	2.324	3.117	1.00000	9.9000×10^{-1}
8	0.11109×10^6	2.287	3.183	1.00000	1.0950×10^0
9	0.52475×10^5	2.270	3.324	1.00000	1.1140×10^0
10	0.19305×10^5	2.260	4.242	1.00000	0.9060×10^0
11	0.91188×10^4	2.251	5.802	1.00000	0.6870×10^0
12	0.43074×10^4	2.220	7.517	1.00000	0.6050×10^0
13	0.20347×10^4	2.139	9.821	1.00000	0.4330×10^0
14	0.96112×10^3	1.981	12.462	1.00000	-4.2230×10^0
15	0.45400×10^3	1.893	16.194	1.00000	-0.5771×10^0
16	0.21445×10^3	2.042	23.945	1.00000	0.9940×10^0
17	0.10130×10^3	2.050	30.856	1.00000	0.6480×10^0
18	0.47851×10^2	2.113	50.970	1.00000	0.1740×10^0
19	0.22603×10^2	2.265	66.412	1.00000	5.6800×10^{-2}
20	0.10677×10^2	2.150	141.940	1.00000	4.6960×10^{-2}
21	0.50435×10^1	2.110	156.513	1.00000	5.8100×10^{-2}
22	0.23824×10^1	2.168	112.130	1.00000	5.3000×10^{-2}
23	0.11254×10^1	1.923	485.400	1.00000	2.6700×10^{-2}
24	0.41399×10^0	2.330	181.490	1.00000	1.6690×10^{-2}

*See Equation (1) for definition of ϵ ; the ratio of fertile to fissile atom density was assumed to be 10.8.

Table B-2-III. Breeding Performance of $(\text{Pu}^{239}-\text{Th}^{232})\text{O}_2$
in D_2O -Cooled Reactor

Energy Group	$E_{\text{lower}}, \text{eV}$	$(\eta)_{\text{Pu-239}}$	$(\nu\sigma_f - \sigma_a)_{\text{Pu-239}}$	ϵ^*	$\frac{1}{(\nu\sigma_f - \sigma_a)(\eta\epsilon - 2)}$
1.	6.0653×10^6	3.983	6.302	2.1394	2.430×10^{-2}
2.	3.6788×10^6	3.541	4.338	1.6559	5.960×10^{-2}
3.	2.2313×10^6	3.259	4.416	1.4799	8.020×10^{-2}
4.	1.3534×10^6	3.094	4.216	1.3342	1.110×10^{-2}
5.	8.2085×10^5	2.974	3.505	1.0082	3.270×10^{-1}
6.	3.8774×10^5	2.796	3.058	1.0000	4.100×10^{-1}
7.	1.8316×10^5	2.596	2.700	1.0000	6.190×10^{-1}
8.	1.1109×10^5	2.525	2.696	1.0000	7.060×10^{-1}
9.	5.2475×10^4	2.464	2.846	1.0000	7.580×10^{-1}
10.	1.9305×10^4	2.165	2.695	1.0000	2.250×10^0
11.	9.1188×10^3	1.891	2.589	1.0000	-3.540×10^0
12.	4.3074×10^3	1.625	2.532	1.0000	-1.050×10^0
13.	2.0347×10^3	1.475	2.820	1.0000	-0.675×10^0
14.	9.6112×10^2	1.603	5.250	1.0000	-5.303×10^{-2}
15.	4.5400×10^2	1.621	8.810	1.0000	-4.300×10^{-2}
16.	2.1445×10^2	1.540	10.110	1.0000	-2.150×10^{-1}
17.	1.0130×10^2	1.652	19.234	1.0000	-1.490×10^{-1}
18.	4.7851×10^1	1.924	54.740	1.0000	-2.400×10^{-1}
19.	2.2603×10^1	1.027	0.810	1.0000	-1.268×10^0
20.	1.0677×10^1	1.706	53.110	1.0000	-6.400×10^{-2}
21.	5.0435×10^0	1.677	28.120	1.0000	-1.100×10^{-1}
22.	2.3824×10^0	2.644	17.730	1.0000	8.760×10^{-2}
23.	1.1254×10^0	2.291	32.020	1.0000	1.070×10^{-1}
24.	4.1399×10^{-1}	1.996	127.150	1.0000	-1.966×10^0

*See Equation (1) for definition of ϵ ; the ratio of fertile to fissile atom density was 10.80.

Table B-2-IV. Breeding Performance of $(\text{Pu}^{239}\text{-U}^{238})\text{O}_2$
in Sodium-Cooled Reactor

Energy Group	$E_{\text{lower}}, \text{eV}$	$(\eta)_{\text{Pu-239}}$	$(\nu\sigma_f - \sigma_a)_{\text{Pu-239}}$	ϵ^*	$\frac{1}{(\nu\sigma_f - \sigma_a)(\epsilon\eta - 2)}$
1	0.36788×10^7	3.6550	4.760	3.955	4.133×10^{-3}
2	0.22313×10^7	3.2620	4.415	3.567	2.344×10^{-2}
3	0.13534×10^7	3.0970	4.231	2.909	3.372×10^{-2}
4	0.82085×10^6	2.9820	3.516	1.422	1.269×10^{-1}
5	0.49787×10^6	2.9620	3.348	1.007	3.039×10^{-1}
6	0.30197×10^6	2.6850	2.859	1.000	5.096×10^{-1}
7	0.18316×10^6	2.5630	2.658	1.000	6.673×10^{-1}
8	0.11109×10^6	2.5260	2.693	1.000	7.053×10^{-1}
9	0.67379×10^5	2.7890	2.813	1.000	4.500×10^{-1}
10	0.40868×10^5	2.3950	2.859	1.000	8.855×10^{-1}
11	0.24788×10^5	2.1970	2.735	1.000	1.856×10^0
12	0.15034×10^5	2.0150	2.606	1.000	25.582×10^0
13	0.91188×10^4	1.9650	2.756	1.000	-10.367×10^0
14	0.43074×10^4	1.6530	2.577	1.000	-2.780×10^{-1}
15	0.26126×10^4	1.5490	2.947	1.000	-7.524×10^{-1}
16	0.20347×10^4	1.3330	2.150	1.000	-6.970×10^{-1}
17	0.12341×10^4	1.5190	4.048	1.000	-5.136×10^{-1}
18	0.96112×10^3	1.6750	6.696	1.000	-4.595×10^{-1}
19	0.58295×10^3	1.5120	5.797	1.000	-3.535×10^{-1}
20	0.27536×10^3	1.8017	14.537	1.000	-3.469×10^{-1}
21	0.10130×10^3	1.5880	17.491	1.000	-1.388×10^{-1}
22	0.29023×10^2	2.0156	49.360	1.000	1.299×10^0
23	0.13710×10^2	1.6400	26.910	1.000	-1.032×10^{-1}
24	0.30590×10^1	1.7230	47.250	1.000	-7.640×10^{-2}
25	0.68256×10^0	2.3710	29.018	1.000	9.288×10^{-2}

*See Equation (1) for definition of ϵ ; the ratio of fertile to fissile atom density was assumed to be 10.8.

Table B-2-V. Group Cross Sections for Slowly Saturating Fission Products (in barns)

Group	Energy interval (ev)	Slowly saturating									
		Mo ⁹⁵	Tc ⁹⁹	Rh ¹⁰³	Xe ¹³¹	Cs ¹³⁵	Nd ¹⁴³	Nd ¹⁴⁵	Pm ¹⁴⁷	Sm ¹⁵²	Eu ¹⁵³
10	1.05 × 10 ⁶ - 8.21 × 10 ⁵	0.04	0.20	0.10	0.07	0.08	0.04	0.04	0.24	0.07	0.5
19	1.11 × 10 ⁵ - 8.65 × 10 ⁴	0.16	0.60	0.36	0.23	0.24	0.11	0.10	0.53	0.18	1.20
28	1.17 × 10 ⁴ - 9.12 × 10 ³	0.78	1.60	1.00	0.69	0.74	0.40	0.37	3.10	1.20	5.30
37	1.23 × 10 ³ -	1.80	2.80	3.30	3.00	3.90	3.00	2.80	19.0	2.80	23.0
38	961-	2.00	3.20	3.60	3.70	4.70	3.70	3.40	23.0	3.00	26.0
39	748-	2.74	3.70	3.90	4.50	5.70	4.70	4.40	27.0	3.30	30.0
40	583-	1.93	4.30	4.40	5.50	6.90	5.80	5.40	33.0	4.10	35.0
41	454-	0	5.00	5.00	6.60	8.40	7.30	7.00	39.0	5.20	40.0
42	354-	0	5.80	5.70	8.00	11.0	9.20	8.70	48.0	6.50	47.0
43	275-	0	6.70	4.66	9.70	18.3	11.0	11.0	57.0	8.20	55.0
44	215-	0	21.8	9.44	12.0	8.2	14.0	14.0	67.0	10.0	63.0
45	167-	3.99	16.4	21.7	14.0	15.1	17.0	17.0	80.0	12.0	72.0
46	130-	0	9.8	1.92	17.0	27.8	21.0	21.0	96.0	15.0	83.0
47	101-	0	0	2.87	20.0	24.7	26.0	26.0	110	19.0	96.0
48	78.9-	0	0	0.41	11.9	0	0	32.0	130	24.0	110
49	61.4-	0	7.00	0	0	0	54.1	0	77.8	0	125
50	47.9-	387	6.20	2.19	44.0	60.0	0.11	210	397	0	140
51	37.3-	0.39	0	0	0	0	0.20	0	59.5	0	160
52	29.0-	0.44	0	0	0	0	0.35	0	0	0	41.1
53	22.6-	0.50	87.2	0	0	100.4	0.61	0	72.5	0	392
54	17.6-	0.56	0	0	2,850	0	1.02	0	65.7	0	44.7
55	13.7-	0.64	0	0	5.49	0	1.64	0	0	0	222
56	10.68-	0.72	0	0	6.22	0	2.57	0	0	0	38.2
57	8.32-	0.82	0	0	7.05	0	3.89	0	1,100	9,600	22.7
58	6.48-	0.93	320	0.75	7.98	1,330	5.72	0	7,200	14.4	156
59	5.04-	1.05	1.66	1.65	9.05	2.11	8.13	5.20	0	16.3	595
60	3.93-	1.20	1.88	3.92	10.3	2.40	11.3	5.13	0	18.5	696
61	3.06-	1.35	2.13	10.4	11.6	2.70	15.1	5.81	0	20.9	1,742
62	2.38-	1.52	2.41	33.6	13.2	3.10	19.7	6.58	0	23.7	0
63	1.86-	1.73	2.73	183	14.9	3.50	25.2	7.46	0	26.8	164
64	1.44-	1.96	3.10	2,940	16.9	3.90	31.4	8.45	41.7	30.4	22.0
65	1.125-	2.22	3.51	480	19.1	4.50	38.5	9.57	27.0	34.5	26.7
66	0.876-	2.51	3.98	170	21.7	5.10	46.5	10.8	31.0	39.1	35.2
67	0.683-	2.85	4.51	106	24.6	5.70	55.5	12.3	35.0	44.2	40.0
68	0.532-	3.23	5.11	83.4	27.9	6.50	65.5	13.9	40.0	50.1	48.5
69	0.414-	3.66	5.79	74.0	31.6	7.40	76.7	15.8	45.0	56.8	59.0
70	0.322-	4.14	6.56	71.0	35.8	8.30	89.1	17.9	51.0	64.4	71.0
71	0.251-	4.69	7.43	71.0	40.5	9.50	103	20.3	58.0	72.9	90.0
72	0.196-	5.32	8.42	74.0	45.9	10.7	119	23.0	66.0	82.7	105
73	0.152-	6.03	9.54	78.0	52.0	12.1	136	26.0	75.0	93.7	127
74	0.119-	6.83	10.8	84.0	59.0	13.8	156	29.5	85.0	106	154
75	0.0924-	7.74	12.2	91.0	66.8	15.6	178	33.4	96.0	120	186
76	0.0719-	8.77	13.9	100	75.7	17.7	203	37.8	109	136	225
77	0.0561-	9.93	15.7	111	85.8	20.0	231	42.9	124	154	273
78	0.0436-	11.3	17.8	124	97.2	22.7	262	49.0	140	175	333
79	0.0340-	12.8	20.2	138	110	25.7	298	55.1	159	198	400
80	0.0265-	14.5	22.9	155	125	29.1	339	62.4	180	225	485
81	0.0206-	16.4	25.9	174	141	33.0	384	70.7	204	254	592
82	0.0161-	18.6	29.4	196	160	37.4	436	80.1	231	288	715
83	0.0125-	21.0	33.3	221	182	42.4	494	90.8	262	327	865
84	0.0097-	23.8	37.7	250	206	48.0	561	103	297	370	1,070
85	0.0076-	27.0	42.7	282	233	54.4	636	117	337	419	1,300
86	0.0059-	30.6	48.4	319	264	61.6	723	132	382	475	1,600
87	0.0046-	34.7	54.8	359	299	69.8	814	150	433	539	1,900
88	0.0036-	39.3	62.2	407	339	79.1	905	170	491	610	2,300

Table B-2-VI. Group Cross Sections for Rapidly Saturating and Nonsaturating Fission Products and Xe¹³⁵ (in barns)

Group	Energy interval (ev)	Rapidly saturating					Xe ¹³⁵	Nonsaturating ^a		
		Cd ¹¹³	Sm ¹⁴⁹	Sm ¹⁵¹	Gd ¹⁵⁵	Gd ¹⁵⁹		233	235	239
10	1.05 × 10 ⁶ -	0.10	1.20	0.50	0.40	0.24	—	0.026	0.028	0.044
	8.21 × 10 ⁵ -									
19	1.11 × 10 ⁵ -	0.35	3.00	1.00	1.40	0.57	—	0.091	0.10	0.15
	8.65 × 10 ⁴ -									
28	1.17 × 10 ⁴ -	1.20	7.20	5.20	6.20	3.10	—	0.33	0.36	0.51
	9.12 × 10 ³ -									
37	1.23 × 10 ³ -	2.70	18.0	25.0	17.0	7.70	—	1.07	1.13	1.53
38	961-	3.10	22.0	29.0	20.0	9.30	—	1.07	1.14	1.59
39	748-	3.60	26.0	34.0	24.0	11.0	—	1.36	1.47	2.01
40	583-	4.20	32.0	40.0	28.0	13.0	—	2.38	2.61	3.26
41	454-	5.00	38.0	46.0	33.0	16.0	—	4.62	5.76	6.83
42	354-	6.00	46.0	54.0	38.0	19.0	—	2.99	2.97	4.07
43	275-	7.20	55.0	63.0	44.0	23.0	—	4.13	4.14	4.84
44	215-	12.9	66.0	73.0	52.0	27.0	—	1.99	2.05	3.63
45	167-	0	78.0	84.0	60.0	32.0	—	2.12	1.67	3.28
46	130-	13.7	93.0	97.0	69.0	37.0	—	1.81	1.85	2.81
47	101-	29.4	123	110	80.0	44.0	—	9.24	8.94	10.3
48	78.9-	12.6	300	130	92.0	52.0	—	8.12	9.26	11.8
49	61.4-	0	210	150	100	66.1	—	2.43	2.63	4.46
50	47.9-	0	238	170	157	37.8	—	5.16	5.51	7.34
51	37.3-	0	110	200	326	0	—	3.74	3.33	14.7
52	29.0-	0	194	230	93.7	0	1	7.97	4.49	3.50
53	22.6-	6.69	0	260	349	0	2	0.21	0.13	0.23
54	17.6-	0	279	300	81.7	472	4	4.02	6.61	7.93
55	13.7-	0	75.4	340	78.7	0	7	0.59	0.93	4.43
56	10.68-	0.25	79.6	390	14.4	0	12	0.21	0.20	0.28
57	8.32-	0.50	0	440	791	0	20	0.21	0.20	0.24
58	6.48-	1.14	154	956	0	0	36	2.34	1.80	78.6
59	5.04-	2.16	723	314	0	0	67	0.29	0.27	0.49
60	3.93-	4.15	1.93	0	0	0	127	0.39	0.33	0.58
61	3.06-	8.01	3.67	0	2854	350	241	0.43	0.37	0.53
62	2.38-	15.4	6.94	1040	567	17.0	454	0.51	0.43	0.61
63	1.86-	30.6	13.4	847	8.09	32.9	871	3.09	1.74	5.67
64	1.44-	61.1	25.9	1490	15.2	62.0	1670	0.72	0.59	0.82
65	1.125-	125	4300	2000	28.8	117	3250	0.84	0.68	0.95
66	0.876-	265	4400	23.0	54.5	223	6360	1.05	0.84	1.10
67	0.683-	583	204	43.0	103	425	12,700	1.24	0.99	1.30
68	0.532-	1380	426	78.0	198	815	25,600	1.44	1.16	1.50
69	0.414-	3587	924	143	378	1571	53,200	1.66	1.32	1.70
70	0.322-	10,700	2120	256	726	3043	1.14 × 10 ⁵	1.99	1.50	2.00
71	0.251-	34,400	5250	455	1400	5910	2.48 × 10 ⁵	2.08	1.71	2.17
72	0.196-	59,000	14,600	790	2670	11,400	5.55 × 10 ⁵	2.42	1.94	2.50
73	0.152-	44,900	45,500	1340	5020	21,900	1.18 × 10 ⁶	2.75	2.20	2.80
74	0.119-	30,200	104,000	2200	9210	40,700	2.14 × 10 ⁶	3.16	2.51	3.20
75	0.0924-	23,500	111,000	3450	15,900	70,700	2.86 × 10 ⁶	3.52	2.80	3.56
76	0.0719-	20,400	74,000	5200	24,900	111,000	2.98 × 10 ⁶	4.00	3.20	4.04
77	0.0561-	19,100	54,900	7400	35,200	154,000	2.86 × 10 ⁶	4.62	3.63	4.63
78	0.0436-	18,800	46,100	10,100	44,900	192,000	2.74 × 10 ⁶	5.20	4.10	5.23
79	0.0340-	19,200	42,100	13,100	53,100	221,000	2.69 × 10 ⁶	5.90	4.65	5.95
80	0.0265-	20,200	40,800	16,500	60,200	246,000	2.73 × 10 ⁶	6.70	5.28	6.76
81	0.0206-	21,600	41,200	20,100	66,700	269,000	2.83 × 10 ⁶	7.60	5.95	7.70
82	0.0161-	23,400	42,900	24,100	73,600	294,000	3.00 × 10 ⁶	8.60	6.75	8.70
83	0.0125-	25,600	45,500	28,400	80,800	320,000	3.23 × 10 ⁶	9.72	7.70	9.80
84	0.0097-	28,300	49,200	33,300	89,600	352,000	3.52 × 10 ⁶	11.0	8.80	11.1
85	0.0076-	31,400	53,700	38,500	98,900	389,000	3.88 × 10 ⁶	12.5	9.90	12.6
86	0.0059-	35,000	59,200	44,300	110,000	431,000	4.30 × 10 ⁶	14.2	11.2	11.3
87	0.0046-	39,100	65,200	50,500	123,000	478,000	4.76 × 10 ⁶	16.0	12.7	15.8
88	0.0036-	43,600	72,000	56,900	138,000	540,000	5.30 × 10 ⁶	18.2	14.3	18.4

^aEach nonsaturating fission product has been multiplied by its yield from U²³³, U²³⁵, and Pu²³⁹ fission, separately. These products have been summed to obtain the combined group cross sections tabulated in the last three columns.

B.2.2 Doubling Time and Specific Power

The concept of breeding ratio and breeding gain is straightforward and simple, but apparently there is no definition for the breeding ratio that is universally accepted. The difficulty arises from the fact that the fuel composition of the initial loading in a breeder reactor differs from the ultimate, equilibrium composition in a closed cycle. In a closed cycle at equilibrium, the composition of a fuel charge is closely related to the discharge composition. Part of the discharged bred fuel is used back into the same reactor; surplus fuel is used to fuel other reactors. By contrast, the fuel in an open cycle operation always reflects the composition of the feed fuel, consequently the breeding ratio in open cycles is time-dependent. Additional complications in the definition of the breeding ratio come from inconsistencies in what is considered fissile isotopes. For example, some consider U^{235} in natural uranium as fissile fuel; others discount it. Some adjust the critical mass as a function of burnup to compensate for fission product buildup; this obviously affects the breeding gain. Others reduce all isotopes of plutonium to equivalent Pu^{239} . A comprehensive discussion of these considerations is found in Ref. 72-76. In this work the following definitions, patterned after Ref. 75 are chosen as a frame of reference for comparison. The breeding ratio and breeding gains are time averaged quantities over one fuel cycle which begins with start-up and ends with refueling.

$$\text{Breeding Gain (BG)} = \frac{(\text{Fissile})_{\text{EOC}} - (\text{Fissile})_{\text{BOC}}}{\text{Fissile Destroyed}} \quad (1)$$

$$= \frac{\text{Fissile Gain}}{\text{Fissile Loss}}$$

where EOC = end of cycle

BOC = beginning of cycle

$$\text{Breeding Ratio (BR)} = \frac{\text{Fissile Produced}}{\text{Fissile Loss}} = \frac{\text{Fissile Loss} + \text{Fissile Gain}}{\text{Fissile Loss}} \quad (2)$$

$$= 1 + \text{BG}$$

$$\text{Reactor Doubling Time (RDT)} = \frac{(\text{Fissile})_{\text{BOC}}}{\frac{\text{Fissile Gain}}{\text{Fuel Cycle}} \times \text{Fuel Cycles/Year}} \quad (3)$$

$$\text{Inventory Doubling Time (IDT)} = \frac{(\text{Fissile})_{\text{BOC}} (1 + \text{fex})}{\frac{\text{Fissile Gain} - \text{Loss}_{\text{ex}}}{\text{Fuel Cycle}} \times \text{Fuel Cycles/Year}} \quad (4)$$

where fex = fraction of fissile inventory external to reactor in critical mass units

Loss_{ex} = out-of-reactor losses during the course of reprocessing and fabrication plus losses associated with radioactive decay.

$$\text{Compound Inventory Doubling Time (CIDT)} = 0.693 (\text{IDT}) \quad (5)$$

$$\text{RDT} = \frac{(\text{Fissile})_{\text{BOC}}}{(\text{BR}-1) \times \frac{\text{Fissile Loss}}{\text{Fuel Cycle}} \times \text{Fuel Cycles/Year}} \quad (6)$$

But

$$\frac{\text{Fissile Loss}}{\text{Fuel Cycle}} = \frac{\text{Energy Produced (MWD)}}{\text{Fuel Cycle}} \times \frac{\text{Fuel Consumed}}{\text{MWD}} \times \frac{\text{Fissions in Fissile}}{\text{Total Fissions}} \times \frac{\text{Fissile Loss (Capture + Fissions)}}{\text{Fissile Fissioned}} \quad (7)$$

Combining (7) into (6) one gets

$$(\text{RDT}) = \frac{1}{(\text{BR}-1) \frac{\text{Energy Produced (MWD)/Fuel Cycle}}{(\text{Fissile}) \text{ BOC}} (\text{ABC}) \times \frac{\text{Fuel Cycles}}{\text{Year}}} \quad (8)$$

where

A = the conversion factor of fuel fissioned per MWD

B = the ratio of fissions originating in fissile to total fissions

C = the fissile loss due to capture and fission divided by the loss due to fission only or $(1+\alpha)$

A is not system dependent, B depends on the relative fissions in fissile and fertile materials and C depends on the α , the capture to fission ratio of the fissile isotopes only.

From Eq. (8) we see that RDT is inversely proportional to the breeding gain and the specific energy, MWD/kg fissile for one fuel cycle. The average specific power, in MW/kg of fissile material, is obtained by dividing the specific energy by the length of the fuel cycle in days.

For a cylindrical fuel element with a radius a cm and a clad of thickness Δ cm surrounded by a coolant having a heat transfer coefficient h , it can be shown^(77,78,79) that the specific power and heat generation are related to the engineering characteristics of the reactor by the relation

$$\text{Specific Power (SP)} = Q/d = (T_{MF} - \bar{T}_c) / \left(d \frac{a^2}{4k_F} + \frac{a^2}{2} \left(\frac{1}{k_{cl}} \ln \frac{b}{a} + \frac{1}{hb} \right) \right) \quad (9)$$

where

Q = heat generation rate per unit volume of fuel

d = fissile fuel density

T_{MF} = maximum fuel temperature at pin center

\bar{T}_c = average coolant temperature

a = fuel radius

b = a + clad thickness Δ

k_F, k_{cl} = thermal conductivity of fuel and clad, respectively

h = average heat transfer coefficient.

By substituting Eq. (9) into Eq. (8) one gets

$$\text{RDT} = \frac{\left[d \left[\frac{a^2}{4k_F} + \frac{a^2}{2} \left[\frac{1}{k_{cl}} \ln \frac{b}{a} + \frac{1}{hb} \right] \right] \right]}{(BR-1) (T_{FM} - \bar{T}_c) \frac{\text{Days}}{\text{Fuel Cycle}} (ABC) \times \frac{\text{Fuel Cycles}}{\text{Year}}} \quad (10)$$

With Eq. (10), it is possible to make several observations:

- (1) The relationship between the density of fissile material, d , and the breeding ratio is such that if d decreases while the fuel volume fraction is held constant (equivalent to decreasing the enrichment), the volume of the reactor increases and the breeding ratio in typical, $^{239}\text{Pu} - ^{238}\text{U}$ LMFBR system, decreases. On the other hand, transport calculations have shown that the D_2O -cooled $(^{233}\text{U} - \text{Th})\text{O}_2$ system would have a conversion ratio

of 1.16 at 8.5% enrichment and 1.14 at 12% enrichment. The fissile density was .37 kg/liter and .48 kg/liter at the lower and higher enrichments, respectively. These results support the conclusion that the U²³³-Th system would exhibit better RDT performance at relatively soft (not necessarily thermal) neutron spectra.

- (2) The fuel which would give the lowest RDT is the fuel with the highest thermal conductivity (see Table B-2-VII).
- (3) The RDT for a particular fuel increases as the square of the radius of the fuel pin. Consequently, the smallest pin diameter consistent with economic constraints is desired.
- (4) While it is desirable to have a high heat transfer coefficient for the coolant, it may not have significant effects on RDT if

$$\frac{1}{hb} \ll \frac{1}{4k_F} + \frac{1}{2k_{cl}} \ln \frac{b}{a} .$$

B.2.3 Breeder Strategy

Based on data shown in Fig. A-4-1, it was stated that, if projected energy requirements are to be met and if no major new deposits of uranium are found, other sources than fission energy would have to be used extensively regardless of the LMFBR program. In this section we show that thorium-based breeders could realistically compete with current designs of LMFBR's. In fact, thorium-based breeders can have not only comparable breeding ratios but superior doubling time regardless of the form of fuel, i.e. oxide, carbide or metal.

For completeness we will only mention that various schemes to improve, or stretch, fuel utilization⁽⁸¹⁻⁸³⁾ have been studied and that such schemes

Table B-2-VII. Thermal Conductivity k_f of Some Fuel Materials*
(Btu/hr-ft-°F)

Temperature, °F	Uranium	UO ₂	UC	PuO ₂	Thorium	ThO ₂
200	15.80	4.5	14.77	3.60	21.75	7.29
300	16.40	...	14.07	22.18	6.25
400	17.00	3.5	13.48	22.60	5.34
500	17.50	...	13.02	23.00	4.61
600	18.10	2.8	12.67	23.45	4.03
700	18.62	...	12.39	23.90	3.59
800	19.20	2.5	12.19	24.30	3.21
900	19.70	...	12.02	24.65	2.91
1000	20.25	2.2	11.91	25.75	2.68
1100	20.75	25.60	2.47
1200	21.20	2.0	11.82	26.13	2.30
1300	21.60	2.17
1400	22.00	1.6	11.76	1.57	2.07
1600	1.5	11.70	1.90
1800	1.4	11.67	1.80
2000	1.3	11.57	1.70
2200	1.2	1.69
2400	1.1	1.68
2600	1.1
2800	1.1
3000	1.1
3200	1.1

* Values given are for unirradiated materials and usually decrease on irradiation. The percent decrease is a function of both irradiation temperature and burnup. The ceramics (UO₂, ThO₂, and UC) in particular suffer a large decrease. For example, k_f for UO₂ decreases by some 60 percent on irradiation at 200°F and after 4,000 Mw-day/ton burnup. For UC the decrease is about 58 percent on irradiation at 1000-1500°F and after 7,500-10,000 Mw-day/ton burnup. (Source Ref. 84)

may prove to be too little and too late, especially if the uranium reserve picture does not change dramatically for the better. In the same category as the improved converters is the LWBR. Our analysis showed that the LWBR will be a good converter but not a true breeder. Apparently ERDA sees a potential for this concept and is proceeding with a demonstration reactor in Shippingport.⁽⁵²⁾ There are three major drawbacks to the LWBR:

- (1) In the initial phase, the demand for new uranium to fuel the "pre-breeder" reactors would be about 2.5 times more than the demand for the current LWR fuel cycle.⁽⁵²⁾ This increase in demand, apparently, would not taper off to LWR levels for a period of 12 years. At a time when there is so much uncertainty about uranium reserves, the LWBR could be the straw that breaks the camel's back!
- (2) The "pre-breeder" of the LWBR concept would also require a significant increase in the enrichment capacity.
- (3) The LWBR could not possibly provide a solution to electrical energy demands on a timely schedule unless a dramatic increase in uranium reserves is realized. Basically this concept emphasizes long term conservation rather than making abundant supplies of fuel possible.

The Molten Salt Breeder Reactor (MSBR) has an attractive potential for reasonable doubling times, perhaps 15 years.⁽⁶¹⁾ This program, however, has been out of funds for some time presumably because of material problems with graphite expansion after irradiation. Experience has shown⁽⁶¹⁾ that dimensional changes occur as a result of irradiation, first contraction then expansion. The rate of volumetric expansion after the graphite reaches its

initial volume again becomes large and this limits its performance. Graphite irradiation limit was estimated at 3×10^{22} neutrons/cm². This corresponds to 2-4 years lifetime exposure. Another concern with graphite is its permeability to xenon isotopes. This adversely affects the breeding ratio. A third concern is the embrittlement of Hastelloy-N by helium, which is produced in the metal when irradiated.

In addition to the material problems of the MSBR, there are logistical problems. Currently the U²³³ inventory is very limited. To get this program to any kind of start would require using U²³⁵ which would further limit the supply for LWR's. Consequently, the way in which breeder concept impacts current technology and how readily it could bring relief to power demand become very important.

The AEC's and now ERDA's plan is to use LWR generated plutonium with U²³⁸ as oxide fuel in LMFBR's. The breeding ratio of such systems is low, perhaps as low as 1.1, or lower, and the doubling time is high, perhaps as high as 60 years (see Ref. 60). This low performance when added to the uncertainty in safety and economics fully justifies a search for alternatives.

Our strategy is to use plutonium-thorium fuel in metallic form in either sodium cooled or helium cooled fast reactors as interim breeders. In time, U²³³ - Th²³² fuel will be recycled in the same reactor with beryllia, if needed, to enhance the breeding ratio and minimize the critical mass. Justification for this approach is delineated below.

B.2.3.1 Metallic Pu-Th Interim Breeders

Our investigations indicate that metallic Pu-Th fuels with high burnup, good thermal conductivity, high power density, and low doubling time in either sodium cooled or helium cooled reactors are technologically possible. There has been limited irradiation of thorium-uranium metallic fuel. The results showed that thorium-based fuels exhibit superior irradiation stability over uranium alloys. (23,25,61) The consensus is that such fuel would perform well in power reactors. No experimental data have been reported on the irradiation tolerance of metallic Pu-Th fuels. What is needed is an immediate program designed to establish the temperature and irradiation limits of these fuels. EBR-II is operating and could immediately be used for this purpose.

The thermal conductivity for metallic fuel is at least 10 times more than oxide fuel and this would contribute significantly to the reduction of RDT (see Eq. 10).

The breeding ratio for metallic Pu-Th fuel is expected to be comparable to that for $(\text{Pu-U}^{238})\text{O}_2$ because of the difference in the neutron spectrum. The spectrum with oxide fuels is relatively soft due to the scattering with oxygen which results in lower total fissions in U^{238} . The hardness of the spectrum in metallic fuel improves the breeding ratio on two counts: (1) the η of Pu increases, and (2) the total fissions in Th^{232} increases. Both have positive effects on the breeding ratio.

The good thermal conductivity and the small diameter particles when combined with the excellent heat transfer properties of sodium or the relative good properties of helium should produce high power densities and low RDT's.

The use of thorium instead of U^{238} in the fuel would improve the sodium void coefficient and thus contribute to the safety features of those reactors.

It is not certain that including beryllia in the design would improve the breeding ratio with Pu-Th fuel because the $n, 2n$ and γ, n production of neutrons in Be is offset by a decrease in η^{239} as a result of spectrum softening. But since η^{233} is not sensitive to changes in the neutron spectrum, including beryllia in the U^{233} -Th cycle would improve the breeding ratio.

The technology for metallic fuel and sodium cooled reactors is reasonably at hand. EBR-II has been operating for about 14 years and represents a vast experience to draw upon. We only lack experimental data on the behavior of the Pu-Th²³² and U^{233} -Th²³² fuels under reactor irradiation conditions.

B.2.4 Coolant Void Coefficient

The coolant-void coefficient is a design parameter of considerable importance to the safe operation of a nuclear power plant. The sodium-cooled fast breeder reactors, fueled with Pu²³⁹-U²³⁸, have a positive void coefficient in a large region about the center of the core. Loss of flow and/or sodium boiling in this region could initiate transients with severe consequences. ERDA currently is funding large programs concerned with safety issues directly related to the void coefficient.

The major reasons for the sodium-void being positive in Pu-U²³⁸ systems may be seen from Fig. B-2-3 in which the fission cross sections for U²³³, U²³⁵ and Pu²³⁹ are shown as a function of energy. As a consequence of the

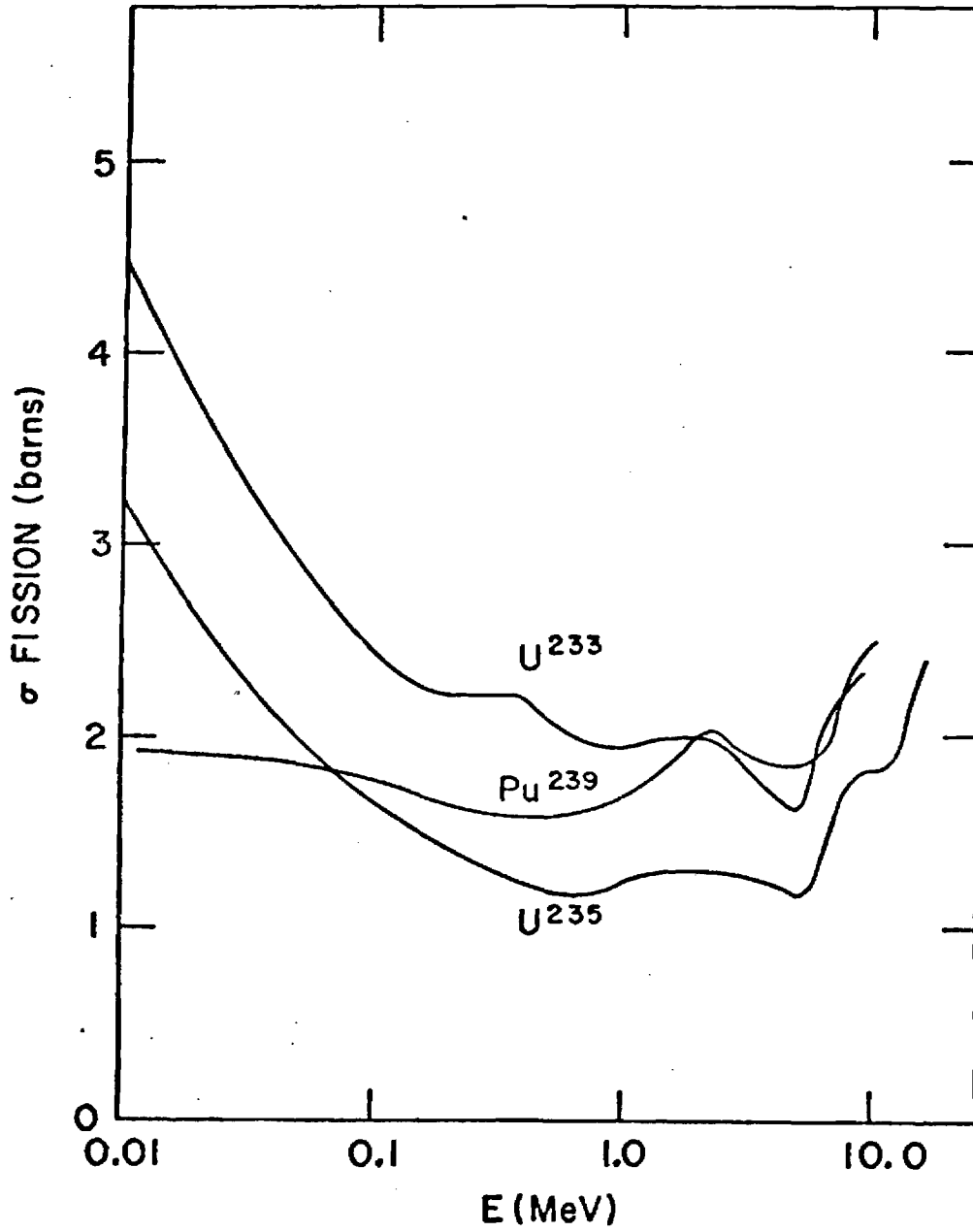


Fig. B-2-3. Fission Cross Sections of U^{233} , U^{235} , and Pu^{239} as a Function of Energy (source Ref. 61).

voiding, the neutron spectrum hardens, i.e., the average energy increases resulting in lower parasitic captures in Pu^{239} , U^{238} , and structural material and a higher fission rate in U^{238} . The Pu^{239} fission cross section below about 1 MeV is not sensitive to variation in the neutron energy. Above 1 MeV the spectral hardening would increase the fission rate in Pu^{239} . All of these effects increase the reactivity of the system.

In thorium-based reactors, cooled with sodium or helium, the same analysis applies except in this case a significant reduction in the fission rate of U^{233} takes place, as a result of spectral hardening, offsetting any increase in the thorium fission rate. Thus, it is possible to design sodium-cooled U^{233} - Th^{232} systems with negative void coefficients. Helium cooled thorium-based reactors have a negative void coefficient.

B.2.5 Doppler Coefficient

The Doppler coefficient of fissile material is usually small and perhaps positive. The Doppler effect of fertile material is large and negative. When both the fissile and fertile materials are homogeneously mixed, either fuel cycle can have a large negative Doppler effect. When the neutron spectrum is relatively soft, as should be the case for the He cooled $(\text{U}^{233}-\text{Th}^{232})\text{C}_2$ system, the Doppler coefficient should be significantly larger and negative.

B.2.6 Protactinium Production

A neutron capture in Th^{232} results in Pa^{233} which decays with a 27-day half-life. As a result, Pa^{233} will build up such that the build-up of U^{233} is delayed. This gives rise to several special problems of safety

and operation. The build-up of ^{233}Pa increases the excess reactivity to be controlled for burnup and the decay of ^{233}Pa to ^{233}U causes an increase in reactivity after shutdown. In a study by Sofer et al. ⁽⁸⁵⁾ it was concluded that these characteristics of the ^{233}U - ^{232}Th reactor do not materially affect the operation and safety of the reactor.

The absorption of a neutron by a ^{233}Pa atom is of more importance to breeding considerations because not only a neutron is lost but also the eventual breeding of one ^{233}U atom. The full impact of the conversion of ^{233}Pa to ^{234}U and its effects on the breeding ratio has not, as far as we are aware, been assessed comprehensively in the epithermal region. The effects of ^{234}U presence on the sodium-void coefficient in ^{233}U - ^{232}Th fast reactors were considered by Lowenstein and Blumenthal. ⁽⁸⁶⁾ The breeding ratio in a fast ^{233}U - ^{232}Th system ⁽⁸⁵⁾ was not, apparently, adversely affected by the presence of ^{233}Pa ; in fact, the total breeding ratio for the fuel cycle was higher than the initial conversion ratio.

B.2.7 Uranium-232 Production

The transmutations by nuclear reactions in thorium-based reactors are shown in Fig. B-2-4. For comparison, the transmutations in U-based reactors are shown in Fig. B-2-5. The production of ^{232}U comes from the $n,2n$ reactions in ^{233}U , ^{233}Pa , and ^{232}Th . The daughter products of ^{232}U are also shown in Fig. B-2-4. The daughter products Bi-212 and Tl-208 emit high energy gamma rays, 0.4 - 2.1 MeV from Bi-212 and 2.6 MeV from Tl-208.

For a limited time after chemical purification of the ^{233}U from a reactor, the material will emit weak radiation. However, as Bi-212 builds up, the radiation becomes more intense and it becomes necessary to use

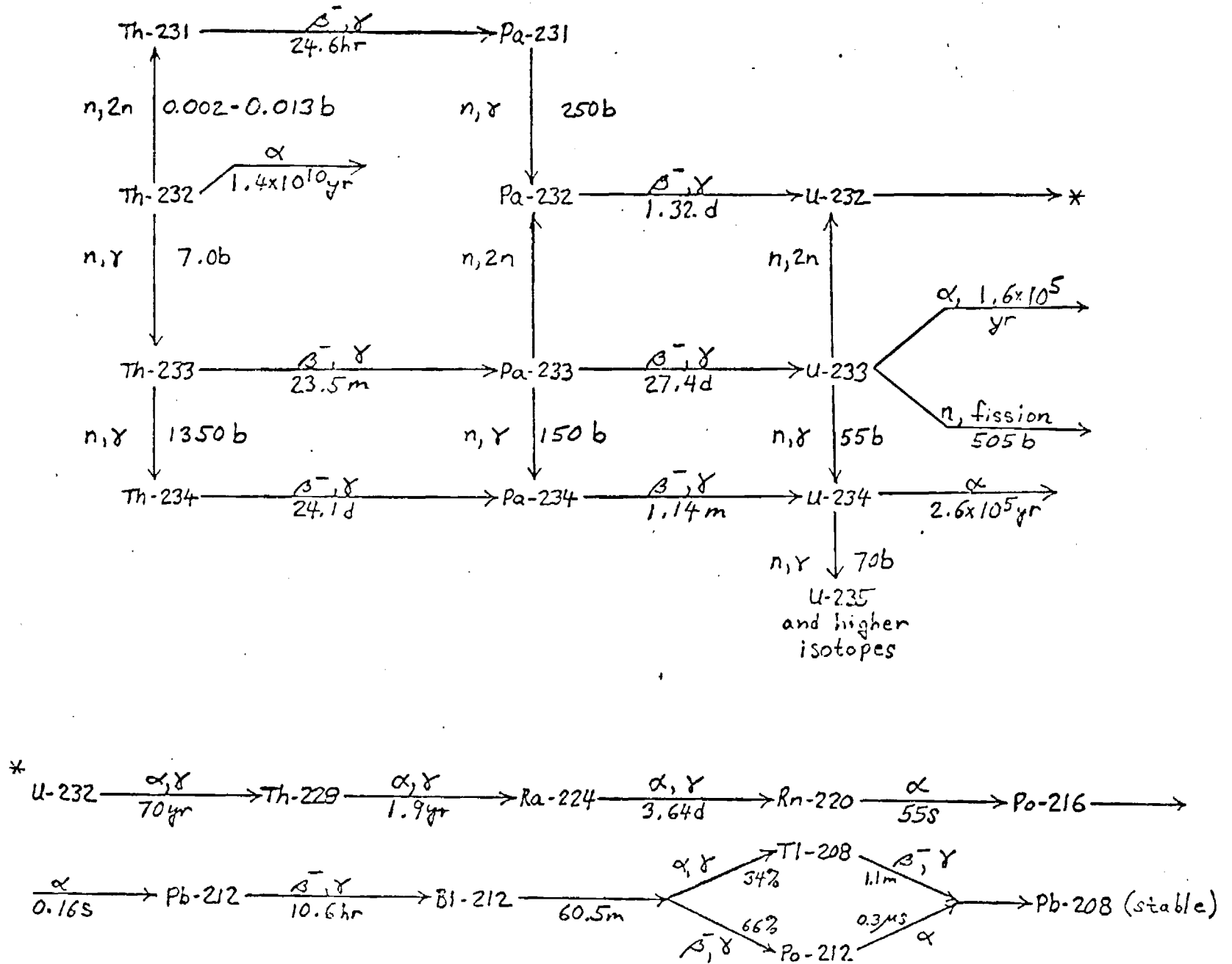
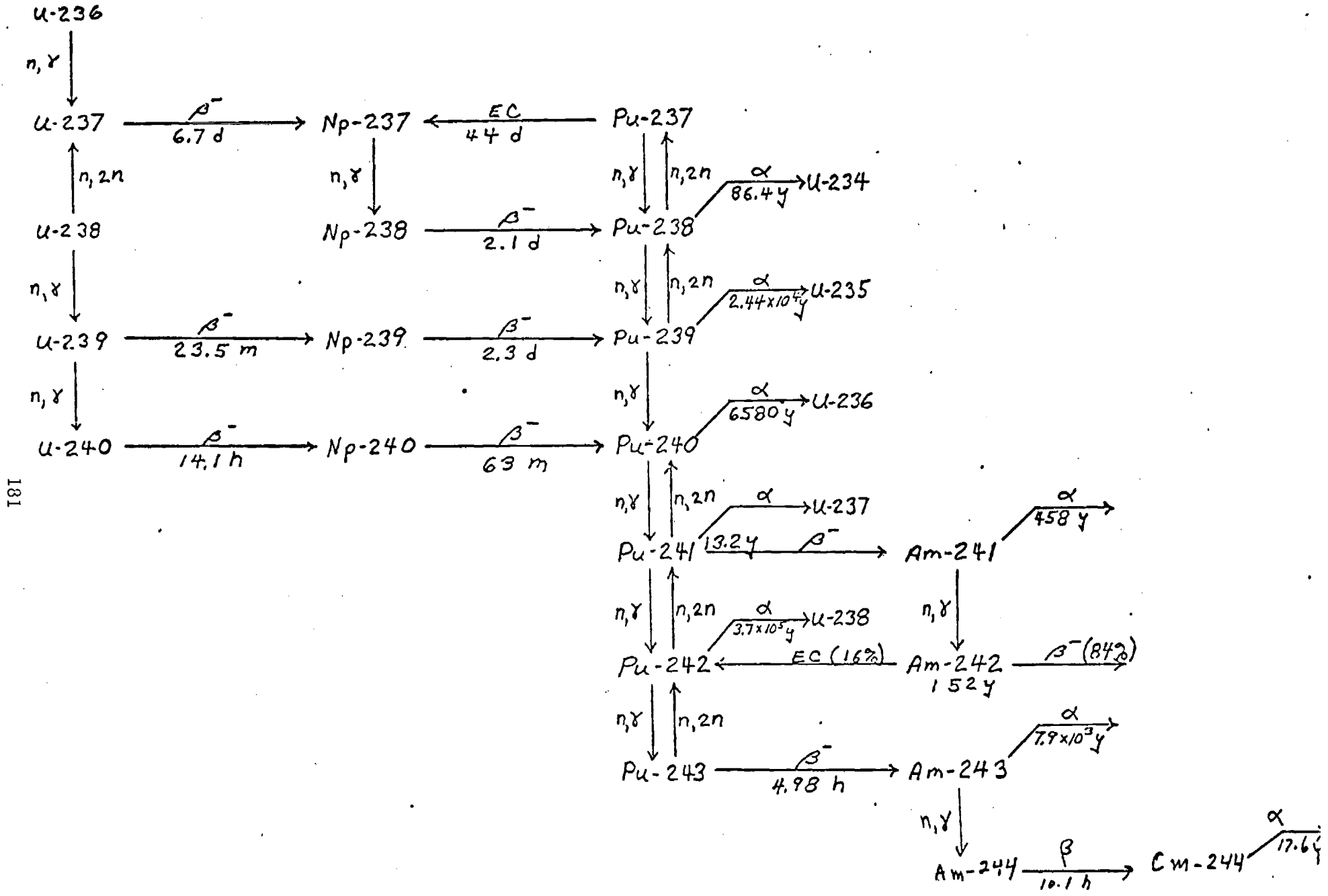


Fig. B-2-4. Nuclear Reactions Occurring in the Neutron Irradiation of Thorium



181

Fig. B-2-5. Nuclear Reactions Occurring in the Neutron Irradiation of Uranium

remote handling procedures. The radiation intensity from spheres of U^{233} contaminated by U^{232} was calculated by Devaney⁽⁸⁷⁾ and the results are as follows:

Results:

1. The radiation level at the surface is given by:

$$r = 2 \text{ cm } 14.0 \text{ x (T.F.)}$$

$$r = 3 \text{ cm } 14.8 \text{ x (T.F.)}$$

$$r = 4 \text{ cm } 15.0 \text{ x (T.F.)}$$

$$r = 5 \text{ cm } 15.2 \text{ x (T.F.)}$$

is units of roentgens
 232
per hr-ppm U

(T.F.) is the time factor and may be read from Fig. B-2-6.

2. The energy intensity at the surface is:

$$r = 2 \text{ cm } 1.56 \text{ x } 10^{10} \text{ x (T.F.)}$$

$$r = 3 \text{ cm } 1.67 \text{ x } 10^{10} \text{ x (T.F.)}$$

$$r = 4 \text{ cm } 1.71 \text{ x } 10^{10} \text{ x (T.F.)}$$

$$r = 5 \text{ cm } 1.74 \text{ x } 10^{10} \text{ x (T.F.)}$$

in units of MeV/hr-
 232
cm²-ppm U

3. In order to get irradiations and intensities at a distance $R (< r)$ from the center of the sphere, multiply the numbers of 1 and 2 by $(r/R)^2$.

The time factor to be used with these results is given in Fig. B-2-6. The equilibrium concentration of U^{232} in uranium was estimated by Sofer et al.⁽⁸⁵⁾ at 5000 ppm which would not be reached until 100 years of irradiation.

The U^{232} problem is a distinct disadvantage of the U^{233} - Th 232 fuel cycle. Fuel fabrication, however, can still be carried out without remote handling equipment if the U^{233} is chemically separated from trace

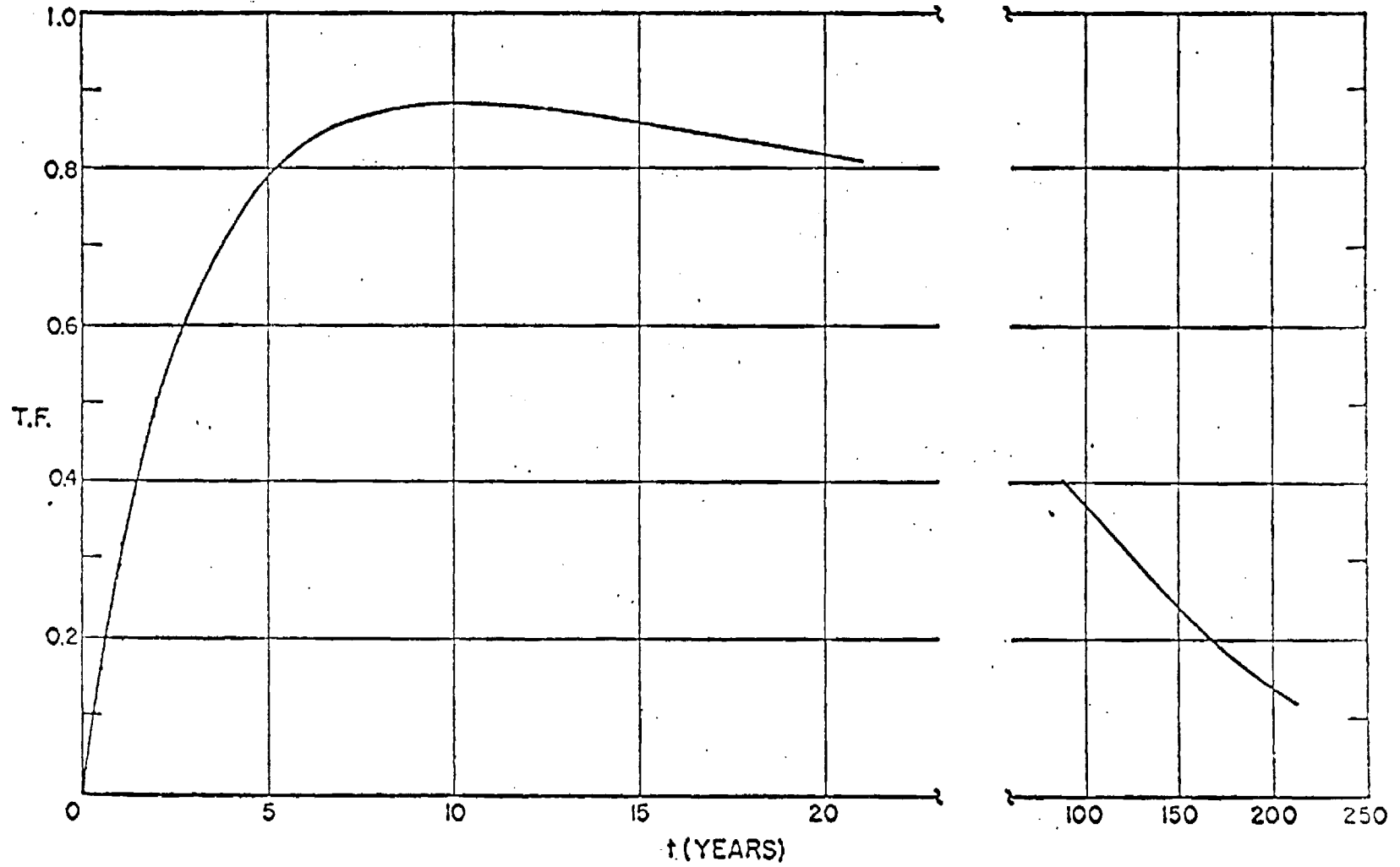


Fig. B-2-6. Time Factor (T.F.) $\equiv (e^{-0.0099t} - e^{-0.3647t})$ vs t (years)

amounts of Th^{228} and all other daughter products of U^{232} just before fabrication. Experimental procedures to remove Th^{228} have been successfully demonstrated at Los Alamos. ⁽⁸⁸⁾

In one regard, the suggestion advanced as a solution to safeguarding fissile material enroute from reprocessing plants or fuel fabrication plants to power stations that the fuel be spiked by gamma emitting isotopes to discourage potential saboteurs from attempts on the material, applies naturally to U^{233} .

B.2.8 Transuranium Element Production

Figures B-2-4 and B-2-5, cited earlier, show the isotopic build up in thorium and uranium systems. Although the relative hazards assessment associated with each fuel cycle would require knowledge of the absolute quantities of each of the isotopes at equilibrium conditions, it is safe to say that Pu^{238} , Pu^{239} , Pu^{240} , Am^{241} , and Am^{243} are more hazardous than U^{232} , U^{233} , U^{234} , U^{235} , and U^{236} . Morgan et al ⁽⁸⁹⁾ studied the relative hazards of various radionuclides. Assigning a relative hazard of 1.0 for Ra^{226} , they computed the relative hazards listed in Table B-2-VIII for the main transuranium elements listed above.

Table B-2-VIII, Relative Hazards of Transuranium Elements in Th²³² and U²³⁸ Fuel Cycles

Thorium Cycle	Relative Hazard	U ²³⁸ Cycle	Relative Hazard
Thorium-232	1.11 x 10 ⁻⁷	U-238	1.37 x 10 ⁻⁷
Pu-233	1.67 x 10 ⁻³	Np-239	4.46 x 10 ⁻⁴
U-233	2.38 x 10 ⁻³	Pu-238	152.0
U-234	1.49 x 10 ⁻³	Pu-239	1.04
U-235	4.85 x 10 ⁻⁷	Pu-240	384
U-236	1.48 x 10 ⁻⁵	Pu-241	3.23
Np-237	4.91 x 10 ⁻³	Pu-242	6.21 x 10 ⁻²
		Am-243	.97

B.2.9 Delayed Neutron Fraction

The delayed neutron fraction is an important control parameter in the safe operation of nuclear reactors. The number of delayed neutrons per fission for the relevant fissile and fertile isotopes are given in Table B-2-IX. Although the delayed neutron fraction for U²³³ is larger than that for Pu²³⁹, the effective delayed neutron fraction in Pu²³⁹-U²³⁸ systems is comparable to that in U²³³-Th²³² systems because of the larger number of fissions in U²³⁸ relative to Th²³².

Table B-2-IX. Delayed Neutrons per Fission (Source Ref. 90).

Delayed Neutrons per Fission	Th ²³²	U ²³³	U ²³⁵	U ²³⁸	Pu ²³⁹	Pu ²⁴⁰
	.0496	.0070	.0165	.0412	.0063	.0088
	± 0.002	± 0.004	± 0.0005	± .0017	± .0003	± .006

APPENDIX C

HEAT CONDUCTION THROUGH
SUCCESSIVE SPHERICAL SHELLS

HEAT CONDUCTION THROUGH SUCCESSIVE SPHERICAL SHELLS

C.1 Heat Conduction Through A Single Spherical Shell

The steady state heat equation with no heat generation is generally in the form of Laplace's equation in three dimensions. For spherically symmetric problems, however, it would reduce to one dimensional, second order, ordinary differential equation.

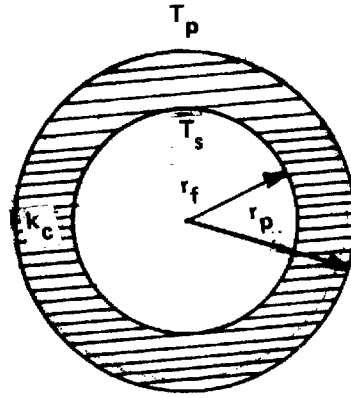


Fig. C-1. Sketch of a Single Spherical Shell With Inside and Outside Radii of r_f and r_p respectively

The Laplace's Equation is

$$\nabla^2 T(r, \theta, \phi) = 0 \quad (C-1)$$

For spherically symmetric problem $T(r, \theta, \phi) \equiv T(r)$. Thus

$$\frac{1}{r^2} \frac{d}{dr} \left(r^2 \frac{d}{dr} T(r) \right) = 0 \quad (C-2)$$

$$r^2 \frac{d}{dr} T(r) = A' \equiv \text{constant} \quad (C-3)$$

$$\frac{d}{dr} T(r) = \frac{A'}{r^2} \quad (C-4)$$

By integration:

$$T(r) = -\frac{A'}{r} + B' \quad A' \text{ and } B' \text{ are constants} \quad (C-5)$$

Now applying boundary conditions:

$$\text{at } r = r_f \implies T = T_s \quad (C-6)$$

$$r = r_p \implies T = T_r \quad (C-7)$$

to Eq. (C-5) yields

$$\left\{ \begin{array}{l} T_s = -\frac{A'}{r_f} + B' \\ T_p = -\frac{A'}{r_p} + B' \end{array} \right. \quad (C-8)$$

$$(C-9)$$

Solving Equations (C-8) and (C-9) for A' , one gets

$$A' = \frac{\frac{T_s - T_p}{\frac{1}{r_p} - \frac{1}{r_s}}}{\frac{1}{r_p} - \frac{1}{r_s}} \quad (C-10)$$

But from the Fourier Equation for heat conduction, we have

$$q = -A_f K_c \left. \frac{dT(r)}{dr} \right|_{r=r_f} \quad (C-11)$$

or equally

$$q = -A_p K_c \left. \frac{dT(r)}{dr} \right|_{r=r_p} \quad (C-12)$$

where $q \equiv$ amount of heat conducted

$K_c \equiv$ thermal conductivity of the shell

$A_f =$ area of sphere of radius r_f

$A_p =$ area of sphere of radius r_p

Upon substitution of equations (C-9) and C-10) in (C-11) and (C-12) one gets

$$q = A_f \left[\frac{K_c}{r_f \left(1 - \frac{r_f}{r_p} \right)} \right] (T_s - T_p) \quad (C-13)$$

$$q = A_p \left[\frac{K_c}{r_p \left(\frac{r_p}{r_f} - 1 \right)} \right] (T_s - T_p) \quad (C-14)$$

Equations (C-13) and (C-14) are exactly the same. In terms of the diameter of a particle the above equations could be written as:

$$q = A_f \left[\frac{2K_c}{D_f \left(1 - \frac{D_f}{D_p} \right)} \right] (T_s - T_p) \quad (C-15)$$

$$q = A_p \left[\frac{2K_c}{D_p \left(\frac{D_p}{D_f} - 1 \right)} \right] (T_s - T_p) \quad (C-16)$$

C.2 Heat Conduction Through Three Layer Spherical Shell

Since the amount of heat conducted through each layer is the same, the above equations could be generalized for each of the successive layers.

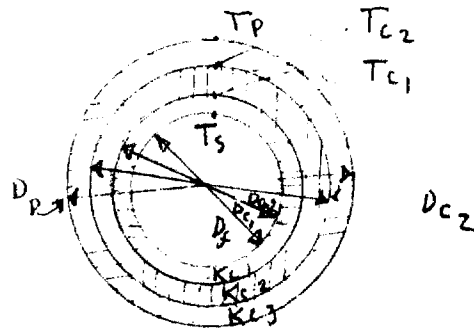


Fig. C.II: Sketch of Three Successive Spherical Shells

$$q = A_f \left[\frac{2K_{c1}}{D_f \left(1 - \frac{D_f}{D_{c1}} \right)} \right] (T_s - T_{c1}) \quad (C-17)$$

$$q = A_{c1} \left[\frac{2K_{c2}}{D_{c1} \left(1 - \frac{D_{c1}}{D_{c2}} \right)} \right] (T_{c1} - T_{c2}) \quad (C-18)$$

$$q = A_p \left[\frac{2K_{c3}}{D_p \left(\frac{D_p}{D_{c2}} - 1 \right)} \right] (T_{c2} - T_p) \quad (C-19)$$

Since the concern is with the temperature drop through the three layers, the above equations, namely (C-17), (C-18), and (C-19) for the temperature differences through each layer are:

$$T_s - T_{c1} = \frac{q}{A_f} \frac{D_f \left(1 - \frac{D_f}{D_{c1}} \right)}{2K_{c1}} \quad (C-20)$$

$$T_{c1} - T_{c2} = \frac{q}{A_{c1}} \left[\frac{D_{c1} \left(1 - \frac{D_{c1}}{D_{c2}} \right)}{2K_{c2}} \right] \quad (C-21)$$

$$T_{c2} - T_p = \frac{q}{A_p} \left[\frac{D_p \left(\frac{D_p}{D_{c2}} - 1 \right)}{2K_{c3}} \right] \quad (C-22)$$

By adding all three equations (C-20), (C-21), and (C-22) one gets

$$T_s - T_p = q \left[\frac{1}{A_f} \frac{D_f \left(1 - \frac{D_f}{D_{c1}} \right)}{2K_{c1}} + \frac{1}{A_{c1}} \frac{D_{c1} \left(1 - \frac{D_{c1}}{D_{c2}} \right)}{2K_{c2}} + \frac{1}{A_p} \frac{D_p \left(\frac{D_p}{D_{c2}} - 1 \right)}{2K_{c3}} \right] \quad (C-23)$$

But q is the amount of heat generated in the fuel particle, as

$$q = q''' \times V_f \quad (C-24)$$

where $V_f =$ volume of the fuel kernel $\equiv \frac{\pi}{6} D_f^3$

$q''' =$ volumetric heat source strength

substituting (C-24) in (C-23) yields

$$T_s - T_p = q''' \left[\frac{D_f}{6} \cdot \frac{D_f \left(1 - \frac{D_f}{D_{c1}} \right)}{2K_{c1}} + \frac{D_f}{6} \cdot \left(\frac{D_f}{D_{c1}} \right)^2 \cdot \frac{D_{c1} \left(1 - \frac{D_{c1}}{D_{c2}} \right)}{2K_{c2}} + \frac{D_f}{6} \cdot \left(\frac{D_f}{D_p} \right)^2 \cdot \frac{D_p \left(\frac{D_p}{D_{c2}} - 1 \right)}{2K_{c3}} \right] \quad (C-25)$$

This relationship describes the temperature drop through three spherical shells with heat generation in the fuel kernel, for a constant volumetric heat source strength.

C.3 Heat Generation in Spherical Geometry

The steady state heat equation with heat generation is generally in the form of Poisson's Equation:

$$\Delta^2 T + \frac{q'''}{K_f} = 0 \quad (C-26)$$

where $T = T(r, \phi, \theta) \equiv$ temperature distribution

$q''' =$ volumetric heat source strength

$K_f =$ thermal conductivity of fuel kernel



Fig. C-III: Sketch of the Spherical Fuel Kernel With Radius r_f and thermal conductivity K_f .

Equation (C-26) is a general form of the temperature distribution with internal heat production. However, in the case of a spherically symmetric problem with flat volumetric heat source strength (constant q'''), the problem is greatly simplified:

$$\frac{1}{r^2} \frac{d}{dr} \left(r^2 \frac{d}{dr} T(r) \right) + \frac{q'''}{K_f} = 0 \quad (C-27)$$

Upon integration, one gets:

$$\frac{dT(r)}{dr} = -\frac{q'''}{K_f} \cdot \frac{r}{3} + \frac{A}{r^2}, \quad A \equiv \text{constant} \quad (C-28)$$

Integration of Eq. (C-28) yields,

$$T(r) = -\frac{q'''}{K_f} \frac{r^2}{6} - \frac{A}{r} + B, \quad B \equiv \text{constant} \quad (C-29)$$

Applying boundary conditions

$$\text{at } r = 0 \implies T = T_m \quad (C-30)$$

$$\text{at } r = r_f \implies T = T_s \quad (C-31)$$

The first boundary condition, Eq. (C-30), implies that $A = 0$, and the second one, (C-31), yields $B = T_m$. By substituting the results into Eq. (C-29), one gets

$$T_m - T_s = \frac{q'''}{K_f} \cdot \frac{r_f^2}{6} \quad (C-32)$$

But amount of heat generated is

$$q = q''' V_f = \frac{\pi}{6} D_f^3 \quad (C-33)$$

Solving for q''' , one gets

$$q''' = \frac{q}{\frac{\pi}{6} D_f^3} \quad (C-34)$$

Substituting (C-34) into (C-33) and solving for q one gets

$$q = A_f \left(\frac{4K_f}{D_f} \right) (T_m - T_s) \quad (C-35)$$

APPENDIX D
THERMAL HYDRAULICS CODE

COMPUTER PROGRAM

Definition of Variables

- ROC1 \equiv density of the first coating layer (low density pyrolytic carbon
gr/cm³)
- ROC2 \equiv density of the second coating layer (SiC)
- ROC3 \equiv density of the third coating layer (ZrC)
- ROF \equiv density of the fuel kernel
- TCC11 \equiv thermal conductivity of the first coating layer (low density prolytic
carbon) $\frac{\text{watt}}{^{\circ}\text{C}\cdot\text{cm}}$
- TCC22 \equiv thermal conductivity of the second coating layer
- TCC33 \equiv thermal conductivity of the third coating layer (ZrC)
- TCFF \equiv thermal conductivity of the fuel kernel
- CPP \equiv specific heat of gas $\frac{\text{watt}\cdot\text{sec}}{\text{gr}\cdot^{\circ}\text{C}}$
- GPRESS \equiv gas static press [psi]
- TGI \equiv core gas inlet temperature [^oF]
- SUPFV \equiv superficial velocity of the gas [m/sec]
- HC \equiv height of the core [m]
- void \equiv gas volume fraction in core
- CONST \equiv a constant used in pressure drop formula for fixed bed

D_p ≡ fuel particle diameter (cm)
THICK ≡ total coating thickness (cm)
THICK1 ≡ thickness of the first layer (carbon coating)
THICK2 ≡ thickness of the second layer (SiC)
THICK3 ≡ thickness of the third layer (ZRC)

```

1          PROGRAM FIXRUN2(INPUT,OUTPUT,TAPE5=INPUT,TAPE6=OUTPUT)
C
C
C THIS PROGRAM CALCULATES POWER DENSITY OF A HE-GAS-SUSPENDED-BED
C NUCLEAR REACTOR AS A FUNCTION OF FUEL PARTICLE SIZE WITH MAXIMUM
C THREE LAYERS COATINGS OVER FUEL KERNEL .
      READ(5,1) ROC1,ROC2,ROC3,ROF
      READ(5,1) TCC11,TCC22,TCC33,TCFF,CPP
65      READ(5,2) GPRESS,TGI,SUPFV,HC,VOID,CONST
      IF(GPRESS.LT.100.) GO TO 999
      ROGI=(0.00595/(TGI+460.))*GPRESS
75      READ(5,3) DP,THICK,THICK1,THICK2
      IF(DP.LT.1.00E-06) GO TO 888
      1  FORMAT(7F10.5)
      2  FORMAT(6F10.5)
      3  FORMAT(4F10.5)
      PI=3.14159
      DF=DP-(2.*THICK)
      DC1=DF+(2.*THICK1)
20      DC2=DC1+(2.*THICK2)
      VP=(PI/6.)*(DP**3.)
      VF=(PI/6.)*(DF**3.)
      VC1=(PI/6.)*(DC1**3.)
      VC2=(PI/6.)*(DC2**3.)
25      W=(VF*ROF)+(VC1-VF)*ROC1+(VC2-VC1)*ROC2+(VP-VC2)*ROC3
      ROP=W/VP
      DR=DF/DP
      DR1=DF/DC1
      DR12=DC1/DC2
30      DR2=DP/DC2
      TCC1=TCC11*5./9.
      TCC2=TCC22*5./9.
      TCC3=TCC33*5./9.
      TCF=TCFF*5./9.
35      CP=CPP*5./9.
      A=(DF*(1.-DR1))/(2.*TCC1)
      ACA=(DR1**2.)*(DC1*(1.-DR12))/(2.*TCC2)
      AA=(DR**2.)*(DP*(DR2-1.))/(2.*TCC3)
      B=DF/(4.*TCF)
40      C=1./(DR**3.)
      D=DF/6.
      CC=78.2
      G=981.

```

```

45      PR=0.67
      PR23=PR**(.2/.3.)
      HE=HC/.874
      PLH=PI*HC/(2.*HE)
      TC=273.1
50      TGO1=1500.
      T1=(5./9.)*(TGI-32.)
      T2=(5./9.)*(TGO1-32.)
      T12=(T1+T2)/2.
      ROG=((T1+TC)/(T12+TC))*ROGI
55      VISCG=0.000187*((TC+CC)/(T12+TC+CC))*(((T12+TC)/273.1)**1.5)
      DELRO=(ROP-ROG)/ROG
      DVIS2=(VISCG/ROG)**2.
      AR=((G*(DP**3.))/DVIS2)*DELRO
PROGRAM FIXRUN2      73/74      OPT=1

```

FTN 4.6+420

```

60      ARSQ=SQRT(AR)
      RETERM=AR/(18.+0.61*ARSQ)
      TERVEL=RETERM*VISCG/(DP*ROG*100.)
211     GOPT=SUPFV*100.*ROGI
      REOPT=(GOPT*DP/VISCG)*(ROG/ROGI)
      REMOD=REOPT/(1.-VOID)
65     IF(REMOD.GT.30.) GO TO 20
      C THE FOLLOWING HTC(HEAT TRANS. COEF.) IS BASED ON CHU EQ
      HTC=(5.7/PR23)*(1./(REMOD**0.78))+CP*GOPT
      HTTC=HTC*9./5.
      GO TO 30
70     20 HTC=(1.77/PR23)*(1./(REMOD**0.44))+CP*GOPT
      HTTC=HTC*9./5.
      30 DD=DP/(6.*HTC)
      PGCV=PI*GOPT*CP/(1.-VOID)
      ZCFMAX=(HC/PI)*ATAN(100.*HE/(PGCV*(DD+D+C*(A+ACA+AA+B))))
      PZH=(PI*ZCFMAX)/HE
75     QQ1=(PI/PGCV)*(1./C)*(HE/PI)*(SIN(PZH)+SIN(PLH))
      QQ2=DD*(1./C)*COS(PZH)
      QQ3=D*AA*COS(PZH)
      QQ4=D*ACA*COS(PZH)
      QQ5=D*A*COS(PZH)

```

```

80      QQ6=D*B*COS(PZH)
      DTZ=2400.-TGI
      QQQC=DTZ/(QQ1+QQ2+QQ3+QQ4+QQ5+QQ6)
      TGO=TGI+(PI/PGCV)*(1./C)*QQC*(HE/PI)*(2.*SIN(PLH))
      TGZ=TGI+(PI/PGCV)*(1./C)*QQC*(HE/PI)*(SIN(PZH)+SIN(PLH))
85      TPZ=TGZ+DD*(1./C)*QQC*COS(PZH)
      TC2Z=TPZ+D*AA*QQC*COS(PZH)
      TC1Z=TC2Z+D*ACA*QQC*COS(PZH)
      TSZ=TC1Z+D*QQC*A*COS(PZH)
      TMZ=TSZ+D*QQC*B*COS(PZH)
90      DELTGO=TGO1-TGO
      IF(DELGO) 40,50,60
      40  IF(ABS(DELGO).GT.5.) GO TO 41
      GO TO 50
      41  SUPFV=SUPFV+0.1
      GO TO 211
95      60  IF(DELGO.GT.5.) GO TO 61
      GO TO 50
      61  SUPFV=SUPFV-0.1
      GO TO 211
100     50  PWRDEN=(GOPT*CP)*(TGO-TGI)/(HC*100.)
      VFUN=(1.-VOID)/(VOID**3.)
      PRDROP=CONST*(HC*100./DP)*(SUPFV**2.)*(ROG/(.02*G))*VFUN*1.41
      WRITE(6,100)
105     100  FORMAT(//6X,"DP",9X,"THICK",7X,"G-OPT",7X,"VOID",
      17X,"PR.DROP",5X,"ZCFMAX",+X,"GAS IN TEMP",2X,"GAS PRES",2X
      1,"GAS IN DEN",3X,"MEAN G. DEN.")
      WRITE(6,101) DP,THICK,GOPT,VOID,PRDROP,ZCFMAX,TGI,GPRESS,ROG1,ROG
101     101  FORMAT(/1X,10(1PE12.5))
      WRITE(6,200)
110     200  FORMAT(/2X,"HEAT T.C.",3X,"FUEL C.T.",3X,"FUEL S.T.",
      15X,"V.H.SO",3X,"GAS OUT TEMP",1X,"POWER DEN.",2X,"PART. S.T.",
      12X,"TERM. VEL.",2X,"BED HEIGHT",2X,"GAS IN VEL.")
      WRITE(6,201) HTTC, TMZ, TSZ, QQQC, TGO, PWRDEN, TPZ, TERVEL, HC, SUPFV
201     201  FORMAT(/1X,10(1PE12.5))
PROGRAM FIXRUN2      73/74      OPT=1      FTN 4.0+428
115     GO TO 75
      888  GO TO 65
      939  STOP

```

END

SAMPLE OUTPUT

	DP	THICK	G-OPT	VOID	PR.DROP
	1.70000E-01	1.50000E-02	1.59019E+01	5.00000E-01	4.96842E+02
	HEAT T.C.	FUEL C.T.	FUEL S.T.	V.H.SO	GAS OUT TEMP
	3.38774E+00	2.40000E+03	2.05192E+03	2.19756E+05	1.50440E+03
	SCAN 10	EOR 13			
0	OMIT				

NO CORRECTIONS APPLIED.

ZCFMAX	GAS IN TEMP	GAS PRES	GAS IN DEN	MEAN G. DEN.
4.77061E-01	5.54000E+02	1.00000E+03	5.86785E-03	4.00082E-03
POWER DEN.	PARRT. S.T.	TERM. VEL.	BED HEIGHT	GAS IN VEL.
4.38282E+02	1.97409E+03	8.69794E+00	1.00000E+00	2.71000E+01

APPENDIX E
GAS-STEAM BINARY CYCLE

GAS-STEAM BINARY CYCLE

E.1 Steam Cycle

The T-S diagram of the steam cycle with six feed water heaters and no reheat is shown in Fig. (E-1).

The symbols used are:

- h_{mn} , $n=1,2,\dots,6$ \equiv The actual enthalpy of the steam extraction to the n_{th} heater
- h_{mnf} and v_{mnf} , $n=1,2,\dots,6$ \equiv enthalpy and specific volume of the condensed extraction steam (saturated liquid) in the n_{th} heater,
- h_{mnc} , $n=1,2,\dots,6$ \equiv enthalpy of the compressed liquid (feed or condensed water) at the n_{th} heater outlet,
- p_{mn} and t_{mn} , $n=1,2,\dots,6$ \equiv the pressure and corresponding saturation temperature of the n_{th} extraction steam,
- m_n , $n=1,2,\dots,6$ \equiv fraction of the steam extracted from different stages of steam turbine for n_{th} heater.

Once the condition of the steam at the turbine outlet (p_1 and t_1), and condenser (p^* ...), and also pressures of the steam extractions (p_{mn} , $n=1,2,\dots,6$) are specified the rest of the properties of the steam cycle could be obtained from steam-tables taking into account the turbine efficiency at each stages of the steam extractions.

From the simple heat balance for different heaters the fractional steam extractions are obtained under the assumption that compressed liquid (feed water and condensed water) at each heater is heated up to a temperature

which equals the saturated temperature of the extraction steam corresponding to its pressure for that heater. The justification for the assumption is that since most of the extractions are taken where the steam is still superheated, except for the very low pressure heater, it is possible to achieve the prescribed temperatures. For the very low pressure heater the effectiveness of the heater is ignored. Furthermore, one of the heaters, namely heater #3, is open-loop for deaeration purposes, the rest are closed loop heaters. The condensed extraction steam at each closed-loop heater is to be drained to the successive lower pressure heater. For the low pressure heaters the condensed steam is sent to the condensate line.

The fractional quantities of steam extractions are obtained as:

$$m_1 = \frac{h_{m1c} - h_{m2c}}{h_{m1} - h_{m1f}} \quad (1)$$

$$m_2 = \frac{(h_{m2c} - h_{B2}) - m_1(h_{m1f} - h_{m2f})}{h_{m2} - h_{m2f}} \quad (2)$$

$$m_3 = \frac{(1 - m_1 - m_2)(h_{m3f} - h_{m4c}) - (m_1 + m_2)(h_{m2f} - h_{m3f})}{h_{m3} - h_{m4c}} \quad (3)$$

$$m_4 = \frac{(1 - m_1 - m_2 - m_3)(h_{m4c} - h_{m5c})}{h_{m4} - h_{m4f}} \quad (4)$$

$$m_5 = \frac{(1 - m_1 - m_2 - m_3)(h_{m5c} - h_{m6c}) - m_4(h_{m4f} - h_{m5f})}{h_{m5} - h_{m5f}} \quad (5)$$

$$m_6 = \frac{(1 - m_1 - m_2 - m_3 - m_4 - m_5)(h_{m6c} - h_{B1}) - (m_4 + m_5)(h_{m5f} - h_{m6f})}{(h_{m6} - h_{m6f}) + (h_{m6c} - h_{B1})} \quad (6)$$

where $h_{B2} \equiv$ actual enthalpy of the feed pump outlet

$h_{B1} \equiv$ actual enthalpy of the condensate pump outlet

It should be noticed that the effect of the drip pump is neglected because of its very small contribution, but the drip pumping requirements will be considered later.

The turbine is obtained by summing the partial turbine works at different stages of steam extractions as,

$$\omega_{t1} = h_1 - h_{m1} \quad (7)$$

$$\omega_{t2} = (1 - m_1)(h_{m1} - h_{m2}) \quad (8)$$

$$\omega_{t3} = (1 - m_1 - m_2)(h_{m2} - h_{m3}) \quad (9)$$

$$\omega_{t4} = (1 - m_1 - m_2 - m_3)(h_{m3} - h_{m4}) \quad (10)$$

$$\omega_{t5} = (1 - m_1 - m_2 - m_3 - m_4)(h_{m4} - h_{m5}) \quad (11)$$

$$\omega_{t6} = (1 - m_1 - m_2 - m_3 - m_4 - m_5)(h_{m5} - h_{m6}) \quad (12)$$

$$\omega_{t7} = (1 - m_1 - m_2 - m_3 - m_4 - m_5 - m_6)(h_{m6} - h^*) \quad (13)$$

where h_1 \equiv enthalpy of steam at the turbine inlet

h^* = enthalpy of steam at the turbine exit to the condensor.

The total turbine work is given by

$$\omega_t = \omega_{t1} + \omega_{t2} + \omega_{t3} + \omega_{t4} + \omega_{t5} + \omega_{t6} + \omega_{t7} \quad (14)$$

The required work for the condensate pump is obtained as,

$$\omega_{p1} = (1 - m_1 - m_2 - m_3 - m_4 - m_5 - m_6) \frac{v_f^*}{\eta_{p1}} \Delta p_1 \quad (15)$$

where $\Delta p_1 = p_{m3} - p^*$

p^* = absolute pressure in condensor

v_f^* = specific volume of the saturated water in condensor

η_{p1} = efficiency of the condensate pump.

The required work for feed water pump is given as,

$$\omega_{p2} = \frac{v_{m3f}}{\eta_{p2}} \Delta p_2 \quad (16)$$

where $\Delta p_2 = p_1 - p_{m3}$

η_{p2} = efficiency of the feed pump,

and the drip pump required work is written as,

$$\omega_{p3} = (1 - m_1 - m_2 - m_3) \frac{v_{m6f}}{\eta_{p3}} \Delta p_3 \quad (17)$$

The total pumping requirements is obtained by summing up the Eqs. (15), (16), and (17) as,

$$\omega_p = \omega_{p1} + \omega_{p2} + \omega_{p3} \quad (18)$$

The net work done by the steam cycle is simply obtained by subtracting Eq. (18) from Eq. (14),

$$\omega_{\text{net steam}} = \omega_t - \omega_p \quad (19)$$

The amount of heat needed to generate superheated steam at the desired conditions, i.e. p_1 and t_1 , is obtained as,

$$Q_{\text{in steam}} = h_1 - h_{\text{mlc}} \quad (20)$$

Thus, the efficiency of the steam cycle alone is obtained as

$$\eta_{\text{steam}} = \frac{\omega_{\text{net steam}}}{Q_{\text{in steam}}} \times 100 \quad (21)$$

and the quality of steam turbine exit to the condensor is,

$$X = 1 - \frac{h^* - h_f^*}{h_{fg}^*} \quad (22)$$

where h_{fg}^* = total latent heat of steam at the condensor pressure,

h_f^* = enthalpy of the saturated water at the condensor pressure.

E.2 Gas Turbine

The T-S diagram of the gas-cycle is shown in Fig. (E-2). Also, the temperature vs fractional heat exchanged in the steam generator is shown.

The gas turbine work is given by

$$\omega_{t_{\text{gas}}} = C_p \eta_{tg} T_{\text{max}} \left[1 - \left(\frac{\beta}{r_p} \right)^{\frac{\gamma-1}{\gamma}} \right] \quad (23)$$

where

$C_p \equiv$ specific heat of gas

$\eta_{tg} \equiv$ efficiency of the gas turbine

$T_{\text{max}} \equiv$ maximum temperature of the gas (absolute)

$\beta \equiv$ 1 + pressure loss ratio of the cycle

$r_p \equiv$ compressor pressure ratio

$\gamma \equiv$ specific heat ratio.

The gas turbine outlet is obtained as

$$T_{t_{\text{out}}} = T_{\text{max}} - \frac{\omega_{t_{\text{gas}}}}{C_p} \quad (24)$$

By setting T'_b for the gas (see Fig. E-2), and heat balance for the steam generator from pinch point to the high temperature terminal, one obtains an expression for the amount of gas per unit mass of steam generated as,

$$m_g = \frac{h_1 - h_b}{C_p(T_{t_{\text{out}}} - T'_b)} \quad (25)$$

The gas temperature leaving the steam temperature could be obtained straight forwardly as

$$T_{\min} = T_{b'} - \frac{h_b - h_{mlc}}{C_p m_g} \quad (26)$$

The compressor work requirement is obtained as,

$$\omega_{c_{\text{gas}}} = \frac{C_p}{\eta_{cg}} T_{\min} \left(r_p^{\frac{\gamma-1}{\gamma}} - 1 \right) \quad (27)$$

where η_{cg} = efficiency of the compressor

and the gas temperature leaving the compressor is written as,

$$T_{c_{\text{out}}} = T_{\min} + \frac{\omega_{c_{\text{gas}}}}{C_p} \quad (28)$$

The amount of heat required to increase the gas temperature from $T_{c_{\text{out}}}$ to T_{\max} is simply,

$$Q_{\text{in}_{\text{gas}}} = C_p (T_{\max} - T_{c_{\text{out}}}) \quad (29)$$

The efficiency of the gas cycle above is obtained by

$$\eta_{\text{gas}} = \frac{\omega_{t_{\text{gas}}} - \omega_{c_{\text{gas}}}}{Q_{\text{in}_{\text{gas}}}} \times 100 \quad (30)$$

Thus, the net work done by the binary cycle is:

$$\dot{\omega}_{\text{net, binary}} = \dot{m}_g (\dot{\omega}_{\text{t, gas}} - \dot{\omega}_{\text{c, gas}}) + \dot{\omega}_{\text{net, steam}} \quad (31)$$

and finally the overall thermal efficiency of the binary cycle is obtained as

$$\eta_{\text{binary}} = \frac{\dot{\omega}_{\text{net, binary}}}{\dot{m}_g Q_{\text{in, gas}}} \quad (32)$$

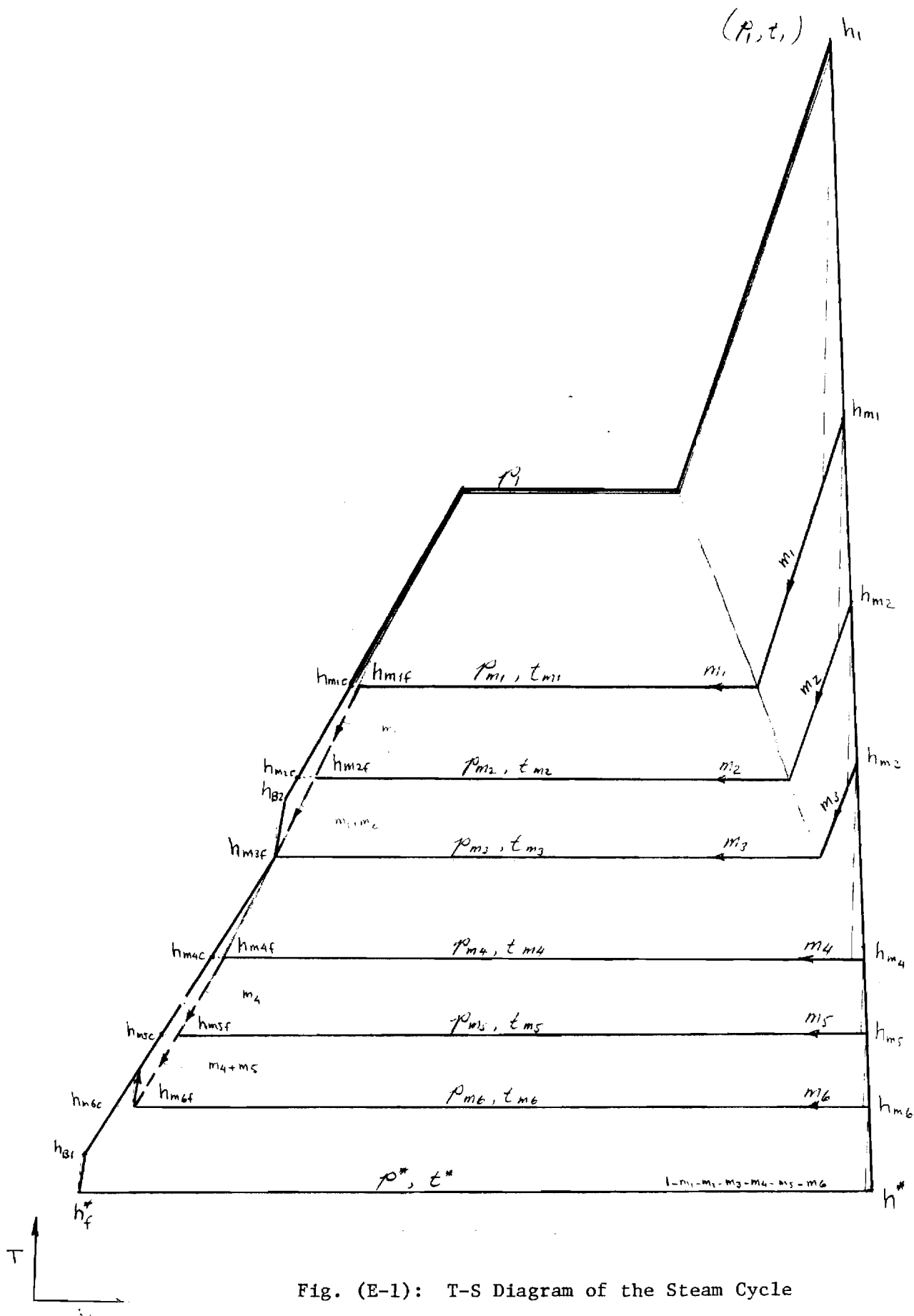


Fig. (E-1): T-S Diagram of the Steam Cycle

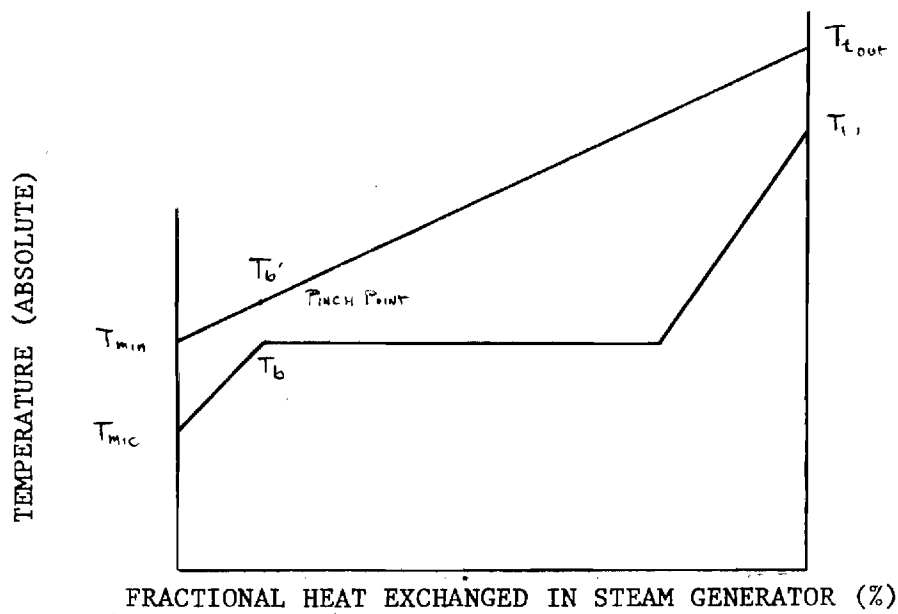
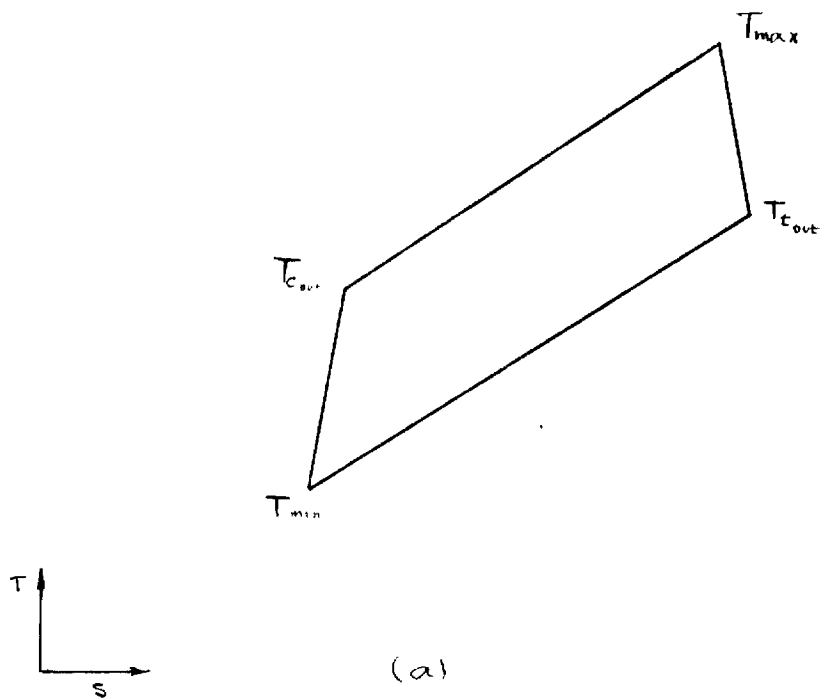


Fig. (E-2): (a) Sketch of T-S Diagram of Gas Cycle (Brayton Cycle)
 (b) Temperature (Absolute) vs Fractional Heat Exchanged in Steam Generator.

REFERENCES

1. Williams, J. R., "Nuclear Power from Space," final report on comparison and evaluation of power plant options for geosynchronous power stations, prepared for NASA under Grant NGR-11-002-181 (November 1974).
2. Fluidized-Bed Reactor Study, Phase 1 - Feasibility, The Martin Nuclear Division, MND-FBR-1696 (1959).
3. Hendrie, J. M., et al., "Rotating Fluidized Bed Reactor for Space Nuclear Propulsion," BNL 50321 (UC-33) (August 1971).
4. Hatch, L. P., W. H. Regan, and J. R. Powell, "Fluidized Solids as a Nuclear Fuel for Rocket Propulsion," American Rocket Society Semi-Annual Meeting, Los Angeles, California (May 1960).
5. Hatch, L. P., W. H. Regan, and J. R. Powell, "Fluidized Bed for Rocket Propulsion," Nucleonics, Vol. 18, No. 12, 102-103 (December 1960).
6. Ludwig, H., "Physics Parameters for a Fluidized Bed Cavity Reactor," Brookhaven National Laboratory Internal Memorandum (June 1971).
7. Gelperin, N. I., and V. G. Einstein, "Heat Transfer in Fluidized Beds," Fluidization, edited by J. F. Davidson and D. Harrison, Academic Press, 513, (1971).
8. Zabrodsky, S. S., "Hydrodynamics and Heat Transfer in Fluidized Beds," M.I.T. Press, 71, (1966).
9. Ibid, 186-188.
10. Botterill, J. S. M., "Fluidized-Bed Heat Transfer," Academic Press, 65, (1975).
11. See reference (8),3.
12. Other references of interest are:
Leva, M., M. Weintraub, M. Grummer, M. Polilchick, and H. H. Storck, "Fluid Flow Through Packed and Fluidized Systems," U. S. Bureau of Mines Bulletin 509, Washington, D. C., (1951).
Lewis, W. K., E. R. Gilliland, and W. C. Bauer, Ind. Eng. Chem., 41, 1104, (1949).
Toomey, R. D., and H. F. Johnstone, Chem. Eng. Prog., 48, 220, (1952).
Leva, M., T. Shivali, and C. Y. Wen, Genie Chemique, 75, 33, (1956).
Frantz, J. F., Chem. Eng. Prog. Symp. Series, 62, No. 62, 21, (1966).

- Kozeny, J., *Ber. Wien. Akad.*, 136A, 271, (1927).
- Todes, O. M., and R. B. Rozenbaum, *Dokl. Akad. Nauk SSSR* 115, 504, (1957).
- Blake, F. C., *Trans. Amer. Inst. Chem. Eng.*, 14, 415, (1922).
- Carman, P. C., *Trans. Inst. Chem. Eng.*, 15, 150, (1937).
- Ergun, S., *Chem. Eng. Prog.*, 48, 89, (1952).
- Todes, O. M., "Applications of Fluidized Beds in the Chemical Industry," Part II, 4-27, *Izd. Znanie, Leningrad*, (1965).
- Todes, O. M., and R. B. Rozenbaum, *Dokl. Akad. Nauk SSSR* 115, 504, (1957).
- Zabrodsky, S. S., 71-73.
- Gelperin, N. I., and V. G. Einstein, "Heat Transfer in Fluidized Beds," edited by J. F. Davidson and D. Harrison, *Fluidization*, 513, Academic Press, (1971).
- Todes, O. M., "Applications of Fluidized Beds in the Chemical Industry," Part II, 4-27, *Izd. Znanie, Leningrad*, (1965).
- Zabrodsky, S. S., 30-31.
- Chu, J. Ch., "Heat and Mass Transfer in Fluidized Beds," Collection *Fluidization*, D. F. Othmer (ed.), *Fluidization*, Reinhold Publishing Corporation, New York, (1956).
- Zabrodsky, S. S., 186-188.
- Lena, M., *Fluidization*, New York, (1959).
- Blake, F. C., *Trans. Amer. Inst. Chem. Eng.*, 14, 415, (1922).
- Carman, P. C., *Trans. Inst. Chem. Eng.*, 15, 150, (1937).
- Ergun, S., *Chem. Eng. Prog.*, 48, 89, (1952).
- Richardson, J. F., and R. A. Meikle, *Trans. Inst. Chem. Eng.*, 39, 348.
- Zabrodsky, S. S., 3.
- Zabrodsky, S. S., 71-73.
- Gelperin, N. I., and V. G. Einstein, "Heat Transfer in Fluidized Beds," edited by J. F. Davidson and D. Harrison, *Fluidization*, 513, Academic Press, (1971).
- Todes, O. M., and R. B. Rozenbaum, *Dokl. Akad. Nauk SSSR* 115, 504, (1957).
13. Wirtz, Karl, "Development of Advanced Power Reactor in the Federal Republic of Germany," *Advanced Reactors: Physics, Design and Economics*, edited by J. Kallfelz and R. A. Karam, Pergamon Press, (1975).
14. Fortescue, P., and R. N. Quade, "Direct Cycle and Process Heat, HTGR Development," *Gas-Cooled Reactors: HTGR and GCFBR*, American Nuclear Society Topical, May 7-10, 397-417, Gatlinburg, Tennessee, (1974).
15. Donne, M. Dalle, et al., "High Temperature Gas Cooling for Fast Breeders," *Symposium on Advanced- and High-Temperature Gas-Cooled Reactors*, IAEA, Julich, October 21-25, 345-357, (1968).

16. Donne, M. Dalle, et al., "Gas Cooled Fast Breeder Reactor Design Development and Safety Features," Gas Cooled Reactors: HTGR and GCFBR, ANS Topical, May 7-10, Gatlinburg, Tennessee, (1974).
17. de Nordwall, H. J., and J. B. Sayers, "The Value of Silicon Carbide Barrier in High Temperature Reactor Fuels," High Temperature Nuclear Fuels, a symposium sponsored by Nuclear Committee of the Institute of Mining, Metallurgical, and Petroleum Engineers, Delvan, Wisconsin, (October 1966).
18. "Thorium Fuel Cycle," Proceedings of Second Inter. Thorium Fuel Cycle Symposium," Gatlinburg, Tennessee, May 3-6, 1966, U.S.A.E.C. Div. of Technical Inf., (February 1968).
19. Proceedings of the Gas-Cooled Reactor Inf., meeting at Oak Ridge National Laboratory, April 27-30, 1970, Oak Ridge, Tennessee (937 pages).
20. Gas-Cooled Reactors: HTGR and GCFBR, ANS Topical Meeting, Gatlinburg, Tennessee, May 7-10, (1974).
21. Tokar, Michael, "Evaluation of High Temperature Gas Cooled Reactor Fuel Particle Coating Failure Models and Data," NUREG-0111, (November 1976).
22. Lane, R. K., et al., "High Conversion and Near-Breeding HTGR," GA-A 14029 (UC-77), (July 1976).
23. "Utilization of Thorium in Power Reactors," Technical Report Series No. 52, International Atomic Energy Agency, Vienna (1966).
24. Schumar, T. F., "Research on Metallic Fuel," in Education and Research in the Nuclear Fuel Cycle, D. M. Elliott and Lynn Weaver (eds.), University of Oklahoma Press, Norman, (1972).
25. Kittel, T. H., J. A. Haruk, W. F. Murphy, and S. H. Paine, "Effects of Irradiation of Th and Th-U Alloys," ANL 5676, (1963).
26. "The Use of Thorium in Nuclear Power Reactors," WASH 1097, (1969).
27. Bohm, H., "The Effect of Neutron Irradiation on High Temperature Mechanical Properties of Vanadium-Titanium-Alloys," Defects and Defect Clusters in BCC Metals and Their Alloys, Institute of Metals Div. Am. Inst. of Metallurgical Eng., 163, (1963).
28. Kasten, P. R., "Assessment of the Thorium Fuel Cycle in Power Reactors," ORNL/TM-5565, (January 1977).

29. Chang, Y. I., "Review of the French Concept of Heterogeneous Core to Improve the Doubling Time," FRA-TM-77, Argonne National Laboratory, (August 1975).
30. Toppel, B. J., A. L. Rago and D. M. O'Shea, "Mc², A Code to Calculate Multi-group Cross Sections," Argonne National Laboratory, ANL-7318, (1967).
31. Sehgal, B. R., et al., "Thorium Based Fuels in Fast Breeder Reactors," Trans. Am. Nucl. Soc., 21, 422, (1975).
32. Wirtz, K., "Development of Advanced Power Reactors in the Federal Republic of Germany," Advanced Reactors: Physics, Design and Economics, J. Kallfelz and R. A. Karam (eds.), Pergamon Press, (1975).
33. Rostaker, William, "The Metallurgy of Vanadium," publisher by John Wiley & Sons, Inc., (1958).
34. Miller, G. L., "Zirconium," 2nd edition, Academic Press, Inc., London, (1957).
35. Clark, R. J. H., "The Chemistry of Titanium and Vanadium," Elsevier Publishing Company, New York, (1968).
36. Masamune, S., and J. M. Smith, "Thermal Conductivity of Beds of Spherical Particles," Industrial and Engineering Chemistry Fundamentals, 2, No. 2, 136-142, (May 1963).
37. "Mineral Resources and the Environment," a Supplementary Report on Reserves and Resources of Uranium in the United States, prepared by Committee on Mineral Resources and the Environmental (COMRATE), National Academy of Sciences, Washington, D. C., (1975).
38. Information from ERDA, Weekly Announcements, (March 19, 1976).
39. "Proposed Final Environmental Statement, Liquid Metal Fast Breeder Reactor Program," Vol. III, 6C, 2-12, (December 1974).
40. "Uranium Resources to Meet Long Term Requirements," Summary of EPRI Special Report 5, (November 1974).
41. Patterson, John A., USAEC, at the Gulf Coast Association of Geological Societies Annual Meeting, Corpus Christi, Texas, "Nuclear Power and Uranium," 11, cited in Ref. 3, Section GA. 1-11, (October 13, 1972).
42. "Assessment of Uranium and Thorium Resources in the U.S. and the Effect of Policy Alternatives," NSF, Office of Energy R&D Policy, work performed by Battelle Pacific Northwest Laboratories, (1974).

43. Chapman, D. F., and N. D. Martimer, "Energy Inputs and Outputs for Nuclear Power Stations," Research Report ERG 005, Open University, Energy Research Group, Milton Keynes, U. K., (1974).
44. See Reference 39, Section 6A, 1-17.
45. "Energy Alternatives: A Comparative Analysis," prepared for CEQ, ERDA, EPA, FPC, DOI and NSF by the University of Oklahoma, (May 1975).
46. Nuclear News, 18 (13), 50, (October 1975).
47. Hogerton, John F., "Uranium Supply in the U.S.: A Current Assessment," Nuclear News, 19, 73, (June 1976).
48. Nuclear News, 19, 60, (May 1976).
49. Nininger, R. D., Appendix for 1967 Supplement to the 1962 Report to the President on Civilian Nuclear Power, U.S. AEC, (February 1967).
50. Olsen, J. C., U.S. Geological Survey Bulletin - 1204, (1964).
51. See Reference 39 Section 6A, 1-87.
52. Draft, Environmental Statement, Light Water Breeder Reactor Program, Vol. I, ERDA - 1541, (July 1975).
53. Gunst, S. B., D. E. Conway and D. R. Harris, "Integral Measurement of Neutron Capture and Fission in U²³³ (LWBR Development Program)," WAPD-TM-760, Bettis Atomic Power Laboratory, Pittsburg, Pennsylvania (August 1968).
54. Taylor, S. R., "Abundance of Chemical Elements in the Continental Crust, A New Table," Goeochem. Cosmochem. Acta., 28, 173-1285, (1964).
55. "Comparative Risk-Cost-Benefit Study of Alternative Sources of Electrical Energy," WASH-1224, (December 1974).
56. "Nuclear Power Growth 1974-2000," WASH-1139, (1974).
57. Draft, "Generic Environmental Statement on Mixed Oxide Fuel," WASH-1327, (August 1974).
58. Dietrich, J. R., "The Problem of Fast Breeder Inventory," Trans. Am. Nucl. Soc., 9, 548, (November 1966).
59. See Reference 39, Section 6A, 1-4.
60. Lake, J. A., R. A. Doncals, R. W. Rathbun and H. C. Robinson, "Breeding and Doubling Time Characteristics of the Clinch River Breeder Reactor," 665-676, Advanced Reactors: Physics, Design and Economics, J. Kallfelz and R. A. Karam, Eds., Pergamon Press, (1975).

61. "The Use of Thorium in Nuclear Power Reactors," 1, WASH-1097, (1969).
62. "Administrator's Findings on the Liquid Metal Fast Breeder Reactor Program-Final Environmental Statement," (December 31, 1975).
63. Mougnot, J. C., et al., "Breeding Gains of Sodium-Cooled Oxide-Fueled Fast Reactors," Trans. Am. Soc., 20, 348, (1975); also, ORNL-TR-2994.
64. Chang, Y. I., "Review of the French Concept of Heterogeneous Core to Improve the Doubling Time," Applied Physics Div., FRA-TM-77, Argonne National Laboratory, (August 1975).
65. Orlov, V. V., and L. A. Kochetkov, "Status of the Fast Reactor Development in the U.S.S.R.;" see discussion of this paper on p. 88, Advanced Reactor: Physics, Design and Economics, J. M. Kallfelz and R. A. Karam, Eds., Pergamon Press, (1975).
66. Final Environment Statement, Liquid Metal Fast Breeder Reactor Program, Vol. I, III-B-52, WASH-1535, (December 1975).
67. Okrent, David, "Neutron Physics Considerations in Large Fast Reactors," Power Reactor Technology, 7 (2), (Spring 1964).
68. Karam, R. A., "A Proposal to Assess the Breeding Potential of the $U^{233} - Th^{232}$ Fuel Cycle in Sodium-Cooled and Heavy Water-Cooled Reactors," Georgia Institute of Technology, (June 1976).
69. Perry, A. M., and A. M. Weinberg, "Thermal Breeder Reactors," Am. Rev. of Nuclear Science, 22, 317-353, (1972).
70. Kasten, P. R., et al., "Assessment of the Thorium Fuel Cycle in Power Reactors," ORNL/TM-5565, (January 1977).
71. Garrison, J. D., and B. W. Roos, "Fission-Product Capture Cross Sections," Nucl. Sci. and Eng., 12, 115-134, (1962).
72. Spinrad, B. I., "On the Definition of Breeding," Proc. of Conf. on Physics of Breeding, October 19-21, 1959, 23-32, ANL-6122, (1959).
73. Ott, K. O., "An Improved Definition of the Breeding Ratio for Fast Reactors," Trans. Am. Nucl. Soc., 12, 719, (1969).
74. Adkins, C. R., "The Breeding Ratio with Correlation in Doubling Time and Fuel Cycle Reactivity Variation," Nuclear Technology, 13, 114-130, (February 1972).
75. Wyckoff, Harvey L., and Paul Greebler, "Definitions of Breeding Ratio and Doubling Time," Nuclear Technology, 21, 158-164, (1974).

76. Ott, Karl O., and Robert C. Borg, "Derivation of Consistent Measures for the Doubling of Fast Breeder Reactor Fuel," PNE-76-108, Purdue University, West Lafayette, Indiana, (1976).
77. Srikantiah, G., and J. Chernick, "Plutonium Fueled Thermal Reactors with High Conversion Ratios," Nuclear Science and Eng., 21, 165-178 (1965).
78. Glasstone, S. and A. Sesonske, Nuclear Reactor Engineering, 358, D. Van Nostrand Co. Inc., New York (1963).
79. Colburn, A. P., Trans. Am. Inst. Chem. Eng., 29, 174 (1933).
80. "Evaluation of Advanced Converter Reactors," Advanced Converter Task Force, WASH-1087, (April 1969).
81. "An Evaluation of Heavy-Water-Moderated Organic-Cooled Reactors," WASH-1083, (March 1968).
82. "Evaluation of High-Temperature Gas-Cooled Reactors," WASH-1085, (December 1969).
83. Lewis, W. Bennet, "The Super-Converter or Valuebreeder," A Near-Breeder Uranium-Thorium Nuclear Fuel Cycle," Atomic Energy of Canada Limited, AECL-3081, (May 1968).
84. Kittel, J. H., J. A. Horak, W. F. Murphy and S. H. Paine, "Effects of Irradiation on Th and Th-Uranium Alloys," ANL-5674 (1963).
85. Sofer, G. A., A. H. Kazi and J. Bober, "Economic and Safety Aspects of Large Ceramic U-Th Fast Breeder Reactors," Proc. of the Conf. on Breeding, Economics and Safety in Large Fast Power Reactors, October 7-10, 1963, ANL-6792 (1963).
86. Lowenstein, W. B., and B. Blumenthal, "Mixed Fuel-Cycle Fast Breeder Reactors; Nuclear, Safety, and Material Considerations," Proc. of the Conf. on Safety, Fuels, and Core Design in Large Fast Power Reactors, October 11-14, 1965, ANL-7120 (1965).
87. Devaney, J. J. "Radiation Intensity from Spheres of U²³³ Contaminated with U²³²," Los Alamos Scientific Laboratory, LAMS-1892 (1955).
88. Bortino, J. P., and J. A. Kircher, "U²³³ Purification and Metal Production," Los Alamos Scientific Laboratory, LA-2245 (1959).
89. Morgan, Karl, Z., W. S. Snyder and M. R. Ford, "Relative Hazards of the Various Radioactive Materials," Health Physics, 10, 151-169 (1964).
90. Reactor Physics Constant, Argonne National Laboratory, ANL-5800, 2nd Ed. (1963).